

https://dspace.org/

Physico-chemical properties and treatment of scale formation in dust scrubber discharge lines at a PGM Smelter in South Africa

Fungene, Thandiwe

2024

University of the Witwatersrand, Johannesburg

https://hdl.handle.net/10539/45408

Fungene, Thandiwe. (2024). Physico-chemical properties and treatment of scale formation in dust scrubber discharge lines at a PGM Smelter in South Africa [Masters dissertation, University of the Witwatersrand, Johannesburg]. WIReDSpace. https://hdl.handle.net/10539/45408

Downloaded from a DSpace repository. https://dspace.org/



PHYSICO-CHEMICAL PROPERTIES AND TREATMENT OF SCALE FORMATION IN DUST-SCRUBBER DISCHARGE LINES AT A PGM SMELTER IN SOUTH AFRICA

Thandiwe Fungene

A Dissertation submitted to the Faculty of Engineering and the Built Environment, University of Witwatersrand, Johannesburg, in fulfilment of the requirements for the degree of Master of Science in Engineering

Johannesburg, 2023

Declaration

I, Thandiwe Fungene, declare that this dissertation is my own unaided work. It is being submitted for the degree of Master of Science in Engineering to the University of the Witwatersrand, Johannesburg. It has not been submitted before for any other degree or examination in any other University.



13th day of October 2023

Dedication

In memory of my mother

Nelisiwe Kuky Elyve Phiri-Ramahali

1957–2019

Publications

This work has produced some publications

Journal Publications

1. Thandiwe Fungene, Sehliselo Ndlovu & Elias Matinde (2023) Scale formation in wet scrubbers and the current state of anti-scaling and softening methods for hard waters: A review, Separation Science and Technology, DOI: 10.1080/01496395.2023.2189051

Conference Proceedings

1. T. Fungene, S. Ndlovu, E. Matinde. Physico-chemical properties and treatment of scale formation in dust scrubber discharge lines. Mine-Impacted Water Conference: Impacting The Circular Economy, Closing The Loop. SAIMM Online Conference, 12th – 13th October 2022.

Abstract

Several technologies in the field of flue-gas desulphurization (FGD) have been created to address the issue of sulphur dioxide (SO_2) emission from gas streams. Among these, wet scrubbing, particularly the use of lime/ limestone ($Ca(OH)_2$/ $CaCO_3$) scrubbing, stands out as the primary method for reducing SO_2 emissions from power plants. These methods are simple and cost-effective, making them suitable for various industrial facilities that emit SO_2, including refineries and smelters. In $Ca(OH)_2$ or $CaCO_3$ scrubbing systems, calcium (Ca) compounds are introduced in the form of slurries into the scrubber liquid. However, this process leads to the undesired creation of solid Ca salts. Consequently, the solubility of Ca salts in the slurry restricts the efficiency of wet scrubbing techniques containing Ca. If the ion concentration in the water exceeds the solubility limit of Ca salts like calcium sulphate ($CaSO_4$), it can result in the development of supersaturated $CaSO_4$, which may lead to scale accumulation or deposition in the scrubber. This scaling issue, in turn, requires frequent plant shutdowns to open and remove scale from pipelines.

The aim of this research is to propose a process for the prevention of hard water scale or its removal in FGD systems, particularly scrubbers commonly utilized in PGM smelters. To accomplish this goal, analyses were conducted to both physically and chemically characterize the scale or deposit, as well as all the feed materials within and around the variable throat scrubber (VTS) system at a local PGM smelter. By leveraging the physical and chemical properties of these materials, this study explores the application of traditional chemical "water softening" techniques like ion exchange and precipitation, as well as an emerging physical method known as magnetic water treatment (MWT), to combat scale formation in scrubbers.

The water samples obtained from the Sibanye-Stillwater scrubbing circuit were characterized by extremely high levels of Ca and magnesium (Mg) hardness (1000—8000 mg/L $CaCO_3$) and high levels of total dissolved solids (TDS) (3000—9000 mg/L). Both a strong acid cation exchange resin (SAC) and weak acid cation exchange resin (WAC) were employed in the treatment process. The WAC resin, commonly used for high TDS solutions, displayed better removal of Ca and Mg compared to SAC, effectively bringing the total hardness levels down to 120—180 mg/L $CaCO_3$. Chemical precipitation using a lime and soda ash pre-treatment step prior to cation exchange resulted in residual hardness levels of 0—120 mg/L as $CaCO_3$.

The use of MWT remains a topic of debate as a non-chemical option for water softening due to concerns about its scientific validity. This research aims to investigate the potential of a magnetic field to reduce hard water scaling. Several factors, including pH, dissolved oxygen (DO), electrical conductivity (EC), calcium ion concentration ($[Ca^{2+}]$), and scaling potential, were compared between treated and untreated water. The treated water displayed notable changes in these factors. Most significantly, the precipitation in treated water indicated a shift from calcite to aragonite formation, essentially inhibiting the overall scaling potential. These findings are substantiated by a mechanistic theory based on a comprehensive review of successful applications in the existing literature. This study holds significance in questioning the sustainability of chemical-based water treatment methods and explores the feasibility of non-chemical alternatives.

Acknowledgements

My Lord and Saviour, Jesus Christ – all glory and honour are Yours. You are the author of my faith and my strength in times of weakness. May Your name be praised.

To my husband and daughter, Nkosinathi and Lulama Fungene, as well as my sisters Ntombenhle and Nkosazana Ramahali: Thank you for your unwavering support, encouragement, and unconditional love during this challenging time. I hold you deeply in my heart and forever cherish you.

To my supervisor, Professor Sehliselo Ndlovu: Words cannot adequately convey my sincere gratitude for everything. Your dedication, including taking time from your holidays, and your unwavering push, especially when I felt overwhelmed, have been invaluable. Your frustrations motivated me, and I am profoundly grateful. This journey would not have been possible without you. Thank you for enriching not only my life but also that of my family. May God continue to bless and keep you.

To my co-supervisor, Dr Elias Matinde: Your insights and your commitment to this project, even amid your busy schedule, have been invaluable. Your stern yet constructive comments have helped reshape my thoughts on paper. May God bless you abundantly.

I must also acknowledge my fellow colleagues in the Metal Extraction and Recovery group (MERG), as well as Mr Bruce Mothibedi. Your collective strength and support, whether in the labs or the office, have been vital – thank you. My prayers are with all of us as we navigate this journey. A special mention to Ellen Chiyangwa and Amanda Vilakazi: Our weekly calls have provided comfort during challenging times, and the shared victories and losses have been deeply appreciated.

Ecclesiastes 12:12-13

"12 And further, by these, my son, be admonished: of making many books there is no end; and much study is a weariness of the flesh. 13 Let us hear the conclusion of the whole matter: Fear God, and keep His commandments: for this is the whole duty of man."

Table of Contents

Declaration II

Dedication III

Publications IV

Abstract V

Acknowledgements VII

Table of Contents VIII

List of Tables XIII

List of Figures XV

Nomenclature 1

Abbreviation 1

Description 1

AAS 1

Atomic Absorption Spectroscopy 1

Chapter 1 Introduction 3

1.1 Background 3

1.2 Problem identification 7

1.3 Research aims and objectives 9

1.4 Research questions 9

1.5 Research hypothesis 10

1.6 Research methodology 10

1.7 Thesis layout 10

1.8 References 11

Chapter 2 Literature review 15

2.1 Introduction 15

2.2 Flue gas desulphurisation systems 16

2.2.1 Non-Regenerable Processes 19

2.2.2 Regenerable Processes....25
2.3 Scale formation in lime based systems....30
2.3.1 Scale formation mechanism....33
2.3.2 Common scale deposits....34
2.3.3 Scale formation in wet scrubbers....39
2.4 Scale reduction techniques....42
2.4.1 Calcium sulphate scale....42
2.4.1.1 Oxidation inhibition....42
2.4.1.2 Softening....43
2.4.1.3 Sodium chloride....43
2.4.2 Calcium carbonate scale....44
2.5 Traditional Water Treatment Methods....45
2.6 Hard water and the process of softening to prevent scale formation....46
2.6.1 Water hardness and alkalinity relation....48
2.6.2 Water softening using ion exchange resins....56
2.6.3 Water softening through lime and soda ash (chemical precipitation)....59
2.6.4 The SAVMIN process....63
2.7 Magnetic water treatment....66
2.8 Application of magnetic treatment on hard water....67
2.8.1 The development of MWT parameters....69
2.8.2 Magnetization and the exhibition of a magnetic field on charged particles....80
2.8.3 Mechanisms of magnetic mater treatment....84
2.9 References....88
de Dardel, F., 2020, Basic ion exchange processes in water treatment, viewed 18 November 2019, http://dardel.info/IX/processes/processes.html/.....91
Chapter 3 Materials and Methods....102
3.1 Introduction....102

3.2 Experimental methods 102
3.2.1 Solid and liquid sample characterization 103
3.2.2 Chemical precipitation using lime and soda ash 105
3.2.3 The efficiency of ion exchange resins on hard water 110
3.2.4 The effect of magnetic water treatment (MWT) on hard water 114
3.3 Reagents 121
3.3.1 Neodymium magnet properties 121
3.4 Analytical methods and techniques 123
3.6 References 124
Chapter 4 Characterisation of solid scale and liquid samples 125
4.1 Introduction 125
4.2 Results and discussion 125
4.2.1 Solid scale samples 125
4.2.2 Liquid samples 131
4.3 Summary 141
4.4 References 142
Chapter 5 The effect of lime and soda ash addition on hard water 145
5.1 Introduction 145
5.2 Results and Discussion 146
5.2.1 The effect of varying lime concentration on hardness removal at ambient/room temperatures 146
5.3 Summary 167
5.4 References 168
Chapter 6 The efficiency of ion exchange resins on hard water 170
6.1 Introduction 170
6.2 Results and discussion 170
6.2.1 Resin loading/regeneration 170

6.2.2 Determining optimal operating parameters for resin batch reactions.....171

6.2.3 Summary of determined optimal operating parameters for resin batch reactions.183

6.2.4 Determining cation resin efficiency in the removal of calcium and magnesium for all samples 184

6.2.5 Determining resin efficiency with lime-soda ash pre-treatment of hard water (combined softening treatment).....187

6.3 Summary of cationic resin efficiency of WAC (Amberlite IRC 83H) and SAC (Amberlite IRC 120Na).....192

6.4 References.....193

Chapter 7 The effect of magnetic water treatment on hard water.....195

7.1 Introduction.....195

7.2 Results and discussion 196

7.2.1 Preliminary MWT time exposure effects on solution pH and dissolved oxygen (DO) 196

7.2.2 Effect of adjusted MTD exposure on electrical conductivity, calcium concentration, dissolved oxygen and DO and oxidation-reduction potential 197

7.2.3 Influence of the magnetic strength variation on hard water 203

7.2.4 The influence of flow rate on calcium concentration in MTD. 209

7.2.5 The influence of pipe material of a MTD on calcium concentration 210

7.2.6 The effect of MTD on the scale produced.....211

7.2.7 Proposed Mechanism of MWT.....216

7.3 Summary.....217

7.4 References.....219

Chapter 8 The proposed conceptual water treatment process and the techno-economic evaluation.....221

8.1 Proposed conceptual water treatment process 221

8.2 The techno-economic evaluation of the proposed water treatment process 223

8.2.1 Lime- soda softening evaluation.....224

8.2.2 Ion- exchange softening evaluation using the Amberlite IRC83H (WAC).....230
8.3 Summary.....232
8.4 References.....233
Chapter 9 Conclusions and recommendations.....234
Appendices:.....236
Appendix 1.....236
Appendix 2:.....247
Appendix 3:.....251
Appendix 4:.....252

List of Tables

Table 2. 1 FGD available technologies (Poullikkas, 2015) 18
Table 2. 2 Current and future distribution of FGD plants on coal-fired generating units (modified from Poullikkas, 2015) 18
Table 2. 3 XRD quantitative analysis of scrubber samples from a typical plant dealing with scale build-up. 40
Table 2. 4 Degree of hardness (United States Geological Survey, 2020) 48
Table 2. 5 The acceptance criteria for charge balance error (Rice et al., 2012). 51
Table 2. 6 Interpretation of P and M alkalinity (Bates, 2001; Dara, 2008; Ibanez et al., 2008). 52
Table 3. 1 Lime and soda ash dosages 107
Table 3. 2 N35 characteristic magnetic properties at room temperature (25°C) (*kjmagnets.com, 2022)*. 121
Table 4. 1 X-ray diffraction average results (Relative Abundance). 127
Table 4. 2 Average unit cell parameters for the mineral phases of gypsum and calcite. 128
Table 4. 3 XRD quantitative analysis of scrubber samples. 129
Table 4. 4 EDS element analysis of gypsum, calcite and talc crystals. 131
Table 4. 5 Received AAS and pH analysis on process water and dust thickener overflow sample. 133
Table 4. 6 ICP-OES analysis of all four liquid samples. 134
Table 4. 7 Additional analysis of physico-chemical water parameters. 135
Table 4. 8 Establishment of the hardness distribution. 137
Table 4. 9 Calculated TDS and EC values. 138
Table 4. 10 TDS and water quality relationship (Oram, 1989). 139
Table 5. 1 Varying lime dosage parameters 147
Table 5. 2 Effect of temperature on lime softening parameters for scrubber bleed and process water samples 152
Table 5. 3 Lime-soda ash-softening parameters 155
Table 5. 4 Calcium and magnesium concentrations after lime-soda ash treatment at room temperature (25°C) 155
Table 5. 5 Effect of temperature on lime-soda ash softening parameters for scrubber bleed and process water samples 157
Table 5. 6 Rand water elemental quality report (SANS 214:2015) 160

Table 5. 7 Initial concentrations of elements present in highest concentration for scrubber bleed and process water samples 162
Table 5. 8 Final concentrations after respective softening treatment (scrubber bleed sample) 162
Table 5. 9 Final concentrations after respective softening treatment (process water sample) 164
Table 6. 1 Total hardness after lime -soda ash and ion-exchange combined softening treatment 190
Table 6. 2 TDS values after combined softening treatment..... 191
Table 7. 1 X-ray diffraction average results (Relative Abundance) after 60 minutes exposure to the MTD..... 213
Table 7. 2 X-ray diffraction average results (Relative Abundance) after a 3-hour exposure to the MTD..... 214
Table 8. 1Process design criteria for the Neutralisation Reactor and Thickener/Settler 225
Table 8. 2 The Capital expenditure for a lime-soda ash treatment and alternative gypsum crystallization stream 227
Table 8. 3 Monthly reagent costs..... 228
Table 8. 4 Electrical costs 229
Table 8. 5 Labour costs..... 229

List of Figures

Figure 1. 1 Block flow diagram of the off-gas handling equipment. Figure adapted from Bezuidenhout et al. (2012, pg. 2) 6
Figure 1. 2 Simplified flow diagram of the dual-alkali system. Figure adapted from Bezuidenhout et al. (2012, pg. 2) 7
Figure 2. 1 FGD process classification (adapted from Lisnic and Jinga, 2018) 17
Figure 2. 2 General flow diagram for a wet FDG process (adapted from Živković et al., 2014) 20
Figure 2. 3 Flow diagram of the limestone scrubbing method (adapted from Poullikkas, 2015) 21
Figure 2. 4 Seawater FGD process (adapted from Lisnic and Jinga, 2018) 23
Figure 2. 5 Schematic diagram of the (a) open-loop FGD process, (b) closed-loop FGD process (Long et al., 2020). 24
Figure 2. 6 Flow diagram of the Wellman-Lord process (adapted from Poullikkas, 2015) 26
Figure 2. 7 Flow diagram of the Walther method (adapted from Poullikkas, 2015). 28
Figure 2. 8 Typical dry sorbent injection process (adapted from Lisnic and Jinga, 2018) 29
Figure 2. 9 Mechanism of scale formation (Safari et al., 2014) 33
Figure 2. 10 Crystal structure of aragonite (a, b) and calcite (c, d) (Soldati et al., 2016). 36
Figure 2. 11 Stability of aragonite and calcite with respect to pressure and temperature (Nelson, 2014). 37
Figure 2. 12 X-ray diffraction (XRD) pattern for a mixture of aragonite and calcite, highlighting significant peaks for the purpose of identification (Railsback, 2006). 38
Figure 2. 13 Scrubbing circuit for A PGM smelter (Sibanye-Stillwater, 2019) 47
Figure 2. 14 Relationship between pH and alkalinity (HCO_3^-, CO_3^{2-} and OH^-) (Minnesota Rural Water Association, 2009, page 5). 50
Figure 2. 15 Structure of a weak acid cation resin (left) and a strong acid cation resin (right) 56
Figure 2. 16 SAVMIN process (Van Niekerk, 2002) 64
Figure 2. 17 MWT effect: Left (c) is the steel pipe without MWT. Right (d) shows a similar pipe treated with a magnetic field (Lipusa and Dobersek, 2007) 68
Figure 2. 18 The crystal structure of Nd (red), Fe (green), B (blue) (Coey, 1995). 71
Figure 2. 19 Axially magnetized (*kjmagnets.com, 2022)* 72
Figure 2. 20 Radially magnetized (*kjmagnets.com, 2022)* 73

Figure 2. 21 Diametrically magnetized (*kjmagnets.com, 2022*) 74
Figure 2. 22 Scheme of the MTD with alternated magnetic poles (inverted), (B) scheme of the MTD without inversion of the magnetic poles (non-inverted) (Gabrielli et al., 2001). 76
Figure 2. 23 Variation of the magnetic induction for inverted pairs of permanent magnets (Gabrielli et al., 2001). 77
Figure 2. 24 Variation of the magnetic induction in the gap for non-inverted pairs of permanent magnets (Gabrielli et al., 2001) 78
Figure 2. 25 Typical MTD setup for water treatment (Gabrielli et al., 2001). 79
Figure 2. 26 Variations in Installation of Magnets (Rathilal, 2004). 79
Figure 2. 27 Effect of a magnetic field on polar (top) and nonpolar (bottom) molecules (Sawaftah, 2017) 81
Figure 2. 28 Dipole moment of a water molecule (McMahon, 2009) 82
Figure 2. 29 Representation of the electrical double layer (Stern and diffuse layer) (Suopajarvi, 2015). 83
Figure 2. 30 The Laplace-Lorentz force on a moving charged ion is at a right angle of both the ion flowing direction and the magnetic field direction (Sawaftah, 2017) 85
Figure 2. 31 An electric wire with cross-section A flown by a current I is submitted to a force F when placed into a magnetic field B (Sawaftah, 2017) 86
Figure 3. 1 Experimental procedures and stages necessary to achieve the objectives assigned in this study 103
Figure 3. 2 Scrubber circuit at Sibanye-Stillwater indicating sampling points (1. Scrubber feed, 2. Scrubber bleed, 3. Dust-thickener overflow and 4. Process water). 104
Figure 3. 3 Diagrammatic representation of the lime softening process 108
Figure 3. 4 Diagrammatic representation of the lime-soda ash process 110
Figure 3. 5 Preliminary MWT setup for effect on pH and DO 115
Figure 3. 6 Inverted magnet orientation on MTD 115
Figure 3. 7 Adjusted MTD for further tests 116
Figure 3. 8 Non-inverted magnetic pole orientation MTD 118
Figure 3. 9 Direction of magnetic field for the neodymium magnets used, axially magnetized (*kjmagnets.com, 2022)* 122
Figure 4. 1 SEM photomicrographs of three of the samples collected presenting major crystal phases 130
Figure 4. 2 Liquid sample points from the scrubbing circuit 132

Figure 4. 3 EPA Secondary TDS Regulations for water (adapted from U.S. Environmental Protection Agency, 2009). 140
Figure 5. 1 Effect of varying lime dosage on pH 148
Figure 5. 2 Variation of calcium for varying lime dosages 149
Figure 5. 3 Variation of magnesium for varying lime dosages 149
Figure 5. 4 Variation of total hardness for varying lime dosages 150
Figure 5. 5 Effect of varying lime dosage on precipitate mass 151
Figure 5. 6 Relationship between temperature and mass of precipitate formed for lime treatment 153
Figure 5. 7 Calcium removal with increasing temperature for lime softening procedure 154
Figure 5. 8 Magnesium removal with increasing temperature for lime softening procedure 154
Figure 5. 9 Lime-soda ash treatment for Ca and Mg removal 156
Figure 5. 10 Relationship between temperature and mass of precipitate formed for lime-soda ash treatment 158
Figure 5. 11 Calcium removal efficiency with increasing temperature for lime-soda softening 158
Figure 5. 12 Magnesium removal efficiency with increasing temperature for lime-soda softening 159
Figure 6. 1 Proton (H^+) loading on WAC resin (*Amberlite IRC83H)* 171
Figure 6. 2 Sodium (Na^+) loading on SAC resin (*Amberlite IRC120Na*) 171
Figure 6. 3 Removal of calcium and magnesium by WAC resin as a function of initial pH of the solution (Initial [Ca^{2+}] = 521 mg/L; initial [Mg^{2+}] = 111 mg/L; stirring speed = 150 rpm, contact time = 60 minutes; Temperature = 25°C) 172
Figure 6. 4 Removal of calcium and magnesium by SAC resin as a function of initial pH of the solution (Initial [Ca^{2+}] = 521 mg/L; initial [Mg^{2+}] = 111 mg/L; stirring speed = 150 rpm, contact time = 60 minutes; Temperature = 25°C) 173
Figure 6. 5 (a) Mg- H_2O and (b) Ca-H_2O Pourbaix diagram (temperature= 25°C; Concentration $1*10^{-3}$) 175
Figure 6. 6 Removal of calcium and magnesium by WAC resin as a function of resin mass. (Initial [Ca^{2+}] = 521 mg/L; initial [Mg^{2+}] = 111 mg/L; stirring speed = 150 rpm, contact time = 60 minutes; Temperature = 25°C; initial natural pH = 4.85). 177
Figure 6. 7 Removal of calcium and magnesium by SAC resin as a function of resin mass. (Initial [Ca^{2+}] = 521 mg/L; initial [Mg^{2+}] = 111 mg/L; stirring speed = 150 rpm, contact time = 60 minutes s; Temperature = 25°C; initial natural pH = 4.85). 177

Figure 6. 8 Removal of calcium and magnesium by WAC resin as a function of shaking speed. (Initial [Ca^{2+}] = 521 mg/L; initial [Mg^{2+}] = 111 mg/L; contact time = 24hrs; Temperature = 25°C; initial natural pH = 4.85). 179
Figure 6. 9 Removal of calcium and magnesium by SAC resin as a function of shaking speed. (Initial [Ca^{2+}] = 521 mg/L; initial [Mg^{2+}] = 111 mg/L; contact time = 24hrs; Temperature = 25°C; initial natural pH = 4.85). 180
Figure 6. 10 Removal of calcium and magnesium by WAC resin as a function of contact time. (Initial [Ca^{2+}] = 521 mg/L; initial [Mg^{2+}] = 111 mg/L; Contact time = 24hrs; Temperature = 25°C; Initial natural pH = 4.85). 182
Figure 6. 11 Removal of calcium and magnesium by SAC resin as a function of contact time. (Initial [Ca^{2+}] = 521 mg/L; initial [Mg^{2+}] = 111 mg/L; Contact time = 24hrs; Temperature = 25°C; Initial natural pH = 4.85). 182
Figure 6. 12 Removal of calcium and magnesium by WAC resin. (Contact time = 60 minutes; Temperature = 25°C; Shaking speed 150 rpm; Resin mass = 10 g; Solution pH 4 –10). 185
Figure 6. 13 Removal of calcium and magnesium by SAC resin. (Contact time = 60 minutes; Temperature = 25°C; Shaking speed 150 rpm; Resin mass = 10 g; Solution pH 4 –10). 186
Figure 6. 14 Final Ca concentration after dual softening of water samples with lime-soda ash and WAC resin..... 188
Figure 6. 15 Final Mg concentration after dual softening of water samples with lime-soda ash and WAC resin..... 188
Figure 6. 16 Final Ca concentration after dual softening of water samples with lime-soda ash and SAC resin 189
Figure 6. 17 Final Mg concentration after dual softening of water samples with lime-soda ash and SAC resin 189
Figure 7. 1 MWT effect on solution pH 196
Figure 7. 2 MWT effect on solution DO..... 196
Figure 7. 3 Effect of MTD on [Ca^{2+}] for all four water samples 197
Figure 7. 4 Effect of MTD on EC for all four water samples..... 198
Figure 7. 5 Relationship between TDS and EC for all water samples..... 199
Figure 7. 6 Effect of MTD on pH for all four water samples 200
Figure 7. 7 Effect of MTD on DO for all four water samples 200
Figure 7. 8 Effect of MTD on E_h for all four water samples 201
Figure 7. 9 Percent change of [Ca^{2+}], DO, E_h pH and EC without and with an MTD 203

Figure 7. 10 Relationship between number of magnets/ effective magnetic strength and [Ca^{2+}] 204
Figure 7. 11 Inverted vs non-inverted magnetic poles and the effect on [Ca^{2+}] of the scrubber bleed sample.....205
Figure 7. 12 Inverted vs non-inverted magnetic poles and the effect on [Ca^{2+}] of the process water sample 205
Figure 7. 13 Schematic representation of waveforms for inverted (left) and non-inverted (right) magnetic pole orientation for MTD (Redrawn from Gabrielli et al (2001)).....206
Figure 7. 14 Variation of [Ca^{2+}] against the number of magnets and orientation of magnetic poles for the scrubber bleed sample.....207
Figure 7. 15 Variation of [Ca^{2+}] against the number of magnets and orientation of magnetic poles for the process water sample 207
Figure 7. 16 Variation of the concentration of the ionic calcium against the length of the magnetic device obtained by varying the number of inverted or non-inverted pairs of permanent magnets (Gabrielli et al., 2001).....208
Figure 7. 17 Effect of flowrate on the MTD removal efficiency.....209
Figure 7. 18 Variation of [Ca^{2+}] against the pipe material of the MTD 210
Figure 7. 19 [Ca^{2+}] and E_h as a function of time.....211
Figure 7. 20 DO and pH as a function of time.....212
Figure 7. 21 EC as a function of time 212
Figure 7. 22 XRD analysis for crystals formed after 60 minutes exposure to MTD.....213
Figure 7. 23 XRD analysis for crystals formed after 3 hours exposure to MTD.....215
Figure 8. 1 Proposed flowsheet for the water softening process 221

Nomenclature

Abbreviation	Description
AAS	Atomic Absorption Spectroscopy
BOD	Biochemical Oxygen Demand
$CaCl_2$	Calcium Chloride
$CaCO_3$	Calcium Carbonate
CaO	Calcium Oxide
$CaSO_3$	Calcium Sulphite
$CaSO_4$	Calcium Sulphate
$CaSO_4 \cdot 2H_2O$	Calcium Sulphate Dihydrate (Gypsum)
$CaSO_4 \cdot 1/2H_2O$	Calcium Sulphate Hemihydrate (Plaster of Paris)
$CaSO_X$	Generic term for Calcium Sulphates/Sulphites
$Ca(OH)_2$	Calcium Hydroxide
CAPEX	Capital Expenditure
CO	Carbon Monoxide
DTO	Dust Thickener Overflow
EC	Electrical Conductivity
EPA	Environmental Protection Agency
ESP	Electrostatic Precipitator
FGD	Flue Gas Desulphurization
H	Hydrogen
H_2S	Hydrogen Sulphide
H_2SO_4	Sulphuric Acid
HCl	Hydrochloric Acid
HCO_3^-	Bicarbonate Ion
ICP-OES	Inductively Coupled Plasma Optical Emission Spectrometry
LSI	Langelier Saturation Index
MHD	Magnetohydrodynamic
ML	Megalitre
MTD	Magnetic treatment device
MWT	Magnetic water treatment
N	Nitrogen
Na	Sodium
Na_2CO_3	Sodium Carbonate
Na_2SO_3	Sodium Sulphite
Na_2SO_4	Sodium Sulphate
NaCl	Sodium Chloride
$NaHSO_3$	Sodium Bisulphite
NEMAQA	National Environmental Management: Air Quality Act
NH_3	Ammonia

$(NH_4)_2SO_3$	Ammonium Sulphite
$(NH_4)_2SO_4$	Ammonium Sulphate
NO_X	Nitrogen Oxides (generic term for NO and NO2)
OPEX	Operating Expenditure
PGM	Platinum Group Metals
PM	Particulate Matter
PSI	Puckorius Scaling Index
PW	Process Water
RSI	Ryznar Stability Index
S	Sulphur
SAC	Strong Acid Cation (resin)
SB	Scrubber Bleed
SEM	Scanning Electron Microscopy
SF	Scrubber Feed
SO_2	Sulphur Dioxide
TDS	Total Dissolved Solids
TSAP	Thematic Strategy on Air Pollution
VTS	Variable Throat Scrubber
WAC	Weak Acid Cation (resin)
XRD	X-ray Diffraction

Chapter 1 Introduction

1.1 Background

Sulphur dioxide (SO_2), a significant contributor to air pollution, primarily enters the atmosphere through the combustion of sulphur (S)-rich fuels and industrial processes. The majority of SO_2 emissions originate from sources such as power plants, base metal smelters, as well as residential and vehicular combustion of materials high in S content. SO_2 is corrosive and can cause eye and skin irritation even at low concentrations, posing a fatal risk when exposure exceeds 3497 ppm for more than 10 minutes (Cordoba, 2015; Poullikkas, 2015). Additionally, when released into the atmosphere, SO_2, along with nitrogen oxides (NOx), plays a major role in the formation of acid rain. When SO_2 reacts with moisture, oxygen, and sunlight, it produces varying concentrations of sulphuric acid (H_2SO_4), which contributes to the detrimental effects of acid rain on plant life, marine animals, and infrastructure (Cordoba, 2015; Poullikkas, 2015).

Worldwide, legislation is becoming increasingly stringent regarding air quality and the control of toxic emissions. For example, the Clean Air Act, enacted in 1970, has significantly reduced pollution levels in the United States as of 2020, according to the Environmental Protection Agency (EPA) (United States Environmental Protection Agency, 2021) (Rogers, 1990). Similarly, the European Union established Ambient Air Quality and Clean Air standards in 2008 under the Thematic Strategy on Air Pollution (TSAP), with specific goals of reducing the health impacts and environmental damage caused by air pollution (Kuklinska et al., 2015). In South Africa, the National Environmental Management Air Quality Act (NEMAQA) (No. 39 of 2004) was enacted in 2010, aiming to establish air quality standards and focus on reducing emissions (Gubb, 2009; Mohlala, 2020; Rycroft, 2014). The Ambient Air Quality Act in South Africa sets maximum SO_2 concentration limits and the frequency of allowable exceedances for SO_2 emitters (Gubb, 2009; Mohlala, 2020; Tshehla and Wright, 2019). The ambient concentrations of SO_2 may not exceed:

1. a ten-minute peak of 0.191 ppm 25 °C
2. an instant peak of 500 g/m^3 at 25 °C
3. a 24-hour average of 0.048 ppm
4. an annual average of 0.019 ppm

Significant sources of SO_2 emissions include utility companies that generate power by burning fossil fuels, petroleum refineries, as well as pyrometallurgical processes in PGM and base metal

smelters (Cordoba, 2015; Gololo, 2017; Gubb, 2009; Mohlala, 2020; Poullikkas, 2015; Tshehla and Wright, 2019). To minimize SO_2 emissions, various methods can be employed, including removing S from fuel prior to combustion, capturing SO_2 during combustion, or treating exhaust gases to remove SO_2 after combustion (Wirsching et al., 1994). The selection of low-S fuels (typically containing less than 0.5 % S) is a common approach before combustion, albeit at a substantial capital and operational cost (Saikia et al., 2015). However, due to the high costs associated with pre-combustion S removal, the use of "low-rank" coal, which is high in S, nitrogen(N), and other trace metals, has become more prevalent (Gani et al., 2021). It becomes essential to reduce SO_2 emissions from the combustion of high-S content fuels to meet appropriate emission standards (Poullikkas, 2015).

Flue gas desulphurization techniques serve as controls for reducing sulphur dioxide (SO_2) emissions after combustion, and various processes have been developed for this purpose. These processes are largely grouped into regenerable and non-regenerable categories and are further divided into wet, semi-dry, and dry processes, as discussed in detail in Section 2.2 (Jahnig and Shaw, 1981; Pike, 1984; Poullikkas, 2015). Removing SO_2 during combustion involves in-furnace injection of sorbents that react with the SO_2. These sorbents are typically Ca compounds such as lime and limestone, which can remove 30—60 % of SO_2 emissions (Poullikkas, 2015; World bank, 1999). Methods like the oxidation or reduction of SO_2 to produce sulphuric acid (H_2SO_4) or S, absorption by various types of solids and liquids followed by absorbent regeneration, and washing with sodium (Na)-active species, lime, and limestone slurry are examples of these methods (Jahnig and Shaw, 1981; Pike, 1984; Slack et al., 1972). While water alone is only partially effective as an SO_2 absorption medium (achieving 20 % removal efficiencies), solutions with suitable chemical absorbers demonstrate higher SO_2 removal efficiencies ranging from 50—99.8 % (Chin et al., 2002; Li et al., 2020; Poullikkas, 2015).

The use of hydrogen (H_2) and renewable energy sources have been suggested as more sustainable fuel technologies, however, this transformation from “dirty energy” to cleaner and alternative energy is expected to be concluded only after 2030—2040 (Fokaides et al., 2014; Ehteshami and Chan, 2014; Poullikkas, 2015). Therefore, while these proposed sustainable technologies are being integrated across all major emitters of flue gas as alternatives of energy sources, it remains necessary to improve the efficiency and to reduce the associated costs and issues of existing emission control technologies, such as FGD processes.

The metallurgical and mining processes in South Africa, particularly the pyro-metallurgical process of PGM and base metal smelting, are high emitters of SO_2. This is mainly because the

smelter feed (concentrate) has high sulphide minerals (> 6 wt.%). The smelters and furnaces generate hydrogen sulphide (H_2S) in addition to SO_2 as well as significant amounts of fugitive emissions (Bezuidenhout et al., 2012; Eksteen et al., 2011; Gololo, 2017; Jones, 2005).

Sibanye-Stillwater (formerly known as Lonmin) stands as one of four primary producers of platinum in South Africa alongside Anglo American Platinum Corporation Ltd (Amplats), Impala Platinum and Northam Platinum. Sibanye-Stillwater is also one of the three largest producers of platinum in the world thus establishing South Africa as the world's largest producer of PGMs. Each company has its own approach to smelting as this is mostly governed by the type(s) of ore they process. Amplats mines the Platreef ore while the other three companies mine both the Merensky and UG2 ores (Jones, 2005).

Sibanye-Stillwater processes a blend of Merensky and UG2 ore that is concentrated through the flotation process and smelted to form a distinct matte and slag. During smelting, an off-gas is formed in the furnace with varying SO_2 concentrations that could be as low as 0.5 % and as high as 6 % depending on furnace and converter operations (Bezuidenhout et al., 2012; Eksteen et al., 2011; Jones, 2005). At its highest concentration, the SO_2 in the off-gas was too high to be handled by pure lime-based scrubbing, while at its lowest, the SO_2 concentration in the off-gas did not make the construction and operation of an acid plant economically viable. This meant that Sibanye-Stillwater was faced with the challenge of finding an FGD system that could handle or treat a wide range of SO_2 concentration in the off-gas. At the time, prior to an SO_2 abatement installation in 2002, pure lime/ limestone-based scrubbing were the popular choice in FGD systems for the absorption of SO_2 from flue gas but the high SO_2 concentrations could not be handled using these systems.

The dual-alkali scrubber was the technology of choice for Sibanye-Stillwater in 2002. It was seemingly able to handle both the high SO_2 concentrations of converter off-gas and the swings in SO_2 concentration. With minor variation, the dual-alkali process is much like the lime/ limestone scrubbing process in that $Ca(OH)_2$/ $CaCO_3$ is consumed, and a calcium sulphite/sulphate ($CaSO_3$/$CaSO_4$) wet solid waste product is produced. In the case of the dual-alkali process, a Na-Ca alkali is used for the absorption of SO_2 and production of $CaSO_3$/$CaSO_4$, hence the name "dual-alkali" (Nissen et al., 1976).

The dual-alkali plant was installed at Sibanye-Stillwater due to the technology's ability to overcome $Ca(OH)_2$/ $CaCO_3$ scrubbing issues such as scaling and low reactivity. At the time, dual-alkali scrubbing was considered the only technology to achieve good scrubbing efficiencies and had the ability to handle SO_2 concentrations ranging from 3—9 % (Bezuidenhout et al., 2012).

The dual-alkali plant forms part of the off-gas cleaning circuit at the Sibanye-Stillwater smelter with an electrostatic precipitator (ESP) and a variable throat scrubber (VTS). Figures 1.1 and 1.2 show a block flow diagram of the off-gas handling equipment and a simplified flow diagram of the dual-alkali system installed at Sibanye-Stillwater, respectively.

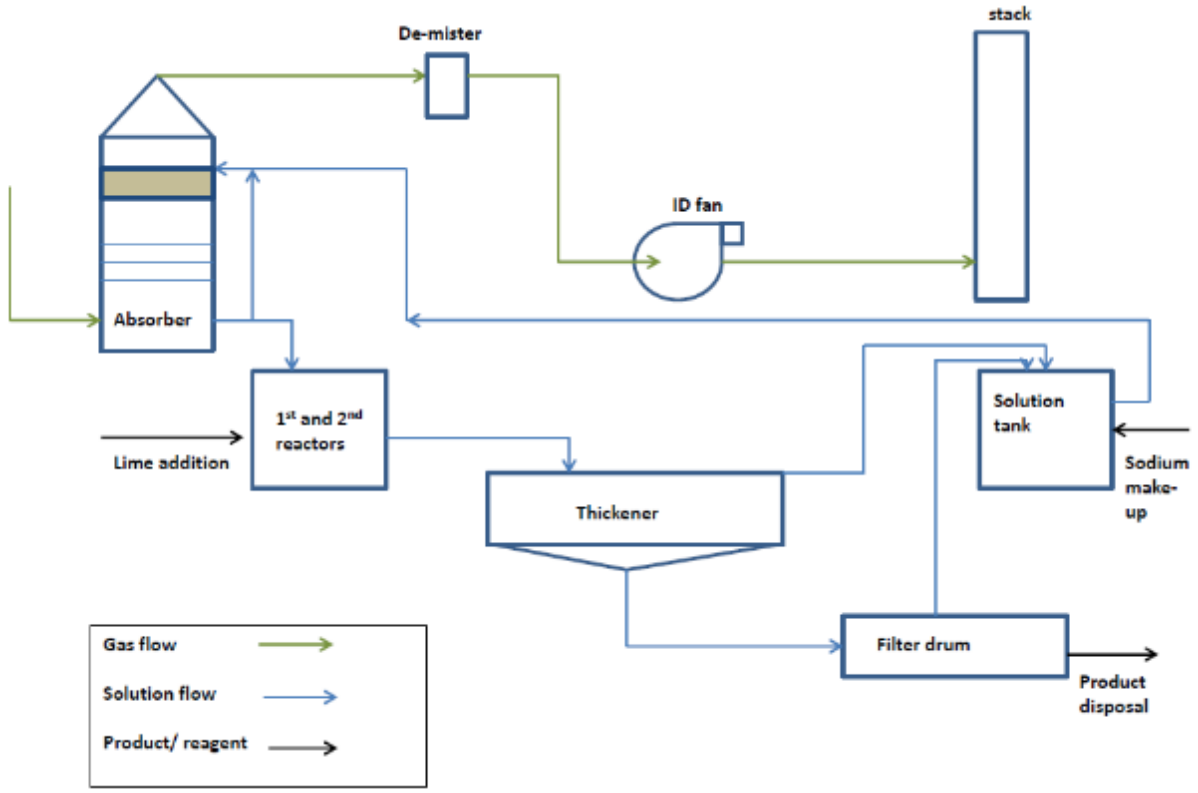


Figure 1. 1 Block flow diagram of the off-gas handling equipment. Figure adapted from Bezuidenhout et al. (2012, pg. 2)

The off-gases from the smelters and converters typically contain various elements, including SO_2. They also contain particulate matter (PM), which includes fine particles of metal oxides and other compounds. Carbon monoxide (CO) is present from incomplete combustion, and nitrogen oxides (NOx) are formed during high-temperature processing. Additionally, volatile metals, including small amounts of PGMs and chromium (Cr), are present (Aylmore et al., 2001; Habashi, 2005; Schlesinger, 2011; Xstrata Technology, 2009).While most PGMs are recovered in the smelting process, small amounts can be carried over in the off-gas as fine particulate matter, leading to minor losses of valuable metals and contributing to scale formation if these particles deposit within the gas treatment systems. Additionally, Cr, often present in the ore and smelting materials, can volatilize at high temperatures and then condense as chromium oxide (Cr_2O_3) in cooler parts of the system, resulting in hard, refractory scale build-up. Additionally, the off-gas includes hydrogen chloride (HCl) and fluorides (HF) from

chlorinated and fluorinated compounds in the feed materials (Aylmore et al., 2001; Habashi, 2005; Schlesinger, 2011; Xstrata Technology, 2009). The SO_2 rich off-gases from the furnace and the converter are combined and sent to the scrubber where the SO_2 is absorbed into solution using sodium sulphite (Na_2SO_3). Lime is then added to precipitate out a product referred to as $CaSO_X$, which is made up of an 80/20 ratio of $CaSO_3/CaSO_4$ (Bezuidenhout et al., 2012; Eksteen et al., 2011; Nissen et al., 1976).

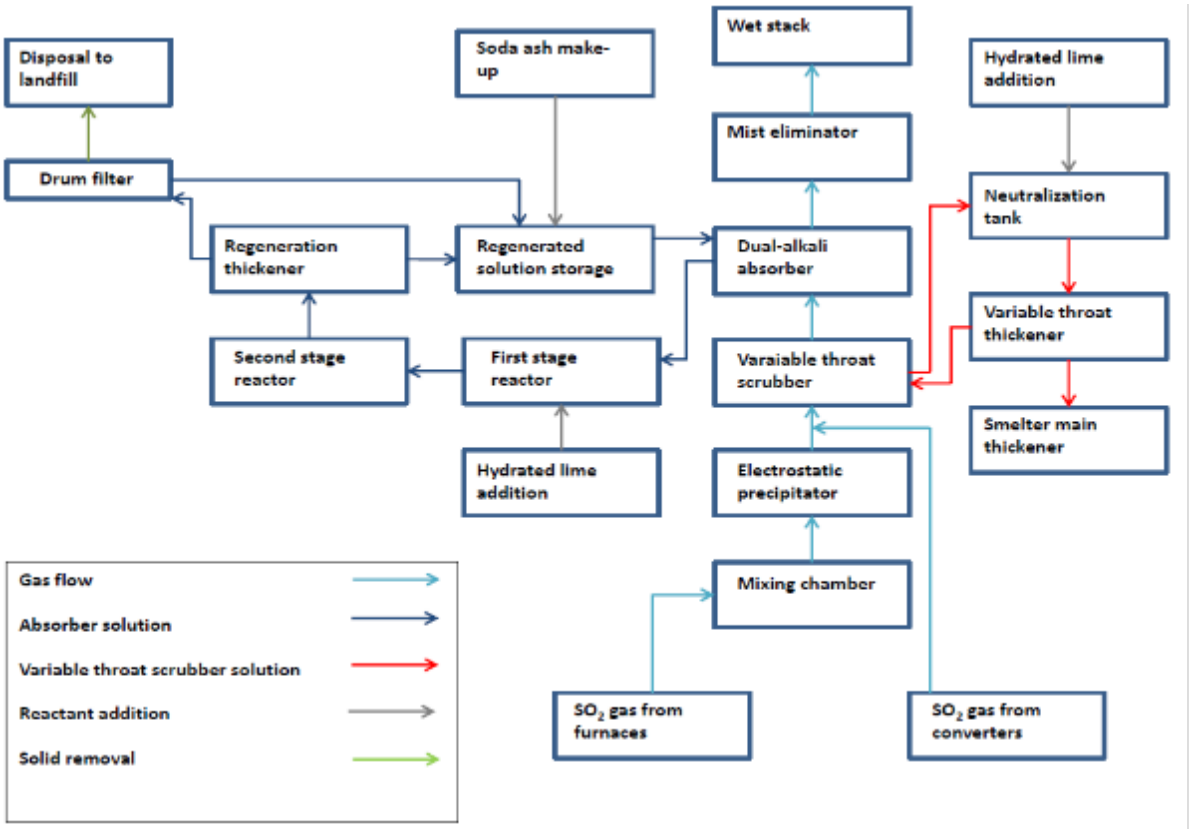


Figure 1. 2 Simplified flow diagram of the dual-alkali system. Figure adapted from Bezuidenhout et al. (2012, pg. 2)

1.2 Problem identification

Although the initial tests of the dual-alkali technology indicated little to no scaling (Newman et al., 1975), Sibanye-Stillwater has, for the past few years, been dealing with the build-up of scale in the pipes joining the scrubber to the thickener. Scaling in the scrubber can result from two sources: through the water make-up and the chemical additions made in the scrubbing process. The elements present in the off-gasses can also significantly influence scale formation within the smelting and off-gas treatment systems. Sulphur dioxide (SO_2) combines with moisture to form sulphuric acid, leading to sulphate scales. Particulate matter (PM) deposits on

cooler surfaces, causing metal oxide scale buildup. Volatile metals, like chromium, form oxides that contribute to hard, refractory scales. Carbon monoxide (CO) and nitrogen oxides (NOx) react with other elements to form complex compounds that precipitate as scale. Additionally, hydrogen chloride (HCl) and fluorides (HF), being corrosive, lead to the formation of difficult-to-remove chloride and fluoride scales (Aylmore et al., 2001; Habashi, 2005; Schlesinger, 2011; Xstrata Technology, 2009). In $Ca(OH)_2$/ $CaCO_3$ scrubbing, scaling has most commonly resulted from the precipitation of $CaSO_3$/ $CaSO_4$ / $CaCO_3$ from supersaturated water sources, and, in some cases, unstable calcium sulphate hemihydrate ($CaSO_4.1/2H_2O$) may also form (Rosenberg and Grota, 1979; WL Badger and Associates, 1959). High concentrations of specifically Ca (along with Mg) in water render the water "hard" – indicating a high mineral content. As this water continues to re-circulate the scrubber, scale deposits form over time. The formation of these Ca compounds in such systems also creates a problem of scaling or deposition in the scrubber and its connected pipes. This scale interferes with the operation and efficiency of the SO_2 removal system as a result of blockages, leading to the plant's shutdown almost four times a year to remove the scaling (Rosenberg and Grota, 1979; Wen et al., 1975). Anti-scaling additives and chemical methods like sodium carbonate (Na_2CO_3) and dilute acids have been proposed for $Ca(OH)_2$/ $CaCO_3$ scrubbing in the past, with some demonstrating effective control of sulphate (SO_4^{2-}) scaling by up to 75 % (WL Badger and Associates, 1959; Chan and Leung, 1979). Currently, Sibanye-Stillwater relies solely on high-pressure cleaning to remove scale build-up in the scrubber. While this approach is effective, it is not a sustainable long-term solution for the plant.

This study proposes the use of ion exchange and chemical precipitation techniques for treating water from four distinct sources within the scrubber circuit, specifically identified as Scrubber bleed, Scrubber feed, Dust-thickener overflow, and Process water. These water sources, being the primary contributors to scale formation, are treated using ion exchange resins known for their effectiveness in handling high levels of "hard water" ion concentrations (Amber series, 2022). This proposed treatment is evaluated both exclusively and in combination with chemical precipitation as a pre-treatment for extremely "hard water", allowing for the determination of an optimal treatment approach. As an alternative to the current practice of using pressurized water for scale removal, this study propose a relatively debated and emerging physical water treatment technique - magnetic water treatment (MWT). The efficacy of this technique has a history of controversy regarding in countering hard water scaling (Baker and Judd, 1996; Busch et al., 1997; Fathi et al., 2006; Lipus and Dobersek, 2007; Parsons et al., 1997). Nonetheless,

this study aims to understand its treatment mechanism(s) and assess its effectiveness, if any. The objective is to propose an alternative approach to chemical-based hard water treatment.

1.3 Research aims and objectives

The main objective of this study was to explore and develop effective methods for the removal and mitigation of scale formation in the $Ca(OH)_2$/ $CaCO_3$ scrubber circuit, with the ultimate goal of minimizing or completely avoiding shutdowns to the smelter. To achieve this aim, the following objectives were pursued:

1 Investigation of the physical and chemical characteristics of the scale that forms in the scrubber circuit.
2 Analysis of the factors and mechanisms involved in scaling formation in the scrubber thickener lines, including an examination of water composition and chemical additions to identify the source of scale.
3 Explore and propose appropriate treatment methods for the removal and prevention of scale formation. This involves considering well-established techniques such as ion exchange and chemical precipitation, as well as the application of an emerging water treatment technique known as MWT.

1.4 Research questions

The study aims to address the following research questions, which are crucial for achieving the objectives and overall purpose of the research:

1. What is the chemical and physical composition of the scale build-up? Which minerals or compounds constitute the majority of the scale deposit?
2. Where within the scrubbing process does the scale formation occur? What specific reactions take place during the formation of scale?
3. What is the chemical composition of the scale source, including water, chemical additives, and elements present?
4. How effective are the proposed chemical treatment methods in removing ions responsible for hard water? Can the desired soft water conditions of 0—60 mg/L as $CaCO_3$ or practical limits of 0—180 mg/L be achieved, thus preventing significant scale formation?

5. To what extent can the proposed alternative physical method, MWT, prevent scale formation? What mechanisms contribute to its efficiency?

1.5 Research hypothesis

The development and application of a physical and/or chemical treatment process(es) can aid in the prevention of scale formation in wet $Ca(OH)_2$/ $CaCO_3$ scrubber systems. This would thus ensure that production shutdowns are reduced if not avoided.

1.6 Research methodology

The main approach employed in this study was a quantitative scientific investigation aimed at generating systematically manipulated data that could be statistically analysed. The research methodology implemented in this investigation encompassed various tasks, including a comprehensive literature review, detailed description of materials and methods, conducting laboratory test work, analysing the collected data, performing a techno-economic evaluation, drawing conclusions based on the obtained results, and providing recommendations for future research.

1.7 Thesis layout

This section provides a summary of the chapters and sections that are covered in this study. Each chapter ends with a summary on what has been covered and a lead into the subsequent chapters.

- **Chapter 1 Introduction:**

  This chapter provides the motivation for the research, the problem statement, and the overall objectives of the study.
- **Chapter 2 Literature review:**

  This chapter sets out to extensively review literature on the current research concepts as well as to conceptualize a framework in which this work lies.
- **Chapter 3 Materials and methods:**

  This chapter describes the materials and analytical methods and techniques used in the study.
- **Chapter 4—7 Results and discussion:**

These chapters describe the results observed as well as the discussion of the findings from the laboratory tests carried out. The test work carried out include:

1. Solid scale sample and liquid process sample characterization
2. Treatment of liquid process samples with lime and lime and soda ash
3. Treatment of liquid process samples with ion exchange
4. Investigating the efficiency of MWT

- **Chapter 8 Techno-economic evaluation:**

  This chapter summarises the potential installation of a full-scale lime-soda ash treatment process followed by ion exchange with an alternative gypsum crystallization stream. The capital expenditure (CAPEX) and operating expenditure (OPEX) are presented for treatment of 10 megalitres (ML)/day of process water.

- **Chapter 9 Conclusions and recommendations for future work:**
  This chapter concludes the research undertaken with a summary of the findings and recommendations.

References to all articles used in the study are provided at the end of each chapter. An appendix section is also included at the end of the dissertation to provide relevant laboratory test results and other supporting data.

1.8 References

Amber series (2022). Home. Available at: https://wwww.dupont.com/brands/amber-series.html/(accessed: January 19, 2022).

Aylmore, M. G., & Muir, D. M. (2001). Thiosulfate Leaching of Gold—A Review. *Minerals Engineering*, 14(2), pp.135-174.

Baker, J.S. and Judd, S.J., 1996. Magnetic amelioration of scale formation. Water research, 30(2), pp.247-260.

Bezuidenhout, G.A., Davis, J., Van Beek, B. and Eksteen, J.J., 2012. Operation of a concentrated mode dual-alkali scrubber plant at the Lonmin smelter. Journal of the Southern African Institute of Mining and Metallurgy, 112(7), pp.657-665.

Busch, K.W., Busch, M.A., Darling, R.E., Maggard, S. and Kubala, S.W., 1997. Design of a test loop for the evaluation of magnetic water treatment devices. Process safety and environmental protection, 75(2), pp.105-114.

Cappelle, M.A. and Davis, T.A., 2016. Ion Exchange Membranes for Water Softening and High-Recovery Desalination. Emerging Membrane Technology for Sustainable Water Treatment; Elsevier: Amsterdam, The Netherlands, pp.163-179.

Chan, Y.K. and Leung, K.K., 1979. Chemical removal of calcium sulphate scale-plant experience of Lok on Pai desalter. Desalination, 30(1), pp.359-371.

Chin, M., Ginoux, P., Kinne, S., Torres, O., Holben, B.N., Duncan, B.N., Martin, R.V., Logan, J.A., Higurashi, A. and Nakajima, T., 2002. Tropospheric aerosol optical thickness from the GOCART model and comparisons with satellite and Sun photometer measurements. Journal of the atmospheric sciences, 59(3), pp.461-483.

Coey, J.M.D. and Cass, S., 2000. Magnetic water treatment. Journal of Magnetism and Magnetic materials, 209(1-3), pp.71-74.

Cordoba, P., 2015. Status of Flue Gas Desulphurisation (FGD) systems from coal-fired power plants: Overview of the physic-chemical control processes of wet limestone FGDs. Fuel, 144, pp.274-286.

Cordoba, P. and Staicu, L.C., 2018. Flue gas desulphurization effluents: An unexploited selenium resource. Fuel, 223, pp.268-276.

Dey, D.; Herzog, A.; Srinivasan, V., 2007. Chemical Precipitation: Water Softening; Michigan State University: East Lancing, MI.

Ehteshami, S.M.M. and Chan, S.H., 2014. The role of hydrogen and fuel cells to store renewable energy in the future energy network–potentials and challenges. Energy Policy, 73, pp.103-109.

Eksteen, J.J., Van Beek, B. and Bezuidenhout, G.A., 2011. Cracking a hard nut: an overview of Lonmin's operations directed at smelting of UG2-rich concentrate blends. Journal of the Southern African Institute of Mining and Metallurgy, 111(10), pp.681-690.

Fathi, A., Mohamed, T., Claude, G., Maurin, G. and Mohamed, B.A., 2006. Effect of a magnetic water treatment on homogeneous and heterogeneous precipitation of calcium carbonate. Water research, 40(10), pp.1941-1950.

Fokaides, P.A., Kylili, A., Pyrgou, A. and Koroneos, C.J., 2014. Integration potentials of insular energy systems to smart energy regions. Energy Technology & Policy, 1(1), pp.70-83.

Gani, A., 2021. Fossil fuel energy and environmental performance in an extended STIRPAT model. Journal of Cleaner Production, 297, p.126526.

Gololo, K. V., 2017. Industrial Emissions Management: The Good, the Bad and the Ugly; Department of Environmental Affairs; Pretoria, October2-3. [PowerPoint presentation].

Gubb, A., 2009. National Environmental Management Air Quality Act (39 of 2004). Wildlife and Environmental Society of South Africa. Retrieved from http://www. enviropaedia. com/topic/default. php.

Habashi, F. (2005). *Handbook of Extractive Metallurgy*. Wiley-VCH.

Invent a better now. 2022. Dupont. Available at: https://www.dupont.com/

Jahnig, C.E. and Shaw, H., 1981. A Comparative Assessment of Flue Gas Treatment Processes Part I—Status and Design Basis. Journal of the Air Pollution Control Association, 31(4), pp.421-428.

Jones, R.T., 2005. An overview of Southern African PGM smelting. Nickel and Cobalt, pp.147-178.

Kuklinska, K., Wolska, L. and Namiesnik, J., 2015. Air quality policy in the US and the EU–a review. Atmospheric Pollution Research, 6(1), pp.129-137.

Li, B., Wu, H., Liu, X., Zhu, T., Liu, F. and Zhao, X., 2020. Simultaneous removal of SO_2 and NO using a novel method with red mud as absorbent combined with O3 oxidation. Journal of hazardous materials, 392, p.122270.

Lipus, L.C. and Dobersek, D.J.C.E.S., 2007. Influence of magnetic field on the aragonite precipitation. Chemical Engineering Science, 62(7), pp.2089-2095.

Mohlala, K., 2020. A critical evaluation of local government air quality management: the Gauteng experience (Doctoral dissertation, North-West University (South Africa)).

Newman, L., Forrest, J. and Manowitz, B., 1975. The application of an isotopic ratio technique to a study of the atmospheric oxidation of sulphur dioxide in the plume from an oil-fired power plant. Atmospheric Environment (1967), 9(11), pp.959-968.

Nissen, W.I., Elkins, D.A. and McKinney, W.A., 1976. Citrate Process For Flue Gas Desulphurization A Status Report. In Proceedings: Symposium on Flue Gas Desulphurization, New Orleans, March 1976 (Vol. 2, p. 843). US Environmental Protection Agency, Office of Research and Development.

Parsons, S.A., Judd, S.J., Stephenson, T., Udol, S. and Wang, B.L., 1997. Magnetically augmented water treatment. Process safety and environmental protection, 75(2), pp.98-104.

Pike, D.E., Airpol Inc, 1984. Double alkali process for removal of sulphur dioxide from gas streams. U.S. Patent 4,452,766.

Poullikkas, A., 2015. Review of Design, Operating, and financial considerations in flue gas desulphurization systems. Energy Technology & Policy, 2(1), pp.92-103.

Rogers, P.G., 1990. The clean air act of 1970. EPA J., 16, p.21.

Rosenberg, H.S. and Grotta, H.M., 1979. Scale suppression in lime and limestone scrubbers (No. US 4177245).

Rycroft, M., 2014. Air quality regulations− playing the numbers game with power stations. Energize, 1, pp.25-29.

Saikia, J., Saikia, P., Boruah, R. and Saikia, B.K., 2015. Ambient air quality and emission characteristics in and around a non-recovery type coke oven using high sulphur coal. Science of the Total Environment, 530, pp.304-313.

Schlesinger, M. E., King, M. J., Sole, K. C., & Davenport, W. G. (2011). *Extractive Metallurgy of Copper*. Elsevier.

Slack, A.V., Falkenberry, H.L. and Harrington, R.E., 1972. Sulphur oxide removal from waste gases: Lime-Limestone scrubbing technology. Journal of the Air Pollution Control Association, 22(3), pp.159-166.

Tshehla, C. and Wright, C.Y., 2019. 15 years after the National Environmental Management Air Quality Act: Is legislation failing to reduce air pollution in South Africa?. South African Journal of Science, 115(9-10), pp.1-4.

United States Environmental Protection Agency, 2021. Progress Cleaning the Air and Improving People's Health. https://www.epa.gov/clean-air-act-overview/progress-cleaning-air-and-improving-peoples-health

United States Geological Survey. Imagens Landsat. 2020, 5.

Wen, C.Y., Wjm Jr, R.D., Nelsen Jr, J.B., Werkowitz, D.S., Ketteringham, J.M., Davidsson, L.M. and Wiig, K.M., 1975. Scale Control in Limestone Wet Scrubbing Systems. US EPA, EPA-650/2-75-031.

World Bank, 1999. Pollution prevention and abatement handbook, 1998: Toward cleaner production. The World Bank

Wirsching, F., Hüller, R. and Olejnik, R., 1994. FGD Gypsum Definitions and Legislation in the European Communities, in the OECD and in Germany. In Studies in Environmental Science (Vol. 60, pp. 205-216). Elsevier.

WL Badger and Associates, 1959. Critical review of literature on formation and prevention of scale.

Xstrata Technology. (2009). The ISASMELT™ Furnace: Collaborative Technology Development. *Journal of The South African Institute of Mining and Metallurgy*, 109(10), 567-572.

Chapter 2 Literature review

2.1 Introduction

Numerous mitigation techniques have been incorporated to capture or remove SO_2 with flue gas desulphurization FGD being the most common method. Over the past 80 years, SO_2 emissions have raised concerns, leading to the development and refinement of desulphurization processes. Flue gas desulphurization can be accomplished using wet or dry methods. The most prevalent FGD technique involves wet desulphurization employing $Ca(OH)_2$/ $CaCO_3$ and accounts for around 85 % of all desulphurization processes (Hanif et al., 2020; Nissen et al., 1976; Pan et al., 2012). While this process does not recover the SO_2 in a useful form, it is relatively simple and less costly and can be applied to other processing plants that emit SO_2 such as refineries and smelters. In a $Ca(OH)_2$/ $CaCO_3$ process, the absorption of SO_2 and the production of waste occur (to some extent) simultaneously in a single reaction system. This, at times, may results in poor SO_2 absorption efficiencies and poor dissolution of $Ca(OH)_2$/ $CaCO_3$, the latter leading to scaling and plugging (Nissen et al., 1976; Pan et al., 2012) of the system's connected pipes. The formation of scale is most commonly preceded by supersaturated, hard water- particularly characterized by high concentrations of calcium (Ca) as a result of the $Ca(OH)_2$/ $CaCO_3$ addition. The presence of scale or deposit formation in an FGD system interferes with the efficient removal of SO_2 leading to production halts in order to remove the scale from the affected areas. To mitigate these issues, it is important to understand the origin of scale formation and what steps can be taken to pre-empt their formation.

This chapter provides a general overview and review of the FGD systems that are used to control SO_2 emissions and the common issue of hard water scaling or deposit formation that occurs in $Ca(OH)_2$/ $CaCO_3$ FGD scrubbing, in particular. More importantly, this chapter reviews current and potential methods that are and have been employed in the successful removal or prevention of scaling and deposition, by focusing on the treatment of hard water, which is a precursor in the formation of scale.

2.2 Flue gas desulphurisation systems

Flue gas desulphurization systems were initially introduced in coal-fired power plants in the United States and Japan during the early 1970s, and they later became prevalent in Europe during the 1980s (Córdoba, 2015). These systems, often referred to as wet scrubbers because of their primary function of removing SO_2 emissions, are widely acknowledged in the literature due to their efficient removal of SO_2 (up to 99 %) and cost-effectiveness (Bezuidenhout et al., 2012; Córdoba, 2015; Poullikkas, 2015). In the FGD process, flue gas is mixed with an absorbent medium within an absorber/scrubber vessel, resulting in a high solid slurry. Flue gas desulphurization technologies are classified as either regenerable or non-regenerable processes, depending on whether the S compounds produced are separated from the absorbent as a by-product or disposed of along with the absorbent as waste (Córdoba and Staicu, 2018; Dzhonova-Atanasova et al., 2011). Other authors have categorized FGD systems as wet scrubbers, spray dry scrubbers, sorbent injection, and regenerable processes. Each of these basic categories can be further subdivided based on the specific chemical processes and flow conditions involved, as illustrated in Figure 2.1 (Córdoba, 2015; Lisnic and Jinga, 2018; Nygaard et al., 2004; Soud, 2000; Srivastava and Controlling, 2000).

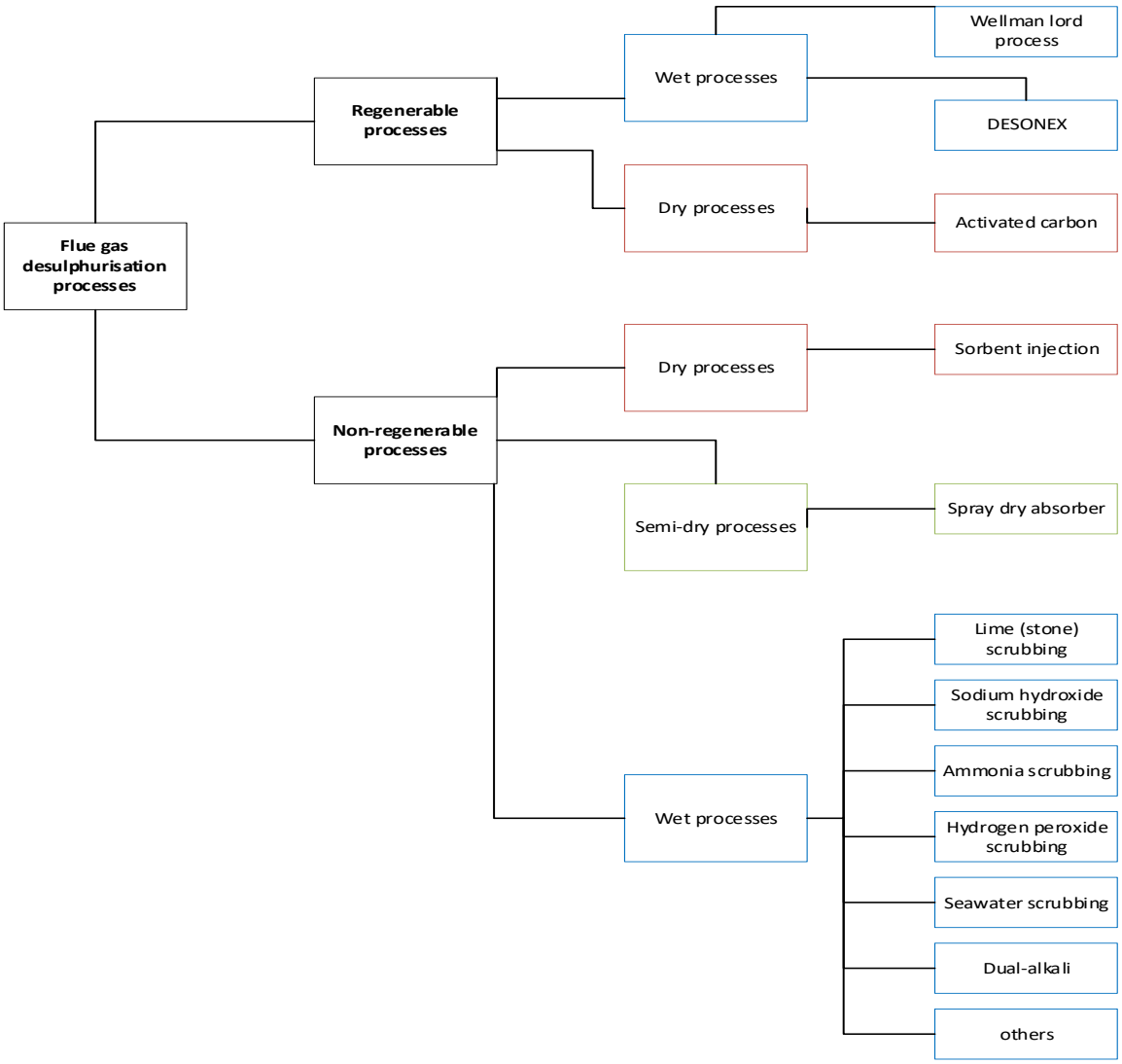


Figure 2. 1 FGD process classification (adapted from Lisnic and Jinga, 2018)

Scrubber systems are typically designed either for the removal of entrained particulate matter, such as dust, or for the removal of gases. In order to comply with air emission standards, most plants emitting flue gases have turned to scrubbing as a solution for reducing SO_2 emissions (Bezuidenhout et al., 2012; Córdoba, 2015; Eksteen et al., 2011). Table 2.1 provides a comparison of the various FGD technologies presently available. The table outlines the primary raw materials used in each technology, their by-products, S content, and the effectiveness of SO_2 removal.

Table 2. 1 FGD available technologies (Poullikkas, 2015)

Technology	Raw materials	By-products	Max fuel S content	Max SO_2 removal efficiency
Wet scrubbers				
1. Limestone scrubbing	Limestone and water	Marketable gypsum, sludge, wastewater	3.5 %	95 –99 %
2. Lime scrubbing	Lime and water	Marketable gypsum, sludge, wastewater	3.5 %	95 – 99 %
3. Seawater scrubbing	Seawater and limestone or lime	Waste treated seawater	3.5 %	90 – 95 %
Spray dry scrubbers	Lime or calcium oxide and water	Mixture of calcium sulphate, sulphite and flying ash	3.5 %	90 – 95 %
Sorbent injection processes	Limestone or hydrated lime	Mixture of calcium sulphate, sulphite and flying ash	N/A	50 %
Dry scrubbers	Limestone or lime or dolomite	Mixture of calcium sulphate, sulphite and flying ash	1 %	50 %
Regenerable processes	Sodium sulphite or ammonia	S or SO_2 or H_2SO_4 or ammonium sulphate	3.5 %	90 – 99 %

Table 2.2 illustrates the worldwide distribution of operational FGD facilities in 2015. The most prevalent and widely adopted wet scrubbing methods involve the use of lime or limestone, which generates valuable gypsum as a by-product. Additionally, significant processes include sorbent injection systems, spray-dry scrubbers, regenerable processes, and seawater scrubbing. As indicated in Table 2.2, wet systems remain predominant due to their superior efficiency compared to dry methods.

Table 2. 2 Current and future distribution of FGD plants on coal-fired generating units (modified from Poullikkas, 2015)

Technology	Current Distribution (%)	Future Distribution (%)
Limestone or lime wet scrubbing	45.4	68.5
Sea water scrubbing	36.3	20.9
Spray dry scrubbing	10.3	4.3
Regenerable processes	4.6	5
Sorbent injection	3.5	1.3

Along with other wet scrubbing processes such as seawater scrubbing, wet scrubbers will make up for nearly 90 % of new FGD plants. With the advent use of cleaner fuels slow approaching

(2040—2050), the increasing demands of electricity and dependence on the use of fossil fuels requires current wet FGD systems to be very efficient in SO_2 reductions (Lisnic and Jinga, 2018). Therefore, the global market for FGD systems will continue to see growth in the coming years. This growth will depend on the legal constraints of SO_2 emissions (Gubb, 2009; Mohlala, 2020; Rycroft, 2014) and the useful (or not) waste generation as recovery and re-use becomes more important in the ongoing conversation of a “circular economy”.

The following sections briefly review the FGD technologies under non-regenerable and regenerable processes. Flue gas desulphurization technologies are divided into these two categories based on the life cycle of the sorbent used to absorb SO_2 from the flue gas. The technologies’ process descriptions, technical characteristics, capital and operating costs as well as some of their key advantages and disadvantages are summarised.

2.2.1 Non-Regenerable Processes

Non-regenerable processes involve the use of a sorbent to absorb SO_2, and in these processes, the sorbent cannot be reused. Consequently, these processes result in the creation of a product that is either discarded as waste or sold as a by-product, often referred to as "throw-away" or "once-through" processes. The most prominent example of such processes is the lime/limestone method, which generates a sludge containing $CaSO_3$/ $CaSO_4$ (Aly et al., 1999; Hanif et al., 2020).

2.2.1.1 Lime/ limestone scrubbers

Wet scrubbers, the most widely used type of FGD system, employ a liquid to capture, dissolve, or chemically react with pollutants in a gas stream. Several branded designs of commercial wet scrubbing systems are accessible, $Ca(OH)_2$/ $CaCO_3$ being the preferred sorbents for this method (Córdoba, 2015; Koech et al., 2021). Lime/limestone wet scrubbers, especially those that yield marketable gypsum as a by-product, are the most commonly employed ones. This helps address the stricter regulations regarding by-product disposal. Wet scrubbing using $Ca(OH)_2$/ $CaCO_3$ currently dominates the FGD market, particularly in applications such as smelters that release substantial quantities of SO_2 (Bezuidenhout et al., 2012; Córdoba, 2015; Eksteen et al., 2011; Poullikkas, 2015; Slack et al., 1972). In the South African context, platinum group metals (PGM) and base metal smelters generate notably high levels of SO_2 emissions due to the high sulphide mineral content (typically 3—6 wt. % S) found in smelter feedstock (Gololo, 2017;

Jones, 2005). According to the 12th Air Quality Governance Lekgotla held in Pretoria in 2017 (Gololo, 2017), South Africa's metallurgical and mineral processing sectors host a significant number of operational facilities, with 173 in metallurgy and 137 in mineral processing. Together, these sectors are responsible for approximately 55 % of the nation's particulate matter emissions, primarily stemming from cement kilns, metallurgical smelters, and the brick manufacturing industry (Gololo, 2017). The metallurgical and mineral processing industries also contribute 18 % of the total SO_2 emissions, with the main sources being base metals and PGM smelters. According to the 2020 air quality criteria, the adoption of FGD technology is expected to reduce SO_2 emissions from base metal smelters and PGM operations by around 70 % and 80 %, respectively (Gololo, 2017). This substantial reduction in emissions can be attributed to historical advancements in cleaning techniques. The lime/ limestone wet cleaning technique, for instance, was patented by Eschellman in 1909, marking the beginning of its first commercial application in London. Subsequently, the initial unit operation was established at the Battersea Power Station in 1931, where small quantities of chalk were introduced into the river water as a solvent. This method has served as the foundation for numerous modern and improved $Ca(OH)_2$/ $CaCO_3$ processes (Živković et al., 2014). The general flow diagram illustrated in Figure 2.2 closely resembles that of the wet $Ca(OH)_2$/ $CaCO_3$ process (Živković et al., 2014).

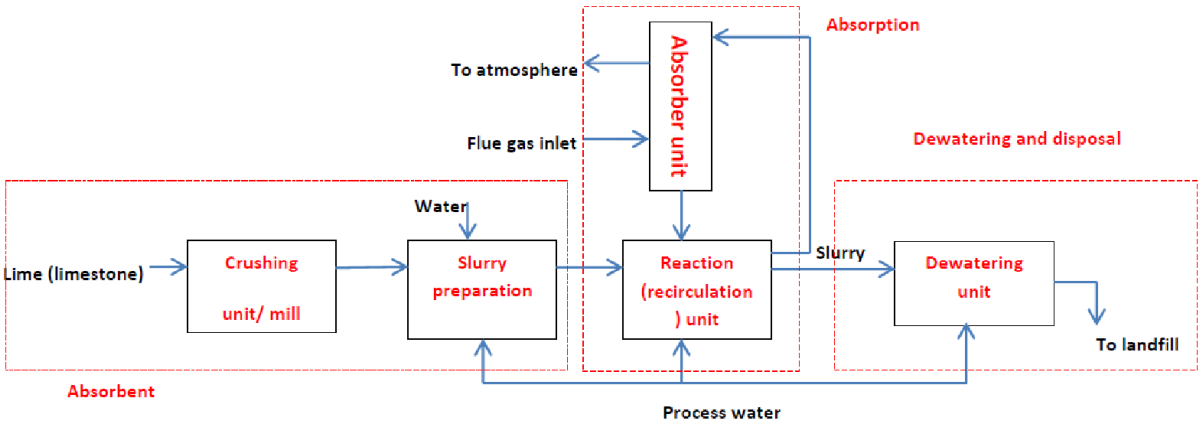


Figure 2. 2 General flow diagram for a wet FDG process (adapted from Živković et al., 2014)

In a standard lime/limestone process, the reagent components include water, along with either $Ca(OH)_2$ or $CaCO_3$. This alkaline mixture is subsequently injected into the absorber unit, where

it encounters exhaust gases containing SO_2. This exposure results in the formation of insoluble precipitates, $CaSO_4$ and $CaSO_3$, which are then separated from the liquid and ultimately disposed of in a landfill. The gas is further purified through a separator before being released into the atmosphere (Figure 2.3).

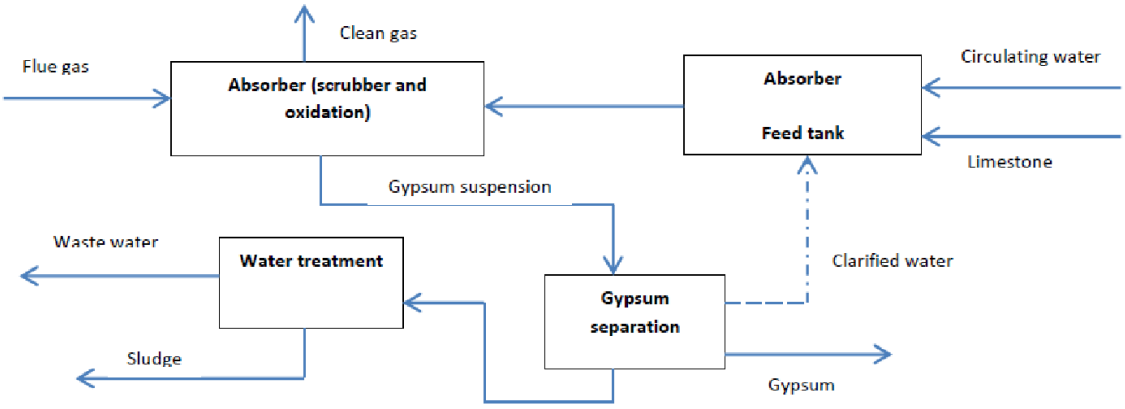


Figure 2. 3 Flow diagram of the limestone scrubbing method (adapted from Poullikkas, 2015)

The simplest setup for wet scrubbers involves conducting all chemical reactions within a single absorber, resulting in savings on both capital and energy expenses. This approach is space-efficient and allows for easy adjustments to existing plant layouts. Absorber linings made of rubber, stainless steel, or nickel alloy are commonly utilized to prevent corrosion and wear. Additionally, fiberglass scrubbers are employed because of their ability to effectively handle high humidity, elevated temperatures, and gas streams that could be flammable or explosive. The chemical reactions outlined in Equations 2.1 and 2.2, as well as the equipment design, remain consistent regardless of whether a lime or limestone water mixture is utilized.

$$Limestone: CaCO_3\,(s) + SO_2\,(g) + 2\,H_2O \rightarrow CaSO_3.\,2H_2O\,(s) + CO_2\,(g) \quad [2.1]$$

$$Lime: Ca(OH)_2\,(s) + SO_2\,(g) + H_2O \rightarrow CaSO_3.\,2H_2O\,(s) + H_2O\,(l) \quad [2.2]$$

The scrubber or a different reaction chamber is used for a forced oxidation stage (Equation 2.3) that yields marketable gypsum ($CaSO_4.2H_2O$) in the presence of air:

$$CaSO_3\ (s) + ½\ O_2\ (g) + 2\ H_2O\ (l) \rightarrow CaSO_4.\ 2H_2O\ (s) \quad [2.3]$$

The key differentiation among most wet scrubbers pertains to how they facilitate contact between the liquid and gas. Various methods are employed, such as introducing liquid into collection chambers, allowing liquid to flow over weirs into chambers, bubbling gas through liquid-filled trays or beds, and injecting liquid into rapidly moving gas streams. Additionally, wet scrubbers can be categorized based on their preference for particulate matter or gaseous pollutants. However, a significant drawback of wet scrubbers is the accumulation of solids, which presents ongoing maintenance challenges. This issue will be explored in greater detail in Section 2.3.

2.2.1.2 Seawater-based scrubbers

This process dates back to the 1970s when Berkeley demonstrate the feasibility of using seawater in desulphurisation (Bromley, 1972). In seawater-based FGD systems, the natural alkalinity of seawater with a pH range of ~ 7—8, which includes CO_3^{2-} and HCO_3^- ions, is utilized to neutralize SO_2, eliminating the need for chemicals. The dust is collected using an electrostatic precipitator (ESP). Afterward, the exhaust gases are passed through a heat exchanger to lower their temperature before being directed upward into a seawater scrubber against the flow of saltwater. This process results in the absorption and conversion of SO_2 from the flue gas into SO_4^{2-} ions. This technique relies on the following chemical reactions:

$$SO_2\ (g) \rightarrow SO_2\ (aq) \quad [2.4]$$

$$SO_2\ (aq) + 2\ HCO_3^-\ (aq) + ½\ O_2\ (aq) \rightarrow SO_4^{2-}\ (aq) + 2\ CO_2\ (aq) + H_2O\ (aq) \quad [2.5]$$

In this procedure, the SO_4^{2-} product entirely dissolves within the saltwater, eliminating the necessity for waste disposal. The resultant seawater, now possessing a pH of ~ 3, gets mixed with additional seawater to raise the pH and aerated to eliminate the CO_2 produced during acidification. Any existing SO_3^{2-} undergo conversion to SO_4^{2-} as the oxygen levels are increased (Behrends and Liebezeit, 2003; Cordoba, 2015; Poullikkas, 2015). Following aeration, the water is typically discharged into the ocean, as depicted in Figure 2.4.

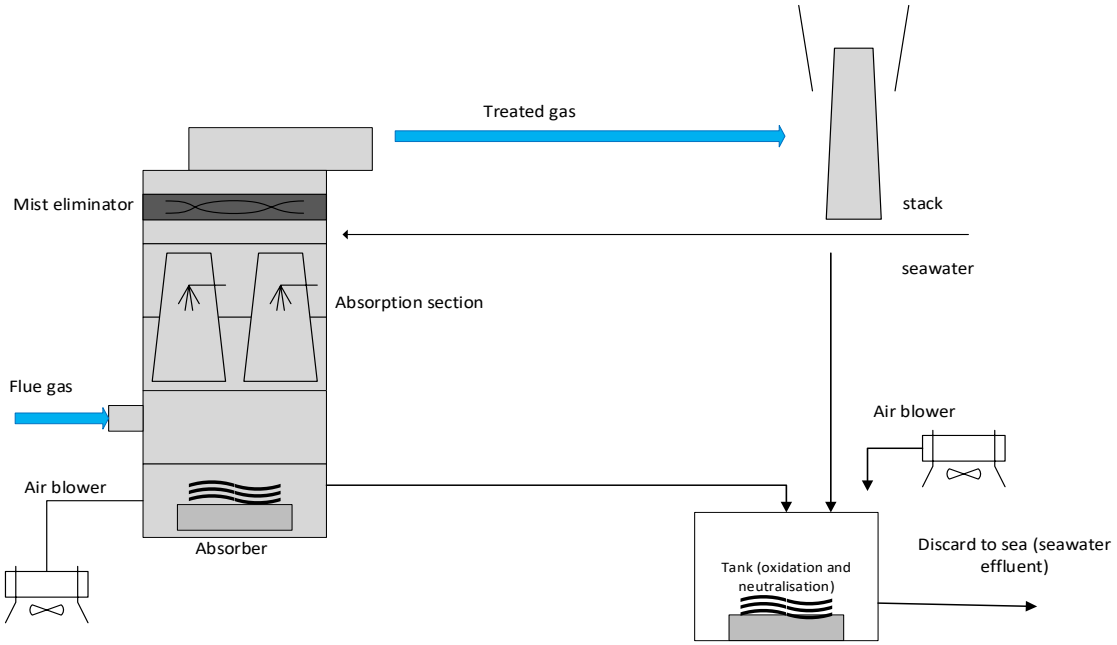


Figure 2. 4 Seawater FGD process (adapted from Lisnic and Jinga, 2018)

Seawater FGD systems have demonstrated an efficiency range of 85—98.5 % in removing SO_2 (Cordoba, 2015; Poullikkas, 2015). The use of seawater scrubbing can offer certain advantages, such as a simple design, minimal reliance on bulk chemicals, and generally low capital and operational costs (Cordoba, 2015; Poullikkas, 2015). However, it's important to note that the discharged water from such systems can have an impact on the local marine ecosystem due to its high biochemical oxygen demand (BOD). Biochemical oxygen demand refers to the amount of oxygen required by organisms to meet their oxygen needs (Behrends and Liebezeit, 2003; Cordoba, 2015; Poullikkas, 2015). Figure 2.5 illustrates the open-loop and closed-loop systems for two simplified FGD procedures. In the open-loop mode (Figure 2.5a), untreated saltwater is introduced into the scrubber system. The naturally occurring carbonate (CO_3^{2-}) and bicarbonate (HCO_3^-) ions present in saltwater effectively absorb and neutralize SO_2.

In the closed-loop mode (Figure 2.5b), the scrubber system operates with a continuous circulation of freshwater or seawater, without any emissions into the ocean. A water cleaning apparatus is necessary to treat the discharged water as per the requirements. Before re-entering the scrubber, the wash water undergoes cooling through a heat exchanger.

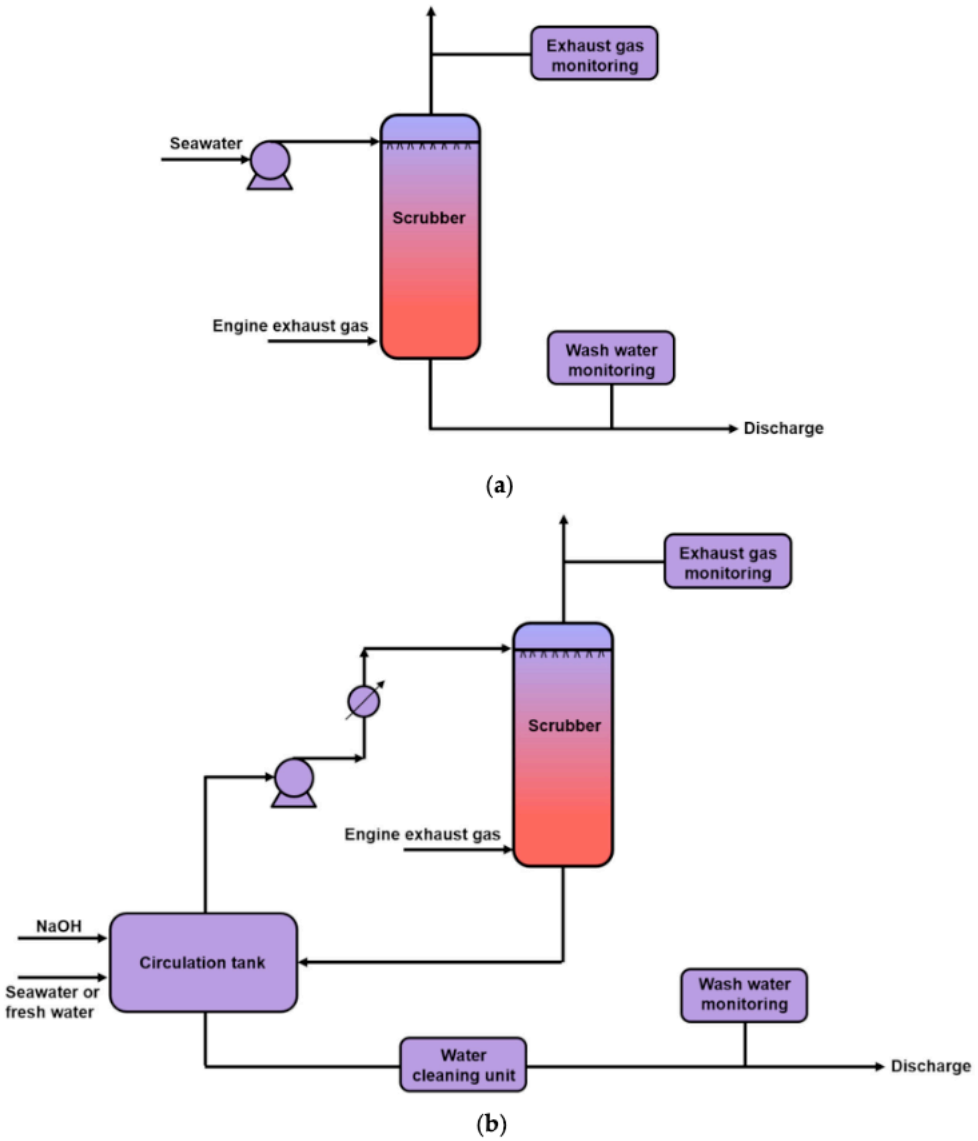


Figure 2. 5 Schematic diagram of the (a) open-loop FGD process, (b) closed-loop FGD process (Long et al., 2020).

2.2.1.3 Dry spray scrubbing

In dry spray scrubbing, salts are formed through the reaction of SO_2 with a lime suspension to eliminate it from flue gases. These dry FGD systems involve the reaction of SO_2 with a sorbent like CaO or $Ca(OH)_2$, which is mixed with additional water or slaked to create a lime slurry. This liquid absorbs and reacts with SO_2 in the flue gas. As documented by Cordoba (2015), Poullikkas (2015), Srivastava et al (2001), and Strömberg and Karlsson (1988), the resulting by-product consists of a dry mixture containing $CaSO_3.12H_2O$, $CaSO_4.2H_2O$, unreacted $Ca(OH)_2$, and fly ash. This mixture is carried along with the flue gas downstream of a particulate collection device, typically an ESP or fabric filter. To enhance calcium oxide (CaO)

consumption, the residue is recycled and blended with fresh CaO slurry. While this approach is more cost- and energy-efficient, saving between 30 % and 50 % compared to the wet limestone process (Cordoba, 2015; Poullikkas, 2015; Srivastava et al., 2001; Strömberg and Karlsson, 1988), operational costs increase with rising sorbent (lime) expenses (Fischer and Darling, 2015; Koech et al., 2021). Dry spray FGD systems can achieve SO_2 removal efficiencies ranging from 85 % to 95 % (Cordoba, 2015; Poullikkas, 2015). These scrubbers are also capable of handling high-volume flow rates, making them the second most popular FGD technology.

2.2.2 Regenerable Processes

The sorbent used for SO_2 adsorption in regenerable processes can be used again. These processes are appealing because the spent sorbent can be restored and re-used multiple times for absorbing and releasing SO_2 until its removal capacity decreases significantly (Hanif et al., 2020; Koralegedara et al., 2019). Regenerable processes often produce little waste water and do not need to dispose of waste. While incorporating a regeneration unit may increase the initial investment and operating expenses, this can be offset by the reduced waste and by-product formation. The adsorbed SO_2 undergoes thermal or chemical regeneration to recover SO_2 gas, sulphuric acid, or elemental sulphur (Cordoba, 2015; Hanif et al., 2020; Koralegedara et al., 2019; Poullikkas, 2015; Srivastava et al., 2001).

The systems presently employed are the Walther method and the Wellman-Lord process (Cordoba, 2015; Koralegedara et al., 2019; Poullikkas, 2015; Srivastava and Jozewicz, 2001). Despite the excellent efficiency of these technologies in removing SO_2 (> 95%), they come with significant initial costs and overall power consumption (Cordoba, 2015; Poullikkas, 2015). The capital cost is determined by the flue-gas flow rate, as well as the quality and composition of the fuel utilized. Operational expenses, on the other hand, are heavily influenced by factors such as the number of full-load working hours per year and the quality and composition of the fuel (Cordoba, 2015; Koralegedara et al., 2019; Poullikkas, 2015; Srivastava and Jozewicz, 2001).

(a) Wellman-Lord Process

The Wellman-Lord technique uses sodium sulphite (Na_2SO_3) solution as a sorbent to reduce SO_2 emissions (Cordoba, 2015; Koralegedara et al., 2019; Poullikkas, 2015; Srivastava and Jozewicz, 2001). Figure 2.6 depicts the Wellman-Lord process' main flow diagram.

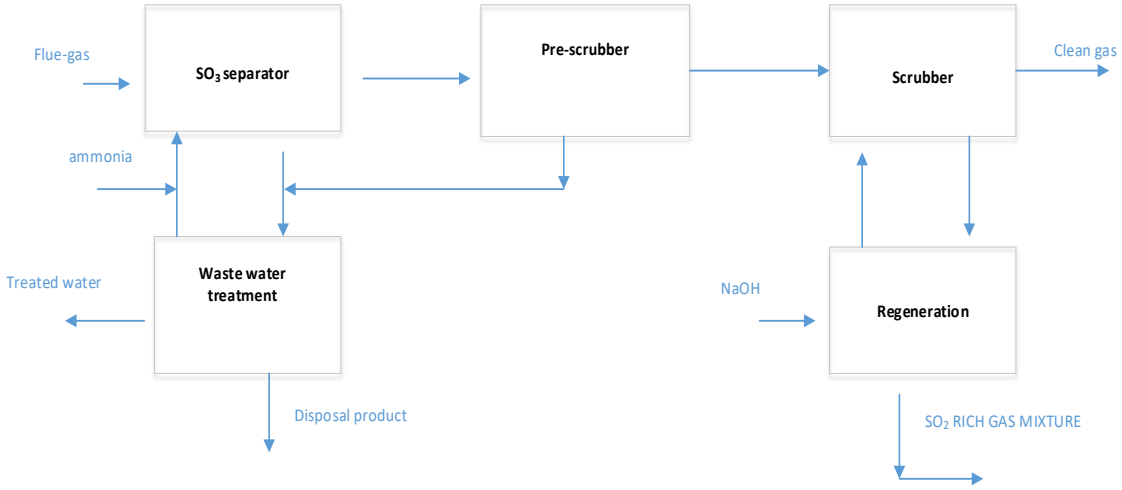


Figure 2. 6 Flow diagram of the Wellman-Lord process (adapted from Poullikkas, 2015)

The process can be divided into six primary steps: sulphite separation, pre-scrubbing of flue gas, absorption of SO_2, regeneration, processing of SO_2-rich gas, and waste management. Ammonia (NH_3) water is introduced into the flue gas stream (Cordoba, 2015; Koralegedara et al., 2019; Poullikkas, 2015; Srivastava and Jozewicz, 2001), resulting in the precipitation of ammonium sulphate ($(NH_4)_2SO_4$) along with the dust particles. The leftover mixture is then treated in a wastewater treatment unit. At the bottom of the scrubber, the pre-scrubber removes chlorides and fluorides (Cordoba, 2015; Koralegedara et al., 2019; Poullikkas, 2015; Srivastava and Jozewicz, 2001). To achieve maximum removal efficiency, hydrochloric acid is used to lower the pH of the liquid pre-scrubber sorbent to 2. The pre-scrubber also reduces the exhaust gas temperature, which is essential for the absorption process (Cordoba, 2015; Koralegedara et al., 2019; Poullikkas, 2015; Srivastava and Jozewicz, 2001).

A concentrated Na_2SO_3 sorbent is employed, circulating and absorbing SO_2, resulting in the formation of sodium bisulphite ($NaHSO_3$). Oxygen in the flue gases partially oxidizes Na_2SO_3, leading to sodium sulphate (Na_2SO_4) formation. The absorber operates using a counterflow mechanism and typically consists of three closely packed beds, each with a height of about 1.6

m (Koralegedara et al., 2019; Poullikkas, 2015). The average pressure drop in the scrubber is similar to that of other wet scrubber systems, ranging from 40 to 70 mbar. The sorbent is pumped at each stage to prolong its interaction with the flue gases. The excess solution from the lowest absorber stage is collected in the buffer tanks and subsequently directed to the reactor (Koralegedara et al., 2019; Poullikkas, 2015). To regenerate the scrubbing liquid, a regeneration unit is used to remove sulphur dioxide, producing SO_2-rich gas composed of 92 % vapor and 8 % SO_2 (Cordoba, 2015; Koralegedara et al., 2019; Poullikkas, 2015; Srivastava and Jozewicz, 2001). The vapor content in the SO_2-rich gas is subsequently reduced to 3 % to enable compression and processing into a final product (Cordoba, 2015; Koralegedara et al., 2019; Poullikkas, 2015; Srivastava and Jozewicz, 2001).In the described process, the two-stage catalytic reduction of SO_2 involves the use of natural gas as a reducing agent, typically in the presence of an aluminium and calcium oxide catalyst (Cordoba, 2015; Koralegedara et al., 2019; Poullikkas, 2015; Srivastava and Jozewicz, 2001):

First Stage:

Reaction with Methane (CH4): Sulphur dioxide reacts with methane in the presence of the catalyst to produce hydrogen sulphide (H_2S) and sulphur (S).

$$SO_2 + CH_4 \rightarrow H_2S + S \quad [2.6]$$

Second Stage:

Conversion of Remaining SO_2 and H_2S into Elemental Sulphur: The remaining sulphur dioxide and hydrogen sulphide are converted into elemental sulphur (S) and water (H_2O).

$$SO_2 + H_2S \rightarrow S + H_2O \quad [2.7]$$

In the described system, sulphur tanks maintain condensed sulphur gas in a liquid state at 150 °C, facilitating its storage and handling. Lime plays a crucial role in wastewater treatment by adjusting the pH of ammonia-containing wastewater to a level of 10, ensuring proper treatment and disposal. Recycling of recovered ammonia back into the sulphite separator is efficiently achieved through the use of a stripper, enhancing the overall sustainability of the process. When confronted with flue gases resulting from the combustion of fuels with high sulphur concentrations, reaching up to 3.5 %, this process demonstrates impressive efficiency, capable of achieving a 95 % removal of SO_2 at a maximum flow rate of 0.6 x 106 Nm^3/h. Additionally,

to handle substantial flue gas flow rates, multiple lines are used for flue FGD, ensuring effective mitigation of sulphur emissions (Cordoba, 2015; Koralegedara et al., 2019; Poullikkas, 2015; Srivastava and Jozewicz, 2001).

(b) Walther Process

The Walther process involves reacting SO_2 with ammonia water to produce ammonium sulphite $(NH_4)_2SO_3$, which is subsequently oxidized to produce ammonium sulphate $((NH_4)_2SO_4)$ that is subsequently used to desulphurize flue gases (Cordoba, 2015; Koralegedara et al., 2019; Poullikkas, 2015; Srivastava and Jozewicz, 2001). Figure 2.7 depicts the main flow diagram of the Walther process.

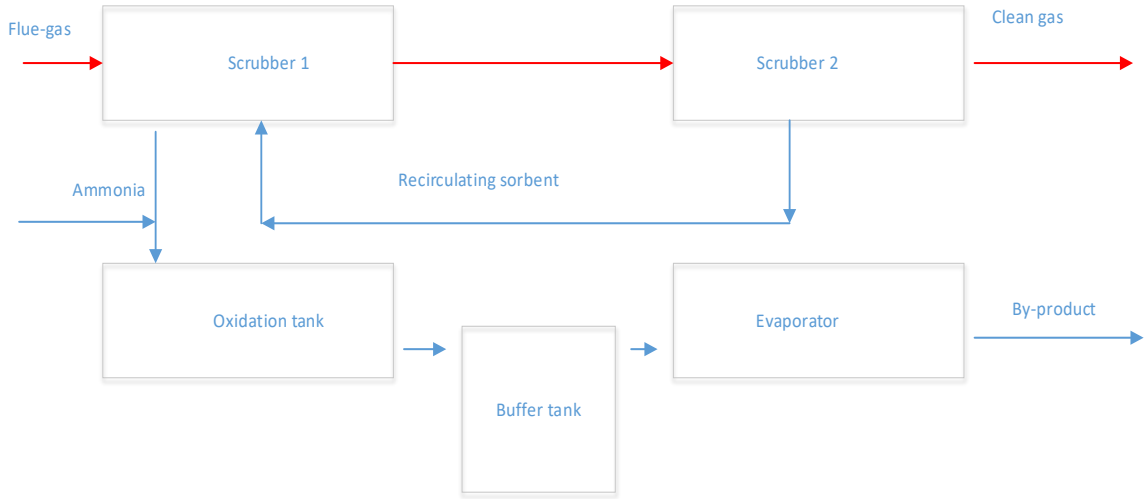


Figure 2. 7 Flow diagram of the Walther method (adapted from Poullikkas, 2015).

The process consists of two main components: the scrubbing system, which includes two interconnected scrubbers in a series, and the treatment of by-products. This treatment involves an oxidation unit, a buffer tank, and an evaporator. The recirculated sorbent solution from the scrubber comes into contact with flue gases that have been rid of dust particles. To achieve a sorbent solution with a 25 % NH_3 concentration, water and ammonia are mixed. It is important to maintain a lower limit of 200 mg/Nm^3 SO_2 concentration in clean gases, as lower SO_2 concentrations lead to significantly increased NH_3 emissions in clean gases. In the first scrubber, ammonium salts settle at the bottom (Cordoba, 2015; Koralegedara et al., 2019; Poullikkas, 2015; Srivastava and Jozewicz, 2001). The cleaned gases are then directed to the second scrubber, where they are heated to temperatures ranging from 50—90 °C before being released into the station's flue system. In the oxidation tank, the cleaning solution from the first scrubber is thoroughly mixed with air to facilitate the conversion of $(NH_4)_2SO_3$ to $(NH_4)_2SO_4$. When powdered $(NH_4)_2SO_4$ is granulated, it can be utilized as a commercial fertilizer with a nitrogen concentration of 20—25 %. The Walther process is effective in cleaning flue gases generated from the combustion of fuels with sulphur concentrations as high as 1.2 %. When dealing with a high flow rate of flue gases, FGD is performed using two or more lines (Cordoba, 2015; Koralegedara et al., 2019; Poullikkas, 2015; Srivastava and Jozewicz, 2001).

2.2.2.1 Dry Sorbent injection

In a dry sorbent injection (DSI) system, a commercially available sorbent like $CaCO_3$ or $Ca(OH)_2$ is commonly used (Figure 2.8). When the flue gas passes through the convective pass, the sorbent reacts with SO_2 and O_2, resulting in the formation of $CaSO_4$. This $CaSO_4$, along with any unused sorbent and fly ash, is collected in either a cloth filter or an ESP.

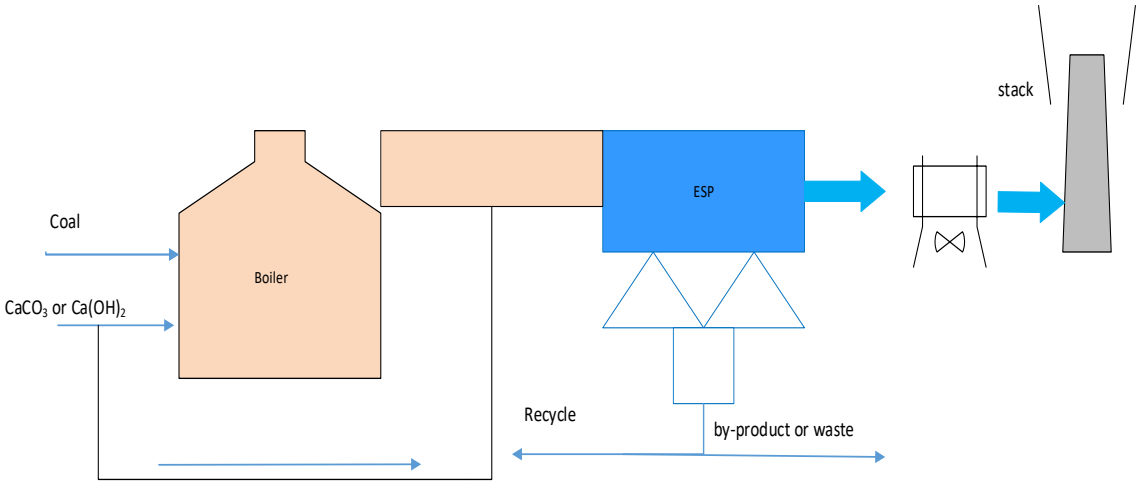


Figure 2. 8 Typical dry sorbent injection process (adapted from Lisnic and Jinga, 2018)

In the economizer sorbent injection process, hydrated lime is introduced into the flue gas stream when the temperature falls within the range of 300—650 °C in the economizer zone. At this lower temperature, $Ca(OH)_2$ does not fully dehydrate but directly reacts with SO_2. On the other hand, in the furnace sorbent injection method, the reaction temperature is much higher, approximately 1100 °C (Cordoba, 2015; Dal Pozzo et al., 2020; Helfritch et al., 1992; Hunt and Sewell, 2015; Poullikkas, 2015). In this method, the primary product is $CaSO_3$ instead of $CaSO_4$, and the reaction rates are similar to those at 1100 °C. The resulting by-products, along with the unused sorbent and fly ash, are captured in a cloth filter or ESP (Cordoba, 2015; Dal Pozzo et al., 2020; Helfritch, et al., 1992; Hunt and Sewell, 2015; Poullikkas, 2015). After the reaction between the ductwork and SO_2 in the flue gas, the resulting by-product is collected downstream in a filter. In the hybrid sorbent injection process, furnace and duct sorbent injection systems are often combined to enhance sorbent utilization and reduce SO_2 levels. Hybrid systems include additional post-furnace steps, such as humidification in a specially designed vessel and injection of supplementary sorbents, particularly sodium compounds, into the duct (Cordoba, 2015; Dal Pozzo et al., 2020; Helfritch et al., 1992; Hunt and Sewell, 2015; Poullikkas, 2015). Sorbent injection systems offer several advantages, such as compact equipment that requires less installation space and provides cost-effective capital and operational expenses. They are also easy to retrofit, simple to operate, and do not require slurry handling. However, their effectiveness in removing SO_2 is limited to approximately 50 % (Poullikkas, 2015).

A summary of wet FGD technologies and their processes has been provided in the earlier sections (Section 2.2.1). The predominant FGD method is wet $Ca(OH)_2$/ $CaCO_3$, which has gained widespread acceptance owing to its efficiency, solvent utilization, and positive environmental effects. Nevertheless, there are drawbacks to these methods. As mentioned previously, the issue of scale accumulation in and around their internal components is a concern that diminishes their efficiency.

2.3 Scale formation in lime based systems

Scale formation is the process of depositing inorganic salts with limited solubility from aqueous solutions, as highlighted by Baker and Judd (1996), Kelland (2011), and Silva et al (2015). This process is influenced by various factors such as temperature, pressure, pH, and the chemical composition of the water. The process typically begins with the supersaturation of

the solution, where the concentration of dissolved salts exceeds their solubility limit. As a result, the salts nucleate and form tiny crystals, which then grow and aggregate onto surfaces, eventually forming solid scale deposits. These scales can adhere to nearly any surface, and once they start forming, they tend to grow thicker unless managed (Baker and Judd, 1996;, Kelland, 2011; Silva et al., 2015). In water-related production scenarios, scale formation is a major challenge as it can obstruct pipelines, valves, and other critical equipment, leading to reduced efficiency and increased maintenance costs. This issue, alongside corrosion and gas hydrates, significantly impacts the operational reliability and economic performance of production systems. The control of scales can pose a significant operational expense in various industries. It can result in the formation of deposits on the surfaces of equipment like electric submersible pumps, sliding sleeves, and manifolds, leading to disruptions in operations. Mineral scales can accumulate at different points within the production conduit, narrowing the internal diameter and obstructing the flow. Furthermore, scale build-up can occur within production and processing facilities. Similar challenges are observed in processes such as seawater desalination and industrial wastewater treatment. The specific types of scales formed are influenced by the chemical composition of the water. For instance, in oilfield formation water, the concentrations of ions like Ca^{2+}, Ba^{2+}, Sr^{2+}, Fe^{2+}, HCO_3^-, and SO_4^{2-} are often higher than those in seawater.

Scale precipitation occurs when process conditions cause supersaturation with respect to one or more sparingly soluble salts. This challenge is encountered in both evaporation and membrane desalination processes. Without preventive measures, the concentration effect inherent in every desalination process triggers the precipitation of sparingly soluble salts, such as $CaCO_3$ and $CaSO_4$.

The formation of scale involves a complex interplay between crystallization and transport mechanisms. From a thermodynamic standpoint, crystallization or precipitation becomes possible when the activity of ions in the solution exceeds their saturation limit, resulting in supersaturation. Once supersaturation reaches a critical level, scale nucleation on particle surfaces initiates crystal growth, and the scarcity of nucleation sites slows down crystallization kinetics.

Dawson (1990) defined the 'supersaturation ratio' in Equation 2.8 to determine whether a water sample can scale:

$$S_r = ([Ca^{2+}]_a[CO_3^{2-}]_a) / ([Ca^{2+}]_{eqm}[CO_3^{2-}]_{eqm}) \quad [2.8]$$

Where 'a' refers to the actual concentrations and 'eqm' refers to the equilibrium concentrations. Scaling can happen if Sr > 1; if Sr 1, scaling cannot happen but dissolution can. If Sr = 1, the system is saturated and neither precipitation nor dissolution would occur, assuming no modifications are made to the system's physical characteristics. The equilibrium and free ion concentrations of Ca^{2+} and CO_3^{2-} play a crucial role in regulating scaling in water systems. (Dawson, 1990). When water contains dissolved Ca^{2+} and CO_3^{2-}, the system tends towards equilibrium, where these ions can combine to form $CaCO_3$, a common component of scale deposits. The concentration of these ions, as well as the pH of the water, determines the saturation level with respect to $CaCO_3$. Two pathways for scale formation have been documented: surface crystallization and bulk crystallization (Gilron and Hasson, 1987;Lee and Lee, 2000; Lee et al., 1999). The presence of scaling in pipe systems is the result of a combination of these two mechanisms and is influenced by the operational conditions within the pipes. Surface crystallization refers to the heterogeneous crystallization of scale deposits on the inner surface of pipes, which ultimately leads to pipe obstruction and reduced flow. In contrast, bulk crystallization occurs when crystal particles form within the bulk phase through homogeneous crystallization and may settle on pipe surfaces as sediment or particles, forming a layer that impedes fluid flow. Furthermore, when conditions become supersaturated with scale-forming substances, it results in scale growth and the aggregation of scale particles, as elaborated on in the following section.

2.3.1 Scale formation mechanism

The mechanism of scale formation may be summarized in the following steps (Al-Roomi and Hussain, 2016; Hasson and Semiat, 2006) as depicted in Figure 2.9.

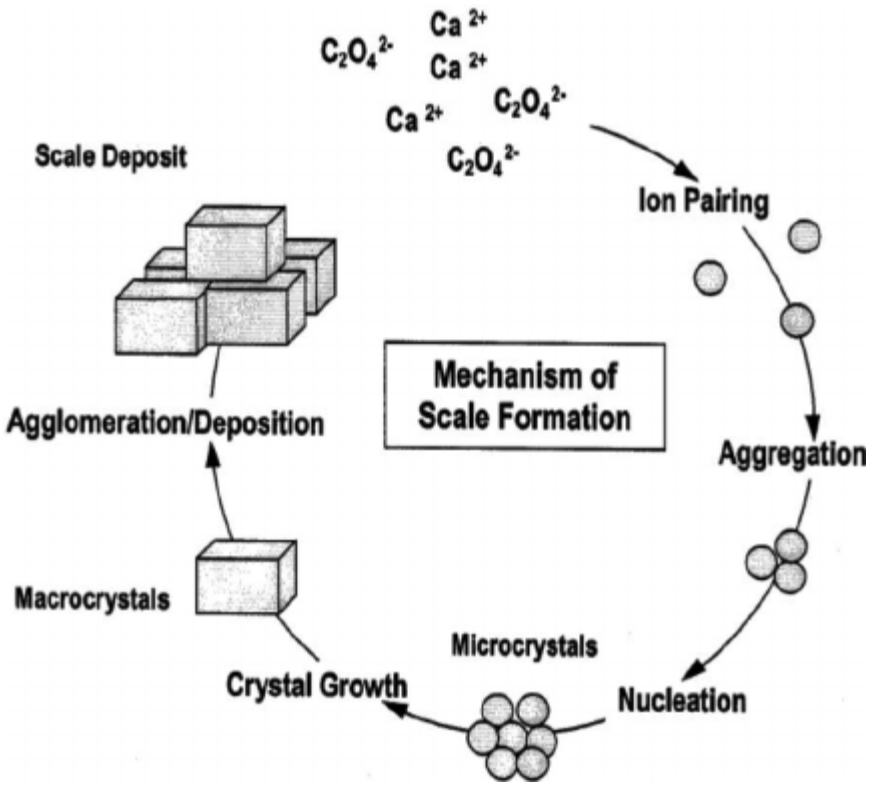


Figure 2. 9 Mechanism of scale formation (Safari et al., 2014)

2.3.1.1. Aggregation and Nucleation

The supersaturation level of deposit-forming species is the primary factor affecting the scaling intensity. Cationic and anionic species, such as Ca^{2+} and CO_3^{2-}/SO_4^{2-}, collide to create ion pairs in the solution after a supersaturation system is established. The next step for these pairings is to produce microaggregates, which are tiny crystals, embryos, micronuclei, or seed centres. Some of these microaggregates serve as crystallization nucleation sites, leading to the development of microcrystals. In practical systems, nucleation is predominantly heterogeneous rather than homogeneous. This means that the formation of nuclei, the initial clusters of atoms or molecules that serve as the building blocks for crystals, occurs predominantly on existing surfaces or interfaces within the system, rather than in the bulk solution (Al-Roomi and Hussain, 2016; Hasson and Semiat, 2006; Safari et al., 2014). Heterogeneous nucleation is favoured because the presence of a deposition surface provides a site for the assembly of

molecules or ions into stable nuclei. These surfaces often possess properties that promote nucleation, such as roughness, irregularities, or chemical functionalities that attract or bind certain ions or molecules, leading to the subsequent formation and growth of scale deposits on the surfaces (Al-Roomi and Hussain, 2016; Hasson and Semiat, 2006; Safari et al., 2014).

2.3.1.2. Crystal growth

In solution, microcrystals agglomerate and/or adsorb to surfaces, growing into larger microcrystals that finally fuse to produce adherent macro crystals.

2.3.1.3. Agglomeration

These macrocrystals continue to expand by adsorbing more scaling ions from the solution until they initiate the formation of the initial layer of a scale film on the surface. Once this initial scale layer is established, subsequent deposition becomes more facilitated. The growth of a crystal layer on a surface subjected to fluid flow involves a series of interconnected processes:

1. The diffusion of crystal-forming ions to the layer where crystallization occurs.
2. The incorporation of these ions into the growth sites of the crystal lattice.
3. Adhesion and removal processes.

Several operational factors can influence scale formation, including pH, temperature, operating pressure, penetration rate, flow velocity, and the presence of additional salts or metal ions (Antony et al., 2011).

2.3.2 Common scale deposits

For the purpose of this study, the focus on lime/ limestone FGD is emphasized. These FGDs commonly have issues with scale that is high in Ca- typically sulphates and carbonates. The two most common minerals, gypsum and calcite, are discussed.

2.3.2.1 Calcium sulphate dihydrate (gypsum)

Calcium sulphate minerals ($CaSO_4$) can precipitate in three crystallographic forms: gypsum or calcium sulphate dihydrate ($CaSO_4.2H_2O$), plaster of Paris or calcium sulphate hemihydrate ($CaSO_4.1/2H_2O$), and calcium sulphate anhydrite ($CaSO_4$) (Antony et al., 2011; Yehia et al., 2011). Among the non-alkaline scales, calcium sulphate dihydrate, or gypsum, is the most common. The formation of calcium sulphate scales presents significant challenges in various

applications, including desalination, geothermal energy production, and petroleum engineering (Aquilano et al., 2016). Gypsum is also an undesirable scaling agent in oil and gas production processes, water-cooling towers, and various metallurgical processes. Managing this type of scale can require costly remedial work (Kashchiev and Van Rosmalen et al., 2003; Van Rosmalen et al., 1981).

The formation of $CaSO_4$ scale might have a number of negative consequences. When these scales grow on surfaces engaged in heat transfer, they obstruct the flow of heat and can build within pipelines, orifices, and other passages, creating severe disturbances in the process flow. Furthermore, $CaSO_4$ scales, in conjunction with $CaCO_3$ scales, are the principal causes of fouling in reverse osmosis membranes. This fouling causes a constant drop in desalinated water output, diminishing overall efficiency and increasing operational and maintenance expenses (Prisciandaro et al., 2013).

2.3.2.2 Calcium carbonate

Calcium carbonate can crystallize in three distinct crystal forms: calcite, aragonite, and vaterite. Calcite is typically associated with hard scale, while aragonite and vaterite result in a softer scale that can be easily removed. Among carbonate scales, $CaCO_3$ scale is the most commonly encountered (Lakshmi et al., 2013). Calcite, being the most stable form of $CaCO_3$ scale under reservoir conditions, is more prevalent than aragonite and vaterite, which are other variations of calcium carbonate scale. The formation of $CaCO_3$ scale is influenced by the concentrations of Ca ions, ionic strength, pH, temperature, and HCO_3^- concentration in the water. It occurs due to the chemical equilibrium among these ions and CO_2. The presence of both Ca and HCO_3^- ions can lead to the development of $CaCO_3$ scale. The deposition of $CaCO_3$ scale increases with elevated temperatures, reduced pH levels, and increased pressure (Hamid et al., 2016; Ramstad et al., 2004).

2.3.2.2.1 Properties of Calcite and Aragonite

Aragonite and calcite, both members of the $CaCO_3$ family, are frequently found in scale formations, with calcite being the primary constituent. These two minerals, aragonite and calcite, are categorized as polymorphs, indicating they share the same chemical composition but possess distinct structures, symmetries, and crystal shapes (Nelson, 2014). Additionally, vaterite, another crystalline form, is also considered a polymorph of calcite and aragonite, collectively forming a trimorph system. Aragonite exhibits orthorhombic symmetry, calcite displays trigonal symmetry, and vaterite has hexagonal symmetry (Kelland, 2009; Szkatula et

al., 2002; Van Rosmalen et al., 1981). The structural disparities become evident when examining the arrangement of CO_3^{2-} within these minerals. Aragonite has a denser structure, characterized by triangular CO_3^{2-} groups where three oxygen atoms form the corners of a triangle, with the carbon atom at the centre. These CO_3^{2-} are oriented in two perpendicular planes. In contrast, calcite's CO_3^{2-} are situated within a single plane, all pointing in the same direction, resulting in its trigonal symmetry (Kelland, 2009; Szkatula et al., 2002; Van Rosmalen et al., 1981), as depicted in Figure 2.10.

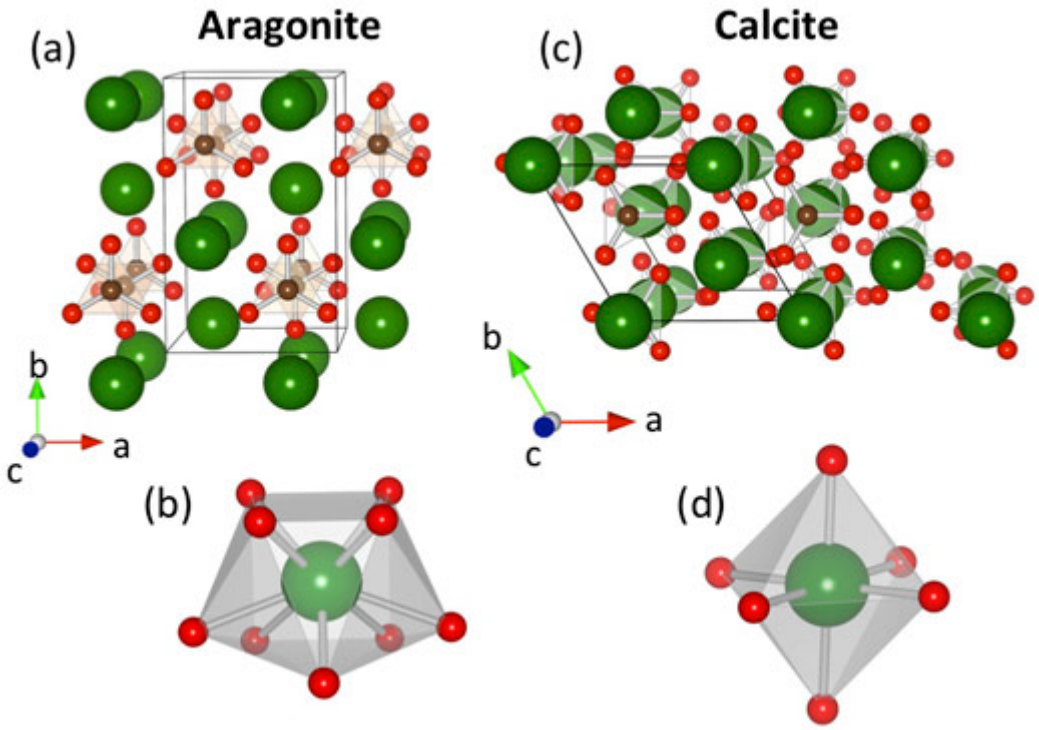


Figure 2. 10 Crystal structure of aragonite (a, b) and calcite (c, d) (Soldati et al., 2016).

Under normal pressures and temperatures, aragonite is typically unstable. However, it becomes stable when higher pressures are applied, without any corresponding increase in temperature. The formation of aragonite is favoured when specific conditions during crystallization prevent calcite from forming, as depicted in Figure 2.11. Factors such as the presence of magnesium and salt in the crystallizing fluid, its turbidity, and the duration of crystallization are some of the influencing factors. Importantly, it should be noted that aragonite is likely to transform into calcite after a certain period of time has passed (Van Rosmalen et al., 1981).

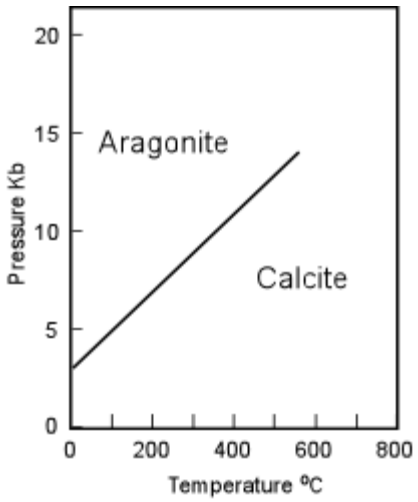


Figure 2. 11 Stability of aragonite and calcite with respect to pressure and temperature (Nelson, 2014).

The key physical difference between calcite and aragonite is that calcite is a hard crystal that adheres to surfaces and pipes, whereas aragonite does not. Due to its much softer nature and inability to attach to surfaces, aragonite cannot form solid limescale. According to Kelland (2009), Szkatula et al. (2002), and Van Rosmalen et al. (1981), aragonite will instead precipitate out of the solution and remain in suspension until it settles out. At room temperature, calcite is somewhat more soluble than aragonite, with a solubility of 0.0014 g/100g of water compared to 0.0012 g for aragonite.

2.3.2.2.2 X-ray diffraction (XRD) of aragonite and calcite

X-ray diffraction offers a straightforward way to differentiate between the two polymorphs forms of $CaCO_3$, aragonite and calcite. These minerals exhibit distinct peak patterns at different angles, making their identification relatively simple. Aragonite's most pronounced peak (111) occurs at a smaller angle (°2Θ), accompanied by several smaller peaks. On the other hand, calcite displays a strong peak (104) just to the right of aragonite's primary peak, along with fewer and smaller additional peaks (Railsback, 2006; Ryu et al., 2010).

While these distinct patterns are useful for identifying pure samples quickly, analysing mixtures becomes more intricate. Calcite's robust 104 peak often overshadows aragonite's 111 peak, even when aragonite makes up 75 % of the mixture. Conversely, the aragonite peak tends to blend into the background noise of a calcite XRD pattern if aragonite accounts for less than 25 % of the sample, as seen in Figure 2.12.

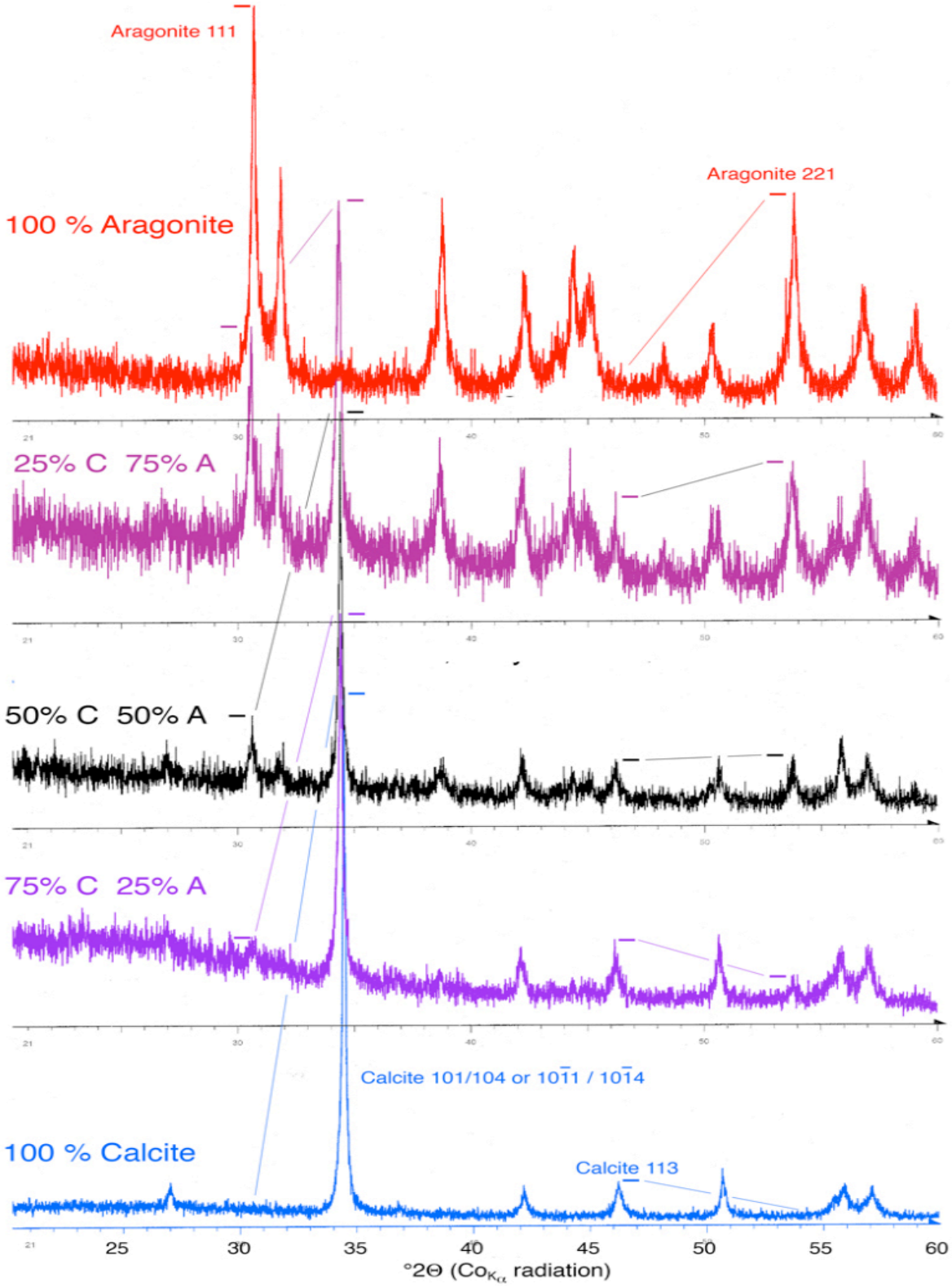


Figure 2. 12 X-ray diffraction (XRD) pattern for a mixture of aragonite and calcite, highlighting significant peaks for the purpose of identification (Railsback, 2006).

Consequently, comparing the most intense peaks can be complex and possibly misleading. A common approach to address this challenge involves using the aragonite 221 peak as an indicator of aragonite concentration. For example, Dickinson and McGrath (2001) utilized the ratio of integrated peak areas for calcite's 104 peak and aragonite's 221 peak to establish a quantitative relationship between aragonite and calcite ratios. This method yields accurate quantitative results, though with the caveat that a 50:50 mixture of the polymorphs results in a 104/221 intensity ratio significantly greater than 1, due to calcite's unusually strong 104 peak. Another option, providing a more intuitively understandable result, involves comparing calcite's 113 peak with aragonite's 221 peak. This method is particularly helpful for quick assessments. When using CoKα radiation, these peaks are around 46 and 54 °2Θ, symmetrically positioned near 50 °2Θ. For patterns generated with CuKα radiation, the peaks are around 40 and 46 °2Θ, slightly less symmetric around 43 °2Θ but still easily identifiable.

2.3.3 Scale formation in wet scrubbers

Depending on the gas stream's composition and the chemicals introduced into the water in the scrubber, the operational conditions inside the scrubber can lead to the creation of highly corrosive or scaling water. When $Ca(OH)_2$/ $CaCO_3$ is used for scrubbing, the addition of Ca compounds to the scrubber liquid can result in the formation of solid Ca salts in the form of a slurry. These $Ca(OH)_2$/ $CaCO_3$ slurries react with SO_2 to produce insoluble chemicals, which must be separated in a thickener. Although the primary goal of the $Ca(OH)_2$/ $CaCO_3$ wet scrubbing method is to convert SO_2 into solid $CaSO_3$ for removal from the gas phase, the occurrence of solid-phase precipitation cannot be overlooked. As SO_2 solidifies upon extraction from the flue gas, it requires careful handling and disposal outside the scrubber. In the absence of additional reactants, Ca^{2+} and SO_3^{2-} ions will precipitate as hemihydrate, as illustrated in Equations 2.1 and 2.2 (Bezuidenhout et al., 2012; Buecker, 2008; Kemmer, 1979; Poullikkas, 2015; Rosenberg et al., 1979; Wen et al., 1975). The presence of oxygen in the flue gas, as shown in Equation 2.3, significantly affects the chemistry, as aqueous SO_3^{2-} ions react with oxygen to produce SO_4^{2-} (Buecker, 2008; Poullikkas, 2015). The formation of supersaturated $CaSO_4$ in such systems poses a scaling or deposition challenge within the scrubber and the associated pipes, potentially disrupting the efficiency of the SO_2 removal systems (Buecker, 2008; Kemmer, 1979; Rosenberg et al., 1979; Wen et al., 1975).

Depending on the moisture content or dew point in the SO_2 gas stream, gas cooling can lead to either condensation or evaporation, potentially resulting in the concentration or dilution of

scrubber water (Bezuidenhout et al., 2012; Kemmer, 1979). When recycled water is utilized in wet scrubbing and the gas stream is above the dew point, issues related to scale formation, which arises from gases or particles removed from the gas stream, become more pronounced (Bezuidenhout et al., 2012; Kemmer, 1979). However, in certain systems where the gas contains significant amounts of water vapor, condensation and subsequent dilution of the recycled water may occur, reducing the likelihood of scaling and deposits (Bezuidenhout et al., 2012; Kemmer, 1979). Scale deposits resulting from the interaction of water with suspended particles are typically formed in systems operating at a pH level above 7 (Bezuidenhout et al., 2012; Kemmer, 1979). Due to the wide variability in process gases, water properties, and scrubber designs, it is challenging to make generalizations about the composition of these deposits. Nevertheless, the most commonly encountered deposits include metal sulphides, $CaCO_3$, $CaSO_4$, and $Ca(OH)_2$ (Bezuidenhout et al., 2012; Buecker, 2008; Kemmer and McCallion, 1979; Poullikkas, 2015; Rosenberg et al., 1979; Tseng and Rochelle, 1986; Wen et al., 1975). Table 2.3 provides an example of the typical composition of scaling samples from the VTS for the purposes of this study. Components such as inlet gas ports, induced draft fans, and stacks are just a few parts of the scrubber system that can become clogged with deposits. In this scenario, deposits can also form at the mist removal pumps, trays, liquid recycling lines, and supply lines for the clarifier (Bezuidenhout et al., 2012; Buecker, 2008; Poullikkas, 2015).

Table 2. 3 XRD quantitative analysis of scrubber samples from a typical plant dealing with scale build-up.

Sample	Actinolite $Ca_2Si_8O_{22}(OH)_2$ (wt. %)	Calcite $CaCO_3$ (wt. %)	Gypsum $CaSO_4$ (wt. %)	Quartz SiO_2 (wt. %)	Talc $Mg_3Si_4O_{10}(OH)_2$ (wt. %)	Dolomite $CaMg(CO_3)_2$ (wt .%)	Muscovite $KAl_2(F, OH)_2$ (wt. %)	Arnothite $CaAl_2Si_2O_8$ (wt. %)
1	1.99	4.02	83.68	4.04	5.24	-	1.03	-
2	1.55	4.95	73.25	1.32	9.87	7.03	2.03	-
3	2.03	7.69	85.87	0.64	1.89	-	-	1.88
4	-	-	98.72	1.28	-	-	-	-
5	-	8.77	85.41	2.13	2.24	-	-	1.46
6	1.82	3.2	80.38	9.4	4.7	-	0.5	12.77
7	2.66	4.68	64.38	2.79	10.74	1.98	-	-

Kemmer's research in 1979 highlighted the major components found in deposits removed from various types of scrubbers, revealing significant differences between industries. While deposit compositions may vary, Ca consistently appeared as the most abundant element. Due to the diverse nature of deposition issues, chemical treatments for managing scale and deposits must be customized for each specific scrubbing system. However, these treatments are generally effective in addressing most deposit-related problems. To combat scaling problems arising from $CaSO_4$ deposition in the absorber, mist eliminator, and piping, as well as to facilitate slurry dewatering, controlled oxidation is often implemented outside the absorber by introducing air into the absorbent slurry (Bogwardt, 1972; Mo et al., 2007; Živković et al., 2014). Controlled oxidation has been proposed as a solution in FGD technology, particularly as the demand for gypsum has decreased over time, and wastewater treatment has become essential (Bogwardt, 1972; Mo et al., 2007; Živković et al., 2014).

Managing the solid chemistry is a challenging but crucial aspect of scrubber operation. Choosing between a fully oxidized or non-oxidized state can reduce scaling in the scrubber, depending on the handling properties and commercial value of the solid. Producing gypsum, a marketable product, is a more practical option since $CaSO_3$/$CaSO_4$ hemihydrates typically retain water and have limited value as a chemical commodity (Bezuidenhout et al., 2012; Buecker, 2008; Poullikkas, 2015). Various techniques have been employed to prevent or reduce scaling in scrubbers, including the use of chemicals such as acids, ammonium carbonate ($(NH_4)_2CO_3$), and sodium hydroxide (NaOH). However, these methods often prove inefficient in terms of speed, comprehensiveness, and cost-effectiveness (Bogwardt, 1972; Mo et al., 2007; Smith et al., 1968).

In order to prevent the accumulation of scale and reduce the oxidation rate in the reaction tank to below 15%, one method involves introducing an emulsion of sulphur and sodium thiosulphate (Na_2S_2O). This specific approach to the process can utilize various reagents such as lime, limestone, magnesium-enhanced lime, and salt, as detailed by Bogwardt (1972), Mo et al. (2007), and Živković et al. (2014). In wet scrubber chemical treatment programs, the primary objective is to ensure that nozzles and collection surfaces remain free from deposits and scale build-up, thus preserving unit efficiency, as emphasized by Bogwardt (1972), Mo et al. (2007), and Živković et al. (2014). Additional methods for reducing scale will be explored in the following section.

2.4 Scale reduction techniques

Several methods are available to prevent the deposition of scale, which is crucial for maintaining the efficiency and longevity of industrial systems. These methods include maintaining appropriate pH levels, utilizing chelating agents, and harnessing the "threshold effect" to hinder nucleation and subsequent scaling. Chelating agents play a vital role in inhibiting scale formation, particularly when the concentrations of calcium or ferric ions (Fe^{3+}) are low. These agents function by forming stable complexes with metal ions, thus preventing them from participating in scale-forming reactions. However, their effectiveness diminishes as the concentrations of these ions increase, as chelating agents typically operate at a 1:1 or 2:1 ratio of Ca to the chelating agent, as outlined by Smith et al. (1968).

The most efficeint and cost-effective methods for scale inhibition involve chemicals that exhibit the "threshold effect". This phenomenon occurs when certain chemicals encapsulate small crystalline nuclei, effectively inhibiting their growth. As a result, the formation of larger scale particles is hindered, and these particles remain suspended in the solution, preventing their deposition. Chemicals demonstrating this characteristic include polyphosphates, organic phosphonates, as well as alkyl and aryl sulphonates, as described by Smith et al. (1968). By employing chemicals with the threshold effect, industries can effectively mitigate scale deposition, ensuring the smooth operation of their systems and reducing maintenance costs associated with scale-related issues.

2.4.1 Calcium sulphate scale

2.4.1.1 Oxidation inhibition

For common scales like calcium sulphate, specialized methods have been developed to address the oxidation of calcium sulphite ($CaSO_3$) to calcium sulphate ($CaSO_4$), a process that contributes to scale formation. Unlike other scales, calcium sulphate scaling requires a distinct approach because complete removal of oxygen from the system, where it's already present in the flue gas, is not feasible (common in limestone wet scrubbing systems). While inhibitors like Na_2S_2O have been tested for preventing or controlling oxidation, they have not proven entirely effective (Mo et al., 2007).

Bogwardt's work in 1972 suggested that most oxidation to sulphite occurs in the holding tank. Therefore, minimizing exposure to air or oxygen can help reduce oxidation. Consequently,

calcium sulphate ($CaSO_4$) can be removed alongside calcium sulphite ($CaSO_3$) as a mixed crystal, provided the oxidation level does not exceed 20 %. Beyond this threshold, increased oxidation leads to scaling issues. This strategy underscores the importance of controlling oxidation levels to effectively manage $CaSO_4$ scaling in industrial systems.

2.4.1.2 Softening

In situations where the $CaSO_4$ scaling issue arises in diluted systems, the solution is to implement a softening process on the regenerated liquor before recycling it back into the scrubber. In contrast, in concentrated systems, $CaSO_4$ doesn't pose a problem because the high concentration of SO_3^{2-} effectively keeps the levels of Ca^{2+} ions low. Softening involves treating the liquor before it is returned to the scrubber system to ensure it remains unsaturated with respect to $CaSO_4$. This is achieved by removing Ca^{2+} and SO_4^{2-} ions, typically through precipitation or ion exchange methods. Therefore, by employing proper softening techniques, even if SO_4^{2-} forms in the scrubber, the liquor won't reach a saturation point with $CaSO_4$, preventing scaling on the inner surfaces of the scrubber. In highly concentrated active alkali systems, there is no need for a specific softening step, as the elevated SO_3^{2-} concentration is maintained throughout the system. This SO_3^2 action keeps the $[Ca^{2+}]$ low (a process known as “sulphite softening”), thereby ensuring that the scrubbing solution remains unsaturated with respect to $CaSO_4$ (Nissen et al., 1976).

This method of scale prevention is discussed further, in detail, in section 2.5.

2.4.1.3 Sodium chloride

The use of sodium chloride (NaCl) solution for the removal of $CaSO_4$ scaling has also been suggested:

$$2\,NaCl + CaSO_4 \rightarrow Na_2SO_4 + CaCl_2 \qquad [2.9]$$

This method proves successful within a concentration range of 10—12 % NaCl by employing a continuous flushing process over the scale surface, as discussed by Axelrad (1956) and Santos et al. (2017). The rate of calcium sulphate removal achieved by a 12 % NaCl solution can reach approximately 4000 mg/L in just a few hours, with the volume of solution adjusted based on the quantity of scale needing removal. Notably, this process is most effective at lower temperatures, as highlighted by Axelrad (1956). This approach demonstrates the efficacy of using sodium chloride solutions for the efficient removal of $CaSO_4$ scale from industrial equipment and surfaces.

2.4.2 Calcium carbonate scale

In the absorber, it's typically crucial to maintain the pH within a range of 6—6.5. Should the pH exceed 9, scaling issues may arise due to the precipitation of $CaCO_3$, resulting from the absorption of CO_2 from the flue gas, as noted by Bezuidenhout et al. (2012) and Little (1975). In situations where scaling contains both $CaCO_3$ and $CaSO_4$, a solution comprising hydrochloric acid (HCl) and NaCl can be employed for removal, as discussed by Axelrad (1956). The addition of HCl, as indicated in Equation 2.10, does not alter the solution's effectiveness in terms of removing $CaSO_4$. Instead, it serves to specifically target and dissolve the CaCO3, which is unaffected by NaCl. This approach enables selective removal of $CaCO_3$ scale while leaving $CaSO_4$ intact, demonstrating a practical method for addressing scaling issues involving multiple types of scale compounds in industrial systems.

$$CaCO_3 + 2\,HCl \rightarrow CaCl_2 + CO_2 + H_2O \qquad [2.10]$$

The amount of HCl to be added to the NaCl solution depends on the amount of $CaCO_3$ present. The HCl reacts with the insoluble $CaCO_3$ and forms soluble calcium chloride ($CaCl_2$). Solutions containing 0.5—10 % of HCl are effective in the removal of $CaCO_3$. Corrosion inhibitors should be added to the solution to prevent corrosion to parts of the scrubber that contain metal due to the addition of a strong corrosive agent, HCl.

In many instances, the initial design of the VTS tends to overlook the presence of Ca^{2+} and SO_4^{2-} ions within the water system. With time, the concentration of these ions in the water can increase significantly, often surpassing the solubility limit of $CaSO_4$. This leads to the development of scale in the scrubber, pipes, and pumps, necessitating downtime for the opening of lines and descaling procedures involving high-pressure water (Bezuidenhout et al., 2012; Rosenberg et al., 2012; Wen et al., 1975). As scale formation results from having

supersaturated and/or hard water, the following section will explore various chemical and physical methods primarily categorized as “water softening” for preventing scale.

2.5 Traditional Water Treatment Methods

Conventional methods for water treatment typically encompass either chemical treatments or ion exchange procedures. Among the widely used commercial systems for addressing hard water problems are chemical water softeners, water filters, and packed-bed water softeners. Chemical water softeners are substances designed to combat water hardness and can be broadly classified into two types: precipitating and non-precipitating. Precipitating water softeners, such as lime and soda ash (explained in more detail in section 2.6.2), form insoluble precipitates when they react with Ca and Mg ions, effectively reducing water hardness. However, these precipitates can make the water appear cloudy and, if not removed, may accumulate on surfaces. Additionally, they increase the water's alkalinity, which could potentially cause damage to various materials, including the skin (Rathilal, 2004; Sawaftah, 2017).

Water filters, on the other hand, come in two primary forms: portable ion exchange and reverse osmosis systems. These filters aim to remove harmful or undesirable particles from the water before it is considered safe for human consumption (Rathilal, 2004; Sawaftah, 2017). Reverse osmosis operates by forcing water through a semi-permeable membrane, effectively blocking specific particles from passing through. Meanwhile, portable water filters use a cartridge containing activated carbon and ion exchange resin. The carbon adsorbs and helps reduce levels of chlorine, chlorine compounds, pesticides, colorants, and other organic substances, thereby improving the taste and appearance of the water (Rathilal, 2004; Sawaftah, 2017).

The ion exchange resin is employed to mitigate temporary hardness, as discussed in section 2.6.1. Packed bed water softeners also function through the ion exchange process. In this process, water flows through a media bed, typically containing sulfonated polystyrene beads saturated with sodium. The elements responsible for water hardness adhere to the resin beads, while Na is simultaneously released into the water. When the resin becomes saturated with Ca and Mg, it undergoes regeneration by passing a brine solution (NaCl) through it. The Na ions replace the Ca and Mg ions, which are then discharged in the wastewater (Rathilal, 2004). However, one drawback of ion exchange treatment is that regenerating the resins may require the use of expensive chemicals. Even modern ion exchange plants that operate automatically involve costly electronic components.

In many instances, chemicals like antiscalants, lime, soda ash, and others can be employed to combat scale formation. However, it's important to note that these chemicals pose environmental risks and may not always be the most suitable or cost-effective means of preventing scale build-up (Rathilal, 2004; Sawaftah, 2017). Chemical treatment does have its disadvantages. It requires precise chemical analysis of the water and accurate dosing of chemicals. Additionally, it can be expensive, both in terms of initial costs and ongoing expenses. There are safety hazards associated with handling chemicals, and it can lead to pollution of the treated water, among other concerns. Chemical treatment may also not be feasible when dealing with large volumes of water. In cases where chemical treatment is impractical, scaling in pipelines and equipment often necessitates disassembly and either mechanical or chemical cleaning, which can be a significant expenditure of time and labour (Rathilal, 2004; Sawaftah, 2017).

2.6 Hard water and the process of softening to prevent scale formation

Water with elevated levels of Ca and Mg ions, causing scaling issues, is commonly known as hard water. Many natural water sources contain increased concentrations of dissolved salts like Ca and Mg carbonates. These compounds are created through the interaction of limestone ($CaCO_3$), a naturally occurring mineral in the earth's crust, with acidic rainfall rich in carbon dioxide. When there is an oversaturation of Ca and Mg ions in hard water, it results in the formation of scale and deposits. To prevent scale build-up, various methods can be employed to treat this water. The process of removing Ca, Mg, and other metal cations from hard water is called "water softening". Softened water helps extend the lifespan of pipes and surfaces (Chen et al., 2018; Entezari and Tahmasbi, 2009; Mercer et al., 2005). Figure 2.13 illustrates a typical scrubbing circuit for a PGM smelter. In this specific case study, four water streams have been identified as potential sources of elements contributing to hard water (exceeding 1000 mg/L). This includes the scrubber feed, which serves as the water source for scrubbing SO_2 and PGM particles entering the scrubber. The water sources collected for analysis are:

1. Scrubber feed
2. Scrubber bleed
3. Dust-thickener overflow
4. Process water

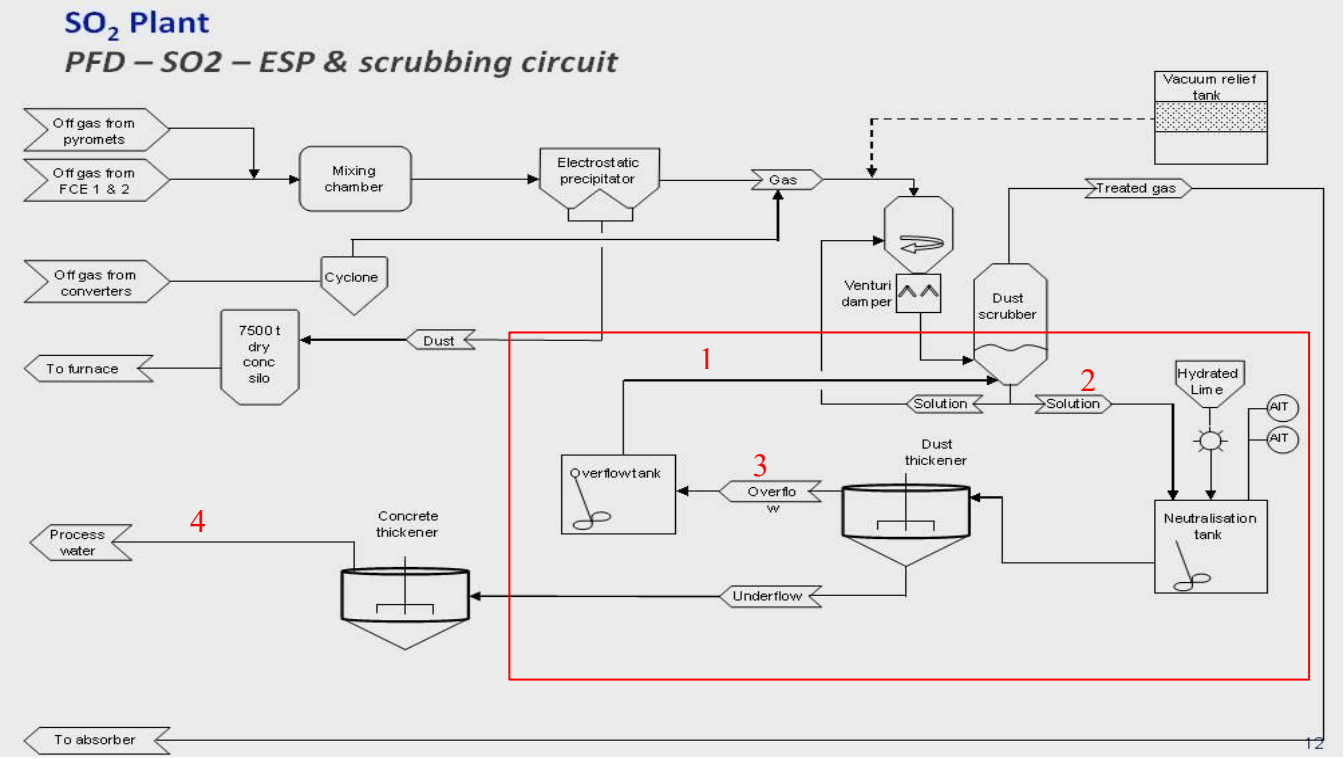


Figure 2. 13 Scrubbing circuit for A PGM smelter (Sibanye-Stillwater, 2019)

Water streams can act as storage reservoirs for certain metals during the process of water recirculation within a plant. This retention process is influenced by several factors, including the water's pH and temperature, as well as the solubility constant of the specific element, among other parameters (Kemmer, 1979; Zivkovic et al., 2014). In practical water recirculation scenarios, metal ions that initially exist in a state of sub-saturation in FGD fluids may gradually approach equilibrium and eventually become saturated in the water stream (Kemmer, 1979; Zivkovic et al., 2014). One method of quantifying water hardness, represented as an equivalent to $CaCO_3$, is depicted in Equation 2.9 as,

$$[CaCO_3](mg/L) = [Ca](mg/L) \times 2.5 + [Mg](mg/L) \times 4.1 \quad [2.9]$$

Each sample can be assigned a degree of hardness based on the calculations, as shown in Table 2.4. It ranges from 120—180 mg/L as $CaCO_3$ and can exceed 180 mg/L as $CaCO_3$ in very hard waters. For soft to moderately hard water, the acceptable hardness range is 17—120 mg/L as $CaCO_3$ (Dey et al., 2007; United States Geological Survey, 2020).

Table 2. 4 Degree of hardness (United States Geological Survey, 2020).

Degree of hardness	mg/L (of $CaCO_3$)
Soft	<17
Slightly hard	17.1-60
Moderately hard	60-120
Hard	120-180
Very hard	>180

The treatment of hard water depends on the degree and type of hardness (Cappelle and Davis, 2016; Dey et al., 2007; Entezari and Tahmasbi, 2009). Temporary or carbonate hardness, caused by the presence of both Ca and HCO_3^- ions in water, can be reduced by adding hydrated $Ca(OH)_2$ or by boiling the water in an open container. Conversely, permanent or non-carbonate hardness, resulting from the presence of Ca and Mg sulphates, becomes more soluble as the temperature rises and cannot be eliminated through boiling (Cappelle and Davis, 2016; Entezari and Tahmasbi, 2009). However, it can be eliminated by using a water softener, which operates based on the principle of ion exchange. This process involves replacing Ca and Mg ions with Na or potassium (K) ions, thereby reducing the concentration of hardness minerals to acceptable levels and softening the water (Cappelle and Davis, 2016; Entezari and Tahmasbi, 2009).

The minerals of Ca and Mg responsible for water hardness also contribute to the ’alkalinity’ of water. These minerals exist in the water as their respective ions (Ca^{2+} and Mg^{2+}), which can react with acids and increase the water's buffering capacity or ‘alkalinity’. In contrast to water hardness, alkalinity is a measure of the water's ability to neutralize acids and maintain a stable pH. It is primarily influenced by the presence of HCO_3^-, CO_3^{2-}, and hydroxide (OH^-) ions in the water. Alkalinity is also expressed in units of mg/L or ppm of $CaCO_3$ equivalent (Cappelle and Davis, 2016; Entezari and Tahmasbi, 2009; Ibanez et al., 2008).

2.6.1 Water hardness and alkalinity relation

Water hardness and alkalinity are related properties influenced by mineral content in water. While water hardness specifically refers to the concentration of Ca and Mg, alkalinity reflects the water's ability to resist changes in pH. Understanding both parameters is crucial for assessing water quality and determining appropriate treatment (Boyd et al., 2016; Cappelle and Davis, 2016; Entezari and Tahmasbi, 2009; Ibanez et al., 2008).

In general, higher water hardness levels are associated with higher alkalinity due to the presence of calcium and magnesium ions. However, it is important to note that alkalinity can also be influenced by other factors, such as HCO_3^- and CO_3^{2-} originating from sources other than water hardness. Water hardness and alkalinity have implications for various applications (Boyd et al., 2016; Cappelle and Davis, 2016; Dara. 2008; Entezari and Tahmasbi, 2009; Ibanez et al., 2008).

1. *Domestic Use*: Hard water can cause mineral build-up in pipes, appliances, and fixtures, reducing their efficiency and lifespan. Alkalinity can influence the pH of water, affecting the taste, suitability for drinking, and the performance of detergents and soaps.
2. *Industrial Processes:* In industrial processes, water hardness and alkalinity are critical parameters that can significantly impact operations. Water hardness, characterized by the presence of dissolved minerals like calcium and magnesium ions, can lead to scaling and equipment damage, disrupting chemical reactions and reducing process efficiency. On the other hand, alkalinity, determined by bicarbonate, carbonate, and hydroxide ions, plays a crucial role in maintaining stable pH conditions, which is vital for ensuring consistent product quality and efficient processes. Controlling water hardness and alkalinity through appropriate treatment and monitoring measures is essential for optimizing industrial processes and minimizing disruptions caused by water quality issues.
3. *Environmental Considerations*: High levels of water hardness and alkalinity can affect aquatic ecosystems. Hard water can have adverse effects on fish and other aquatic organisms, while excessive alkalinity can alter pH levels and disrupt natural habitats.

2.6.1.1 Measuring alkalinity

Two forms of alkalinity represent different components of the overall alkalinity of water. Alkalinity is a collective term that encompasses both M-alkalinity (total alkalinity or carbonate alkalinity) and P-alkalinity (phenolphthalein alkalinity or hydroxide alkalinity). The denotations P and M are given based on the indicator that is used in the titration process; P for phenolphthalein and M for methyl orange (Bates, 2001; Dara, 2008; Ibanez et al., 2008).

1. *M-Alkalinity* (also known as total alkalinity or carbonate alkalinity):

   M-alkalinity primarily represents the concentration of HCO_3^- and CO_3^{2-} in water. These ions contribute to the water's ability to neutralize acids and maintain a stable pH. M-Alkalinity is determined by titrating the water sample with an acid until the HCO_3^- and CO_3^{2-} are converted to CO_2, resulting in a pH endpoint. Therefore, m-alkalinity reflects

the alkalinity due to the presence of HCO_3^- and CO_3^{2-}. Methyl orange is used as an indicator to determine the alkalinity of all OH^-, CO_3^{2-} and HCO_3^- and thus considered as the 'total alkalinity' due to the major role that carbonate species play in the total alkalinity of water. It is determined by titrating to the methyl orange endpoint at pH 4.5 (Bates, 2001; Dara, 2008; Ibanez et al., 2008).

2. *P-Alkalinity* (also known as phenolphthalein alkalinity or hydroxide alkalinity): P-Alkalinity measures the concentration of OH^- and certain weak bases in water. It provides an estimate of the alkalinity contributed by OH^- and other weak bases that can neutralize acids. The phenolphthalein indicator is typically used in the titration process to determine the p-alkalinity. Phenolphthalein alkalinity determines alkalinity of all OH^- and half of the CO_3^{2-} ions and is determined by titrating to the phenolphthalein endpoint at pH 8.3. The phenolphthalein alkalinity endpoint occurs when all the OH^- are consumed and the remaining weak bases contribute to the alkalinity (Bates, 2001). Figure 2.14 illustrates the relationship between alkalinity and pH of a solution.

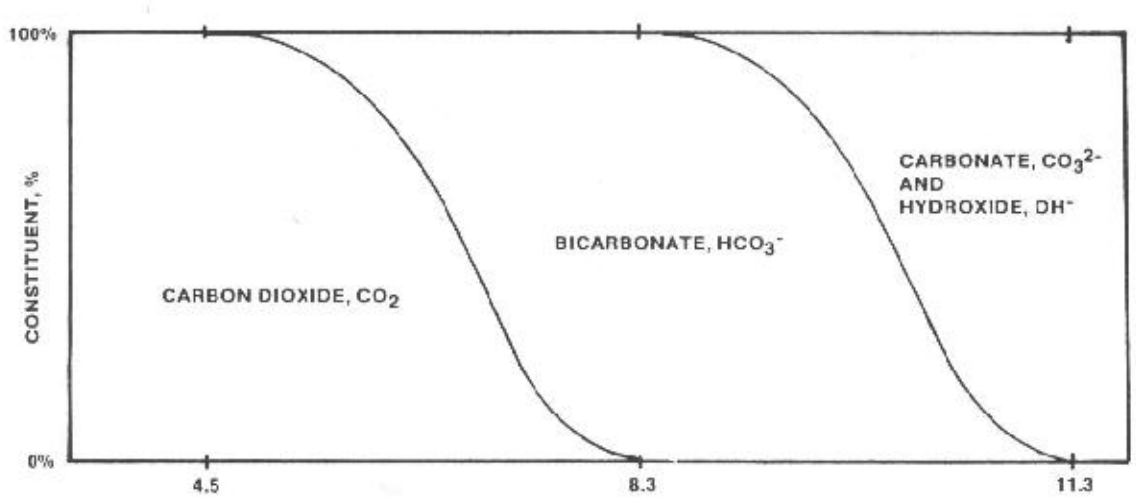


Figure 2. 14 Relationship between pH and alkalinity (HCO_3^-, CO_3^{2-} and OH^-) (Minnesota Rural Water Association, 2009, page 5).

Figure 2.14 can also provide insights into the relationship between the major ions and the alkalinity components. The diagram allows us to observe the relative positions of the data points representing the water samples in relation to the dominant alkalinity constituents. For example, if the data points on the diagram indicate a HCO_3^--dominated region, it suggests that HCO_3^- are the primary alkalinity component. In this case, the anion-cation balance should also reflect the presence of anions (such as HCO_3^-) and corresponding cations (e.g., Ca^{2+}, Mg^{2+},

Na^+, K^+) that maintain electrical neutrality. The concentrations of these cations should be approximately equal to the concentration of HCO_3^- and other anions present. Similarly, if the diagram shows a CO_3^{2-}-dominated region, it indicates that CO_3^{2-} ions play a significant role in the alkalinity. The anion-cation balance should reflect the presence of carbonate and the corresponding cations. An accurate anion-cation balance is crucial because any significant imbalance can suggest the presence of unidentified ions, measurement errors, or incomplete analysis. It is essential to account for all significant anions and cations in water analysis to ensure accurate charge neutrality and reliable data interpretation. Ideally, a potable aqueous solution should always be electrically neutral, and thus the sum of the anions (in Millie equivalents/litre (me/L)) and the cations should balance. It is important to note that all samples were filtered prior to ICP-OES analysis. This was done to ensure removal of suspended solids that may interfere with anion and cation analysis (El Baba et al. 2020; Murray and Wade, 1996; Standard Methods, 1999). The resulting error balance is calculated in Equation 2.10 as follows (El Baba et al. 2020; Greenberg and Navone, 1958; Murray and Wade, 1996):

$$CBE = (\sum Cations - |\sum Anions|/[\sum Cations + |\sum Anions|) * 100 \quad [2.10]$$

The calculated charge-balance error must be within an acceptable limit as presented in Table 2.5.

Table 2. 5 The acceptance criteria for charge balance error (Rice et al., 2012).

Anion Sum (meq/L)	Acceptable % Difference
0–3	± 0.2 meq/L
3–10	± 2%
10–800	± 2 – 5%

The expressions in Table 2.6 provide a quick way to interpret the relationship between P and M alkalinity values and their implications for the water's buffering capacity:

Table 2. 6 Interpretation of P and M alkalinity (Bates, 2001; Dara, 2008; Ibanez et al., 2008).

Value of P and M	Alkalinity due to		
	CO_3^{2-}	HCO_3^-	OH^-
P = 0	0	M	0
P < 1/2 M	2 P	M – 2 P	0
P = 1/2 M	M	0	0
P > 1/2 M	2 (M - P)	0	2 P - M
P = M	0	0	M

1. *P = 0*: This indicates that there is no measurable contribution of OH^- or strong bases to the water's alkalinity. The water's ability to resist changes in pH due to strong acids is limited.
2. *P < 1/2 M*: When p-alkalinity is less than half of m-alkalinity, it suggests that the dominant contributors to the alkalinity are HCO_3^- and CO_3^{2-} ions. The buffering capacity of the water is primarily due to these components.
3. *P = 1/2 M*: This indicates an equal contribution of OH^- and HCO_3^-/CO_3^{2-} to the water's alkalinity. The water has a balanced buffering capacity between OH^- and HCO_3^-/CO_3^{2-}
4. *P > 1/2 M*: When p-alkalinity is greater than half of m-alkalinity, it suggests that OH^- and strong bases play a significant role in the water's buffering capacity. This indicates a relatively higher contribution from OH^- compared to HCO_3^-/CO_3^{2-}.
5. *P = M*: This means that OH^- contribute fully to the water's alkalinity, and there is no measurable contribution from HCO_3^-/CO_3^{2-}. The buffering capacity is dominated by OH^-.

Generally, the relationship between total hardness and alkalinity in water indicates the balance between HCO_3^-/CO_3^{2-} as well as their contribution to water's buffering capacity and potential for scale formation. Understanding this relationship is important for water treatment, industrial processes, and maintaining water quality in various applications. If the total alkalinity is greater than the total hardness (*M-Alkalinity > Total Hardness)*, it suggests that the majority of the alkalinity is due to HCO_3^-/CO_3^{2-}. In this case, there is an excess of HCO_3^-/CO_3^{2-} that can react with acids. Since alkalinity exceeds the total hardness, all of the hardness is attributed to HCO_3^-/CO_3^{2-}. This means that the water is primarily responsible for the buffering of acids and is less

likely to form scale. If the alkalinity is less than the total hardness ***(****M-Alkalinity < Total Hardness***)**, there is a potential for the presence of non-carbonate hardness. Non-carbonate hardness refers to the portion of total hardness that is not associated with carbonate and bicarbonate ions. In this case, carbonate hardness is equal to the alkalinity (M-alkalinity), and the remaining portion of hardness is considered non-carbonate hardness (Rafferty, 1999). The non-carbonate hardness can come from other sources like calcium sulphate ($CaSO_4$) or other divalent cations.

Assessing the overall nature, whether a water sample is prone to forming scale or exhibiting corrosive tendencies, requires the inclusion of various crucial physico-chemical parameters. Alongside determining calcium hardness and M-Alkalinity, it's essential to also measure TDS, EC, pH, and temperature. These combined factors offer a comprehensive insight into the water's attributes, aiding in the assessment of its potential for encountering scale build-up. The level of TDS serves as a general indicator of water source quality. As TDS levels rise, the likelihood of encountering water quality issues increases (Rafferty, 1999).

2.6.1.2 Total dissolved solids and electrical conductivity

From the sums of the cations and anions, both the TDS and EC can be estimated accordingly (Rice et al., 2012; Rusydi, 2017):

$$TDS_{calc} = (0.6 \times \text{Total Alkalinity as } CaCO_3) + \Sigma \text{ cations} + \Sigma \text{ anions} \quad [2.11]$$

Total alkalinity = carbonate hardness as $CaCO_3$ in mg/L

Electrical conductivity is closely related to the concept of TDS in water. It measures the water's ability to conduct an electrical current due to the presence of ions, which are typically dissolved salts and minerals. Higher concentrations of dissolved ions, such as salts, lead to increased electrical conductivity. As TDS increases, so does EC. Electrical conductivity is often used as a practical way to estimate TDS in water samples both are related as:

$$TDS\ (mg/L) = k_e * EC\ (\mu S/cm) \quad [2.12]$$

where k_e is a constant of proportionality. The k_e value varies from 0.55 to 0.85 (Atekwana et al. 2004; Walton, 1989; Rusydi, 2017), and the average (0.7) is most commonly used (Walton, 1989).

2.6.1.3 Scaling indices

Scaling indices are critical tools in water chemistry for assessing the likelihood of scale formation in water systems. Three prominent scaling indices commonly utilized are the Langelier Saturation Index (LSI), Ryznar Stability Index (RSI), and Puckorius Scaling Index (PSI). These indices provide insights into water's corrosive or scaling potential based on its mineral content. The LSI calculates the saturation of $CaCO_3$, indicating whether the water is scaling or corrosive. The RSI estimates the stability of calcium carbonate, offering a measure of the water's scaling tendency. The PSI considers factors like Ca, Mg and silica (SiO_2) concentrations to predict the potential for scale accumulation. These indices collectively aid industries in managing water systems effectively and mitigating scale-related challenges (Abbasnia et al. 2019; Cavano, 2005; Mirzabeygi et al., 2016; Puckorius and Strauss, 1983; Rafferty, 1999; Shah et al., 2023).

All three indices are based on the saturation pH of $CaCO_3$ and use the following physico-chemical parameters:

- Temperature (°C)
- Total dissolved solids (TDS)
- Calcium hardness (expressed as $CaCO_3$)
- Total alkalinity (expressed as $CaCO_3$)

Each index is calculate as follows (Abbasnia et al. 2019; Cavano, 2005; Mirzabeygi et al., 2016; Puckorius and Strauss, 1983; Rafferty, 1999; Shah et al., 2023):

- $LSI = pH - pHs,$ [2.13]

where pH is the actual pH, and pHs is the pH at saturation. pHs is calculated as follows:

$$pHs = (9.3 + A + B) - (C + D) \quad [2.14]$$

where $A = \text{Log}_{10}((TDS) - 1))/10$

$B = (-13.12)\,[\text{Log}_{10}(\text{Temp °C} + 273) + 34.55]$

$C = \text{Log}_{10}(\text{calcium hardness} - 0.4)$

$D = \text{Log}_{10}(\text{total alkalinity})$

If LSI > 0: Water is supersaturated with $CaCO_3$ and scale may form.

If LSI < 0: Water is under saturated with $CaCO_3$ and will dissolve scale.

LSI = 0: Water is neutral- neither scale forming or scale dissolving

- *RSI = 2 (pHs) -pH* [2.15]

If RSI < 6: Water is supersaturated, scale will form
If RSI > 6: Water is under saturated, water will dissolve scale

- *PSI = 2 (pHs) - pHeq,* [2.16]

where pHs is the pH at saturation and pHeq is an equilibrium pH based on the total alkalinity value.

If PSI < 6: Water is supersaturated, scale will form
If PSI > 6: Water is under saturated, water will dissolve scale.

Scaling indices directly influence water treatment strategies by guiding the selection of appropriate methods to counteract scaling issues. Understanding these indices aids in tailoring treatment processes such as chemical dosing, pH adjustment, and ion exchange to effectively prevent or manage scale formation in industrial processes, pipelines, and equipment. Water treatment methods, such as ion exchange and lime softening, can be employed to concurrently reduce water hardness and alkalinity. These processes are designed to effectively eliminate or decrease the concentration of mineral ions accountable for hardness and alkalinity, thereby enhancing water quality to meet specific application needs. Acknowledging the critical significance of water as a resource, Sibanye-Stillwater undertook substantial measures to address its water requisites. In 2017, the company procured a significant quantity of potable water from water boards (18,284 ML), incurring a substantial expense of R200 million. The majority of this water was drawn from the Integrated Vaal River System (IVRS) and subsequently channelled through the Rand Water distribution network. Sibanye-Stillwater has made substantial investments in securing a reliable and sustainable water supply to support its operations (Team, 2021; Water conservation and water demand management, 2022). This reflects the company's strong dedication to managing its water usage efficiently. As a result, the company has increased its investments in various water treatment technologies. The following section provides an overview of methods for addressing hard water issues, with a

particular emphasis on approaches proven to be effective in removing Ca, Mg and other potentially present metal ions and anions.

2.6.2 Water softening using ion exchange resins

Ion exchange resins have played a crucial role in water softening for more than 130 years (Wang and Peng, 2010). Initially, zeolites, which are aluminosilicate minerals known for their cation absorption properties, were used for this purpose (Wang and Peng, 2010). However, with the discovery of synthetic resins over 80 years ago, the applications of ion exchange resins have significantly expanded. Two types of resins can be employed for water softening due to their cation-attracting capabilities: Weak Acid Cation resin (WAC) and Strong Acid Cation resin (SAC) (Apell et al., 2010; Canepa et al., 1996; Cappelle and Davis, 2016; Hoffmann and Martinola, 1988). Weak Acid Cation resin resins feature active carboxylic sites, whereas SAC resins have active sulphonic sites (Figure 2.15).

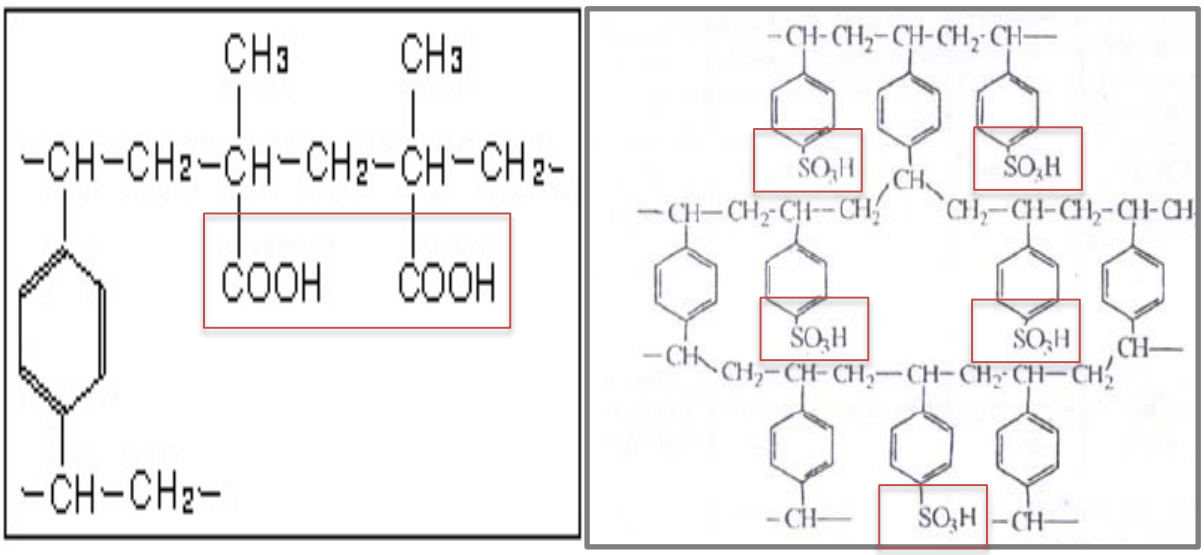


Figure 2. 15 Structure of a weak acid cation resin (left) and a strong acid cation resin (right)

Weak Acid Cation and SAC resins have different properties based on the strength of the functional groups they contain. The affinity of WAC resin for Ca and Mg is stronger than that of SAC resin due to the differences in the acid groups they possess particularly in solutions with high TDS.

Weak Acid Cation resins contain weak acid carboxylic acid functional groups, typically in the form of -COOH which are only partially ionized at typical water treatment pH levels (Hoffmann and Martinola, 1988; Apell et al.,2010; Canepa et al., 1996; Cappelle and Davis,

2016). These functional groups have a weak acidity and have a higher ion exchange capacity for multivalent cations such as Ca^{2+} and Mg^{2+}, present in hard water. The carboxylic acid groups release hydrogen ions (H^+) during the ion exchange process, leading to the replacement of the hardness-causing ions with hydrogen ions, resulting in the softening of water. On the other hand, SAC resins feature stronger acidic functional groups, specifically sulphonic acid groups ($-SO_3H$). These sulphonic acid groups have a higher acidity compared to carboxylic acid groups. SAC resins exhibit enhanced ion-exchange capabilities and can effectively remove both alkaline earth metal cations (e.g., Ca^{2+}, Mg^{2+}) and transition metal cations (e.g., Fe^{2+}, Mn^{2+}) (Hoffmann and Martinola, 1988; Apell et al.,2010; Canepa et al., 1996; Cappelle and Davis, 2016). The weaker ionization of WAC resin allows it to preferentially exchange H^+ ions for Ca^{2+} and Mg^{2+} ions over monovalent cations like Na^+ or K^+. strong acid cation (SAC) resins, with their stronger acid groups, are less selective and can also exchange H+ ions for monovalent cations, which makes them less efficient in removing Ca and Mg when these ions are present in the water along with monovalent ions (Hoffmann and Martinola, 1988; Apell et al.,2010; Canepa et al., 1996; Cappelle and Davis, 2016).

In a typical water softener system, the Ca and Mg ion present in hard water enter a container filled with resin beads containing Na ions (Hoffmann and Martinola, 1988; Apell et al., 2010; Canepa et al., 1996; Cappelle and Davis, 2016):

$$2\ R\text{-}Na + M^{2+} \rightarrow R_2\text{-}M + 2\ Na^+ \qquad [2.17]$$

Where “R-Na” is the resin and “M^{2+}” is the metal absorbed from solution.

Since it's in a state of equilibrium, the reaction mentioned above can be reversed by increasing the sodium concentration on the right side (Equation 2.18). The regeneration process is performed in this manner using NaCl (Apell et al., 2010; Canepa et al., 1996; Cappelle and Davis, 2016; Hoffmann and Martinola, 1988).

$$R_2\text{-}M + 2\ Na^+ \rightarrow 2\ R\text{-}Na + M^{2+} \qquad [2.18]$$

Water softening involves the removal of hardness ions, namely Ca^{2+} and Mg^{2+}, replacing them with Na, without diminishing the water's salinity. The resulting sodium salts have considerably higher solubility, preventing the formation of scale or deposits (de Dardel, 2020).

Weak Acid Cation resins offer a viable means to eliminate hardness from water, even when it contains alkalinity (as indicated in Equation 2.19). Successful regeneration of cation resins is typically achieved using HCl,

$$2\ R\text{-}H + M^{2+}(HCO_3^-)_2 \rightarrow R_2\text{-}M + 2\ H^+ + 2\ HCO_3^- \quad [2.19]$$

and in Equation 2.20, the H+ and HCO_3^- react to create carbon dioxide (CO_2) and water (de Dardel, 2020):

$$H^+ + HCO_3^- \rightarrow CO_2 + H_2O \quad [2.20]$$

Madarász et al. (2014) effectively utilized titanate nanotubes' ion-exchange capabilities to remove Ca^{2+} and Mg^{2+} through three consecutive cycles of water softening and regeneration using a continuous ion exchange unit. Despite readily reversible Mg^{2+}/Na^+ exchange, the irreversible binding of Ca^{2+} ions to exceptionally strong adsorption sites resulted in a decrease in the total ion exchange capacity from 1.2 to 0.66 mmol/g.

Brown and Sheedy (2002) accomplished water softening in treated waters with total dissolved solids (TDS) levels of up to 7000 mg/L using an innovative ion exchange method employing either SAC or WAC resin. Notably, they avoided the use of acid and caustic substances even during the regeneration of weak acid cation resins by utilizing substantial quantities of high-quality brine. The softener equipment exhibited remarkable compactness, featuring resin bed heights as low as 15 cm and flow rates as high as 11.36 m^3/hr.

Handling water samples with very high TDS levels can be a challenging and complex task. This is primarily because the selectivity of SAC resin diminishes at high TDS levels (> 3000 mg/L), leading to increased costs due to frequent regenerations (Brown and Sheedy, 2002). In such instances, weak acid cation resins are typically employed for water softening. However, the main drawback of the WAC process is the need for resin regeneration using hydrochloric acid followed by sodium hydroxide, which can be an expensive procedure (Brown and Sheedy, 2002). When water contains excessively high metal levels, it becomes necessary to employ lime and soda ash dosage for the precipitation of hardness material, a treatment discussed in the following section.

2.6.3 Water softening through lime and soda ash (chemical precipitation)

The chemical precipitation process is a commonly employed method for softening hard water. Commonly used reagents for this purpose include soda ash (Na_2CO_3) and hydrated lime ($Ca(OH)_2$). Lime is effective at removing substances contributing to carbonate hardness, while soda ash is used to eliminate components not associated with carbonate hardness (Dey et al., 2007; de Dardel, 2020; Entezari and Tahmasbi, 2009; Seyrig and Shan, 2007). When lime and soda ash are combined, they result in the formation of insoluble precipitates derived from the minerals responsible for water hardness. Magnesium hydroxide ($Mg(OH)_2$) precipitates as magnesium hardness, while $CaCO_3$ precipitates as calcium hardness. These precipitates are subsequently removed through conventional processes such as coagulation/flocculation, sedimentation, and filtration, all of which are designed to alleviate water hardness (Dey et al., 2007; de Dardel, 2020; Entezari and Tahmasbi, 2009; Seyrig and Shan, 2007). It is worth noting that these precipitates have limited solubility, which means that some degree of hardness remains in the water, preventing issues related to excessive softness and corrosion in the water. Equations 2.21 to 2.24 illustrate how lime reacts with "hardness" (de Dardel, 2020; Entezari and Tahmasbi, 2009; Seyrig and Shan, 2007):

$$CO_2 + Ca(OH)_2 \rightarrow CaCO_3 + H_2O \quad [2.21]$$

$$Ca(HCO_3)_2 + Ca(OH)_2 \rightarrow 2\,CaCO_3 + 2H_2O \quad [2.22]$$

$$Mg(HCO_3)_2 + Ca(OH)_2 \rightarrow CaCO_3 + MgCO_3 + 2H_2O \quad [2.23]$$

$$MgCO_3 + Ca(OH)_2 \rightarrow CaCO_3 + Mg(OH)_2 \quad [2.24]$$

Carbon dioxide does not contribute to water hardness directly, but it reacts with lime and consumes a portion of it before it can effectively reduce hardness. This reaction occurs during the treatment process. “Temporary hardness”, also known as carbonate hardness, can be easily reduced by heating or boiling the water, while “permanent hardness”, also referred to as non-carbonate hardness, requires alternative treatment methods. Furthermore, the process can be reversed by heating the solution, causing the hardness minerals to precipitate out or form scale:

$$Ca(HCO_3)_2 + heat \rightarrow CaCO_3 + H_2O + CO_2 \quad [2.25]$$

In contrast, reducing non-carbonate hardness requires the introduction of chemicals. To induce precipitation, the raw water is subjected to a combination of hydrated lime and soda ash, facilitating the process of softening (as illustrated in Equations 2.26 and 2.27),

$$MgSO_4 + Ca(OH)_2 \rightarrow Mg(OH)_2 + CaSO_4 \quad [2.26]$$

$$CaSO_4 + Na_2CO_3 \rightarrow CaCO_3 + Na_2SO_4 \quad [2.27]$$

Chemical precipitation stands out as the prevalent approach in industrial settings for removing metals from solutions, given its simplicity, effectiveness over a broad temperature spectrum, and cost-effectiveness. This method revolves around pH adjustment to convert heavy metal ions into less soluble forms, such as hydroxides, sulphides, carbonates, or other substances, which can then be physically separated through processes like sedimentation, flotation, or filtration (Chen et al., 2009; Demopoulos, 2009; Mokone et al., 2010).

2.6.3.1 Effect of temperature on hardness removal through lime softening

Temperature also plays an important role in hardness removal through precipitation. An increase in temperature can lead to an effective removal of hardness material in water. Typically, increasing temperature promotes the dissolution of solids in water, as higher temperatures provide more energy for the solvent molecules to overcome the attractive forces between the solid particles and incorporate them into the solution (Fernandez-Prini, 1982; Minnesota rural water association, 2009; Veolia Water Technologies & Solutions, 2023). However, in the context of water hardness removal, more hardness is removed as $CaCO_3$ and $Mg(OH)_2$ when you increase the temperature in lime softening- seemingly counterintuitive based on the general solubility principles. More precipitate is formed primarily due to the improved kinetics of the reactions involved and the better mixing at higher temperatures. There are specific reasons for this behaviour in the context of lime softening:

1. *Increased reaction rate*: Lime softening involves the addition of $Ca(OH)_2$ to water, which reacts with calcium and magnesium ions to form $CaCO_3$ and $Mg(OH)_2$ precipitates. The addition of $Ca(OH)_2$ provides hydroxide ions (OH^-) in the water. The key factor here is that the formation of $CaCO_3$ and $Mg(OH)_2$ precipitates is promoted by the presence of excess OH^-. The reactions involved in lime softening are driven by the availability of OH^- and the adjustment of pH rather than being strongly influenced by the temperature and the direct solubility of these compounds (Fernandez-Prini, 1982; Minnesota rural water association, 2009; Veolia Water Technologies & Solutions, 2023). When the temperature

increases, chemical reactions generally occur at a faster rate due to increased kinetic energy. When a system at equilibrium is subjected to a change in temperature, pressure, or concentration, it will shift its position to counteract that change and re-establish a new equilibrium. In this case, the overall efficiency of the removal process benefits from the enhanced reaction rates as a result of an increase in temperature.

2. *Shift in equilibrium*: When the temperature increases, heat is being added to the system. According to Le Chatelier's principle, the system will shift in the direction that absorbs or consumes heat to counteract the increase in temperature. In this case, the precipitation reactions of $CaCO_3$ and $Mg(OH)_2$ absorb heat (endothermic):

$$Ca^{2+}(aq) + CO_3^{2-}(aq) + \text{heat} \rightarrow CaCO_3(s) \quad [2.28]$$

$$Mg^{2+}(aq) + 2\,OH^{-}(aq) + \text{heat} \rightarrow Mg(OH)_2(s) \quad [2.29]$$

As a result, the reactions involved in the formation of $CaCO_3$ and $Mg(OH)_2$ precipitates become more efficient. Therefore, raising the temperature in a lime softening process, the dissolution reactions of $CaCO_3$ and $Mg(OH)_2$ become less favourable, and the precipitation reactions become more favourable. This means that higher temperatures should lead to better precipitation of hardness ions as $CaCO_3$ and $Mg(OH)_2$, resulting in improved hardness removal (Fernandez-Prini, 1982; Minnesota rural water association, 2009; Veolia Water Technologies & Solutions, 2023).

3. *pH Control and improved mixing*: Higher temperatures can also influence the equilibrium pH of the system in lime softening, making it easier to achieve and maintain the desired pH range for effective precipitation of calcium and magnesium as carbonate and hydroxide precipitates. At higher temperatures, reactions tend to occur more rapidly, and mixing is typically more efficient. This means that the solid precipitates formed in the reactions can grow and settle more effectively, resulting in more efficient hardness removal (Fernandez-Prini, 1982; Minnesota rural water association, 2009; Veolia Water Technologies & Solutions, 2023).

There are generally three lime-softening processes based on temperature: Cold, Warm and Hot lime- softening, depending on the hardness level, water quality and intended application (Fernandez-Prini, 1982; Minnesota rural water association, 2009; Veolia Water Technologies & Solutions, 2023). The difference between cold, warm, and hot water softening lies in the

temperature at which the softening process is conducted. Each temperature range has its advantages and considerations when it comes to effectively removing hardness-causing minerals from water.

1. Cold lime softening:

Cold water softening typically refers to the treatment process conducted at room temperature or lower. It involves the use of chemical agents or ion exchange resins to remove hardness ions from the water. Cold water softening is a common method used in residential and commercial water softening systems. It is relatively simple, cost-effective, and requires less energy compared to warm or hot water softening methods. However, cold water softening may not be as efficient in removing certain types of hardness, such as temporary hardness, which can be addressed more effectively at higher temperatures Fernandez-Prini, 1982; Minnesota rural water association, 2009; Veolia Water Technologies & Solutions, 2023).

2. *Warm lime softening:*

Warm water softening involves conducting the softening process at a moderate temperature, usually between room temperature and 50—60 °C. The increased temperature enhances the solubility of hardness-causing minerals, making it easier to remove them from the water. Warm water softening can be advantageous for effectively removing temporary hardness, which primarily consists of calcium and magnesium bicarbonates that are more soluble at higher temperatures. It may involve methods such as lime softening or precipitation processes to remove hardness ions. Warm water softening strikes a balance between energy efficiency and effective hardness removal (Fernandez-Prini, 1982; Minnesota Rural Water Association, 2009; Veolia Water Technologies & Solutions, 2023).

3. *Hot lime softening*:

Hot water softening refers to conducting the softening process at elevated temperatures, typically above 60 °C. The higher temperature significantly increases the solubility of hardness minerals and improves the effectiveness of their removal. Hot water softening methods often involve processes such as boiling, distillation, or reverse osmosis to remove hardness ions. While hot water softening can be highly effective in removing hardness, it typically requires more energy and may not be practical for large-scale applications (Fernandez-Prini, 1982; Minnesota rural water association, 2009; Veolia Water Technologies & Solutions, 2023).

2.6.3.2 Co-removal of heavy metals through precipitation

The precipitation process in water treatment not only aids in the removal of hardness causing minerals but also provides an effective means for co-removal of heavy metals. Heavy metals, such as lead, copper, cadmium, and zinc, pose significant environmental and health risks even at low concentrations. Precipitation methods, such as lime and soda ash softening, can facilitate the simultaneous removal of these heavy metal ions from water. By adjusting the pH and introducing precipitating agents, the heavy metal ions can form insoluble compounds that precipitate out of the water, enabling their removal. This co-removal of heavy metals through precipitation plays a crucial role in ensuring the purification and remediation of contaminated water sources. In a study conducted by Chen et al in 2018, the utilization of soda ash and lime for the removal of heavy metals from aqueous solutions was examined. The research focused on investigating the influence of precipitant dosage on the removal of heavy metals through various parameters such as pH, particle size, particle Zeta potential, supernatant turbidity, and sludge volume. The findings revealed that lime, as a highly efficient material, exhibited the potential to remove up to 99 % of the heavy metals, indicating its significant effectiveness in the process. Apart from soda ash's capacity to remove dissolved heavy metals from wastewater, carbonate precipitation has proven to be an effective treatment option compared to hydroxide precipitation. To address magnesium hardness, the use of both lime and soda ash may be necessary (Chen et al., 2018; Saloua et al., 2020). Soda ash has the advantage of being simpler to handle than lime, as it involves the use of a single chemical and generates less calcium carbonate sludge. However, it comes with drawbacks, including higher cost, its classification as a hazardous chemical, and the introduction of sodium into the treated water. Due to its elevated operating pH (9.5—10.5), chemical softening also precipitates various heavy elements, such as arsenic, iron, and manganese, effectively removing them from the solution.

2.6.4 The SAVMIN process

Another treatment process that employs the benefits of lime addition for the removal of calcium sulphates and other heavy metals is the SAVMIN process. The SAVMIN process was of particular interest in this study due to the high Ca^{2+} and SO_4^{2-} concentrations that typically precede hard water scaling in the process waters, as is the case with the samples dealt with in thus study. The SAVMIN process is a technique that uses chemical precipitation to lower the levels of Ca^{2+} and SO_4^{2-} in water by precipitating gypsum and ettringite (a hydrous calcium aluminium sulphate mineral, $CaO.3CaSO_4.Al_2O_3.31H_2O$). This process was developed by

Mintek and Savannah Mining. To remove SO_4^{2-} and Ca from acid mine drainage (AMD), lime is added to precipitate metal hydroxides, and then aluminium hydroxide ($Al(OH)_3$) is added to form ettringite (Damons, 2001). The process comprises five important steps that are outlined below and depicted in Figure 2.16.

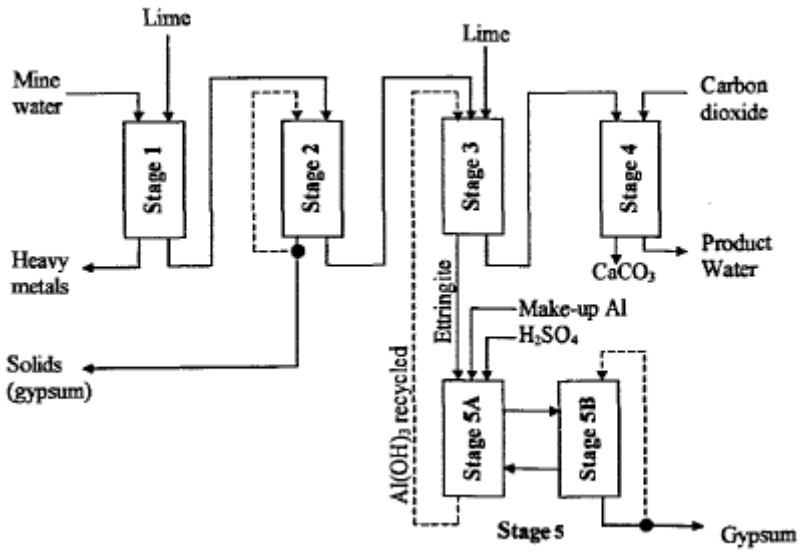


Figure 2. 16 SAVMIN process (Van Niekerk, 2002)

1. The addition of lime to acid mine drainage to create a high pH (> 11.5) environment in which heavy metals can be precipitated as metal hydroxides (Equation 2.30).

$$M^{2+} + 2\ OH^- \rightarrow (OH)_2 \qquad [2.30]$$

where "M^{2+}" refers to divalent heavy metals such as Fe, Ni, Mg and others. While most metal hydroxides generally precipitate at lower pH levels (< 8), a high pH is necessary for precipitation of magnesium. Once the metal hydroxide precipitates have formed, they are filtered out of the system. If the feed water already has a high concentration of sulphates, the solution in stage 1 can become oversaturated with gypsum due to the addition of lime.

2. The solution from stage 1 is mixed with gypsum crystals to catalyse the precipitation of gypsum. The resulting gypsum is then thickened, filtered, and separated from the rest of the solution to be discarded as waste or used as a by-product. The reaction that leads to the

formation of gypsum is represented by the following stoichiometric equation, according to Damons (2001):

$$Ca^{2+} + SO_4^{2-} + 2\ H_2O \rightarrow CaSO_4.2H_2O \quad [2.31]$$

3. The third stage, which is the essence of the SAVMIN process, involves the addition of aluminium hydroxide. This forms insoluble ettringite, removing both sulphate and calcium from solution (Equation 2.32). The pH level of the solution should range between 11.4—12.4 to maximise ettringite formation, and lime is added to maintain the appropriate pH range.

$$6Ca^{2+} + 2\ (OH)_3 + 3\ SO_4^{2-} + 37\ H_2O \rightarrow 3\ CaO{\cdot}3CaSO_4{\cdot}Al_2O_3{\cdot}31H_2O + 6\ H_3O^+ \quad [2.32]$$

4. The fourth stage involves the reduction of pH of the solution from stage 3 to neutral levels (7—8) by using carbon dioxide, resulting in the precipitation of calcium carbonate, which aids in the removal of calcium from solution (Equation 2.33).

$$H_2O + CO_2 \rightarrow CO_3^{2-} + 2H^+ \quad [2.33]$$

The reaction results in the formation of a carbonate ion (CO_3^{2-}) and two hydronium ions, which can lower the pH of the solution (Damons, 2001). Meanwhile, the CO_3^{2-} ions react with the Ca^{2+} ions in the solution to create calcium carbonate, as demonstrated by the Equation 2.34 (Damons, 2001).

$$Ca^{2+} + CO_3^{2-} \rightarrow CaCO_3\ (s) \quad [2.34]$$

By precipitating $CaCO_3$, the process not only changes the pH but also helps to eliminate calcium from the solution.

5. In the fifth and final stage of the process, the ettringite slurry is decomposed with the help of sulphuric acid, and the resulting solution is filtered to extract the insoluble aluminium hydroxide, which is then reused in stage three. This decomposition reaction occurs in water that is already saturated with gypsum at a specific liquid-to-solid ratio, which allows the calcium and sulphate ions to remain in the solution as supersaturated calcium sulphate. The reaction that occurs during decomposition is the reverse of the ettringite formation reaction, as described by Damons (2001). To crystallize the $CaSO_4$, the supersaturated solution is brought into contact with gypsum crystals, which are then removed from the system.

The hard water treatments methods that have been discussed thus far are those that are currently used in the water industry. The following section discusses a potential water treatment that may be used as an alternative physical treatment in reducing scale potential in hard water.

2.7 Magnetic water treatment

While chemical techniques are successful in managing scale in water, they often lead to substantial changes in the solution's chemistry. Many of these chemicals that can inhibit scale formation do not persist in the formation for a sufficient duration to be cost-effective and can be prohibitively expensive. Concerns related to the environment have spurred the investigation of alternative physical methods for preventing the formation of hard-scale, including the utilization of permanent magnets (Baker and Judd, 1996; Sawaftah, 2017). Ion exchange and precipitation using lime or soda ash are established chemical methods that have been used and researched for preventing scale build-up and water softening. These techniques, although effective, come with significant costs and the potential to alter the water's chemical composition substantially. Environmental and economic considerations have driven the development of approaches that focus on altering how scales precipitate (Lipus and Dobersek, 2007). One such physical method designed to avoid introducing chemicals into the water is magnetic water treatment (MWT), currently employed to prevent scale accumulation (Alimi et al., 2007; Lipus and Dobersek, 2007). Over the past few decades, various magnetic treatment devices (MTD) have been developed to achieve highly efficient scale prevention (Gilart et al., 2013; Lipus et al., 2011). In 1873, A.T. Hay was granted the first US patent for a water treatment apparatus utilizing a magnetic field. Nowadays, numerous such devices are readily available on the market (Busch et al., 1997).

Magnetism is a unique physical attribute that, on its own, contributes to water purification by affecting the physical characteristics of impurities in water. Furthermore, when combined with other methods, it enhances the efficiency of water purification technology (Ambashta and Sillanpää, 2010). The effectiveness of this treatment method is still a subject of debate and has been for many decades, with no clear explanation for the phenomenon (Baker and Judd, 1996; Cai et al., 2009; Fathi et al., 2006). Published data often presents conflicting results. While some researchers (Lipus and Dobersek, 2007; Parsons et al., 1997) argue that MWT has a significant impact on reducing scale, others claim it has only a minimal or no effect (Busch et al., 1997). The motivation behind the study on MWT and MTDs stems from the recognition that such a straightforward technology has the potential to bring about beneficial impacts in the

water industry. Magnetic treatment devices, in particular, offer several advantages, including low cost, energy-free operation, and the absence of waste products (Lipus and Dobersek, 2007; McMahon, 2009). In light of this, an extensive review of literature was conducted, focusing on experimental parameters and proposed mechanisms of MWT, with the objective of identifying studies that demonstrate efficiency, reproducibility, and acceptance within the scientific community.

2.8 Application of magnetic treatment on hard water

In contrast to chemical water softening, MWT is believed to not directly impact the chemistry of water. Instead, it is purported to alter the structure and adhesion of precipitates such as $CaCO_3$ scale. Coey and Cass (2000) made a significant discovery regarding the effect of magnetic fields on water in 2000. Carbonates formed by heating water containing more than 120 mg/L of Ca were analysed using X-ray diffraction and electron microscopy. The study involved testing 32 pairs of samples, which established, with a 99.9 % probability level, that drawing water through a static magnetic field (with a strength of 0.1 Tesla and a gradient of 10 Tesla per meter) increased the aragonite/calcite ratio in the deposit. This effect persisted for over 200 hours.

Previous research has demonstrated that MWT influences the crystallization of calcium carbonate, affecting both the type of precipitation (homogeneous and heterogeneous) and its solubility. This is achieved by increasing the overall amount of precipitation and encouraging its formation within the bulk solution rather than as encrustations on surfaces. These findings indicate a greater presence of aragonite in carbonate deposits, with calcite becoming less dominant (Alimi et al., 2009; Alimia et al., 2007; Mahmoud et al., 2016).Various experiments have been conducted on $CaCO_3$ solutions to investigate the effects of magnetic treatment, revealing that its efficiency is influenced by several factors. These factors include the concentration of $CaCO_3$ in the water, solution pH, the material of the pipe used, surface roughness, water flow rate, and the duration of exposure to the magnetic field (Coey and Cass, 2000; Gabrielli et al., 2001; Saksono et al., 2010; Higashitani et al., 1995). These studies shed light on the complex relationship between magnetic treatment and $CaCO_3$ solutions, highlighting the significance of these factors in determining the efficacy of the magnetic treatment process. Knez and Pohar (2005) passed a $CaCO_3$ solution through an electromagnetic chamber and found the amount of aragonite to have increased with time. The work of Holysz et al (2007) involved a solution of mixed salts (sodium chloride, potassium chloride, sodium

phosphate and calcium chloride) being sealed inside a magnetic chamber for varying times. They observed an increase in the conductivity of the electrolyte.

The potential for scaling in hard water following exposure to MWT can be assessed through various techniques, with scaling parameters being defined. These methods can be categorized into two groups: electrochemical and non-electrochemical. In the electrochemical category, the deposited mass can be quantified to determine the scaling rate, or studies involving electrochemical impedance can be conducted (Deslouis et al., 1997; Gabrielli et al., 1996; 2001). Non-electrochemical methods in some cases involve raising pH levels to induce $CaCO_3$ precipitation, while others entail heating or evaporating the solution (Euvrard et al., 1997; Fathi et al., 2006). In 2007, Lipusa & Dobersek achieved positive results by using MTD on a copper pipe spiral used for heating. The scale on a heating copper pipe spiral was 2.5 times thinner when treated with a magnetic field as opposed to untreated water. Additionally they observed a significant difference for the coating in the outlet pipe between magnetically treated and untreated lines. The treated lines had very little coating compared to the untreated water, which had a lot of scale build-up. Figure 2.17 shows the comparison of steel pipes, with the image on the right revealing reduced levels of scale build-up.

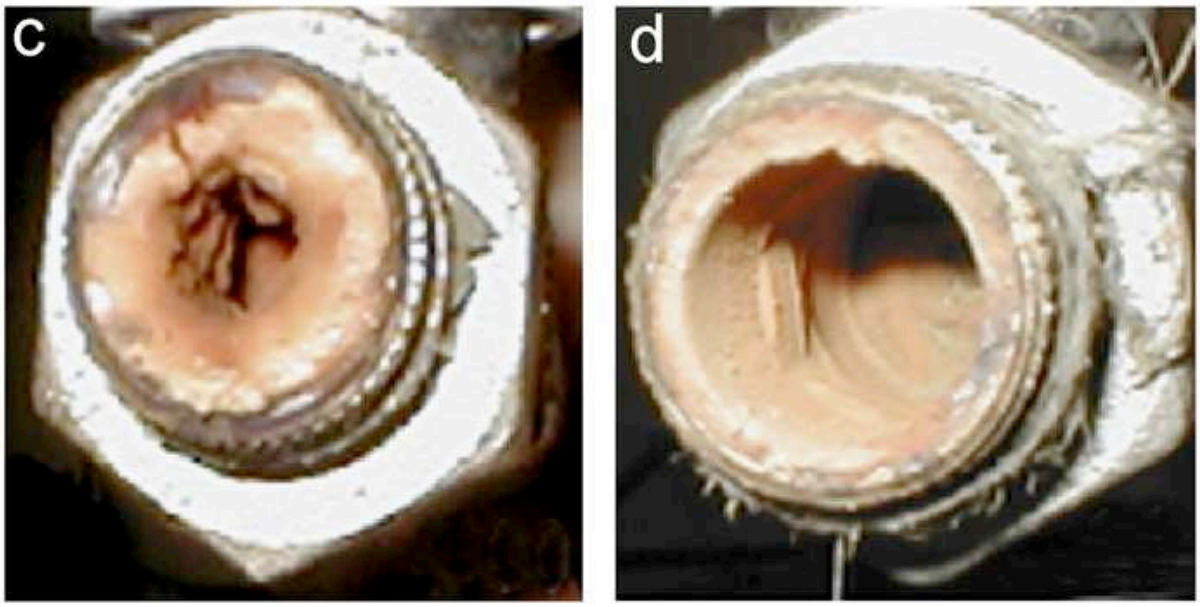


Figure 2. 17 MWT effect: Left (c) is the steel pipe without MWT. Right (d) shows a similar pipe treated with a magnetic field (Lipusa and Dobersek, 2007)

In a non-electrochemical study of scale formation, Mahmoud et al. (2016) examined the impact of magnetic treatment on the potential for scaling in hard water. Their research indicated that a magnetic field exhibits a "memory effect," implying that the scale-inhibiting properties of

treated water persist for an extended duration after magnetic treatment. Additionally, magnetic water treatment alters the crystallization of $CaCO_3$ by delaying its precipitation. A related study by Gryta (2011) also suggested that the flow of water through a magnetic field can significantly influence the form of $CaCO_3$. Much of the research conducted so far has focused on understanding how magnetic fields influence $CaCO_3$ (Alimia et al., 2007; Coey and Cass, 2000; Mahmoud et al., 2016). This focus is not surprising given that $CaCO_3$ is one of the most commonly encountered salts responsible for scale formation, along with $CaSO_4$. Previous studies investigating the impact of magnetic fields on $CaSO_4$ crystal morphology have indicated that subjecting the crystals to a magnetic field alters the direction of their growth. It enhances growth in one direction while suppressing it in others. This phenomenon may lead to the formation of weaker crystals that can be easily carried away by fluid shear forces. Alternatively, the increased surface area may promote bulk crystallization, providing favorable sites for crystal growth. The overall result is a reduction in scale formation on heat transfer surfaces (Alimi et al., 2007; Coey and Cass, 2000; Mahmoud et al., 2016).

While most if not all of these studies differ in solution composition, most of them claim notable observations. These many differences in sample composition make results comparison a difficult task, perhaps also reinforcing why there remains so much controversy on MWT efficiency. Authors agree, however, that while uncertainty exists on which parameters play an important role in experimental studies the main parameters include the type of magnets used, magnetic field strength, the pipe material, orientation of the magnetic poles and flowrate of the sample (Gabrielli et al., 2001; Holysz et al., 2007).

2.8.1 The development of MWT parameters

Magnetic devices can be categorized into two types: those based on electromagnets, which include solenoids and yoke-based electromagnets, and those utilizing permanent magnets. Electromagnets are capable of generating high magnetic field intensities; however, they come with practical challenges, requiring an electrical power supply, cooling, and periodic maintenance (Farshad and Vargas, 2002). On the other hand, permanent magnets are the preferred choice in designing Magnetic Treatment Devices (MTDs) due to their lower operational costs compared to electromagnets.

Neodymium magnets belong to the rare earth magnet family and are known for being the most permanent magnets globally. They are composed of neodymium (Nd), Fe, and boron (B). However, these magnets are susceptible to rust if exposed to environmental elements. To

protect the magnets from corrosion and reinforce the brittle magnet material, they are coated with nickel (Ambashta and Sillanpää, 2010; Coey, 1995, 1996; Croat, 2017; Shewane et al., 2014). Due to their exceptional magnetic properties, neodymium magnets have found widespread application in the field of magnetic treatment for hard water. These magnetic properties also play significant roles in other applications, ranging from designing and evaluating magnetic materials for use in electronics, motors, generators, and magnetic storage devices to understanding magnetic phenomena in materials science and physics (Ambashta and Sillanpää, 2010; Coey, 1995, 1996; Croat, 2017; Shewane et al., 2014). Generally (Croat, 2017; Herbst and Croat, 1991; Shewane et al., 2014), the important magnetic properties include:

1. *Magnetic Field (B):*

The magnetic field is a vector quantity that describes the influence or force that a magnetic material experiences in the presence of other magnets or electric currents (Coey, 1995, 1996; Croat, 2017; de Berg and Chapman, 2001; Herbst and Croat, 1991; Shewane et al., 2014). The magnetic field in neodymium magnets arises from the alignment of magnetic moments in the material's atomic structure. A magnetic moment is a property of a magnetic object or particle that results from the presence of magnetic poles (north and south poles) within the object. It is a vector quantity, which means it has both magnitude and direction. In physics, the magnetic moment can be described as the measure of the strength and orientation of the magnetic field produced by a magnetic object or particle. It is a fundamental property of magnetism and is a result of the alignment of the object's atomic or subatomic magnetic dipoles (Coey, 1995, 1996; Croat, 2017; de Berg and Chapman, 2001; Herbst and Croat, 1991; Shewane et al., 2014). For example, in a magnetic material like a permanent magnet, the magnetic moments of its atoms or atomic dipoles align in a consistent manner, creating a net magnetic field at a macroscopic level. In contrast, in non-magnetic materials, the magnetic moments of individual atoms or dipoles cancel out, resulting in no net magnetic field. The neodymium atoms have strong magnetic moments due to their electron configuration, and when they are combined with iron and boron, they form highly ordered crystalline structures (Figure 2.18) called magnetic domains (Coey, 1995, 1996; Croat, 2017; de Berg and Chapman, 2001; Herbst and Croat, 1991; Shewane et al., 2014).

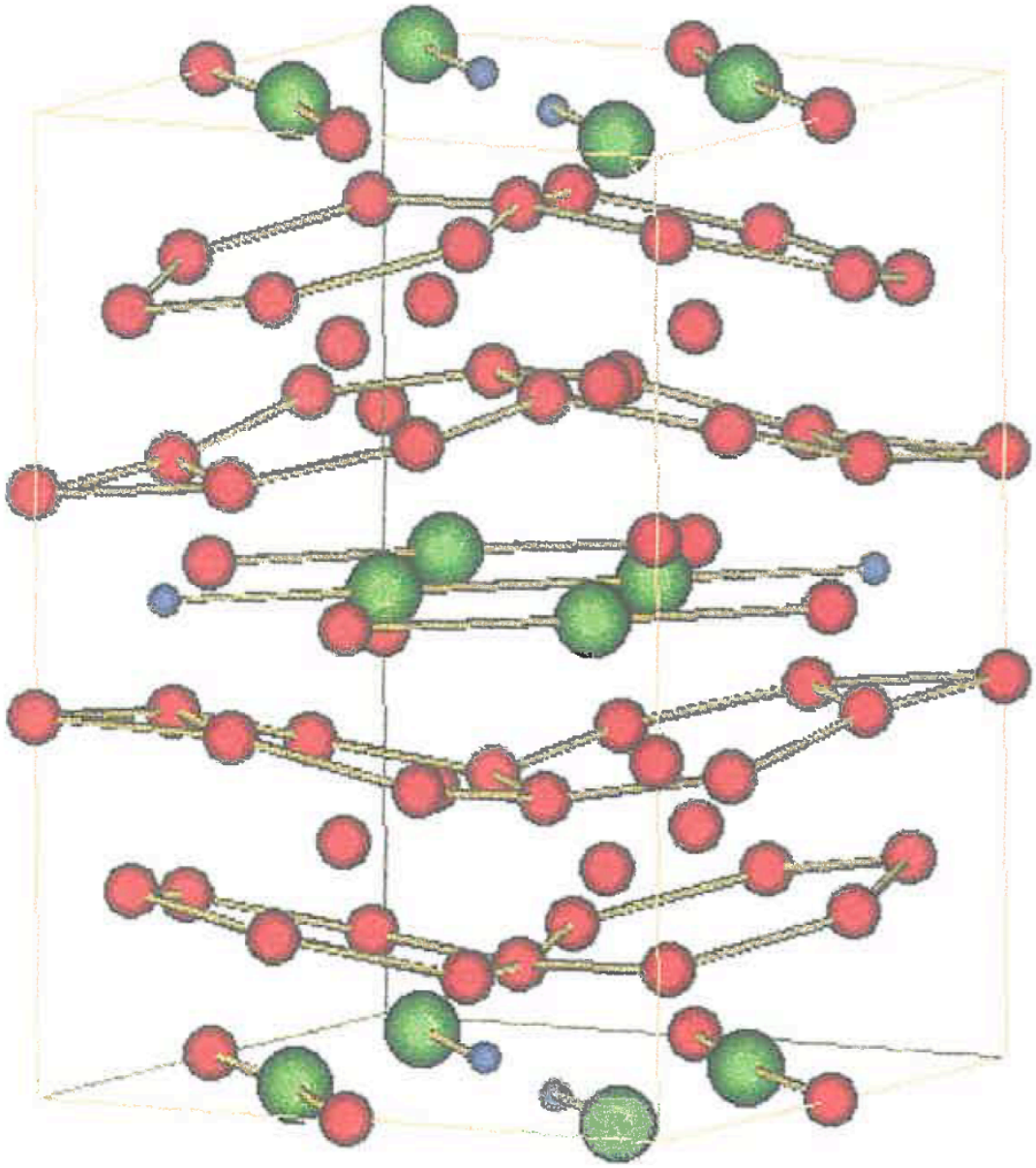


Figure 2. 18 The crystal structure of Nd (red), Fe (green), B (blue) (Coey, 1995).

In each magnetic domain, the atomic magnetic moments align in the same direction, creating a net magnetic field within that domain. In the process of manufacturing the magnets, these magnetic domains are aligned in the desired direction through a process known as magnetization. The magnetization can be done in either an axial, radial or diametrical direction, to achieve the desired magnetic field orientation in the final magnet (Coey, 1995, 1996; Croat, 2017; de Berg and Chapman, 2001; Herbst and Croat, 1991; Shewane et al., 2014). In *axial magnetization* the magnetic domains align along the length of the magnet, from one pole to the other. This is the most common

magnetization direction for cylindrical, rod-shaped and block permanent magnets. The magnetic field lines travel from the North pole to the South pole externally and from the South pole to the North pole internally (Figure 2.19). Block-shaped magnets are characterized by three dimensions: Length (L), width (W), and thickness (T). The thickness dimension is defined along the axis of magnetization (Coey, 1995, 1996; Croat, 2017; de Berg and Chapman, 2001; Herbst and Croat, 1991; Shewane et al., 2014).

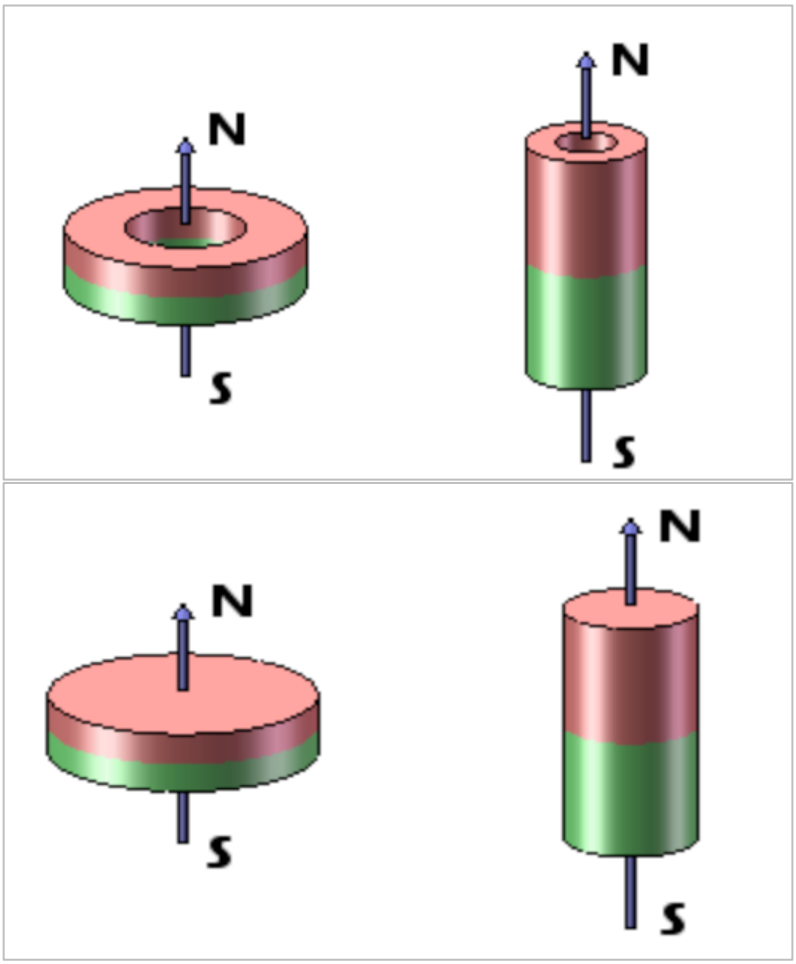


Figure 2. 19 Axially magnetized (*kjmagnets.com, 2022)*

In *radial magnetization* the magnetic domains align along the radial direction of the magnet, from the center to the outer edge. This is often used for ring-shaped or disc-shaped magnets (Coey, 1995, 1996; Croat, 2017; de Berg and Chapman, 2001; Herbst

and Croat, 1991; Shewane et al., 2014). The magnetic field lines form a loop from the inner circumference to the outer circumference of the magnet (Figure 2.20).

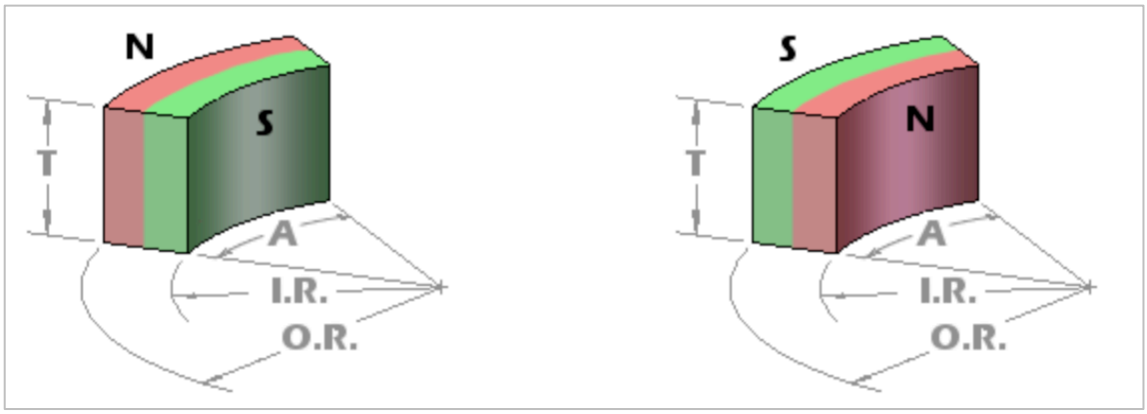


Figure 2. 20 Radially magnetized (*kjmagnets.com, 2022)*

In contrast to axial magnetization direction, *diametric magnetization* direction occurs along the breadth or diameter of the magnet. In diametrical magnetization, the poles are on the curved side of the magnet if the magnet is cylindrical. This means the magnet will be more efficient if the curved side is near the material you want it to attract (Figure 2.21)

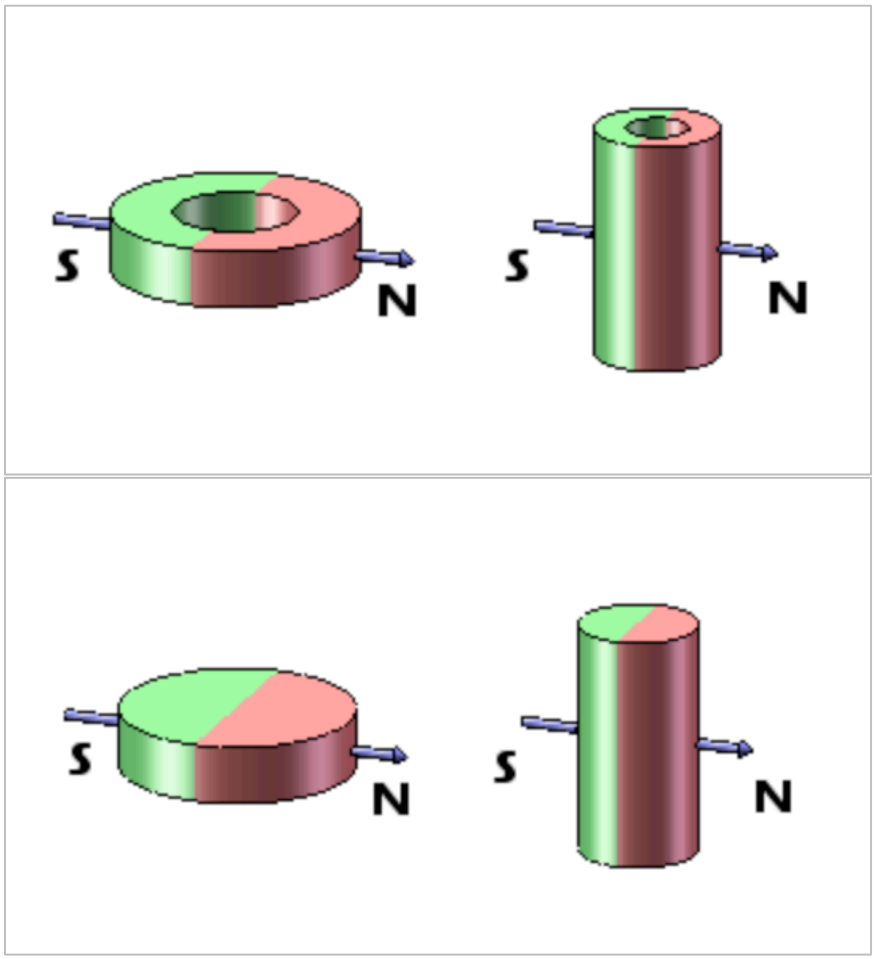


Figure 2. 21 Diametrically magnetized (*kjmagnets.com, 2022*)

2. *Magnetic Flux Density (B):*

Magnetic flux density, also known as magnetic induction, measures the strength of the magnetic field at a particular point in space. It is the amount of magnetic flux passing through a unit area perpendicular to the magnetic field.

3. *Remanence (Br):*

Measured in millitesla (mT) or gauss (G), remanence is the residual magnetic flux density that remains in a magnetic material after an external magnetic field is removed. It represents the material's ability to retain magnetization. Neodymium magnets have an extremely high remanence, typically ranging from 1.1 to 1.4 teslas (11,000 to 14,000 gauss). This means that even after the external magnetic field is removed, they retain a significant amount of magnetization, making them ideal for various applications.

4. *Coercivity (Hcb):*

Coercivity is the magnetic field strength required to reduce the magnetic induction (B) in a material to zero after it has been fully magnetized. It is measured in kiloampere per meter (KA/m) or kilooersted (KOe). High coercivity indicates a strong ability to resist demagnetization. Neodymium magnets have high coercivity values, typically around 800 to 1200 kiloampere per meter (KA/m) or 10 to 15 kilooersted (KOe). This implies that a substantial amount of magnetic field strength is required to demagnetize these magnets once they have been fully magnetized.

5. *Intrinsic Coercivity (Hcj):*

Similar to coercivity, intrinsic coercivity represents the resistance of a magnetic material to demagnetization but is measured under conditions where the external magnetic field is applied in the opposite direction to the initial magnetization. It is also measured in KA/m or KOe. The intrinsic coercivity of neodymium magnets is even higher than the coercivity. It ranges from 800 to 2500 KA/m or 10 to 30 KOe. This makes them very resistant to demagnetization, even under opposing magnetic fields.

6. *Maximum Energy Product ((BH)max)*:

This property quantifies the maximum amount of magnetic energy that a material can store per unit volume. It is measured in kilojoules per cubic meter (KJ/m^3) or mega-gauss-oersted (MGOe). A higher (BH)max value indicates a more powerful magnet. Neodymium magnets exhibit an outstanding maximum energy product, typically ranging from 200 to 400 kilojoules per cubic meter (KJ/m^3) or 25 to 50 mega-gauss-oersted (MGOe). This high (BH)max value means that they can store a significant amount of magnetic energy, making them incredibly powerful for their size.

7. *Pull Strength*:

This property refers to the maximum force or weight that a magnet can hold or attract. It is typically measured in kilograms (Kg) and represents the magnet's ability to provide mechanical holding strength. Due to their high remanence and (BH)max values, neodymium magnets have impressive pull strength. have impressive pull strength. They can exert substantial magnetic force and are widely used in applications where a strong holding force is required, such as in magnetic closures, fasteners, motors, speakers, and magnetic separation systems.

These magnetic properties play significant roles in various applications, ranging from designing and evaluating magnetic materials for use in electronics, motors, generators, and magnetic storage devices to understanding magnetic phenomena in materials science and physics (Ambashta and Sillanpää, 2010; Croat, 2017; Herbst and Croat, 1991; Shewane et al., 2014).

With recent advances in materials, it is possible to increase the magnetic field strength of multiple permanent magnets from ~ 1 Tesla (T) to ~2 T (Kobe et al., 2002). Most studies in scale reduction use multiple permanent magnets to achieve a stronger magnetic field despite producing less than 1 T. Successful treatment can be achieved with a magnetic field of at least 0.5 T, with some studies even claiming reduction in scale with magnetic field lower than 0.5 T (Fathi et al., 2006; Kobe et al., 2002). The studies that have been reviewed typically feature designs with the water sample flowing through the magnetic field or stagnant solutions exposed to the magnetic field from a few minutes to 60 minutes on average (Gabrielli et al., 2001; Holysz et al. 2007; Kobe et al., 2002; Li et al., 2007; Rathilal, 2004; Sawaftah, 2017). These designs also involve the magnetic poles arranged in an alternating and non-alternating design (Figure 2.22 (A, B)) or inverted or non-inverted, respectively.

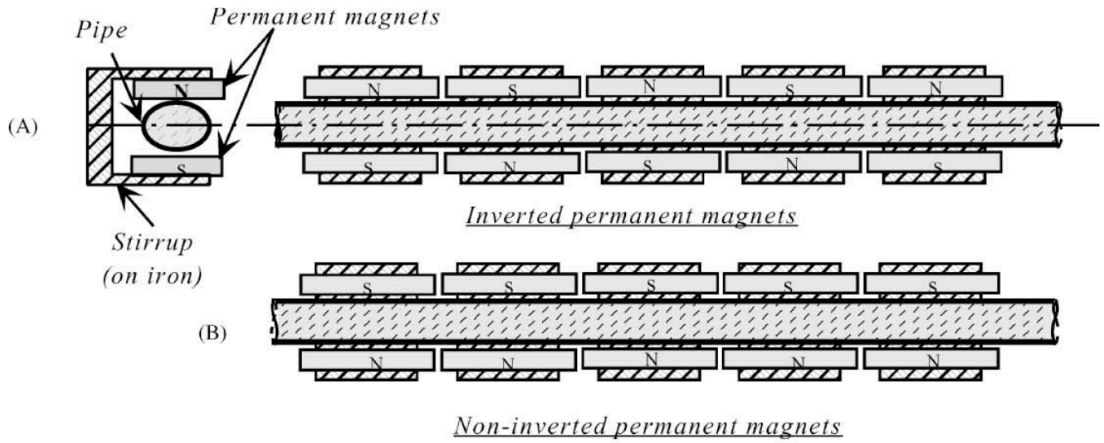


Figure 2. 22 Scheme of the MTD with alternated magnetic poles (inverted), (B) scheme of the MTD without inversion of the magnetic poles (non-inverted) (Gabrielli et al., 2001).

In MWT systems with alternating magnetic poles, magnets with alternating polarity are used. For example, the magnets may be arranged in a configuration where the north pole of one magnet faces the south pole of the next magnet, and so on. The magnetic field lines between the alternating poles create a constantly changing magnetic gradient within the water flow (Figure 2.23).

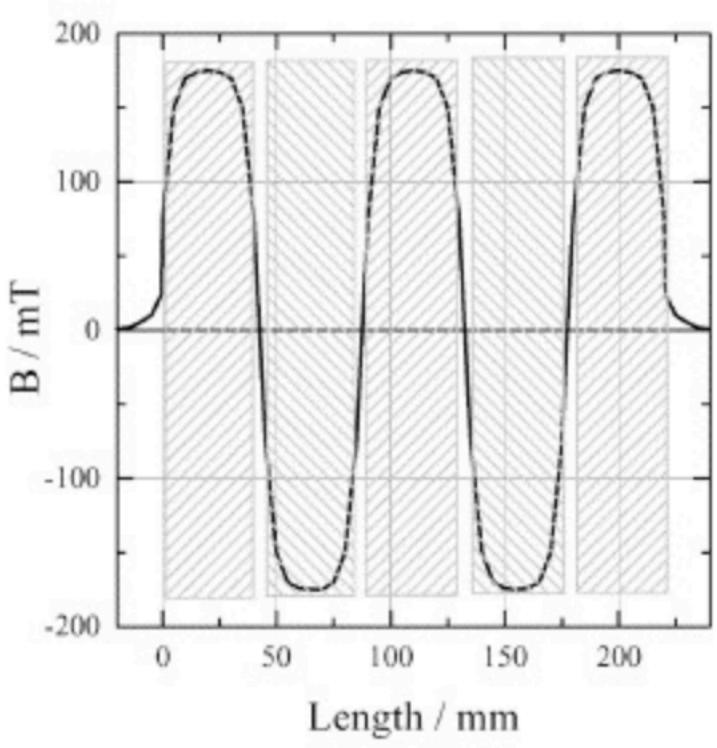


Figure 2. 23 Variation of the magnetic induction for inverted pairs of permanent magnets (Gabrielli et al., 2001).

Advocates of alternating magnetic poles in MWT claim that the changing magnetic gradient induces various effects on the water, potentially reducing scale formation, altering crystal growth, and affecting the behaviour of dissolved minerals (Fathi et al., 2006; Gabrielli et al., 2001; Lipus, and Dobersek, 2007). In MWT systems with non-alternating magnetic poles, magnets with the same polarity (either all north or all south poles) are used. The magnetic field lines from these magnets create a more uniform magnetic gradient within the water flow (Figure 2.24).

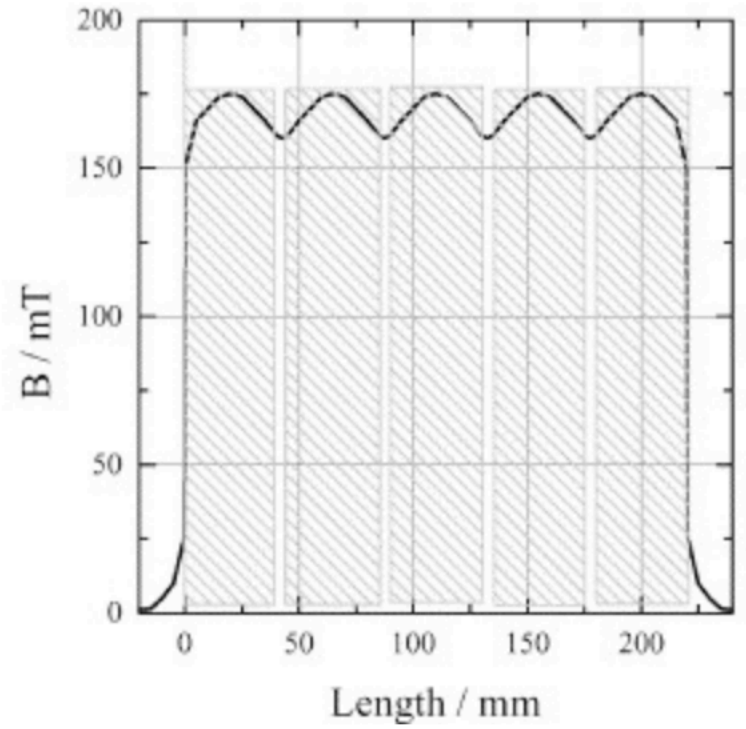


Figure 2. 24 Variation of the magnetic induction in the gap for non-inverted pairs of permanent magnets (Gabrielli et al., 2001).

Some authors argue that a more uniform magnetic field may lead to better results in MWT. They believe that a stable magnetic field can influence the arrangement of water molecules and affect the crystallization process, potentially reducing scale formation and improving water quality.

Fathi et al (2006) and Gabrielli et al (2001) put together a MTD with multiple pairs of permanent magnets arranged with alternating poles facing each other. The design allowed water to be pumped through the system as depicted in Figure 2.25.

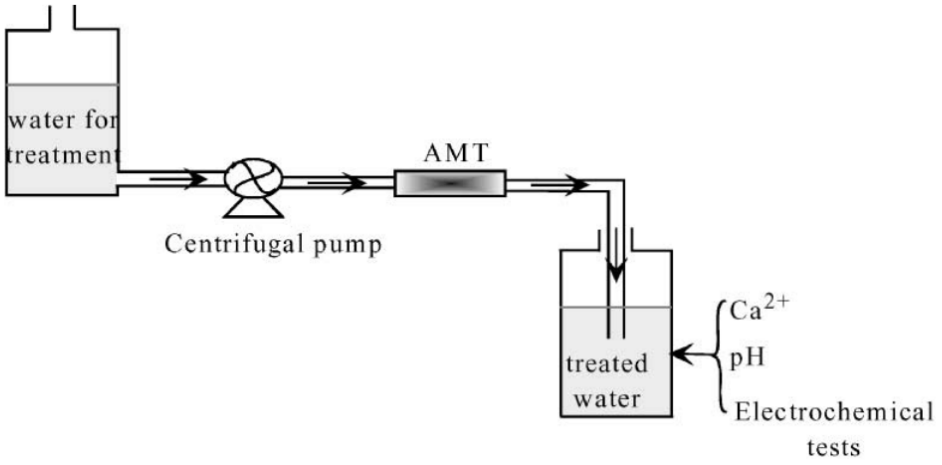


Figure 2. 25 Typical MTD setup for water treatment (Gabrielli et al., 2001).

Regarding the construction of Magnetic Treatment Devices (MTDs), the simplest unit may involve just one magnet attached externally to a water pipe. In certain cases, the magnet is positioned inside the pipe through which the treated water flows (Busch et al., 1986) (as shown in Figure 2.26). Commercial MTDs are available in various configurations and are offered by numerous manufacturers. These devices can utilize either electromagnets or single or arrays of permanent magnets, with varying magnetic field orientations (Rathilal, 2004; Sawaftah, 2017). Some MTDs are considered intrusive, meaning they are integrated into the plumbing and must adhere to relevant regulations. Others are non-intrusive and simply clamped onto the pipes (as seen in Figure 2.26). The cost of these units varies with their size and can range up to thousands of pounds. Additionally, some units employ a magnetic field oriented approximately perpendicular to the direction of water flow, while others primarily use a parallel field (Rathilal, 2004; Sawaftah, 2017).

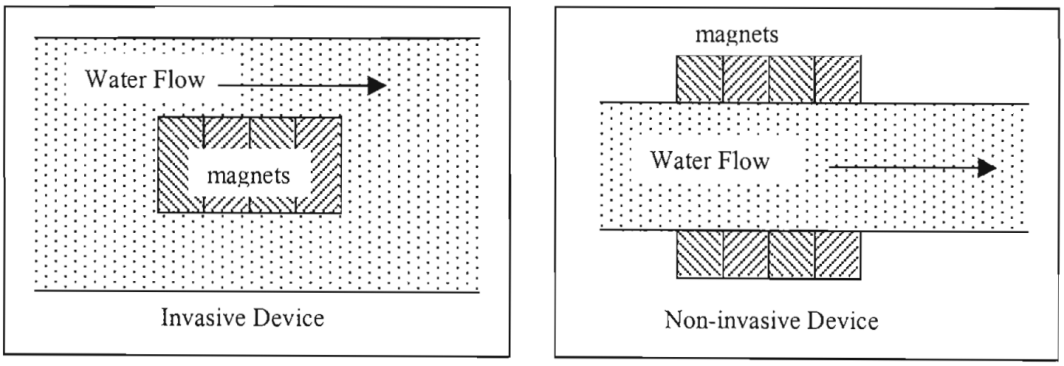


Figure 2. 26 Variations in Installation of Magnets (Rathilal, 2004).

The rate at which the samples flows through the MTD could be an important factor. Kobe et al (2002) states that the sample must pass through the magnetic field at velocities of 0.5—2 m/s for measurable observations. Strazisar et al (2001) carried out static and dynamic (i.e. whether fluid is stagnant or flowing) sample treatment through a MTD and both treatments had higher amounts of aragonite formed from $CaCO_3$ solutions compared to those without treatment. Higher crystal nucleation was observed in the bulk solution as the flow rate increased. Additionally, almost all the studies suggested that the sample flow perpendicular to the applied magnetic field, perhaps to induce the Lorentz force successfully (discussed in detail in section 2.7.3) (Alimi et al., 2009). The material of the pipe of the MTD has shown to be an important factor in the amount of scale that may form on the surface. It is suggested that the combination of the material of the surface and the magnetic field leads to a decrease in scale formation (Alimi et al., 2009). Conclusions were made on magnetic fields being lower for conductive materials such as copper and stainless steel (although less scale was formed) while more scale formation was more evident in non-conducting materials such as PVC and Tygon (Alimi et al., 2009).

2.8.2 Magnetization and the exhibition of a magnetic field on charged particles

Particles or molecules can be categorized as positively charged (positive χ) or negatively charged (negative χ), where χ is their magnetic susceptibility. Their magnetization M can be expressed as

$$M = \chi v.H \qquad [2.35]$$

Here, H represents the applied magnetic field in emu/cm^3, M signifies the magnetization of a particle following exposure to H, and χv denotes the measured magnetic susceptibility arising from the magnetization of the molecules' electrons. Molecular substances can be categorized as either polar or non-polar, as demonstrated in Figure 2.27. In the absence of a magnetic field, polar molecules have a random orientation, which makes it difficult for their positive and negative charges to align, even though molecular collisions occur. However, when exposed to a magnetic field of a certain intensity, polar molecules readily align themselves based on their positive and negative charges (Quinn, 1997; Zaidi et al., 2013).

Conversely, non-polar molecules, when not subjected to a magnetic field, exhibit continuous random movement because their positive and negative charges coincide at the centres of the molecules. This impedes coagulation. Nevertheless, when influenced by a magnetic field, the positive and negative charges within non-polar molecules can be separated.

As a result, the molecules align themselves in accordance with the magnetic field's direction. This orderly arrangement, as depicted in Figure 2.27, leads to the coagulation and aggregation of particles. Furthermore, an increasing field strength results in a higher number of dipoles aligning with the field direction, enhancing the likelihood of particle coagulation and the removal of rare or unnecessary particles or pollutants (Quinn, 1997; Zaidi et al., 2014).

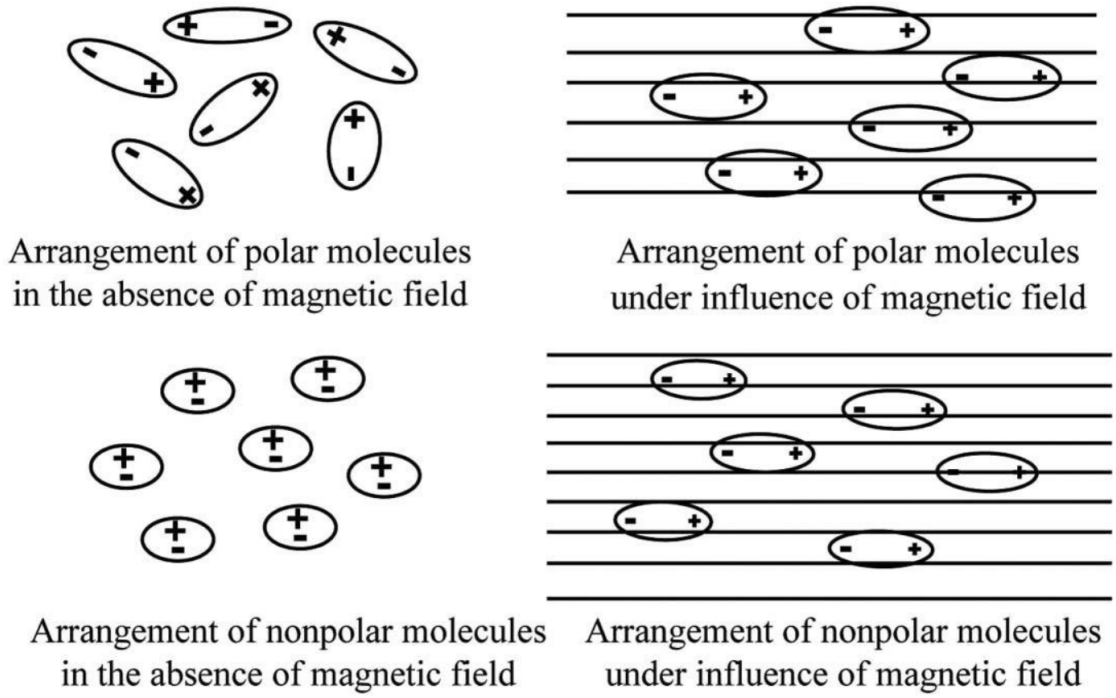


Figure 2. 27 Effect of a magnetic field on polar (top) and nonpolar (bottom) molecules (Sawaftah, 2017)

2.8.2.1 Water chemistry and the effect of an applied magnetic field

Water molecules possess a dipole moment due to the sharing of electrons by the two hydrogen atoms, resulting in a positively charged end and a negatively charged end (Figure 2.28). This dipole moment has been suggested to cause the water molecule to behave like a small magnet. Solubility, which is an important property of water, is influenced by the dipole moment, which is a vectorial quantity. Research has shown that the dipole moment of a water molecule is

similar to that of a magnet. As previously mentioned in section 2.8.2, when exposed to a magnetic field, polar molecules, including water, exhibit distinctive orientation (Figure 2.28) (Quinn, 1997; Zaidi et al., 2014).

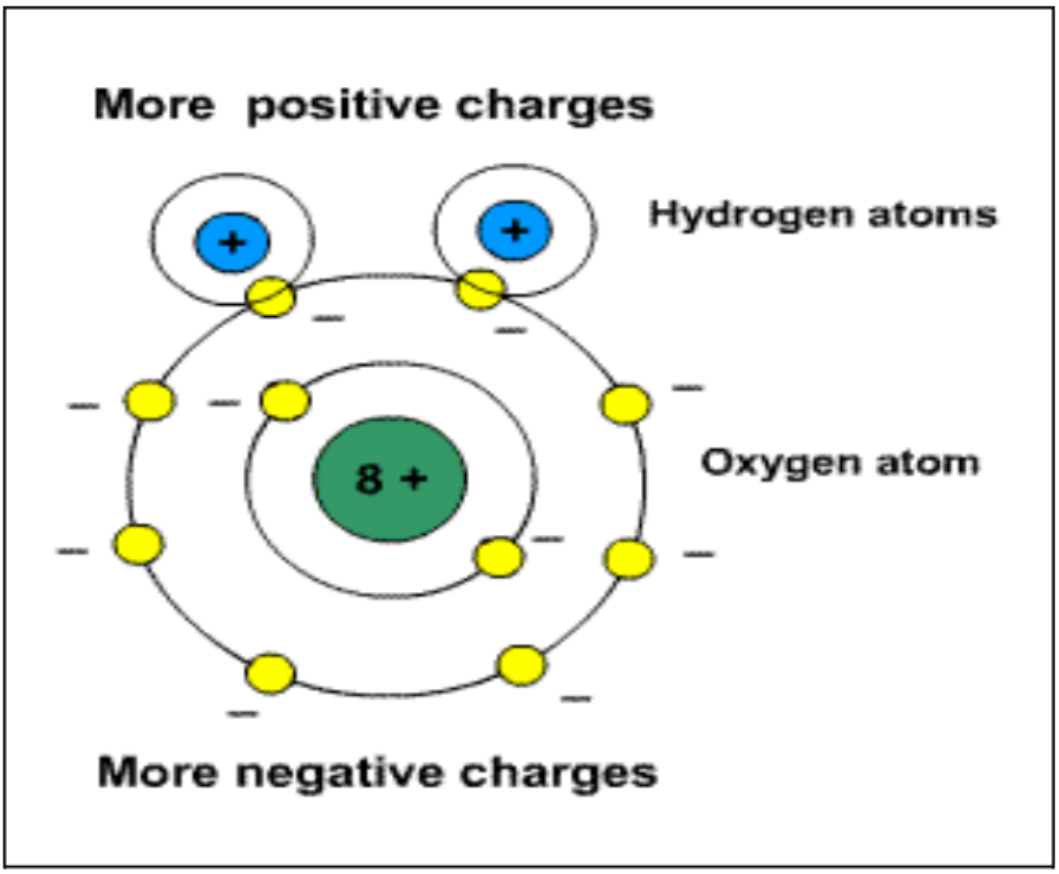


Figure 2. 28 Dipole moment of a water molecule (McMahon, 2009)

When a salt (e.g. $CaCO_3$/$CaSO_4$) dissolves in water, the dipolar water molecules form a hydration shell surrounding the resulting cations and anions. This is called the Stern layer. The Stern layer is made up of made up of water molecules that are closest to the ion and the diffuse layer is made up water molecules further bounded away from the ion (Rathilal, 2004; Su and Wu, 2003) (Figure 2.29).

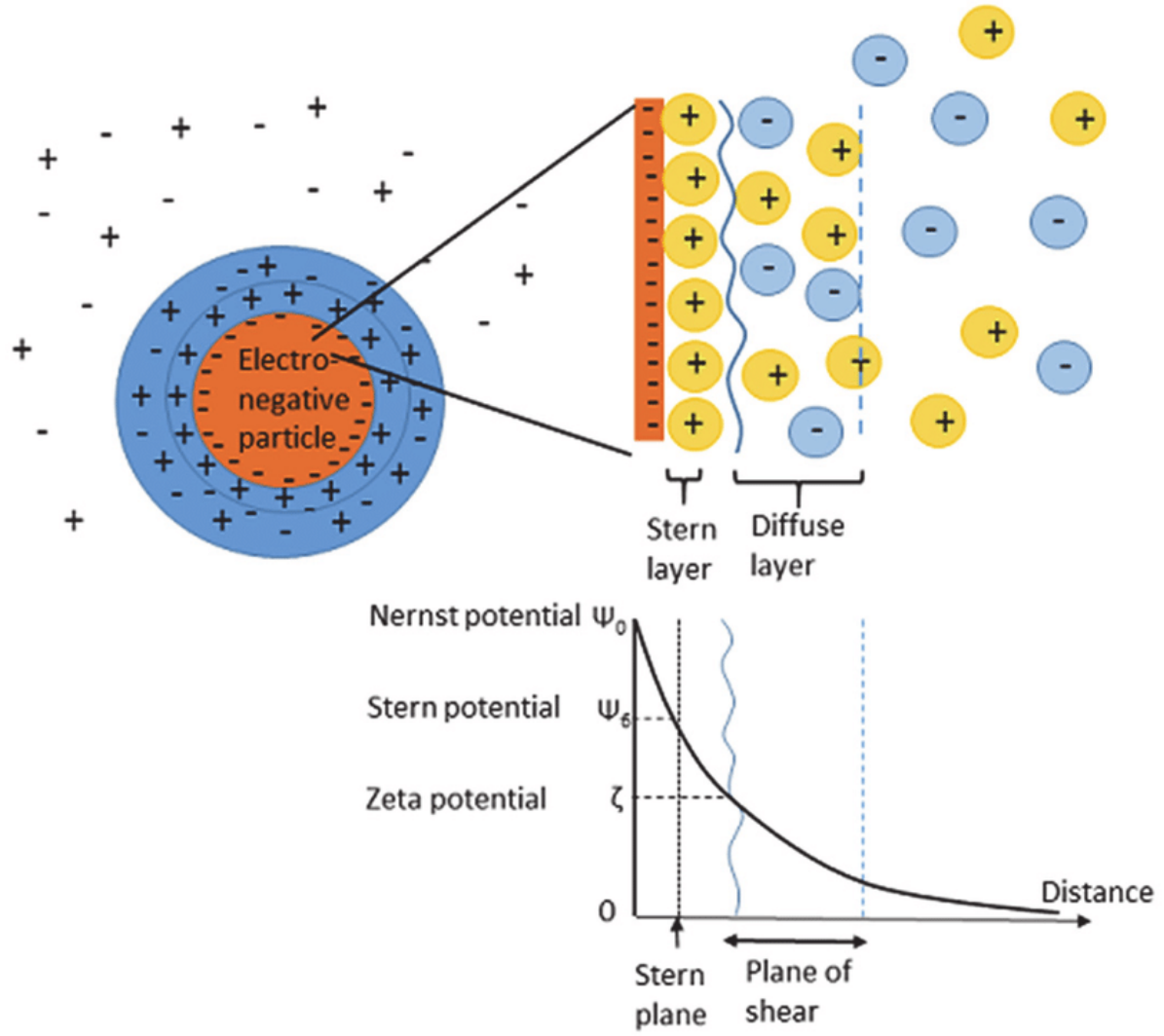


Figure 2. 29 Representation of the electrical double layer (Stern and diffuse layer) (Suopajarvi, 2015).

The hydration shells keep the cations and anions separated and they cannot combine unless there is a disturbance of some kind (such as an applied magnetic field) to the hydration shell, which allows the ions to attract and form a floc. Inside the diffuse layer is a boundary where the ion and its associated water molecules as an entity. This boundary is called the 'surface of hydrodynamic sheer' and its potential is measure by the Zeta potential, which reflects the degree of repulsion or attraction between ions (Rathilal, 2004; Su and Wu, 2003).

According to Holysz et al. (2007), an applied magnetic field changes the hydrogen bonds within water, altering how water molecules arrange themselves around ions within a hydration shell. Holysz et al. (2007) observed that when water is exposed to a magnetic field, it experiences changes in electrical conductivity and evaporation rate. These alterations depend on the type of ions present in the solution and are related to the thickness of the hydration shell around the

ions and the thermodynamic functions of hydration. As a result, Holysz et al. (2007) theorised that the magnetic field modifies the hydration shell, which causes a reduction in scaling. Furthermore, changes in the hydrogen bonding abilities of water during magnetic fluid treatment were identified as the reason for the enhanced evaporation rates observed in the treated samples during the research. Pang and Feng (2003) developed a theoretical framework to describe the relationship between magnetic fields and water structure at the quantum and molecular levels, which was used to explain experimental observations regarding ion mobility and electrical conductivity in water. Cai et al. (2009), Wang et al. (2013) and Pang and Deng (2008) observed that the presence of a magnetic field (~ 0.27 – 0.5 T) enhanced hydrogen bonding among water molecules, which was attributed to the effect of the Lorentz force on protons, promoting bonding with water to form hydronium (H_3O^+).

2.8.3 Mechanisms of magnetic mater treatment

Determining the mechanism on how a magnetic field influences changes in the properties of the water sample is important in justifying any changes that may occur after exposure to a MWT. Various mechanisms can be employed to prevent magnetic scale formation, depending on whether the scaling solution is in a static or dynamic state. Under dynamic conditions, many researchers have proposed that the primary mechanism at play is magnetohydrodynamics (MHD). For this process to be efficient, it's crucial that the magnetic field is perpendicular to the flow of the solution, the fluid should exhibit rapid movement, and the distance between the magnets should be minimal. In this phenomenon, it is suggested that the Lorentz force influences ions and dispersed particles (Alabi et al., 2015; Coey and Cass, 2000; Mosin and Ignatov, 2015a; 2015b).

The Lorentz force affects charged particles when they move through a magnetic field. This force increases proportionally with the particle's charge, velocity, and the perpendicular component of the magnetic field strength (Baker and Judd, 1996). As shown in Figure 2.30, when charged particles move perpendicular to the direction of the magnetic field within the same plane, they generate a Lorentz force. This force acts at a right angle to both the flow direction of the charged particles and the direction of the magnetic field (Baker and Judd, 1996; Spiegel and Yeck, 1998; Zaidi et al., 2014).

It has been established that the Lorentz force plays a role in enhancing various water-related mechanisms, including improving dissolution, promoting the formation of crystallization

nuclei, stabilizing coordinated water, and distorting the double layer (Baker and Judd, 1996; Busch et al., 1986).

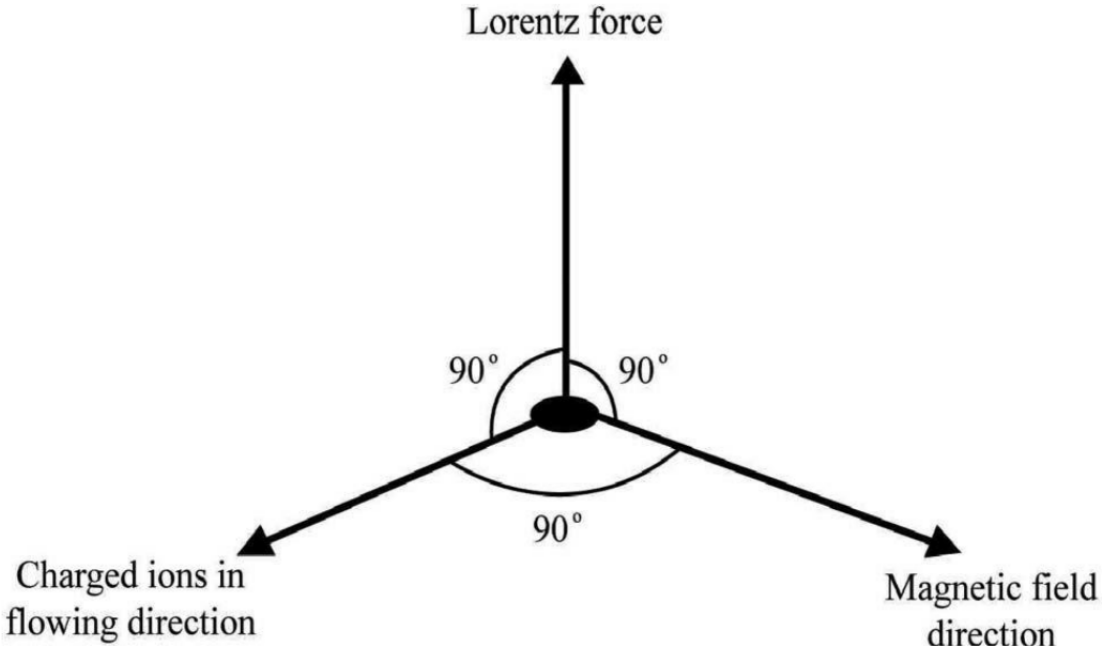


Figure 2. 30 The Laplace-Lorentz force on a moving charged ion is at a right angle of both the ion flowing direction and the magnetic field direction (Sawaftah, 2017)

The operational principle of existing magnetic devices relies on the influence of the exposed magnetic field generated by permanent magnets or electromagnets on dissolved hydrated metal cations, such as Ca^{2+}, Mg^{2+}, Fe^{2+}, and Fe^{3+}, as well as the structure of hydrates and water associations. This leads to a modification in the electrochemical coagulation rate and the stability of aggregated charged particles within a magnetized water stream. It also results in the creation of numerous nucleation sites on the particles of finely dispersed matter (Alabi et al., 2015; Coey and Cass, 2000; Mosin and Ignatov, 2015a; 2015b).

The phenomenon of electrical generators, as depicted in Figure 2.31, provides a common illustration of the Lorentz force. When an electric current I flows through a wire placed in a magnetic field B, each of the moving charged particles within the current experiences the Lorentz force F. This force can also manifest when these moving charged particles are subjected to both magnetic and electric fields (Baker and Judd, 1996). The induced Lorentz force exerts a macroscopic influence on the wire, leading to the creation of a motional electromotive force (EMF). This EMF serves as the driving factor in many electrical

generators. When a conductor moves through a magnetic field, the Lorentz force endeavours to push electrons through the wire, resulting in the generation of EMF.

Equation 2.36 describes the Lorentz force exerted on a charged particle and is given by:

$$F = qvx\ B \qquad [2.36]$$

where, q = charge of the particle (coulomb), v = velocity of the particle (m/s) and B = magnetic field applied (Tesla). This principle was utilized in the development of a Magnetic Treatment Device (MTD) for water applications, with the aim of preventing lime scale deposition on pipe walls (Baker and Judd, 1996; Busch et al., 1986).

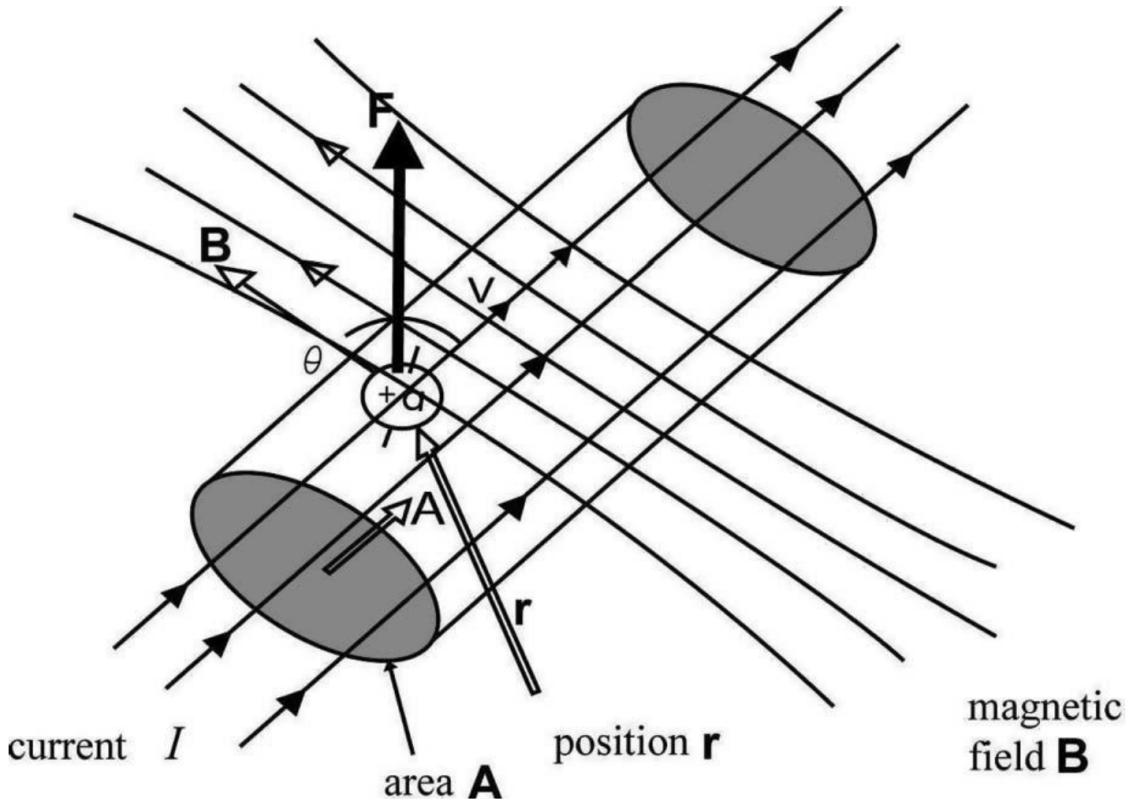


Figure 2. 31 An electric wire with cross-section A flown by a current I is submitted to a force F when placed into a magnetic field B (Sawaftah, 2017)

A few processes are proposed from the literature surveyed thus far to occur during magnetic water treatment:

1. *Increase in the nucleation of dissolved salts in the bulk volume of water:*

Busch (1997) suggested that the magnetic effect is attributed to ferromagnetic impurities, which function as nucleation seeds. A study by Herzog et al. (1989) produced comparable

findings. Their research revealed that minimal Fe^{2+} concentrations significantly impeded the growth of calcite but had no such effect on aragonite. Additionally, trace Fe^{2+} concentrations inhibited the transformation of aragonite into calcite.

2. *Alterations in the coagulation and sedimentation rates of dispersed particles when subjected to a magnetic field treatment:*

Magnetic Water Treatment (MWT) has been shown to reduce nucleation rates while accelerating crystal formation, as reported by several researchers (Higashitani et al., 1993; Parsons et al., 1997). According to Coey and Cass (2000), this alteration in scale formation might be attributed to the preferential growth of the aragonite crystal structure over calcite. According to Gabrielli et al. (2000), aragonite crystals have a needle-like shape with limited adhesion to substrates, making them more susceptible to being carried away by liquid flow. In contrast, calcite, the more stable calcium carbonate polymorph at room temperature, forms dense and resilient layers that are challenging to remove mechanically.

3. *The Lorentz force is credited as the main force behind an applied magnetic field onto a solution as discussed in section 2.8.3.1:*

The underlying processes of MWT seem to vary depending on the specific application. Nevertheless, the literature reviewed has provided valuable insights into determining the ideal configuration of an MTD for scale reduction. An effective MTD for reducing scale should have a magnetic field intensity of at least 0.5 Tesla or higher. Additionally, the solution should pass through the device multiple times, and the piping material should be constructed from conductive materials like steel or copper. It is also advisable to use alternating magnet orientations for the best results. However, to ensure the success of this study and the treatment of the specific water samples, it is crucial to determine the optimal parameters, as detailed in Chapter 3.

When comparing the use of chemicals in water treatment from 1981 to 2018, it is evident that not only has chemical usage increased, but there is also a greater diversity of compounds being employed (Gitis and Hankins, 2018). Therefore, it is worth investigating the potential of MWT as a physical magnetic water treatment method. This approach has the potential to serve as a safe and environmentally friendly alternative to the use of harsh chemicals.

2.9 References

Abbasnia, A., Yousefi, N., Mahvi, A.H., Nabizadeh, R., Radfard, M., Yousefi, M. and Alimohammadi, M., 2019. Evaluation of groundwater quality using water quality index and its suitability for assessing water for drinking and irrigation purposes: Case study of Sistan and Baluchistan province (Iran). Human and Ecological Risk Assessment: An International Journal, 25(4), pp.988-1005.

Ahmed, S., Chughtai, S. and Keane, M.A., 1998. The removal of cadmium and lead from aqueous solution by ion exchange with Na- Y zeolite. Separation and purification technology, 13(1), pp.57-64.

Al-Roomi, Y.M. and Hussain, K.F., 2016. Potential kinetic model for scaling and scale inhibition mechanism. Desalination, 393, pp.186-195.

Alabi, A., Chiesa, M., Garlisi, C. and Palmisano, G., 2015. Advances in anti-scale magnetic water treatment. Environmental Science: Water Research & Technology, 1(4), pp.408-425.

Alimi, F., Tlili, M., Amor, M.B., Gabrielli, C. and Maurin, G., 2007. Influence of magnetic field on calcium carbonate precipitation. Desalination, 206(1-3), pp.163-168.

Alimi, F., Tlili, M.M., Amor, M.B., Maurin, G. and Gabrielli, C., 2009. Effect of magnetic water treatment on calcium carbonate precipitation: Influence of the pipe material. Chemical Engineering and Processing: Process Intensification, 48(8), pp.1327-1332.

Ambashta, R.D. and Sillanpää, M., 2010. Water purification using magnetic assistance: a review. Journal of hazardous materials, 180(1-3), pp.38-49.

Antony, A., Low, J.H., Gray, S., Childress, A.E., Le-Clech, P. and Leslie, G., 2011. Scale formation and control in high pressure membrane water treatment systems: A review. Journal of membrane science, 383(1-2), pp.1-16.

Álvarez-Ayuso, E., Querol, X. and Tomás, A., 2006. Environmental impact of a coal combustion-desulphurisation plant: Abatement capacity of desulphurisation process and environmental characterisation of combustion by-products. Chemosphere, 65(11), pp.2009-2017.

Aly, A.I., Halhouli, K.A. and Abu-Ashur, B.M., 1999. Flue gas desulphurization processes.

Amber series (2022). Home. Available at: https://wwww.dupont.com/brands/amber-series.html/(accessed: January 19, 2022).

Amiri, M.C., Dadkhah Ali, A., 2006. On reduction in the surface tension of water due to magnetic treatment. Colloids and Surfaces A: Physicochemical and Engineering Aspects 278, 252–255.

Andreasen, A. and Mayer, S., 2007. Use of seawater scrubbing for SO2 removal from marine engine exhaust gas. Energy & fuels, 21(6), pp.3274-3279.

Apell, J.N. and Boyer, T.H., 2010. Combined ion exchange treatment for removal of dissolved organic matter and hardness. Water Research, 44(8), pp.2419-2430.

Aquilano, D., Otálora, F., Pastero, L. and García-Ruiz, J.M., 2016. Three study cases of growth morphology in minerals: Halite, calcite and gypsum. Progress in Crystal Growth and Characterization of Materials, 62(2), pp.227-251.

Atekwana, E.A., Atekwana, E.A., Rowe, R.S., Werkema Jr, D.D. and Legall, F.D., 2004. The relationship of total dissolved solids measurements to bulk electrical conductivity in an aquifer contaminated with hydrocarbon. Journal of Applied Geophysics, 56(4), pp.281-294.

Axelrad, B.A., Freeport Sulphur Co, 1959. Removal of calcium sulphate scale. U.S. Patent 2, 884,349.

Bailey, S.E., Olin, T.J., Bricka, R.M. and Adrian, D.D., 1999. Removal of metal ions from aqueous solution by chelating polymeric microsphers. Water Res, 33, pp.2469-2479.

Baker, J.S. and Judd, S.J., 1996. Magnetic amelioration of scale formation. Water Research, 30(2), pp.247-260.

Bates, W., 2001. RO Water Chemistry. Hydranautics Membrane Corp. technical paper posted on website http://www. hydranautics. com/docs/papers/04_ro_water_chemistry. pdf.

Behrends, B. and Liebezeit, G., 2003. Reducing SO2 and NOX emissions from Ships by a seawater scrubber. BP Marine Report, 34.

Bezuidenhout, G.A., Davis, J., Van Beek, B. and Eksteen, J.J., 2012. Operation of a concentrated mode dual-alkali scrubber plant at the Lonmin smelter. Journal of the Southern African Institute of Mining and Metallurgy, 112(7), pp. 657-665.

Borgwardt, R.H. and Harvey, R.D., 1972. Properties of carbonate rocks related to sulphur dioxide reactivity. Environmental Science & Technology, 6(4), pp.350-360.

Boyd, C.E., Tucker, C.S. and Somridhivej, B., 2016. Alkalinity and hardness: critical but elusive concepts in aquaculture. Journal of the World Aquaculture Society, 47(1), pp.6-41.

Braden, J.B., Kolstad, C.D., Woock, R.A. and Machado, J.A., 2001. Is coal desulphurisation worthwhile? Evidence from the market. Energy policy, 29(3), pp.217-225.

Bromley, L. A., 1972. Use of Sea Water to Scrub Sulphur Dioxide from Stack Gases, Int. J. Sulphur Chem., Part B, 7 (1), 77.

Brown, C. and Sheedy, M., 2002, January. A new ion exchange process for softening high TDS produced water. In SPE International Thermal Operations and Heavy Oil Symposium and International Horizontal Well Technology Conference. Society of Petroleum Engineers.

Buecker, B., 2008. Properly monitor your scrubber chemistry. Power Engineering, 112(7), pp.48-51.

Busch, K.W., Busch, M.A., Parker, D.H., Darling, R.E. and McAtee Jr, J.L., 1986. Studies of a water treatment device that uses magnetic fields. Corrosion, 42(4), pp.211-221.

Busch, K.W., Busch, M.A., Darling, R.E., Maggard, S. and Kubala, S.W., 1997. Design of a test loop for the evaluation of magnetic water treatment devices. Process safety and environmental protection, 75(2), pp.105-114.

Cai, R., Yang, H., He, J. and Zhu, W., 2009. The effects of magnetic fields on water molecular hydrogen bonds. Journal of molecular structure, 938(1-3), pp.15-19.

Canepa, P., Garombo, C., Szpyrkowicz, L. and Zilio-Grandi, F., 1996. Comparison between ion exchange and nanofiltration for softening of industrial water. Filtration & separation, 33(2), pp.131-135.

Cappelle, M.A. and Davis, T.A., 2016. Ion Exchange Membranes for Water Softening and High-Recovery Desalination. Emerging Membrane Technology for Sustainable Water Treatment, p.163.

Cavano, R.R., 2005, April. Understanding scaling indices and calculating inhibitor dosages. In NACE CORROSION (pp. NACE-05063). NACE.

Chen, Q., Luo, Z., Hills, C., Xue, G. and Tyrer, M., 2009. Precipitation of heavy metals from wastewater using simulated flue gas: sequent additions of fly ash, lime and carbon dioxide. Water research, 43(10), pp.2605-2614.

Chen, Q., Yao, Y., Li, X., Lu, J., Zhou, J. and Huang, Z., 2018. Comparison of heavy metal removals from aqueous solutions by chemical precipitation and characteristics of precipitates. Journal of water process engineering, 26, pp.289-300.

Chibowski, E., Szczes, A. and Holysz, L., 2005. Influence of sodium dodecyl sulfate and static magnetic field on the properties of freshly precipitated calcium carbonate. Langmuir, 21(18), pp.8114-8122.

Chin, T., Tam, I. and Yin, C.Y., 2021. Comparison of various chemical compounds for the removal of SO_2 and NOx with wet scrubbing for marine diesel engines.

Clifford, D., Sorg, T.J. and Ghurye, G.L., 2011. Ion exchange and adsorption of inorganic contaminants. Water quality & treatment: A handbook on drinking water.

Coey, J.M.D., 1995. Rare-earth magnets. Endeavour, 19(4), pp.146-151.

Coey, J.M.D. ed., 1996. Rare-earth iron permanent magnets (No. 54). Oxford University Press.

Coey, J.M.D. and Cass, S., 2000. Magnetic water treatment. Journal of Magnetism and Magnetic Materials, 209(1-3), pp.71-74.

Comodi, P., Nazzareni, S., Zanazzi, P.F. and Speziale, S., 2008. High-pressure behavior of gypsum: A single-crystal X-ray study. American Mineralogist, 93(10), pp.1530-1537.

Córdoba, P., 2015. Status of Flue Gas Desulphurisation (FGD) systems from coal-fired power plants: Overview of the physic-chemical control processes of wet limestone FGDs. Fuel, 144, pp.274-286.

Córdoba, P. and Staicu, L.C., 2018. Flue gas desulphurization effluents: An unexploited selenium resource. Fuel, 223, pp.268-276.

Croat, J.J., 2017. Rapidly solidified neodymium-Iron-Boron permanent magnets. Woodhead Publishing.

Dal Pozzo, A., Lazazzara, L., Antonioni, G. and Cozzani, V., 2020. Techno-economic performance of HCl and SO_2 removal in waste-to-energy plants by furnace direct sorbent injection. Journal of hazardous materials, 394, p.122518.

Damons, R.E., 2001. Development of an Aspen model for the treatment of acid mine drainage.

Dara, S.S., 2008. A textbook of engineering chemistry. S. Chand Publishing.

Dawson, D.M., 1990. Non-chemical water treatment system. Corrosion Prevention & Control, 37(3), pp.61-64.

de Berg, K.C. and Chapman, K.J., 2001. Determination of the magnetic moments of transition metal complexes using rare earth magnets. Journal of Chemical Education, 78(5), p.670.

de Dardel, F., 2020, Basic ion exchange processes in water treatment, viewed 18 November 2019, http://dardel.info/IX/processes/processes.html/.

Demopoulos, G.P., 2009. Aqueous precipitation and crystallization for the production of particulate solids with desired properties. Hydrometallurgy, 96(3), pp.199-214.

Deslouis, C., Gabrielli, C., Keddam, M., Khalil, A., Rosset, R., Tribollet, B. and Zidoune, M., 1997. Impedance techniques at partially blocked electrodes by scale deposition. Electrochimica acta, 42(8), pp.1219-1233.

Dey, D., Herzog, A. and Srinivasan, V., 2007. Chemical precipitation: water softening. Michigan State University, East Lancing.

Dickinson, S.R. and McGrath, K.M., 2001. Quantitative determination of binary and tertiary calcium carbonate mixtures using powder X-ray diffraction. Analyst, 126(7), pp.1118-1121.

Dzhonova-Atanasova, D.B., Razkazova-Velkova, E.N. and Ljutzkanov, L.A., 2011. Current problems and development in flue gas desulphurization. Materials, methods and technologies (CD-ROM), 5.

Eksteen, J.J., Van Beek, B. and Bezuidenhout, G.A., 2011. Cracking a hard nut: An overview of Lonmin's operations directed at smelting of UG2-rich concentrate blends. Journal of the Southern African Institute of Mining and Metallurgy, 111(10), pp. 681-690.

El Baba, M., Kayastha, P., Huysmans, M. and De Smedt, F., 2020. Evaluation of the groundwater quality using the water quality index and geostatistical analysis in the Dier al-Balah Governorate, Gaza Strip, Palestine. Water, 12(1), p.262.

Entezari, M.H. and Tahmasbi, M., 2009. Water softening by combination of ultrasound and ion exchange. Ultrasonics sonochemistry, 16(3), pp.356-360.

Euvrard, M., Leroy, P. and Ledion, J., 1997. Effects and consequences of electric treatment in preventing scaling of drinking water systems. Aqua- Journal of Water Supply: Research and Technology, 46(2), pp.71-83.

Farshad, F.F. and Vargas, S.M., 2002, October. Scale Prevention, a Magentic Treatment Approach. In SPE Asia Pacific Oil and Gas Conference and Exhibition (pp. SPE-77850). SPE.

Fathi, A., Mohamed, T., Claude, G., Maurin, G. and Mohamed, B.A., 2006. Effect of a magnetic water treatment on homogeneous and heterogeneous precipitation of calcium carbonate. Water research, 40(10), pp.1941-1950.

Fernandez-Prini, R., 1982. Le Chatelier's principle and the prediction of the effect of temperature on solubilities. Journal of Chemical Education, 59(7), p.550.

Fink, J., 2021. Petroleum engineer’s guide to oil field chemicals and fluids. Gulf Professional Publishing.

Fokaides, P.A., Kylili, A., Pyrgou, A. and Koroneos, C.J., 2014. Integration potentials of insular energy systems to smart energy regions. Energy Technology & Policy, 1(1), pp.70-83.

Gabrielli, C., Jaouhari, R., Joiret, S. and Maurin, G., 2000. In situ Raman spectroscopy applied to electrochemical scaling. Determination of the structure of vaterite. Journal of Raman Spectroscopy, 31(6), pp.497-501.

Gabrielli, C., Jaouhari, R., Maurin, G., Keddam, M., 2001. Magnetic water treatment for scale prevention. Water Research 35 (13), 3249–3259.

Gabrielli, C., Keddam, M., Perrot, H., Khalil, A., Rosset, R. and Zidoune, M., 1996. Characterization of the efficiency of antiscale treatments of water Part I: Chemical processes. Journal of applied electrochemistry, 26(11), pp.1125-1132.

Gilart, F., Deas, D., Ferrer, D., López, P., Ribeaux, G. and Castillo, J., 2013. High flow capacity devices for anti-scale magnetic treatment of water. Chemical Engineering and Processing: Process Intensification, 70, pp.211-216.

Gilron, J. and Hasson, D., 1987. Calcium sulphate fouling of reverse osmosis membranes: flux decline mechanism. Chemical Engineering Science, 42(10), pp.2351-2360.

Gitis, V. and Hankins, N., 2018. Water treatment chemicals: Trends and challenges. Journal of Water Process Engineering, 25, pp.34-38

Gololo, K.V., 2017. Industrial Emissions Management: The Good, The Bad and The Ugly [PowerPoint presentation] 2-3 October. Department of Environmental Affairs, Pretoria.

Greenberg, A.E. and Navone, R., 1958. Use of the control chart in checking anion-cation balances in water. *Journal (American Water Works Association)*, *50*(10), pp.1365-1370.

Gryta, M., 2011. The influence of magnetic water treatment on $CaCO_3$ scale formation in membrane distillation process. Separation and purification technology, 80(2), pp.293-299

Gubb, A., 2009. National Environmental Management: Air Quality Act (39 of 2004). Wildlife and Environmental Society of South Africa. Retrieved from http://www. enviropaedia. com/topic/default. php.

Hamid, S., De Jesús, O., Jacinto, C., Izetti, R., Pinto, H., Droguett, E., Edwards, C., Cassidy, J., Zhang, H., Dagenais, P. and Batocchio, M.A., 2016. A practical method of predicting calcium carbonate scale formation in well completions. Spe Production & Operations, 31(01), pp.1-11.

Hanif, M.A., Ibrahim, N. and Abdul Jalil, A., 2020. Sulphur dioxide removal: An overview of regenerative flue gas desulphurization and factors affecting desulphurization capacity and sorbent regeneration. Environmental Science and Pollution Research, 27, pp.27515-27540.

Hasson, D. and Semiat, R., 2006. Scale control in saline and wastewater desalination. Israel journal of chemistry, 46(1), pp.97-104.

Helfritch, D., Bortz, S., Beittel, R., Bergman, P. and Toole-O'Neil, B., 1992. Combined SO_2 and NOx removal by means of dry sorbent injection. Environmental progress, 11(1), pp.7-10

Herbst, J.F. and Croat, J.J., 1991. Neodymium-iron-boron permanent magnets. Journal of magnetism and magnetic materials, 100(1-3), pp.57-78.

Herzog, R.E., Shi, Q., Patil, J.N. and Katz, J.L., 1989. Magnetic water treatment: the effect of iron on calcium carbonate nucleation and growth. Langmuir, 5(3), pp.861-867.

Higashitani, K., Iseri, H., Okuhara, K., Kage, A. and Hatade, S., 1995. Magnetic effects on zeta potential and diffusivity of nonmagnetic colloidal particles. Journal of Colloid and Interface Science, 172(2), pp.383-388.

Hoffmann, H. and Martinola, F., 1988. Selective resins and special processes for softening water and solutions; A review. Reactive Polymers, Ion Exchangers, Sorbents, 7(2-3), pp.263-272

Holysz, L., Chibowski, M., Chibowski, E., 2002. Time-dependent change of zeta potential and other parameters of in situ calcium carbonate due to magnetic field treatment. Colloids and Surfaces A. Physiochemical and Engineering Aspects 208, 231–240.

Holysz, L., Szczes, A. and Chibowski, E., 2007. Effects of a static magnetic field on water and electrolyte solutions. Journal of Colloid and Interface Science, 316(2), pp.996-1002.

Hunt, G. and Sewell, M., 2015, October. Utilizing dry sorbent injection technology to improve acid gas control. In 34th International Conference on Thermal Treatment Technologies & Hazardous Waste Combustors

Ibanez, J.G., Hernandez-Esparza, M., Doria-Serrano, C., Fregoso-Infante, A. and Singh, M.M., 2008. Alkalinity and Buffering Capacity of Water: Reference Chapters: 6, 8.

Ismail, F., Khulbe, K.C. and Matsuura, T., 2018. Reverse osmosis. Elsevier

Jahnig, C.E. and Shaw, H., 1981. A Comparative Assessment of Flue Gas Treatment Processes Part I—Status and Design Basis. Journal of the Air Pollution Control Association, 31(4), pp. 421-428

Jones, R.T., 2005. An overview of Southern African PGM smelting. Nickel and Cobalt, pp.147-178.

K&J magnets- magnetic field visualization.Available at: https://www.kjmagnets.com (accessed: 9 August 2022).
Kashchiev, D. and Van Rosmalen, G.M., 2003. Nucleation in solutions revisited. Crystal Research and Technology: Journal of Experimental and Industrial Crystallography, 38(7-8), pp.555-574.

Kelland, M.A., 2011. Effect of various cations on the formation of calcium carbonate and barium sulfate scale with and without scale inhibitors. Industrial & Engineering Chemistry Research, 50(9), pp.5852-5861.

Kemmer, F.N. ed., 1979. The NALCO water handbook. New York: McGraw-Hill.

Knez, S. and Pohar, C., 2005. The magnetic field influence on the polymorph composition of CaCO3 precipitated from carbonized aqueous solutions. Journal of Colloid and Interface Science, 281(2), pp.377-388.

Kobe, S., Drazic, G., McGuiness, J., Strazisar, J., 2001. TEM examination of the influences of magnetic field on the crystallization form of calcium carbonate: a magnetic water-treatment device. Acta Chimica Slovenica 48,77–86.

Kobe, S., Vedenik-Novak, M., Plavsic, B., Orel, B., 1998. The influence of impurity elements on the crystallization form of calcium carbonate. IChemE Research Event.

Koech, L., Rutto, H., Lerotholi, L., Everson, R.C., Neomagus, H., Branken, D. and Moganelwa, A., 2021. Spray drying absorption for desulphurization: a review of recent developments. Clean Technologies and Environmental Policy, pp.1-22.

Koralegedara, N.H., Pinto, P.X., Dionysiou, D.D. and Al-Abed, S.R., 2019. Recent advances in flue gas desulphurization gypsum processes and applications–A review. Journal of environmental management, 251, p.109572.

Kuklinska, K., Wolska, L. and Namiesnik, J., 2015. Air quality policy in the US and the EU–a review. Atmospheric Pollution Research, 6(1), pp.129-137.

Lakshmi, R., Velmurugan, V. and Sasikumar, S., 2013. Preparation and phase evolution of wollastonite by sol-gel combustion method using sucrose as the fuel. Combustion Science and Technology, 185(12), pp.1777-1785.

Lee, S. and Lee, C.H., 2000. Effect of operating conditions on $CaSO_4$ scale formation mechanism in nanofiltration for water softening. Water Research, 34(15), pp.3854-3866.

Lee, S., Kim, J. and Lee, C.H., 1999. Analysis of $CaSO_4$ scale formation mechanism in various nanofiltration modules. Journal of membrane science, 163(1), pp.63-74.

Li, X., Feng, D., Chai, M., Xu, S., Mohammedomar, A. and Zhao, W., 2020. Efficient SO2 Capture by 2-(Diethylamino) ethanol/Hexadecane Phase Separation Absorbent. Energy & Fuels, 34(11), pp.15039-15047.

Lipus, L.C., Ačko, B. and Hamler, A., 2011. Electromagnets for high-flow water processing. Chemical Engineering and Processing: Process Intensification, 50(9), pp.952-958

Lipus, L.C. and Dobersek, D., 2007. Influence of magnetic field on the aragonite precipitation. Chemical Engineering Science, 62(7), pp.2089-2095.

Lisnic, R. and Jinga, S.I., 2018. Studiu Privind Stadiul Actual Şi Tendinţele Viitoare Ale Tehnologiilor De Desulphurare A Gazelor De Ardere. Revista Romana de Materiale, 48(1), pp.83-90.

Long, N.V.D., Lee, D.Y., Jin, K.M., Choongyong, K., Mok, L.Y., Won, L.S. and Lee, M., 2020. Advanced and intensified seawater flue gas desulphurization processes: Recent developments and improvements. Energies, 13(22), p.5917.

Madarász, D., Szenti, I., Sápi, A., Halász, J., Kukovecz, Á. and Kónya, Z., 2014. Exploiting the ion-exchange ability of titanate nanotubes in a model water softening process. Chemical Physics Letters, 591, pp.161-165.

MAG3, Proceedings of Anti-Scale Magnetic Treatment and Physical Conditions, Cranfield University, UK, 1999.

McIlvaine, R., 2010. FGD is a big but volatile FRP market. Reinforced Plastics, 54(3), pp.43-45.

McMahon, C.A., 2009. Investigation of the quality of water treated by magnetic fields.

Mahmoud, B., Yosra, M. and Nadia, A., 2016. Effects of magnetic treatment on scaling power of hard waters. Separation and Purification Technology, 171, pp.88-92.

Maliou, E., Malamis, M. and Sakellarides, P.O., 1992. Lead and cadmium removal by ion exchange. Water Science and Technology, 25(1), pp.133-138.

Mercer, K.L., Lin, Y.P. and Singer, P.C., 2005. Enhancing calcium carbonate precipitation by heterogeneous nucleation during chemical softening. Journal-American Water Works Association, 97(12), pp.116-125.

Minnesota Rural Water Association. 2009. Lime softening. Minnesota Water Works Operations Manual. 4th edn. Elbow Lake, MN. Chapter 16.

Mirzabeygi, M., Naji, M., Yousefi, N., Shams, M., Biglari, H. and Mahvi, A.H., 2016. Evaluation of corrosion and scaling tendency indices in water distribution system: a case study of Torbat Heydariye, Iran. Desalination and Water Treatment, 57(54), pp.25918-25926.

Mo, J.S., Wu, Z.B., Cheng, C.J., Guan, B.H. and Zhao, W.R., 2007. Oxidation inhibition of sulfite in dual alkali flue gas desulphurization system. Journal of Environmental Sciences, 19(2), pp.226-231.

Mohlala, K., 2020. A critical evaluation of local government air quality management: the Gauteng experience (Doctoral dissertation, North-West University (South Africa)).

Mokone, T.P., Van Hille, R.P. and Lewis, A.E., 2010. Effect of solution chemistry on particle characteristics during metal sulfide precipitation. Journal of colloid and interface science, 351(1), pp.10-18.

Mosin, O. and Ignatov, I., 2015. Practical implementation of magnetic water treatment to eliminate scaling salts. Journal of Health, Medicine and Nursing, 10, pp.111-125.

Mosin, O. and Ignatov, I., 2015. Magnetohydrodynamic cell for magnetic water treatment. Nanotechnology Research and Practice, (2), pp.81-92.

Mousavi Ehteshami, S.M. and Chan, S.H., 2014. Techno-economic study of hydrogen production via steam reforming of methanol, ethanol, and diesel. Energy Technology & Policy, 1(1), pp.15-22.

Murray, K. & Wade, P., 1996. Checking anion-cation charge balance of water quality analyses: Limitations of the traditional method for non-potable waters. Water Sa, 22(1), pp.27-32.

Nanda, D., Tung, K.L., Li, Y.L., Lin, N.J. and Chuang, C.J., 2010. Effect of pH on membrane morphology, fouling potential, and filtration performance of nanofiltration membrane for water softening. Journal of Membrane Science, 349(1-2), pp.411-420.

Neslon, S.A., 2014. Tectosilicates.Carbonates. Oxides and Accessory minerals, Tectosilicates and other minerals.Tulane University. Available at: https://www2.tulae.edu/~sanelson.eens211/tectosilicates&others.htm (accessed: February 19, 2023).

Nissen, W.I., Elkins, D.A. and McKinney, W.A., 1976. Citrate Process For Flue Gas Desulphurization A Status Report. In Proceedings: Symposium on Flue Gas Desulphurization, New Orleans, March 1976 (Vol. 2, p. 843). US Environmental Protection Agency, Office of Research and Development.

Nygaard, H.G., Kiil, S., Johnsson, J.E., Jensen, J.N., Hansen, J., Fogh, F. and Dam-Johansen, K., 2004. Full-scale measurements of SO_2 gas phase concentrations and slurry compositions in a wet flue gas desulphurisation spray absorber. Fuel, 83(9), pp.1151-1164.

Pan, Y., Du, X., Zhao, F. and Xu, B., 2012. Magnetic nanoparticles for the manipulation of proteins and cells. Chemical Society Reviews, 41(7), pp.2912-2942.

Pang, X. and Deng, B., 2008. Investigation of changes in properties of water under the action of a magnetic field. Science in China Series G: Physics, Mechanics and Astronomy, 51(11), pp.1621-1632.

Pang, X.F. and Feng, Y.P., 2003. Mobility and conductivity of the proton transfer in hydrogen-bonded molecular systems. Chemical physics letters, 373(3-4), pp.392-401.

Parsons, S.A., Judd, S.J., Stephenson, T., Udol, S. and Wang, B.L., 1997. Magnetically augmented water treatment. Process safety and environmental protection, 75(2), pp.98-104.

Poullikkas, A., 2015. Review of Design, Operating, and financial considerations in flue gas desulphurization systems. Energy Technology & Policy, 2(1), pp.92-103.

Pike, D.E., Airpol Inc, 1984. Double alkali process for removal of sulphur dioxide from gas streams. U.S. Patent 4,452,766.

Prisciandaro, M., Lancia, A., Mazziotti di Celso, G. and Musmarra, D., 2013. Antiscalants for gypsum precipitation in industrial equipments: comparison among different additives. Chemical Engineering Transactions, 32, pp.2137-2142.

Puckorius, P. and Strauss, S.D., 1983. Get a better reading on scaling tendency of cooling water. Power;(United States), 127(9).

Quinn, C.J., Molden, T.C. and Sanderson, C.H., 1997. Magnetic treatment of water prevents mineral build-up. Iron and steel Engineer, 74, pp.47-52.

Rafferty, K., 1999. Scaling in geothermal heat pump systems.

Railsback, L.B., 2006. Some fundamentals of mineralogy and geochemistry. On-line book, quoted from: www. gly. uga. edu/railsback, 387.

Ramstad, K., Tydal, T., Askvik, K.M. and Fotland, P., 2004, May. Predicting carbonate scale in oil producers from high temperature reservoirs. In SPE International Oilfield Scale Conference and Exhibition? (pp. SPE-87430). SPE.

Rathilal, S., 2004. The study of the mechanism of magnetic water treatment for the prevention of scale and corrosion (Doctoral dissertation).

Rengaraj, S. and Moon, S.H., 2002. Kinetics of adsorption of Co (II) removal from water and wastewater by ion exchange resins. Water research, 36(7), pp.1783-1793.

Rice, E.W., Bridgewater, L. and American Public Health Association eds., 2012. Standard methods for the examination of water and wastewater (Vol. 10). Washington, DC: American public health association.

Rogers, P.G., 1990. The clean air act of 1970. EPA J., 16, pp.21

Railsback, L.B., 2006. Some fundamentals of mineralogy and geochemistry. *On-line book, quoted from: www. gly. uga. edu/railsback*, *387*.

Rosenberg, H.S. and Grotta, H.M., 1979. Battelle Development Corp. Scale suppression in lime and limestone scrubbers. U.S. Patent 4,177,245.

Rusydi, A.F., 2018, February. Correlation between conductivity and total dissolved solid in various type of water: A review. In IOP conference series: earth and environmental science (Vol. 118, p. 012019). IOP Publishing.

Rycroft, M., 2014. Air quality regulations− playing the numbers game with power stations. Energize, pp.25-29.

Ryu, M., Kim, H., Lim, M., You, K. and Ahn, J., 2010. Comparison of dissolution and surface reactions between calcite and aragonite in L-glutamic and L-aspartic acid solutions. Molecules, 15(1), pp.258-269.

Safari, M., Golsefatan, A. and Jamialahmadi, M., 2014. Inhibition of scale formation using silica nanoparticle. Journal of dispersion science and technology, 35(10), pp.1502-1510.

Saksono, N., Bismo, S., Krisanti, E., Manaf, A. and Widaningrum, R., 2010. Magnetic Field Effects on CaCO3 Precipitation Process in Hard Water. Makara Journal of Technology, 10(2), pp.96-101.

Salman, M.A., Safar, M. and Al-Nuwaibit, G., 2015. The effect of magnetic treatment on retarding scaling deposition. Tojsat, 5(3), pp.62-77.

Saloua, J., Mohamed, T., Ahmed, M. and Khadija, M., 2020. Industrial rejection: removal of heavy metals based on chemical precipitation and research for recoverable material in by-products. International Journal of Engineering Technologies and Management Research, 7(2), pp.39-52.

Santos, T.N., Yokoyama, L. and Lage, G.G., 2017. Evaluation of scale inhibitors to prevent calcium sulphate in sulphate removal units.

Sawaftah, N.T.Y., 2017. Optimization of Calcium Sulfate Scale Reduction Using Magnetic Field (Doctoral dissertation, An-Najah National University).

Sensorex, 2021, Wet vs. Dry Industrial Scrubbers, viewed 25 June 2021, https://sensorex.com/blog/2019/12/10/wet-vs-dry-industrial-scrubbers/.

Seyrig, G. and Shan, W., 2007. Chemical precipitation: water softening. ENE, 806.

Shah, M., Shah, V., Dudhat, K. and Patel, D., 2023. Evaluation of geothermal water and assessment of corrosive and scaling potential of water samples in Tulsishyam Geothermal Region, Gujarat, India. Environmental Science and Pollution Research, 30(15), pp.44684-44696.

Shewane, P.G., Gite, M., Singh, A. and Narkhede, A.J.I.J., 2014. An overview of neodymium magnets over normal magnets for the generation of energy. International Journal on Recent and Innovation Trends in Computing and Communication, 2(12), pp.4056-4059.

Silva, I.B., Neto, J.C.Q. and Petri, D.F., 2015. The effect of magnetic field on ion hydration and sulfate scale formation. Colloids and Surfaces A: Physicochemical and Engineering Aspects, 465, pp.175-183.

Singh, R., 2005. Hybrid Membrane systems for Water Purification, chapter 2- water and membrane treatment.

Slack, A.V., Falkenberry, H.L. and Harrington, R.E., 1972. Sulphur oxide removal from waste gases: Lime-Limestone scrubbing technology. Journal of the Air Pollution Control Association, 22(3), pp. 159-166.

Smith, C.F., Nolan III, T.J. and Crenshaw, P.L., 1968. Removal and inhibition of calcium sulfate scale in waterflood projects. Journal of Petroleum Technology, 20(11), pp.1249-1256.

Soldati, A.L., Jacob, D.E., Glatzel, P., Swarbrick, J.C. and Geck, J., 2016. Element substitution by living organisms: the case of manganese in mollusc shell aragonite. Scientific reports, 6(1), p.22514.

Soud, H.N., 2000. Developments in FGD (Vol. 29). London: IEA Coal Research.

Spiegel, E. and Yeck, P., 1998. By A. BRACCO[1], A. PROVENZALE[1], 2. Theory of Black Hole Accretion Discs, p.254.

Srivastava, R.K. and Controlling, S.O., 2000. Emissions: A Review of Technologies, US Environmental Protection Agency. EPA/600/R-00/093, Office of Research and Development, Washington, DC.

Srivastava, R.K. and Jozewicz, W., 2001. Flue gas desulphurization: the state of the art. Journal of the Air & Waste Management Association, 51(12), pp.1676-1688.

Srivastava, R.K., Jozewicz, W. and Singer, C., 2001. SO_2 scrubbing technologies: a review. Environmental Progress, 20(4), pp.219-228.

Strömberg, A.M. and Karlsson, H.T., 1988, January. Limestone based spray dry scrubbing of SO_2. In Tenth International Symposium on Chemical Reaction Engineering (pp. 2095-2102). Pergamon.

Su, N. and Wu, C.F., 2003. Effect of magnetic field treated water on mortar and concrete containing fly ash. Cement and concrete composites, 25(7), pp.681-688.

Suopajärvi, T., 2015. Functionalized nanocelluloses in wastewater treatment applications. Acta Universitatis Ouluensis C, 526.

Szkatula, A., Balanda, M. and Kopeć, M., 2002. Magnetic treatment of industrial water. Silica activation. The European Physical Journal-Applied Physics, 18(1), pp.41-49.

Team, S. W. M. (2021, October 4). Management, treatment, and reuse of water for the mining sector in Latin America. Smart Water Magazine. https://smartwatermagazine.com/news/almar-water-solutions/management-treatment-and-reuse-water-mining-sector-latin-america.

Tseng, P.C. and Rochelle, G.T., 1986. Calcium sulfite hemihydrate: Crystal growth rate and crystal habit. Environmental progress, 5(1), pp.5-11.

Tshehla, C. and Wright, C.Y., 2019. 15 years after the National Environmental Management Air Quality Act: Is legislation failing to reduce air pollution in South Africa? South African Journal of Science, 115(9-10), pp.1-4.

United States Environmental Protection Agency, 2021. Progress Cleaning the Air and Improving People's Health.

United States Geological Survey. Imagens Landsat. 2020, 5.

van Niekerk, A., 2002. Evaluation of the Savmin Sulphate Removal Process. Johannesburg: The Coalteh Research Association.

Van Rosmalen, G.M., Daudey, P.J. and Marchée, W.G.J., 1981. An analysis of growth experiments of gypsum crystals in suspension. Journal of Crystal Growth, 52, pp.801-811.

Veolia Water Technologies & Solutions, 2023. Handbook of Industrial Water Treatment - Chapter 7 Precipitation Softening. [Online] Available at: https://www.suezwatertechnologies.com/handbook/chapter-07-precipitation-softening [Accessed 01 10 2019].

Walton, N.R.G., 1989. Electrical conductivity and total dissolved solids—what is their precise relationship?. Desalination, 72(3), pp.275-292.

Wang, S. and Peng, Y., 2010. Natural zeolites as effective adsorbents in water and wastewater treatment. Chemical engineering journal, 156(1), pp.11-24.

Wang, Y., Babchin, A.J., Chernyi, L.T., Chow, R.S., Sawatzky, R.P., 1997. Rapid onset of calcium carbonate crystallization under the influence of a magnetic field. Water Research 31 (2), 346–350.

Wang, Y., Zhang, B., Gong, Z., Gao, K., Ou, Y. and Zhang, J., 2013. The effect of a static magnetic field on the hydrogen bonding in water using frictional experiments. Journal of Molecular Structure, 1052, pp.102-104.

Water conservation and water demand management - sibanye-stillwater (no date). Available at:https://reports.sibanyestillwater.com/2017/download/sibanye-FS17-water-conservation-water-demand.pdf (Accessed: November 26, 2022).

Wen, C.Y., Wjm Jr, R.D., Nelsen Jr, J.B., Werkowitz, D.S., Ketteringham, J.M., Davidsson, L.M. and Wiig, K.M., 1975. Scale Control in Limestone Wet Scrubbing Systems. US EPA, EPA-650/2-75-031.

Wirsching, F., Hüller, R. and Olejnik, R., 1994. FGD Gypsum Definitions and Legislation in the European Communities, in the OECD and in Germany. In Studies in Environmental Science (Vol. 60, pp. 205-216). Elsevier.

World Bank, 1999. Pollution prevention and abatement handbook, 1998: Toward cleaner production. The World Bank.

Yehia, N.S., Ali, M.M., Kandil, K.M. and El-Maadawy, M., 2011. Effects of some parameters affecting the crystallization rate of calcium sulfate dihydrate in sodium chloride solution. Journal of American Science, 7(6), pp.635-644.

Zaidi, N.S., Sohaili, J., Muda, K. and Sillanpää, M., 2014. Magnetic field application and its potential in water and wastewater treatment systems. Separation & Purification Reviews, 43(3), pp.206-240.

Živković, N.V., Šerbanović, S.P., Živković, E.M., Kijevčanin, M.L. and Stefanović, P.L., 2014. Wet flue gas desulphurisation procedures and relevant solvents thermophysical properties determination. Hemijska industrija, 68(4), pp.491-500.

Chapter 3 Materials and Methods

3.1 Introduction

Chapter 3 provides a comprehensive discussion of the experimental procedures, reagents and analytical methods and techniques utilized in this study to successfully address the specified aims and objectives presented in Chapter 1. The selection and utilization of appropriate reagents was crucial in conducting the necessary tests and analyses required to achieve the outlined objectives.

3.2 Experimental methods

This portion of the study is divided into four sections, each focusing on a specific set of experiments conducted:

1. Solid and liquid sample characterization
2. The impact of lime and soda ash on hard water
3. The effectiveness of ion exchange resins in treating hard water
4. The influence of magnetic water treatment on hard water

Figure 3.1 provides a flow diagram summarizing all the experimental procedures and stages undertaken to accomplish the objectives outlined in this study.

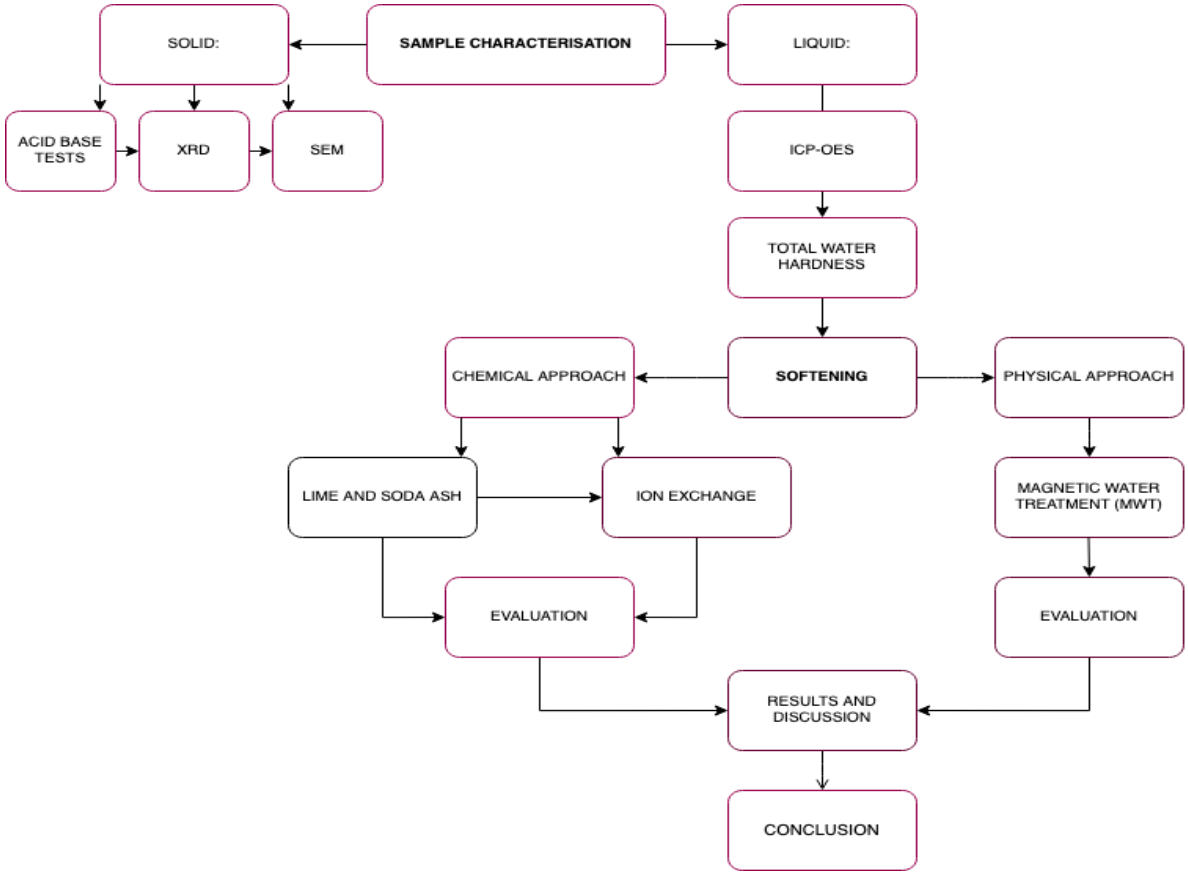


Figure 3. 1 Experimental procedures and stages necessary to achieve the objectives assigned in this study

3.2.1 Solid and liquid sample characterization

3.2.1.1 Acid-base tests (preliminary tests)

The solid scale samples and liquid process water samples utilized in this study were provided by Sibanye-Stillwater (Pty) Ltd, located in South Africa. Initial testing of solid scale samples obtained from the VTS involved a simple acid-base test to identify the presence of SO_4^{2-} and/or CO_3^{2-}. Each of the seven samples, weighing one gram, was placed in a beaker, and a slow addition of 10 mL of an acid solution (0.1 M HCl and $BaCl_2$) was carried out. Observations were made based on the reactions that occurred. To ascertain the presence of carbonates, 10 mL of a 0.1 M HCl solution was added to the samples, and the resulting gas was reacted with 10 mL of lime water ($Ca(OH)_2$ (aq)).

To determine and confirm the mineralogical composition of the solid samples, X-ray diffraction (XRD) analysis was conducted. Unit cell parameters for the predominant phases were calculated with the aid of high score software, which involved refining the unit cell to achieve accurate results. To facilitate imaging and improve the analysis of surface morphology using scanning electron microscopy (SEM), the received scale samples were cut into

petrographic thin sections. These sections, approximately 30 microns thick, were embedded in epoxy resin and placed onto glass slides. Analysis of these sections was performed using a Quanta-400F, FEI, USA model, located in the School of Chemical and Metallurgical Engineering at the University of the Witwatersrand. Liquid samples collected from four points within the scrubbing circuit at Sibanye-Stillwater (Scrubber feed, Scrubber bleed, Dust-thickener overflow, and Process water), as indicated in Figure 3.2, underwent analysis using inductively coupled plasma-optical emission spectroscopy (ICP-OES). This analysis aimed to determine the concentration of elements present in the liquid samples.

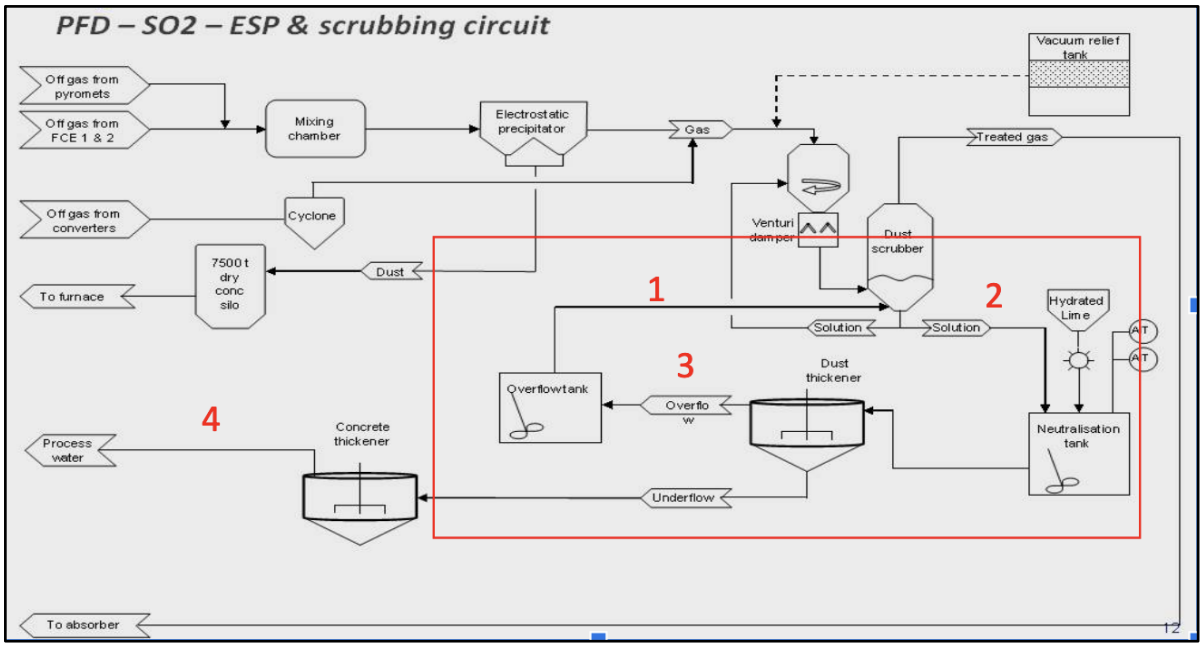


Figure 3. 2 Scrubber circuit at Sibanye-Stillwater indicating sampling points (1. Scrubber feed, 2. Scrubber bleed, 3. Dust-thickener overflow and 4. Process water).

3.2.1.2 Determining water hardness from water samples

By utilizing ICP-OES analysis, the full elemental composition of each of the four samples was determined, enabling the assessment of total hardness, non-carbonate hardness, carbonate hardness, and total alkalinity. In addition to Ca and Mg, other metals present in significant concentrations were identified and became an additional focus of this study. These metals are discussed in Chapter 5.

The measurements of total hardness, non-carbonate hardness, and carbonate hardness are expressed as the equivalent concentration of $CaCO_3$ in milligrams per litre (mg/L) or parts per

million (ppm). The calculations for these parameters are based on Equations 3.1—3.3 (Cappelle and Davis, 2016; Entezari and Tahmasbi, 2009):

Equation 3.1: Total Hardness (mg/L as $CaCO_3$)

Equation 3.2: Carbonate hardness (mg/L as $CaCO_3$)

Equation 3.3 Non-carbonate hardness (mg/L as $CaCO_3$)

These equations allow for the conversion of measured concentrations into standardized units, facilitating the comparison and analysis of hardness-related characteristics in the samples.

Total hardness (TH) =[Ca] (mg/L) 2.497 + [Mg](mg/L) * 4.118* [3.1]

Carbonate hardness (CH) = minimum of total hardness and alkalinity [3.2]

Non-carbonate hardness (NCH) = Total hardness-carbonate hardness [3.3]

The values for all four samples are tabled and presented in Chapter 4, Section 4.1.

3.2.2 Chemical precipitation using lime and soda ash

The objective of these tests was to assess the effectiveness of lime and soda ash (Na_2CO_3) in removing hardness, specifically Ca and Mg, from the water samples. The four water samples obtained from Sibanye-Stillwater (Scrubber bleed, Scrubber feed, Dust-thickener overflow, and Process water) were subjected to treatment. The procedures involving lime and lime and soda ash are described in Sections 3.4.1 and 3.4.2, respectively, and the corresponding results are presented in Chapter 5. The dosages of lime and soda ash were determined based on the levels of carbonate and non-carbonate hardness in the water. Lime was primarily used to remove carbonate hardness, while both lime and soda-ash were employed to eliminate non-carbonate hardness. Comprehensive data obtained from the ICP-OES analyses of all four samples, as well as the test work conducted in Sections 3.4.1 and 3.4.2, are provided in Appendix 1. Given the study's focus, only the contaminants with the highest concentrations along with Ca and Mg were discussed.

3.2.2.1 Lime and soda ash dosage calculations

Table 3.1 provides the calculated concentrations of lime and soda ash using *StaSoft software V5* from the Water Research Commission, South Africa. Alternatively, the dosages can be determined using the conventional dosage method, as described in Equation 3.4 based on the Minnesota Rural Water Association (2009). This method, although more extensive, helps in understanding the chemical and mathematical relationships involved in softening. The lime dosage can be calculated using the following formula (Minnesota Rural Water Association 2009):

$$Lime\ (mg/L) = ((\underline{A + B + C + D) + \%\ EXCESS)}/\ purity\ of\ lime \quad [3.4]$$

Where:

A = Carbon Dioxide (CO_2) concentration in sample (mg/ L)
B = Bicarbonate (HCO_3^-) alkalinity in sample (mg/ L)
C = Hydroxide (OH^-) alkalinity in in sample (mg/ L)
D = Mg concentration in sample (mg/ L)
% Excess = Amount of lime added in excess to ensure pH > 10.5
Lime Purity = 96 % purity was used (as a decimal)

For removal of non-carbonate hardness, soda ash is required. This amount is calculated as follows:

$$Soda\ ash\ (mg/\ L) = Non\text{-}Carbonate\ Hardness\ as\ CaCO_3\ x\ (molecular\ weight\ of\ Na_2CO_3\ /molecular\ weight\ of\ CaCO_3)\ x\ \%\ Excess \quad [3.5]$$

The CO_2 and Mg concentrations were obtained from the ICP-OES analysis and the required reagent dosages were calculated using Equations 3.4 and 3.5 (Minnesota Rural Water Association, 2009).

Table 3. 1 Lime and soda ash dosages

Sample	Lime addition (g/ L)	Soda ash addition (g/ L)
Scrubber bleed	5.37	6.85
Scrubber feed	4.24	6.98
Dust-thickener overflow	3.93	6.74
Process water	1	1.99

Each sample test was conducted in triplicate to ensure the reliability of the results and establish a measure of uncertainty. The filtrate obtained from the tests was then analysed using ICP-OES to determine the remaining concentration of Ca and Mg ions. The precipitates obtained from the tests were sent for XRD analysis to identify the phases present. The average results from these analyses are presented in Chapter 5.

3.2.2.2 The effect of varying lime concentration on hardness removal in ambient/room temperatures

To assess the effects of different lime dosages on various parameters such as total hardness, alkalinity, pH, as well as Ca and Mg ion concentrations, the following experimental steps were performed:

Twenty-eight samples (28), consisting of seven samples from each of the four collected water samples, were prepared. Each sample was 250 mL in volume and treated with lime concentrations corresponding to 20 %, 40 %, 80 %, 100 %, 120 %, 140 %, and 180 % of the stoichiometric amount (as calculated in Table 3.1).The solutions were mixed for 60 minutes at a rotation speed of 100 rpm, during which the temperature and final pH of the solutions were measured. The resulting precipitates were separated from the solution through filtration using a vacuum filter. The collected precipitates were then dried at 80 °C overnight and weighed. The filtrates obtained from the filtration step were carefully labelled and sent for ICP-OES analysis to determine the elemental composition, including the concentrations of Ca and Mg ions. The precipitates obtained from the treatment with 100 % stoichiometric lime dosage were selected for XRD analysis to identify the specific phases present. This dosage was chosen

because it theoretically removes the maximum amount of unwanted material. The XRD analysis was conducted in duplicate to establish a measure of uncertainty. The average results from this analysis are presented in Chapter 5, Section 5.2.

A diagram illustrating the softening procedure is provided in Figure 3.3.

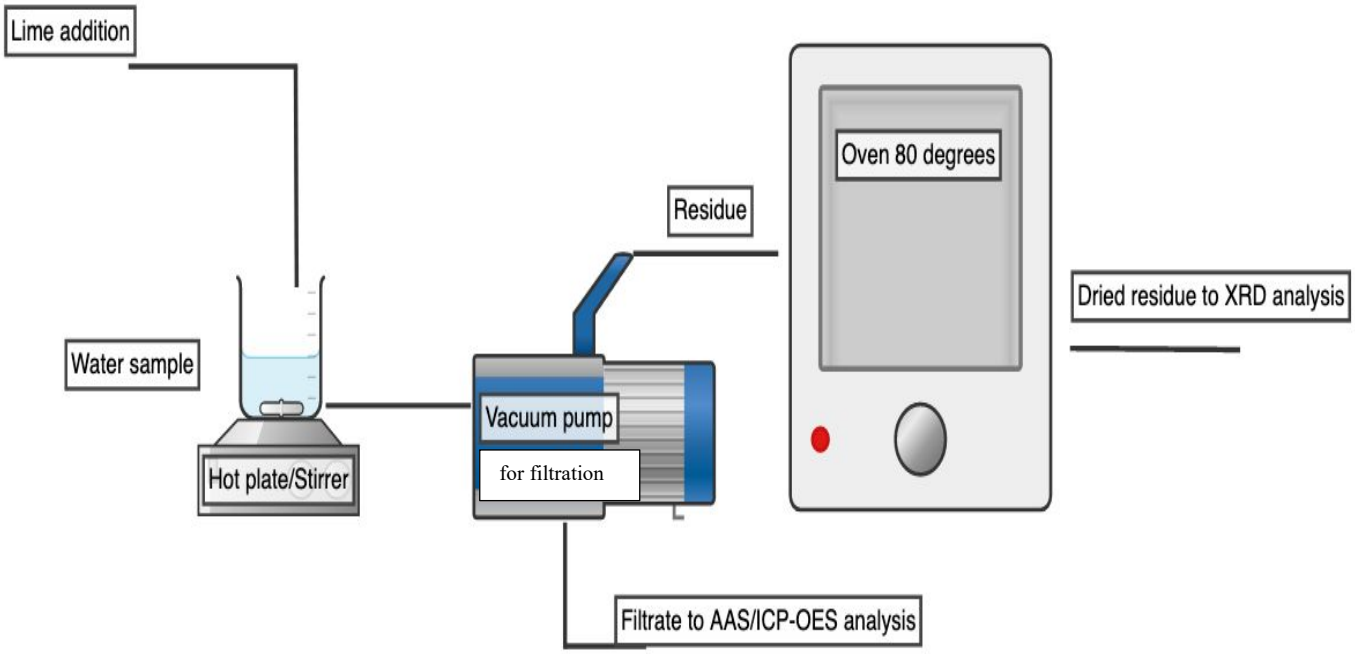


Figure 3. 3 Diagrammatic representation of the lime softening process

3.2.2.3 The effect of temperature on the efficiency of lime softening

In this test work, the focus was on the scrubber bleed and process water samples. The scrubber bleed refers to the sample obtained after the flue gas has been scrubbed and sent for neutralization with lime. The process water serves as a reservoir for topping up the scrubber feed. These two samples were crucial for observing the effects of varying lime dosages and temperature on water hardness. To investigate the impact of temperature on water hardness, the steps taken in Section 3.2.2.2 were repeated at elevated temperatures of 40 °C, 60 °C, 80 °C, and 100 °C. This was done after dosing the samples with the stoichiometric amounts calculated in Table 3.1. A hot plate was utilized to raise the solution temperature, while a thermometer was used for temperature measurement and monitoring. Each sample test was conducted in duplicate to establish a measure of uncertainty. The average results obtained from these tests are presented in Chapter 5, Section 5.2.

3.2.2.4 Traditional excess Lime and soda ash treatment process at ambient/room temperature

To effectively remove the non-carbonate hardness present in the samples, the addition of both lime and soda ash is necessary. The following steps were followed for the lime and soda ash treatment:

The four collected samples, each measuring 250 mL, were dosed with the stoichiometric amounts of lime and soda ash as calculated in Table 3.1. Each solution was mixed for 60 minutes at a speed of 100 rpm, during which the temperature and final pH were measured. The precipitates formed were separated by filtration using a vacuum filter, then dried at 80 °C overnight and weighed. The filtrates were collected, labelled, and sent for ICP-OES analyses. The precipitates were analysed using XRD to determine the phases present. This test was conducted in triplicate to establish a measure of uncertainty, and the average results are presented in Chapter 4, Section 4.2.2.

The following primary reactions (3.6—3.8) occur during the process, as reported by Faust and Aly (2018), Narain et al. (2021), and the Minnesota Rural Water Association (2009):

$$Stage\ 1:\ HCO^- + Ca(OH)_2 \rightarrow CaCO_3\ (s) + H_2O + OH^- \quad [3.6]$$

$$Stage\ 2:\ Mg^{2+} + Ca(OH)_2 \rightarrow Mg(OH)_2\ (s) + Ca^{2+} \quad [3.7]$$

$$Stage\ 3:\ Ca^{2+} + Na_2CO_3 \rightarrow CaCO_3\ (s) + 2\ Na^+ \quad [3.8]$$

In stage 1 of the lime and soda ash softening process, the CO_3^{2-} ions present in the water samples are converted to $CaCO_3$ through the addition of lime. This reaction leads to the precipitation of calcium carbonate, which helps remove carbonate hardness. In stage 2, an additional or excess amount of lime is added, which raises the pH of the solution to approximately 10—11.5. At this elevated pH, Mg^{2+} ions in the water react with OH^- ions to form $Mg(OH)_2$. The $Mg(OH)_2$ precipitates out of the solution, aiding in the removal of Mg^{2+} ions. Finally, in the last stage, the remaining Ca^{2+} ions are removed by the addition of Na_2CO_3. The Na_2CO_3 reacts with the Ca^{2+} ions to form $CaCO_3$, which also precipitates out of the solution.

Figure 3.4 provides a diagrammatic representation of the lime and soda ash softening process, illustrating the sequence of reactions and precipitation steps involved in removing carbonate and non-carbonate hardness from the water samples.

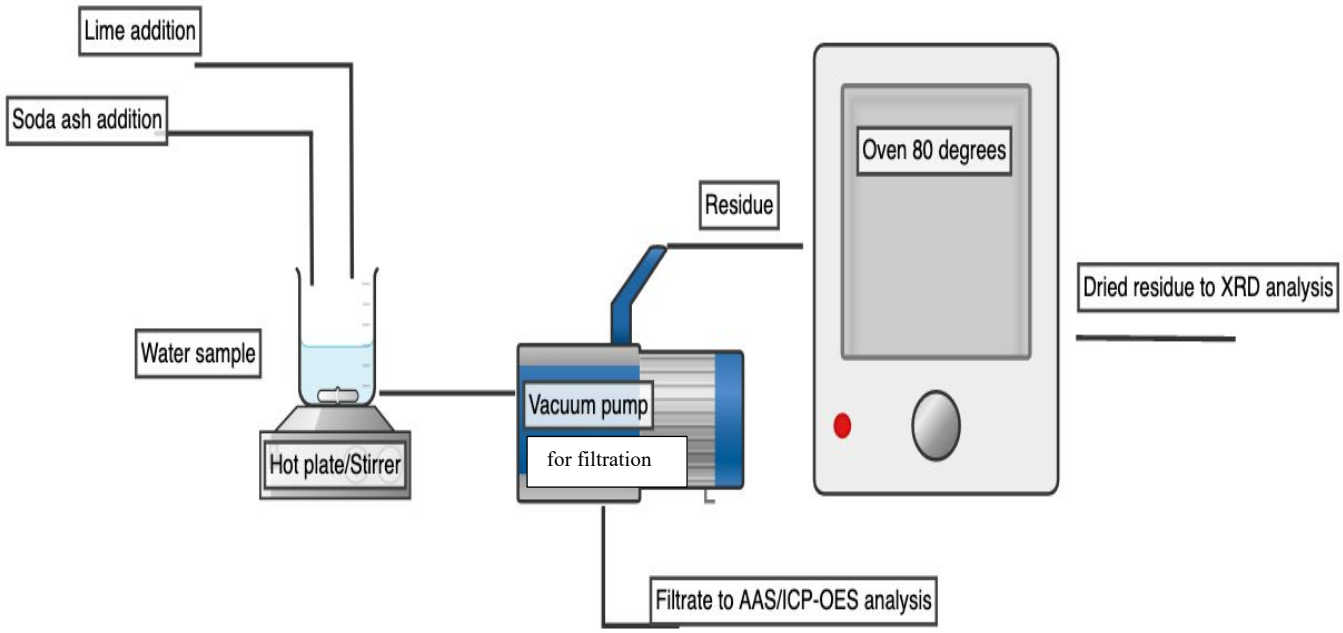


Figure 3. 4 Diagrammatic representation of the lime-soda ash process

3.2.2.5 The effect of temperature on the efficiency of lime and soda ash hardness removal

In a similar manner to section 3.2.2.3, only the scrubber bleed and process water samples were utilized in this experiment. The procedures outlined in the steps of section 3.2.2.4 were replicated, but this time at elevated temperatures of 40 °C, 60 °C, 80 °C, and 100 °C. The samples were dosed with the stoichiometric amounts of lime and soda ash as calculated in Table 3.1. To achieve the desired temperatures, a hot plate was employed, and a thermometer was used to monitor and record the temperature throughout the process. Each sample test was conducted in triplicate to account for any uncertainties or variations in the results. The average outcomes of these tests are presented in Chapter 5, section 5.2, providing valuable insights into the effects of temperature on the efficiency of lime and soda-ash softening for the removal of hardness from the scrubber bleed and process water samples.

3.2.3 The efficiency of ion exchange resins on hard water

3.2.3.1 Resin loading

For the evaluation of Ca and Mg removal efficiency, batch reactions were conducted using both a SAC and WAC resin. The hard water samples used in the experiments were initially filtered to remove any suspended solids. Prior to usage, the SAC resin was treated with 1 M

sodium chloride (NaCl), while the WAC resin was treated with 1 M hydrochloric acid (HCl) to ensure they were in the correct form. In the column setup, a volume equivalent to five bed volumes (bv) of each solution was passed through the respective resin at a flow rate of 2 bv/h. Subsequently, a rinsing step was carried out using deionized water at the same flow rate of 2 bv/h. These procedures were performed following the guidelines provided by DuPont™ (Amber series, 2022). The resulting s-curves, which depict the breakthrough behaviour of the resin and the removal efficiency of Ca and Mg, were plotted. The properties of both the WAC and SAC resins, along with the suggested operating conditions provided by DuPont™ (Amber series, 2022), can be found in Appendix 1, offering further details and information.

3.2.3.2 Determining optimal operating parameters for resin batch reactions

The process water sample was utilized to determine the optimal operating parameters for the resin batch reactions. These parameters include:

3.2.3.2.1 Effect of pH on resin adsorption of calcium and magnesium in hard water

In order to determine the optimal pH for maximum resin efficiency, the process water sample's initial pH was adjusted using 1 M HCl and 1 M NaOH. The pH of the hard water sample plays a crucial role in the resin's ability to adsorb Ca and Mg ions. For the WAC resin, the initial pH range of the process water sample was studied between 1 and 12. This range was selected based on the resin's operating stabilities according to DuPont™. The pH of the solution was measured using a pH meter. Throughout the experiments, the temperature was maintained at 25 °C, stirring speed at 150 rpm, resin amount at 10 g, and contact time at 60 minutes. Each run involved using 250 mL of the process water sample, and samples were taken at 10-minute intervals to determine the residual concentrations of Ca and Mg using atomic absorption spectroscopy (AAS) and ICP-OES. The tests were conducted in duplicate to establish a measure of uncertainty. Similarly, for the SAC resin, the initial pH range of the process water sample was investigated between 4 and 14, again based on the resin's operating stabilities. The experimental setup, conditions, and measurements were carried out in the same manner as described above. By studying the residual concentrations of Ca and Mg at different pH levels, the optimal pH for maximum resin efficiency in removing these ions from the process water sample can be determined. The average results of the experiments are presented in Chapter 6, section 6.2.2.1, along with the analysis of the resin's performance at different pH values.

3.2.3.2.2 Effect resin mass on resin adsorption of calcium and magnesium in hard water

To investigate the removal efficiency of hardness ions from hard water in relation to the mass of resin used, different masses of resin were employed in the experiments. The mass of resin tested ranged from 2 g to 12 g/ 250 mL of water sample based on recommendations from DuPont™. Throughout the experiments, the temperature was maintained at 25 °C, stirring speed at 150 rpm, pH at 4.8 (which was adjusted using an 1 M HCl or base, 1 M NaOH), and contact time at 60 minutes. These conditions were kept constant to ensure consistency in the experimental setup. After the 60 minute contact time, samples were collected to determine the residual concentrations of Ca and Mg ions in the solution. The analysis of Ca and Mg concentrations was performed using AAS and ICP-OES. The experiments were conducted in duplicate, meaning that each condition (specific mass of resin) was tested twice. This duplication helps establish a measure of uncertainty and provides more reliable results. By analysing the residual concentrations of Ca and Mg at different resin masses, the relationship between the mass of resin and the removal efficiency of hardness ions can be determined. The average results of the experiments are presented in Chapter 6, Section 6.2.2.2, alongside the evaluation of the resin's performance at different masses.

3.2.3.2.3 Effect of shaking speed on resin adsorption of calcium and magnesium in hard water.

The effect of shaking speed on the removal efficiency of hardness ions by the resins was investigated by varying the shaking speed in the experiments. Shaking speeds ranging from 50 to 250 rpm were tested. During the experiments, the solutions containing the hard water samples and the resins were placed in a shaking incubator for a duration of 24 hours. The temperature was maintained at 25 °C, and the pH was kept constant at 4.8 throughout the experiments. After the 24 hour shaking period, samples were collected to determine the residual concentrations of Ca and Mg ions in the solution. The analysis of Ca and Mg concentrations was carried out using AAS and ICP-OES. The experiments were performed in duplicate, meaning that each shaking speed was tested twice. This duplication helps establish a measure of uncertainty and enhances the reliability of the results. By comparing the residual concentrations of Ca and Mg at different shaking speeds, the relationship between shaking speed and the removal efficiency of hardness ions by the resins can be examined. The average results of the experiments are presented in Chapter 6, Section 6.2.2.3, providing insights into the influence of shaking speed on the resin's performance in removing hardness ions.

3.2.3.2.4 Effect of contact time on resin adsorption of calcium and magnesium in hard water

The effect of contact time on the removal efficiency of hardness ions by the resins was investigated by varying the duration of contact between the resins and the hard water samples. The experiments were conducted in a shaking incubator for a total duration of 24 hours. During the experiments, the temperature was maintained at 25 °C, the stirring speed was set at 150 rpm, and the pH was kept constant at 4.8. The samples were collected at specific time intervals: 20, 40, 60, 80, 100, 200, 400, 720, and 1440 minutes. After each time interval, samples were taken from the solution to determine the residual concentrations of Ca and Mg ions. The analysis of Ca and Mg concentrations was carried out using AAS and ICP-OES. The experiments were performed in duplicate, meaning that each contact time was tested twice. This duplication helps establish a measure of uncertainty and enhances the reliability of the results. By examining the changes in the residual concentrations of Ca and Mg over different contact times, the relationship between contact time and the removal efficiency of hardness ions by the resins were studied. The average results of the experiments are presented in Chapter 6, section 6.2.2.4, providing insights into the optimal contact time required for effective removal of hardness ions by the resins.

3.2.3.1 Determining cation resin efficiency in the removal of calcium and magnesium for all samples

In order to evaluate the resin capacities for all four water samples, the optimal parameters determined from the previous test work were applied. Two hundred and fifty (250) mL of each water sample were treated with 10 g of both the SAC and WAC resins, respectively. A total of eight (8) samples were prepared, including duplicate runs, for each resin type. The samples were placed in a shaking incubator and agitated at a speed of 150 rpm for a duration of 60 minutes. This contact time was determined as optimal based on previous experiments. After the 60 minute treatment period, the samples were taken for analysis using ICP-OES to determine the resulting concentrations of Ca and Mg ions. The ICP-OES analysis provides accurate measurements of elemental concentrations in the samples. To establish a measure of uncertainty, the test was performed in duplicate for each water sample, ensuring reliability and consistency of the results. The average results obtained from the duplicate runs are presented in Chapter 6, Section 6.2.4, which discusses the resin capacities for the removal of Ca and Mg ions from the four water samples.

3.2.3.2 Resin efficiency with lime and soda ash pre-treatment of hard water

To evaluate the resin efficiencies with lime and soda ash as a pre-treatment, the resulting solutions generated from the excess lime and soda ash test work in Section 3.2.2.4 were used. The experimental procedure followed was the same as in Section 3.2.3.1. Eight (8) samples, including duplicate runs, were prepared using the resulting solutions. These samples were placed in a shaking incubator and agitated for a duration of 60 minutes, maintaining the same conditions of temperature, stirring speed, and pH as in previous tests (25 °C, 150 rpm, and pH 4.8, respectively). After the 60 minute treatment period, the samples were taken for analysis using ICP-OES to determine the resulting concentrations of Ca and Mg ions. The ICP-OES analysis provides accurate measurements of elemental concentrations in the samples. To establish a measure of uncertainty, the test was performed in duplicate for each sample, ensuring reliability and consistency of the results. The average results obtained from the duplicate runs are presented in Chapter 6, Section 6.2.5, which discusses the resin efficiencies with lime and soda ash as a pre-treatment for the removal of Ca and Mg ions.

3.2.4 The effect of magnetic water treatment (MWT) on hard water

3.2.4.1 Preliminary MWT time exposure effects on solution pH AND dissolved oxygen (DO)

The first MWT (Magnetic Water Treatment) setup shown in Figure 3.5 was designed and constructed specifically to investigate the potential effects of a magnetic field on pH (acidity/alkalinity) and DO levels in the process water sample. The process water sample, which was previously described as a reservoir for topping up the scrubber feed, was utilized for these preliminary tests.

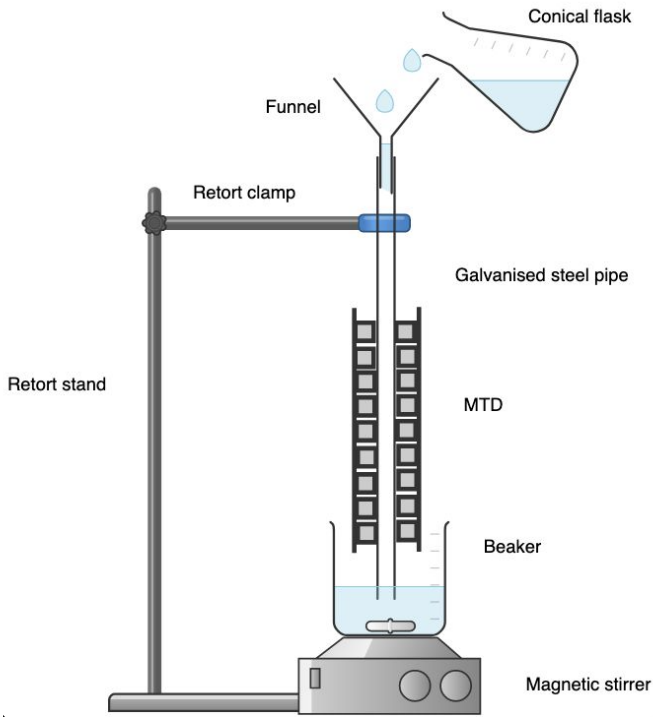


Figure 3. 5 Preliminary MWT setup for effect on pH and DO

The MTD used in the experiment consisted of a galvanized steel pipe with a diameter of 20 mm and a length of 1 m. Along this pipe, a total of 10 pairs of neodymium magnets were arranged in an alternating manner, with north and south poles placed adjacent and opposite to each other as depicted in Figure 3.6.



Figure 3. 6 Inverted magnet orientation on MTD

In the experiment, before subjecting the 250 mL water samples to the MTD, the initial pH and DO values of each sample were measured and recorded. These initial values served as a baseline for comparison. The water samples were then passed through the MTD at different numbers of passes: 1x pass, 2x passes, and 5x passes. The purpose was to evaluate whether successive passes through the MTD would have any effect on the pH and DO levels of the samples. During the magnetic treatment process, the samples were magnetically stirred at low

speeds to ensure proper mixing and interaction with the magnetic field. pH and DO readings were collected at each pass to monitor any changes in these parameters. To account for experimental variability and establish a measure of uncertainty, each test was performed in triplicate. This means that the entire process, including the initial measurement, passing the samples through the MTD, and recording the pH and DO values, was repeated three times for each sample. The resulting data were then used to calculate the average values, and error bars were added to the graphs in Chapter 7, Section 7.2.1, to indicate the level of uncertainty associated with the measurements.

3.2.4.2 Effect of adjusted MTD time exposure on electrical conductivity, calcium concentration, dissolved oxygen and oxidation reduction potential

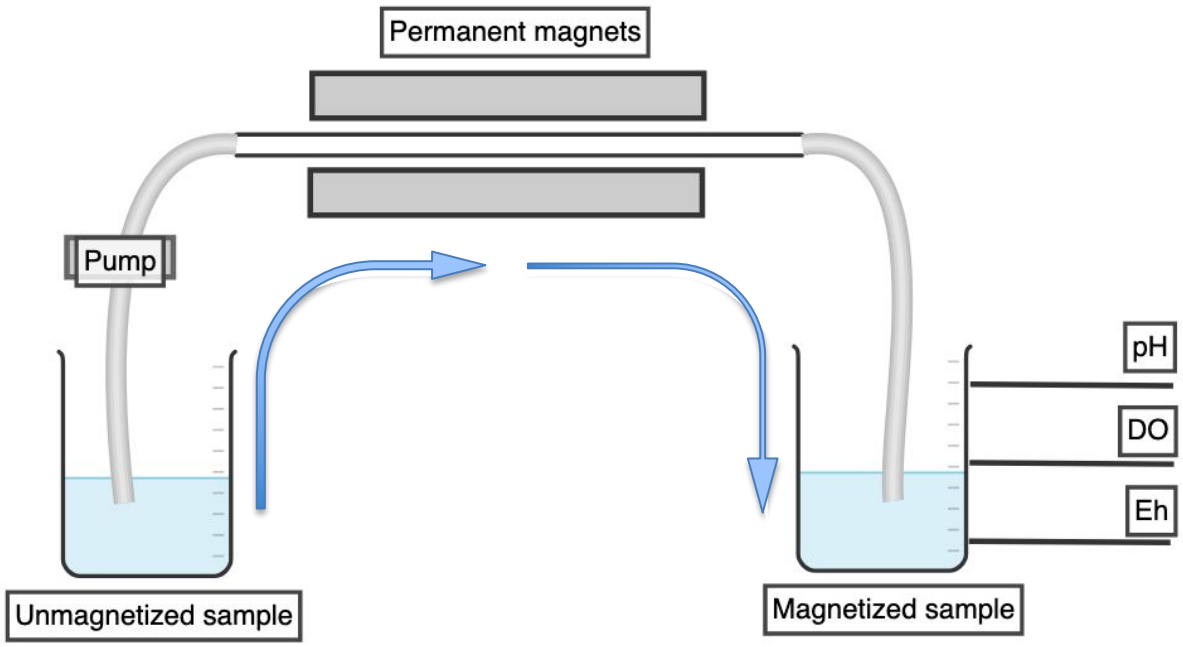


Figure 3. 7 Adjusted MTD for further tests

To assess the effectiveness of the MTD on the water parameters, control experiments were conducted both in the presence and absence of the MTD. The purpose of these control experiments was to validate the influence of the magnetic effect on the measured water parameters. The efficiency of the MTD was determined using Equation 3.9, which calculates the percent change in a parameter before and after exposure to the MTD (Gabrielli et al., 2001). The equation is defined as:

$$Percent\ change\ (\%) = (P_f - P_i/P_i)*100 \quad [3.9]$$

In this equation, P_f represents the final value of the parameter after exposure to the MTD, and P_i represents the initial value of the parameter before exposure. In each experiment, a 250 mL solution was passed through the MTD for a duration of 60 minutes, following the configuration shown in Figure 3.7. Samples were collected every 10 minutes, and the EC, [Ca^{2+}], DO, and E_h were measured. Similarly, the same solutions were passed through a pipe without the MTD to serve as the control. This allowed for a comparison between the results obtained with and without the MTD. To account for experimental variability and establish a measure of uncertainty, each experiment was conducted in duplicate. This means that the entire process, including passing the solution through the MTD or the pipe without the MTD, was repeated twice. The average results of these experiments are presented in Chapter 7, Section 7.2.2, along with the percent change in the measured parameters to assess the efficiency of the MTD.

3.2.4.3 Influence of the magnetic strength variation on hard water

3.2.4.3.1 Effect of number of magnets/ length of MTD on calcium concentration

In this experimental setup, the configuration depicted in Figures 3.6 and 3.7 was utilized, but the strength of the magnetic field was varied by altering the number of magnets used. Specifically, different configurations of the magnetic treatment device (MTD) were created by changing the number of magnet pairs, which resulted in the MTD being shortened or lengthened. Four different configurations were tested, corresponding to 2, 4, 6, and 8 pairs of magnets. The samples were passed through each MTD configuration for a duration of 60 minutes. After the treatment, Ca^{2+}] in the samples was measured again. To ensure reliable results and establish a measure of uncertainty, each test was conducted in duplicate. This means that the entire process, including passing the samples through each MTD configuration, was repeated twice. The average results of these experiments, including the measured [Ca^{2+}] values, are tabulated and presented in Chapter 7, Section 7.2.3, of the report. By analysing the average results obtained for each MTD configuration, the impact of the magnetic field strength on the removal of calcium ions can be assessed and compared. The changes in [Ca^{2+}] can be examined to determine the effectiveness of the different MTD configurations in reducing calcium ion concentration in the treated water samples.

3.2.4.3.2 Effect of magnetic pole orientation on calcium concentration (inverted vs, non-inverted arrangement)

In this experimental setup, the influence of a varied magnetic field on the [Ca^{2+}] was observed by not inverting the magnetic poles as depicted in Figure 3.6. Instead, the MTD pole configuration used was similar to Figure 3.8, where 10 pairs of magnets were arranged along the galvanized steel pipe. By keeping the same pole configuration throughout the experiment, the aim was to compare the effects of different magnetic field strengths on the concentration of calcium ions. The strength of the magnetic field was altered by changing the number of magnets or pairs of magnets used in the MTD, as described in the previous response.



Figure 3. 8 Non-inverted magnetic pole orientation MTD

In this part of the experiment, the water samples were passed through the MTD for a duration of 60 minutes. After passing through the MTD, the parameters including pH, DO, and [Ca^{2+}] were measured again. This allowed for the assessment of any changes in these parameters after exposure to the magnetic treatment. Each test was conducted in duplicate to ensure reliability and establish a measure of uncertainty. The average results obtained from these duplicate tests, including the measurements of pH, DO, and [Ca^{2+}], were recorded and tabulated. These results are presented in Chapter 7, Section 7.2.3, of the report, providing a comprehensive analysis of the effects of the MTD on the measured parameters.

3.2.4.3.3 The combined effect of magnetic pole orientation and number of magnets on calcium concentration (inverted vs, non-inverted arrangement)

In this part of the experiment, the combined influence of a varied magnetic field and the number of magnets was investigated by inverting and not inverting the magnetic poles. This was done for different numbers of magnets, including 2, 4, 6, and 8. For each configuration (inverted and not inverted poles), the water sample was passed through the MTD for a duration of 60 minutes. The [Ca^{2+}] was measured after the treatment. Each test was conducted in duplicate to ensure accuracy and establish a measure of uncertainty. The average results obtained from these duplicate tests, including the measurements of [Ca^{2+}], were recorded and tabulated. These

results will be presented in Chapter 7, Section 7.2.3, of the report, providing a comprehensive analysis of the combined influence of the magnetic field and number of magnets on [Ca^{2+}].

3.2.4.4 The influence of flow rate on calcium concentration in a MTD

In order to examine the influence of flow rate on the effectiveness of the Magnetic Treatment Device (MTD) and its impact on the [Ca^{2+}], all four solutions were passed through the MTD setup depicted in Figures 3.6 and 3.7 at different flow rates. The pH, DO, and [Ca^{2+}] were measured after each run to evaluate the effects of the MTD at varying flow rates. The flow rates were adjusted to simulate different conditions similar to those around the scrubber at Sibanye-Stillwater from low to medium and high flowrates (~ 8—70 m^3/h). This test was conducted in triplicate to ensure reliable results and establish a measure of uncertainty. The average results obtained from these triplicate tests, including the measurements of pH, DO, and [Ca^{2+}], were recorded and presented in Chapter 7, Section 7.2.4, of the report. This provides valuable insights into the performance of the MTD at different flow rates and its impact on [Ca^{2+}].

3.2.3.5 The influence of pipe material of a MTD on calcium concentration

To examine the influence of different pipe materials on the performance of the Magnetic Treatment Device (MTD), various conducting and insulating materials were tested in addition to the galvanized steel that has been used previously. The pipe materials tested include:

1. Copper tube: A 1-meter long tube with a diameter of 20 mm made of copper.
2. Polyvinyl chloride (PVC1) tube: A clear and flexible tube, 1 meter long, with a diameter of 20 mm made of PVC.
3. Polyvinyl chloride (PVC2) tube: A white and rigid tube, 1 meter long, with a diameter of 20 mm made of PVC.

Similar to the previous experiments using galvanized steel, each 250 mL solution was passed through each pipe material using the same MTD configuration shown in Figures 3.6 and 3.7. The residence time for each solution in contact with the pipe material was approximately 60 minutes. The [Ca^{2+}] in each solution was measured after passing through the MTD. In addition, the same solutions were also passed five times through the respective pipe material without the MTD for comparison. This was done to evaluate the effectiveness of the MTD in removing calcium ions compared to the pipe material alone. For each pipe material tested, each of the

four solutions was run three times to establish a measure of uncertainty. The average results obtained from these multiple runs for each pipe material, including the measurements of [Ca^{2+}], are presented in Chapter 7, Section 7.2.5, of the report. This analysis provides insights into the impact of different pipe materials on the performance of the MTD and the removal of calcium ions from the solutions.

3.2.4.6 The effect of MTD on the scale produced

To investigate the potential influence of the Magnetic Treatment Device (MTD) on scale formation, the process water sample was subjected to the MTD under specific conditions:
The MTD configuration consisted of 10 permanent magnets with an effective field strength of 1.3 Tesla. The orientation of the magnetic poles was inverted. A galvanized steel pipe was chosen as the pipe material for water flow during magnetic exposure. The process water sample was passed through the MTD at two different flow rates: 0.75 L/min for 1 hour and 0.75 L/min for 3 hours. Samples were collected every 10 minutes during the treatment period to measure pH, E_h, DO, EC, and [Ca^{2+}]. After passing through the MTD, the treated sample was allowed to sit for 48 hours to allow for evaporation. The crystals that formed were then filtered, dried at 40 °C for 24 hours, and subjected to XRD analysis to identify the mineral phases present. The results obtained from these experiments, including the measurements of pH, E_h, DO, EC, [Ca^{2+}], and the identified mineral phases from XRD analysis, are presented in Chapter 7, Section 7.2.6, of the report.

By examining the changes in these parameters and the mineral phases formed, the study aims to determine whether the MTD has any influence on scale formation. This investigation provides insights into the potential effectiveness of the MTD in mitigating scale formation in the process water system.

3.3 Reagents

In this research, various reagents were utilized to investigate the formation of scale in lime and limestone scrubber circuits and to develop mitigation methods. The following reagents were used:

Sulphuric acid (H_2SO_4, 99 %) was used in the acid-base tests and pH adjustments when necessary. Hydrated lime ($Ca(OH)_2$, 96 %) and soda ash (Na_2CO_3, 99 %) were used in the precipitation reactions. The SAC (Amberlite IRC^{TM} 120Na) and WAC (Amberlite IRC^{TM} 83H) resins used in the treatment of hard water were obtained from DuPont. Sodium hydroxide pellets and HCl (37 %) were used to pre-treat the resins. Calcium carbonate, magnesium oxide (MgO), and NaCl were used in the preparation of stock solutions required for the preparation of standards used in AAS analysis. Distilled water was used in the preparation of all solutions. All reagents used were of analytical-grade quality and were obtained from either Sigma-Aldrich or ACE (Pty) Ltd. All solid and liquid samples used were obtained from Sibanye-Stillwater in Rustenburg.

3.3.1 Neodymium magnet properties

N35 neodymium block magnets measuring 50 mm * 20 mm * 3 mm were obtained from RS South Africa (Pty) Ltd and utilized in this study. The magnetic properties of these magnets are provided in Table 3.2, outlining their relevant characteristics.

Table 3. 2 N35 characteristic magnetic properties at room temperature (25°C) (*kjmagnets.com, 2022).*

Series	Grade	Max operating temperature (°C)	Remanence Br mT (G)	Coercivity Hcb KA/m (KOe)	Intrinsic Coercivity Hcb KA/m (KOe)	Maximum energy product (BH)max KJ/m^3 (MGOe)	Pull strength (Kg)
N	N35	80	1170-1220 (11700-12200)	>868 (>10.9)	> 955 (>12)	263-287 (33-36)	5.8

Figure 3.9 illustrates the orientation of the N35 neodymium block magnets used in this study. The two largest surfaces of the magnets correspond to the north and south poles, while the magnetic field direction is axial. It passes through the centre and thickness of the magnet.

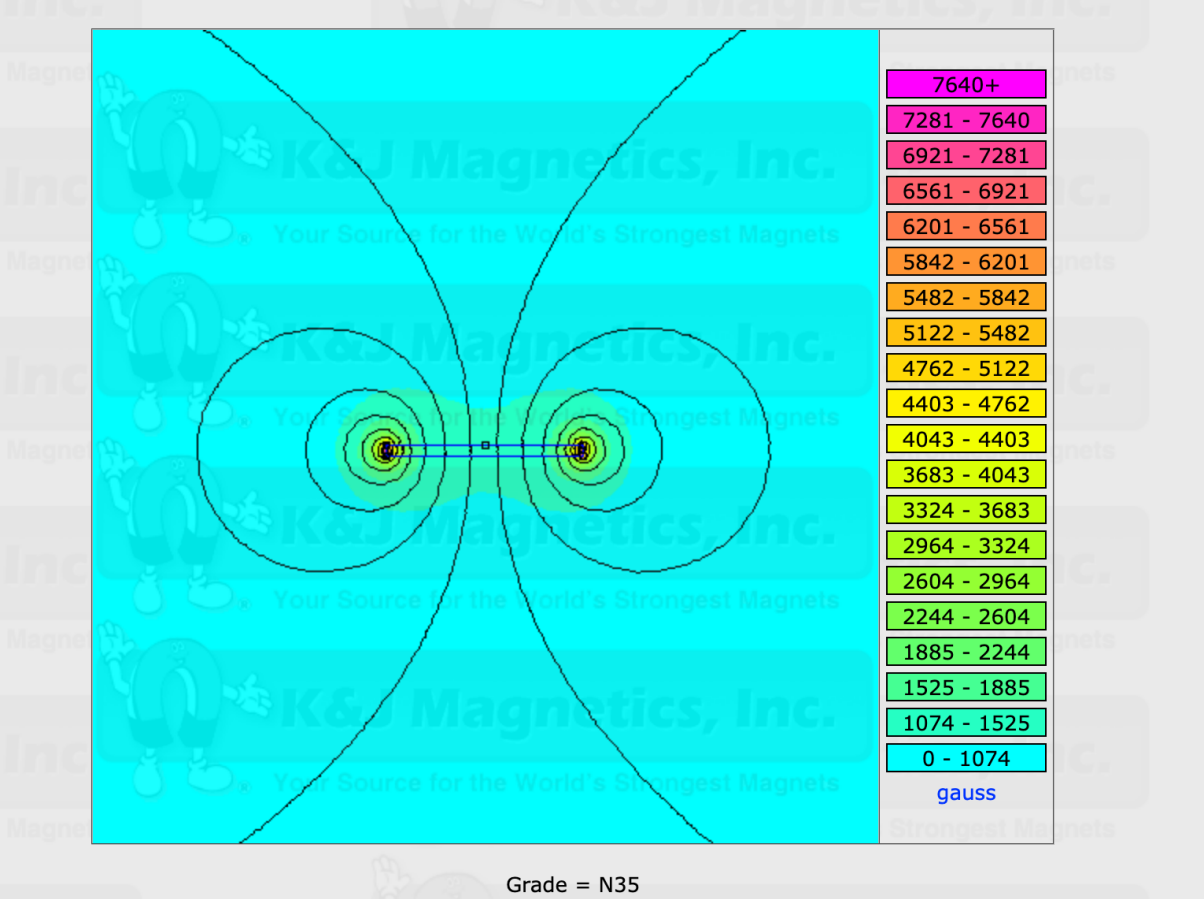


Figure 3. 9 Direction of magnetic field for the neodymium magnets used, axially magnetized (*kjmagnets.com, 2022)*

3.4 Analytical methods and techniques

Solution pH and redox potential (Eh) measurements were conducted using a benchtop Thermo Scientific™ Orion™ Star A211 pH meter equipped with a combination pH and temperature electrode. Prior to measurements, the pH meter and electrode were calibrated using pH 4.00, 7.00, and pH 10.00 buffer solutions. Dissolved oxygen (DO) in the solutions was measured using a HANNA HI2004 edge® DO meter. All solution concentrations were determined using wet chemical analysis methods. Atomic absorption spectroscopy was employed for most analyses, and in cases where applicable, the results were verified using ICP-OES. The AAS analyses were conducted in the School of Chemical and Metallurgical Engineering at the University of the Witwatersrand, while the ICP-OES analyses were carried out at UIS Analytical Services (Pty) Ltd in Pretoria. For the analysis of solid scale samples received and generated during precipitation and magnetic water treatment processes, qualitative and quantitative XRD and scanning electron microscope (SEM) techniques were employed. Thin petrographic samples for SEM analysis were prepared in the School of Geosciences at the University of the Witwatersrand. XRD analysis was performed using a PANalytical X'Pert Pro powder diffractometer in θ–θ configuration with an X'Celerator detector and variable divergence- and fixed receiving slits with Fe filtered Co-Kα radiation at the University of Pretoria. The relative phase amounts (expressed as weight % (wt. %) of the crystalline portion) were estimated using the Rietveld method with the Autoquan program. The magnetic field generated during the magnetic test work was measured using a handheld THM1176 MetroLab magnetometer, specifically a Gauss meter. This device allowed for accurate measurement and quantification of the magnetic field strength during the experiments.

3.5 Summary

This chapter has provided a comprehensive overview of the materials, reagents, methods, experimental design, data collection, and data analysis employed in the study. It has laid the foundation for the subsequent chapters of the dissertation where the experimental results and their discussions will be presented in Chapters 4 to 7.

3.6 References

Amber series (2022). Home. Available at: https://wwww.dupont.com/brands/amber-series.html/(accessed: January 19, 2022).

Cappelle, M.A. and Davis, T.A., 2016. Ion Exchange Membranes for Water Softening and High-Recovery Desalination. Emerging Membrane Technology for Sustainable Water Treatment, p.163.

Entezari, M.H. and Tahmasbi, M., 2009. Water softening by combination of ultrasound and ion exchange. Ultrasonics sonochemistry, 16(3), pp.356-360.

Faust, S.D. and Aly, O.M., 2018. Chemistry of water treatment. CRC press.

Gabrielli, C., Jaouhari, R., Maurin, G., Keddam, M., 2001. Magnetic water treatment for scale prevention. Water Research 35 (13), 3249–3259.

K&J magnets- magnetic field visualization. Available at: https://www.kjmagnets.com (accessed: 9 August 2022).

Minnesota Rural Water Association. 2009. Lime softening. Minnesota Water Works Operations Manual. 4th edn. Elbow Lake, MN. Chapter 16.

Narain, A., Potgieter, J.H., Rencken, G.E. and Smith, J., 2021. Beneficiation of recycled process water at DRDGOLD's ERGO plant, and its effect on gold recovery. Journal of the Southern African Institute of Mining and Metallurgy, 121(7), pp.331-343.

Chapter 4 Characterisation of solid scale and liquid samples

4.1 Introduction

In this chapter, characterisation of solid scale and liquid process water samples was included to provide a comprehensive understanding of their physical and chemical attributes. This characterisation aided in determining appropriate strategies for preventing or minimising scale formation. The composition of scale deposits, as mentioned in Chapter 2, can vary depending on the chemistry occurring in the scrubber and the composition of the water and feed material. The solid samples, such as the precipitates formed after passing the samples through the MTD and allowing precipitation, can be analysed using techniques such as XRD. X-ray diffraction analysis (XRD) can identify the mineral phases present in the precipitates, providing insights into the composition of the scale deposits. The results obtained from the XRD analysis are discussed in this chapter to highlight the specific minerals identified and their relative concentrations. In addition to the solid samples, the liquid samples taken during the experiments were also characterised. This characterisation can involve analysing the chemical composition of the samples using techniques such as ion chromatography or AAS. These analyses can provide information on the concentrations of Ca^{2+}, CO_3^{2-}, SO_4^{2-}, and OH^- ions, which are important constituents in scale formation. Overall, by fully characterising both the solid and liquid samples, the dissertation will provide a comprehensive understanding of the physical and chemical attributes of the samples, leading to a better understanding of scale formation and the potential mitigation strategies.

4.2 Results and discussion

4.2.1 Solid scale samples

4.2.1.1 Acid-base tests (preliminary tests)

Acid-base tests for the solid samples involved observing their reaction to acidic solutions. The solid's effervescence (bubbling) when in contact with an acid indicates the presence of a carbonate or sulphate compound. The tests carried out according to equations (4.1—4.3) below and section 3.2.1.1, indicated the presence of a sulphate as well as a carbonate, respectively in the scale samples:

$$Ba^{2+} + SO_4^{2-} \rightarrow BaSO_4\ (s) \qquad [4.1]$$

$$2\,H^{+} + CO_3^{2-} \rightarrow CO_2 + H_2O \quad [4.2]$$

The CO_2 reacts with a solution of limewater to form the $CaCO_3$ as a precipitate,

$$CO_2 + Ca(OH)_2 \rightarrow CaCO_3\,(s) + H_2O \quad [4.3]$$

While the tests indicated the presence of a sulphate and carbonate in the scale, it was also important to determine the compound or mineral hosting these species through XRD and SEM.

4.2.1.2 XRD analysis of solid scale samples

The X-ray diffraction (XRD) analysis of the scale samples collected from the scrubber between the period 2014 and 2016 revealed that gypsum, talc, and calcite were the predominant mineral phases present. All seven scale samples exhibited a significant composition of these minerals. The detailed average XRD results, showing the relative abundance of each mineral phase, are presented in Table 4.1. To gain a deeper understanding of the mineral phases that were most abundant, the unit cell parameters of the dominant phases were determined. This was achieved through the application of the Rietveld Refinement method using the high score software. This method precisely determines the crystal structure of materials by fitting observed diffraction patterns with calculated patterns, allowing for accurate determination of crystallographic parameters, phase composition, and crystallite size. By refining the unit cell, precise values for the unit cell parameters were obtained. The unit cell parameters provide information about the crystal structure of each mineral phase. Table 4.2 presents the unit cell parameters for the most abundant mineral phases, namely gypsum, talc, and calcite. The comprehensive XRD analysis and determination of unit cell parameters contribute to a thorough characterization of the scale samples. The results confirm the prevalence of gypsum, talc, and calcite in the scale deposits from the scrubber. These findings are of great significance for understanding the mineralogical composition and crystallographic properties of the scales. The data presented in Tables 4.1 and 4.2 provide a foundation for further discussions, focusing on the implications of gypsum, talc, and calcite in scale formation and potential strategies for scale mitigation.

Table 4. 1 X-ray diffraction average results (Relative Abundance).

Mineral	Formula	Mass %	Relative abundance *
Gypsum	$CaSO_4$	81.67	Predominant
Talc	$Mg_3Si_4O_{10}(OH)_2$	4.95	Minor
Calcite	$CaCO_3$	4.76	Minor
Quartz	SiO_2	3.08	Trace
Anorthite	$CaAl_2Si_2O_8$	2.3	Trace
Actinolite	$Ca_2Si_8O_{22}(OH)_2$	1.43	Trace
Dolomite	$CaMg(CO_3)_2$	1.29	Trace
Muscovite	$(KF)_2(Al_2O_3)_3(SiO_2)_6$	0.5	Trace
Total		99.98	

***Predominant (> 50 mass %), Major (20—50 mass %), minor (20—5 mass %) and trace (< 5 mass %).**

The addition of lime in the scrubber for the neutralization of the weak acid stream (H_2SO_3) (as discussed in section 2.3.3) results in the formation of a scale predominantly composed of calcium compounds, which aligns with expectations based on previous studies (Buecker, 2008; Kemmer, 1979; Rosenberg and Grotta, 1979; Wen et al., 1975). The Ca compounds are the main constituents of this particular scale, highlighting the significance of Ca in the precipitation process. These observations further support the understanding of the scale formation mechanism and the role of lime in the scrubbing process.

Table 4.2 provides the unit cell parameters for two of the major mineral phases identified in all the scale samples. It is crucial to determine the crystal structure(s) of these minerals as they significantly contribute to the material's properties and behaviour. Calcium carbonate and calcium sulphate minerals are known to exist in multiple polymorphs (Guo et al., 2019; Koutsoukos and Kapetanaki, 2016; Wang et al., 2013). Through XRD analysis, the unit cell parameters were determined, revealing that the polymorphs of these minerals in the scale samples were gypsum ($CaSO_4.2H_2O$) and calcite ($CaCO_3$) respectively. These findings provide important insights into the specific mineral phases present in the scale deposits, contributing to a better understanding of their composition and behaviour.

Table 4. 2 Average unit cell parameters for the mineral phases of gypsum and calcite.

Unit cell parameters	Gypsum (monoclinic)	Calcite (hexagonal)	Talc (anorthic)
a (Å):	6.28	8.75	5.3
b (Å):	15.21	4.69	9.1
c (Å):	5.68	8.28	18.2
Alpha (°):	90	90	90
Beta (°):	114.0	94.4	101
Gamma (°):	90.0	120.0	90

These unit call parameters are in accordance and agreement with a few studies as well (Comodi et al., 2008; Jacques et al., 2009; Nazzareni, 2010; Pedersen and Semmingsen, 1982). The polymorphs for calcium sulphate are gypsum, anhydrite ($CaSO_4$) and hemihydrate ($CaSO_4.1/2H_2O$) while those of $CaCO_3$ are calcite, aragonite and vaterite (Lisitsin-Shmulevsky et al. 2020; Wang et al., 2012). Gypsum and calcite are known to be the most stable polymorphs with respect to the others of calcium sulphate and calcium carbonate, respectively (Lisitsin-Shmulevsky et al. 2020; Wang et al., 2012). This means that the conditions presented in the scrubber, factors such as temperature, solution concentration and pH, favour the formation of these specific polymorphs as part of the scale.

Table 4.3 gives the quantitative XRD results of all seven samples collected from the scrubber. The surface analysis of these samples was done to further identify the mineral phases present, particularly to distinguish those available in larger quantities. These SEM photomicrographs as well as their corresponding energy dispersive spectroscopy (EDS) spectra are presented and discussed in the next section.

Table 4. 3 XRD quantitative analysis of scrubber samples.

Sample	Actinolite $Ca_2Si_8O_{22}(OH)_2$ (wt %)	Calcite $CaCO_3$ (wt %)	Gypsum $CaSO_4$ (wt %)	Quartz SiO_2 (wt %)	Talc $Mg_3Si_4O_{10}(OH)_2$ (wt %)	Dolomite $CaMg(CO_3)_2$ (wt %)	Muscovite $KAl_2(F, OH)_2$ (wt %)	Arnothite $CaAl_2Si_2O_8$ (wt %)
1	1.99	4.02	83.68	4.04	5.24	-	1.03	-
2	1.55	4.95	73.25	1.32	9.87	7.03	2.03	-
3	2.03	7.69	85.87	0.64	1.89	-	-	1.88
4	-	-	98.72	1.28	-	-	-	-
5	-	8.77	85.41	2.13	2.24	-	-	1.46
6	1.82	3.2	80.38	9.4	4.7	-	0.5	12.77
7	2.66	4.68	64.38	2.79	10.74	1.98	-	-

Samples four, five, and seven were found to have the highest mass percentages of gypsum, calcite, and talc, respectively. These specific minerals were highlighted due to their significance in understanding the physical and chemical properties associated with the scale formation in the scrubber. Investigating the chemistry involved in scale formation is a crucial objective of this study, as outlined in Section 1.4. By focusing on these minerals, we can gain valuable insights into the underlying processes and mechanisms driving the scale formation, contributing to the overall aim of this research.

4.2.1.3 SEM-EDS analysis

Due to the highly carbonaceous nature of the scale samples, it was necessary to prepare petrographic thin sections before conducting surface morphology analysis using SEM-EDS. Figure 4.1 displays the surface morphology of three of the analysed samples. Table 4.3 provides quantitative data on the largest minerals present, with gypsum, calcite, and talc highlighted in grey. Furthermore, Table 4.4 presents three corresponding EDS analyses (samples four, five, and seven) to provide estimates of the elemental abundance within these

three major phase minerals. These findings contribute to a comprehensive understanding of the composition and characteristics of the scale samples.

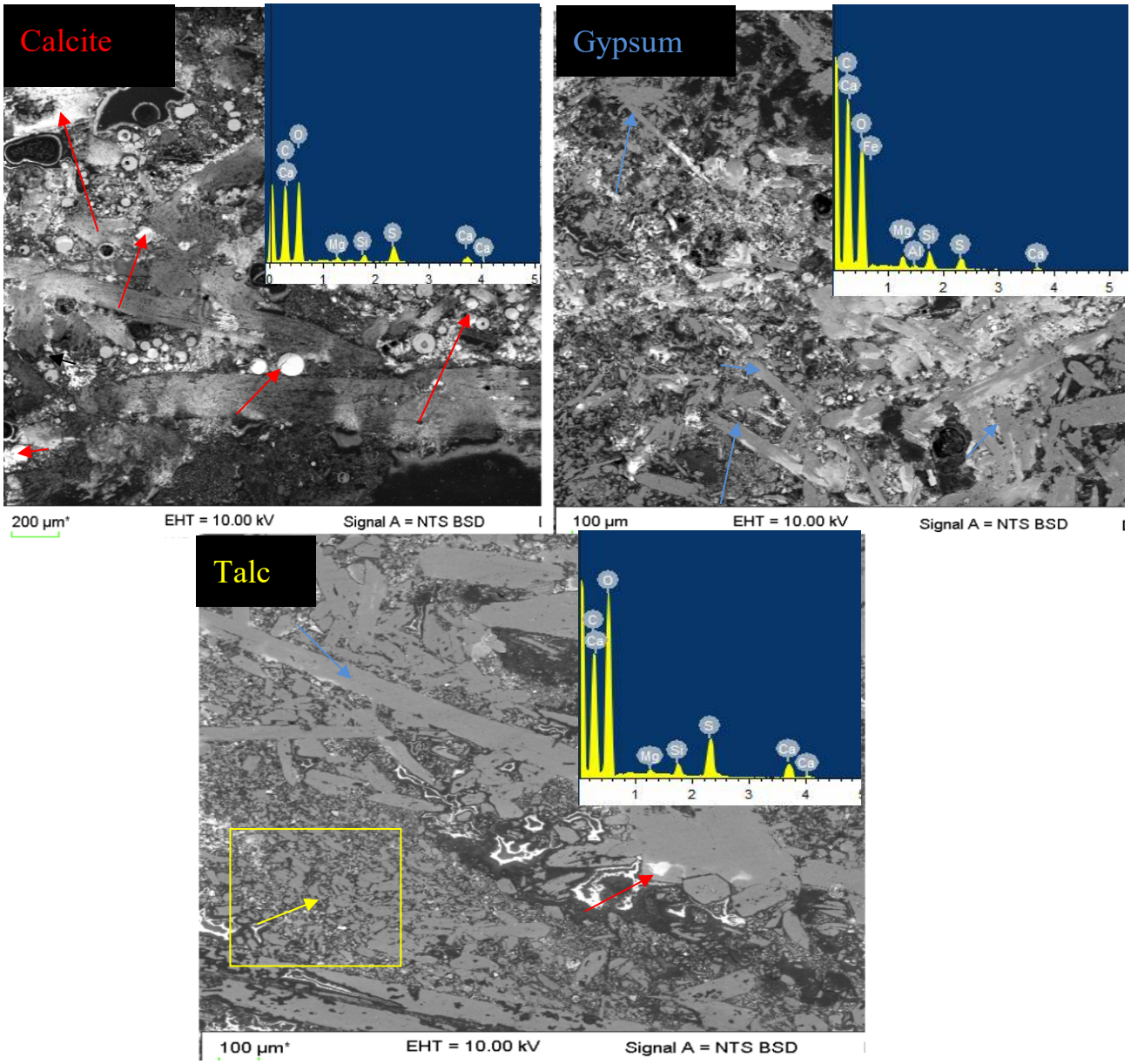


Figure 4. 1 SEM photomicrographs of three of the samples collected presenting major crystal phases

The analysis reveals that gypsum, identified as the largest mineral phase in all the samples, is uniformly distributed and exhibits a distinctive needle-like crystal structure, consistent with observations made by other researchers (Jarc et al., 2017; Kumareson and Devanarayanan, 1987; Van Rosmalen et al., 1976). The photomicrographs clearly show the presence of white areas, indicating the presence of calcite minerals, while talc appears as small grains, particularly

noticeable in sample seven. These distinct mineral phases and their characteristic features provide insights into the composition and morphology of the scale samples.

Table 4. 4 EDS element analysis of gypsum, calcite and talc crystals.

	Sample 5: Calcite ($CaCO_3$)		Sample 4: Gypsum ($CaSO_4$)		Sample 7: Talc ($Mg_3Si_4O_{10}(OH)_2$)	
Element	**Wt. %**	**Atomic%**	**Wt. %**	**Atomic%**	**Wt. %**	**Atomic%**
C	47.03	56.92	3.67	5.35	16.15	25.02
O	42.13	38.28	78.11	85.41	42.97	49.98
Mg	0.64	0.38	-	-	10.35	7.92
Si	1.33	0.69	-	-	20.95	13.88
S	5.70	2.58	11.76	6.42	-	-
Ca	3.17	1.15	6.46	2.82	-	-
Fe	-	-	-	-	9.59	3.19
Totals	100.00		100.00	-	100.00	

4.2.2 Liquid samples

In order to determine the source of scaling and gain insight into the solution chemistry that contributes to scale formation, water samples from the scrubber circuit were also analysed. Four liquid samples were collected, which included:

1. Scrubber feed
2. Scrubber bleed
3. Dust thickener overflow

4. Process water

Figure 4.2 illustrates the scrubbing circuit from which these samples were obtained, with the sample points clearly indicated. These samples were collected to provide a comprehensive understanding of the water chemistry within the scrubber system and to identify any potential sources of scaling.

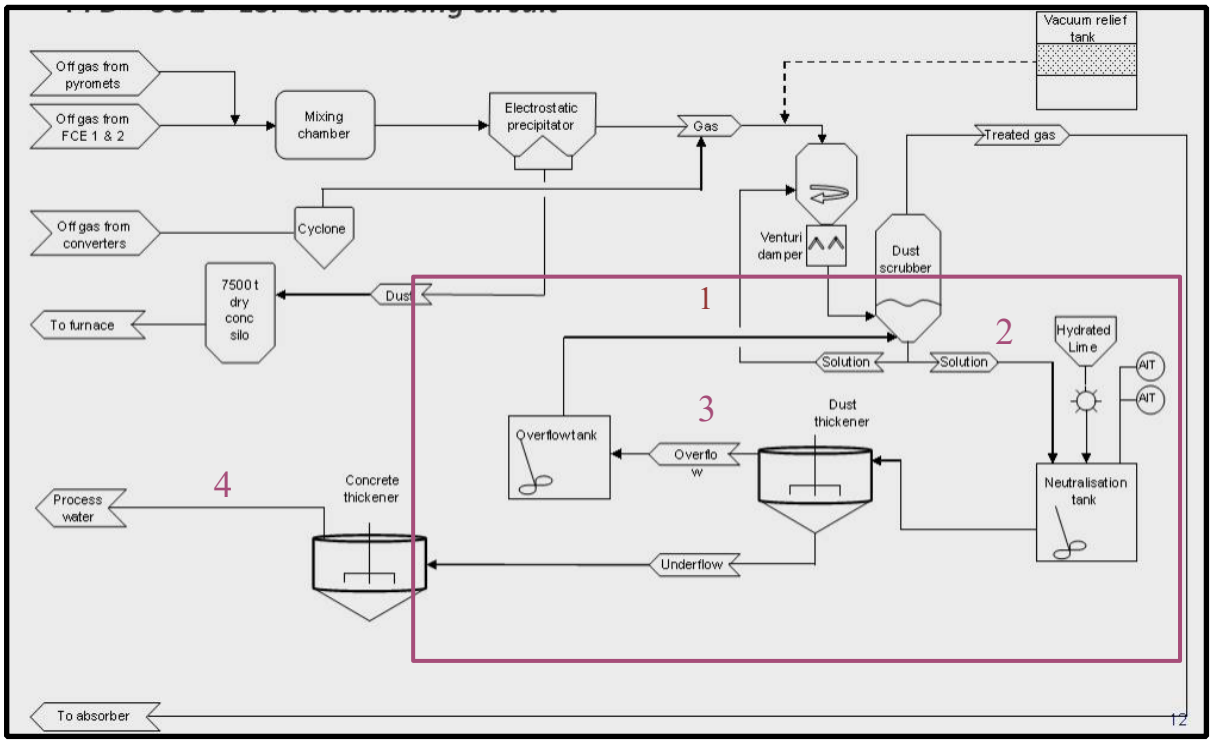


Figure 4. 2 Liquid sample points from the scrubbing circuit

4.2.2.1 Analysing received AAS

Regular analysis using Atomic Absorption Spectroscopy (AAS) was conducted on the process water and dust-thickener overflow samples over the course of a year. The analysis, performed by plant personnel at Sibanye, focused on the determination of sodium (Na) and calcium (Ca) concentrations. Table 4.5 presents the average values obtained from these AAS analyses for the selected elements.

Table 4. 5 Received AAS and pH analysis on process water and dust thickener overflow sample.

Sample	Na (avg.) (mg/L)	Ca (avg.) (mg/L)	pH
Process water	1064	846	6.5
Dust thickener overflow	2196	1145	6.3

In order to fully characterize the source of scaling, a comprehensive elemental analysis was conducted on all four water samples. This analysis included major and trace elements, as well as cations and anions. All four samples were analysed through ICP-OES analysis, which provided information on the elemental composition of the samples. Additionally, the analysis provided insights into the physico-chemical properties of the water samples, such as EC, alkalinity, and TDS. The results of this analysis will be presented in Section 4.2.2.2.

4.2.2.2 ICP-OES analysis

Table 4.6 presents the results of the ICP-OES analysis conducted on the four water samples, indicating the concentrations of relevant elements, particularly those found in the highest amounts. Additionally, the corresponding pH values for each water sample are provided. The analysis allowed for a comprehensive understanding of the chemical composition of the water samples and identified the elements present at significant levels.

Table 4. 6 ICP-OES analysis of all four liquid samples.

Sample	Ca [mg/L]	Fe [mg/L]	Mg [mg/L]	Na [mg/L]	S [mg/L	Si [mg/L]	SO_4^{2-} [mg/L]	Ni [mg/L]	K [mg/L]	Mn [mg/L]	pH
Scrubber bleed	517	478	1740	2180	3110	165	9410	273	71.9	321	3.24
Scrubber feed	574	292	1500	2180	2730	134	7850	40.7	66.5	158	5.18
Dust thickener overflow	497	339	1600	2200	2830	142	8150	9.23	65.5	120	6.38
Process water	521	0.44	111	1530	1220	13.9	3340	30.4	20.1	1.07	4.81

The analysis revealed that all four water samples exhibited remarkably high concentrations of ions, with the following order of predominance: SO_4^{2-} > S > Na > Mg > Fe > Ca > Si > Mn > K > Ni. It became apparent that the AAS analysis conducted on-site by plant personnel, as shown in Table 4.5, was not as accurate as the subsequent ICP-OES analysis for the process water and dust-thickener overflow samples. The ICP-OES results indicated significantly higher levels of sodium (Na) and Ca in comparison. Additionally, the pH values of the water samples were slightly more acidic than those reported by the plant. The high mineral content observed in the water samples aligns with the issue of scaling in the scrubber circuit. The formation of gypsum, calcite, and other mentioned mineral phases can be attributed directly to the presence of these supersaturated waters. The concentrations of Ca and Mg are particularly important, as they provide an indication of the overall hardness of the water samples. In the subsequent section, the hardness of each water sample and additional physico-chemical characteristics will be calculated and discussed.

4.2.2.3 Determining alkalinity and sum of ions

Table 4.7 presents the results of additional ICP-OES analysis conducted to determine the concentrations of phosphorus (P), manganese (Mn), CO_3^{2-} alkalinity, and HCO_3^- alkalinity in the water samples. The sums of the anions and cations were also calculated. These parameters provide further characterization of the samples and contribute to a comprehensive understanding of their physico-chemical properties.

Table 4. 7 Additional analysis of physico-chemical water parameters.

Sample name	Alkalinity (as mg/L $CaCO_3$)					Sum of ions (me/L)		
	M	P	CO_3^{2-}	HCO_3^-	OH^-	Anions	Cations	% Error
Scrubber bleed	3.5	0	0	3.5	0	277	208	14.3
Scrubber feed	26.5	0	0	26.5	0	243	173	16.8
Dust thickener overflow	60.5	0	0	60.5	0	250	182	16.4
Process water	13	0	0	13	0	124	70.5	27.6

From the P and M values obtained from the titration analysis, all four samples indicated a P value of 0. This means that the total alkalinity is in the form of and CO_2 and HCO_3^- and thus no alkalinity in the form of carbonate and hydroxide is present as illustrated in Figure 2.13 (noted in Table 4.7) (Bates, 2001; Minnesota Rural Water Association, 2009). Considering the calculated values for m-alkalinity, namely m = 26.5, 60.5, 3.5 and 13 (mg/L of $CaCO_3$), and the pH of the samples is less than 8.3, the alkalinity data could be analysed in relation to the sample's acidity.

M-Alkalinity: Overall, the m-alkalinity values indicate varying levels of buffering capacity against acidity, with higher values suggesting a stronger ability to resist pH changes. For m = 26.6 mg/L $CaCO_3$ equivalent: This indicates a moderate level of m-alkalinity, suggesting the presence of bicarbonate and carbonate ions in the water. For m = 60.5 mg/L $CaCO_3$ equivalent: This value represents a higher level of m-alkalinity. It indicates a stronger buffering capacity against pH changes due to the higher concentration of bicarbonate and carbonate ions in the water sample. For m = 13 mg/L and 3.5 mg/L $CaCO_3$ equivalent: This value represents a relatively lower m-alkalinity level compared to the previous values. It suggests a weaker buffering capacity against pH changes, indicating a lower concentration of bicarbonate and carbonate ions.

P-Alkalinity: With p = 0 mg/L $CaCO_3$ equivalent: This value indicates that there is no detectable concentration of OH^- or weak bases contributing to the p-alkalinity. The absence of p-alkalinity suggests that the alkalinity attributed to hydroxides and weak bases, as measured by the phenolphthalein indicator, is negligible or absent. In the case of the provided alkalinity values for four samples (m = 26.5, 60.5, 3.5, and 13 mg/L of calcium carbonate) and their corresponding pH measurements (5.18, 6.38, 4.8, and 3.2, respectively), we can observe a clear alignment with this relationship. Let's examine the data in order:

1. Scrubber bleed with m = 3.5 mg/L of $CaCO_3$ exhibits a pH of 4.8.
2. Process water with m = 13 mg/L of $CaCO_3$ displays a pH of 3.2.
3. Scrubber feed with m = 26.5 mg/L of $CaCO_3$ demonstrates a pH of 5.18.
4. Dust thickener overflow with m = 60.5 mg/L $CaCO_3$ with a pH of 6.38.

These values support the general trend that higher alkalinity values correspond to higher pH values (Addy et al., 2004; Sahu and Chaudhari, 2013). This correlation showcases the buffering capacity of alkalinity in maintaining the stability of pH levels in water. According to The South African Water Quality Guidelines (Department of Water Affairs and Forestry, 1993), higher alkalinity values indicate a potential for mild to moderate damage due to scaling or precipitation formation. This is typical for industrial processes such as gas scrubbing. The non-potable nature of the samples tested, along with the large percentage errors observed, suggests the possibility of certain ions being absent in the analysis, such as organic acids. This can be attributed to industrial contamination, which is expected in the case of all four samples.

4.2.2.4 Water Hardness

According to the analysed concentrations of Ca and Mg in Table 4.6, the four water samples can be classified into different degrees of hardness based on established classifications as discussed in Section 2.6 (Dey et al., 2007; United States Geological Survey, 2020). The classification is as follows: Soft (Ca and Mg concentrations ranging from 0—60 mg/L as calcium carbonate), Moderately hard (Ca and Mg concentrations ranging from 61—120 mg/L), Hard (Ca and Mg concentrations ranging from 121—180 mg/L), and Very hard (Ca and Mg concentrations exceeding 180 mg/L).

Table 4. 8 Establishment of the hardness distribution.

Sample	Ca [mg/L]	Mg [mg/L]	Total hardness (as mg/L $CaCO_3$)	Carbonate hardness	Non- carbonate hardness	Degree of hardness
Scrubber bleed	517	1740	8426.5	3.5	8423	Very hard
Scrubber feed	574	1500	7585	26.5	7558.5	Very hard
Dust thickener overflow	497	1600	7802.5	60.5	7742	Very hard
Process water	521	111	1757.6	13	1744.6	Very hard

The total hardness (TH) of each solution was determined through the calculation method in Equation 3.1 as also noted in Equation 4.4.

Total hardness is defined as the sum of the calcium and magnesium concentrations, both

expressed as $CaCO_3$ *in* mg/L (Aqion, 2022; Cappelle and Davis, 2016; Entezari and Tahmasbi, 2009).

$$[CaCO_3](mg/L) = [Ca](mg/L) \times 2.5 + [Mg](mg/L) \times 4.1 \quad [4.4]$$

As discussed in section 2.6.1, if the total hardness is greater than the sum of carbonate and bicarbonate alkalinity, the amount of hardness equivalent to the total alkalinity is called "Carbonate hardness (CH)". This carbonate hardness is a measure of carbonates and bicarbonates dissolved in water (i.e. temporary hardness) therefore:

$$Carbonate\ hardness\ (mg/L) = Alkalinity \quad [4.4a)]$$

If the alkalinity > Total hardness:

$$Carbonate\ hardness\ (mg/L) = Total\ hardness \quad [4.4b]$$

The amount of hardness that remains is called "Non-carbonate hardness (NCH)". These

are associated with sulphate, chloride, and nitrate ions (i.e permanent hardness) and calculated as in Equation (4.4c):

NCH (mg/L) = Total hardness(TH) - Carbonate hardness (CH) [4.4c]

From the values calculated and presented in Table 4.8, as well as the values for total alkalinity, it is therefore evident that all water samples are characterised by ions that result in permanent hardness, owing to the large values determined for non-carbonate hardness (Aqion, 2022; Cappelle and Davis, 2016; Entezari and Tahmasbi, 2009). The South African Water Quality Guidelines, categorises water with a TH > 500 mg/L as $CaCO_3$ as that with a potential to cause significant to major damage to equipment and structures due to heavy scaling. This water can also cause significant interference with processes in industries such as gas scrubbing (Department of Water Affairs and Forestry, 1993).

4.2.2.5 TDS and EC calculations

Table 4.9 lists the calculated TDS and EC values for the water samples. Total Dissolved Solids (TDS) exhibit a positive correlation with EC and influence the pH of a solution. This implies that higher TDS levels are associated with elevated EC values and lower pH, indicating increasing acidity. These observations align with the data presented in Table 4.10.

Table 4. 9 Calculated TDS and EC values.

Sample name	TDS (mg/L)	EC (µS/cm)
Scrubber bleed	9895	14135.7
Scrubber feed	8266	11808.6
Dust thickener overflow	8582	12260.0
Process water	3534.5	5049.3

EC values below 500 µS/cm are commonly categorized as low. Such levels are typically found in freshwater sources like rivers, lakes, and groundwater with minimal dissolved solids. EC values ranging from 500 µS/cm to 2000 µS/cm are considered moderate. Water within this range possesses a moderate concentration of dissolved solids and remains suitable for various

applications, including agriculture, irrigation, and general industrial use. EC values exceeding 2000 µS/cm are generally regarded as high. Water falling into this range exhibits a high concentration of dissolved solids, including salts, minerals, and other substances. High EC levels may indicate suboptimal water quality for certain applications such as drinking water or cultivation of sensitive agricultural crops. According to The South African Water Quality Guidelines (Department of Water Affairs and Forestry, 1993), water with Total Dissolved Solids (TDS) > 1 600 mg/L and EC > 2500 µS/cm indicate that significant to major damage is likely to occur to equipment and structures as a result of corrosion or scaling, particularly in industrial processes such as gas scrubbing. In such cases, additional water treatment or management practices may be necessary to mitigate potential adverse effects associated with high EC water. The measurement of TDS serves as an indicator for assessing the overall quality of water. While the sources of TDS can include all dissolved cations and anions, Table 4.10 provides a generalization of the relationship between TDS levels and water quality issues (Oram, 1989).

Table 4. 10 TDS and water quality relationship (Oram, 1989).

Cations combined with:	Negative impact
Carbonate	Scale formation, bitter taste, nuisance
Chlorides/Sulphates	Salty, brackish taste, corrosion, odours

The high TDS values calculated indicate potential issues with water corrosiveness and scale formation. High TDS levels can contribute to water that is corrosive, resulting in the degradation of plumbing systems and equipment. It can also lead to the formation of scale on surfaces due to the presence of dissolved salts.

Specific TDS thresholds can provide further insights into potential concerns:

- TDS below 50 mg/L: This indicates a potential corrosion problem (there may not be enough dissolved minerals to form a protective scale, leaving the metal vulnerable to corrosion)
- TDS over 250 mg/L: It suggests issues with hardness and general salt content.
- TDS over 500 mg/L: This should raise concerns about the presence of other salts such as bromide, lithium, and aluminium, as well as the scale-forming potential of the water.

- TDS over 1000 mg/L: This raises serious concerns about the direct impacts of human activities on the water samples, such as industrial discharge from mining, manufacturing, and chemical processing (Lehr et al., 1980; Oram, 1989).

Furthermore, Figure 4.3 illustrates the water classification system established by the EPA (Environmental Protection Agency), which categorizes water quality based on TDS values. Notably, the results from this study reveal that all four analysed samples surpass the EPA's set maximum contamination level. This observation further highlights concerns about the water quality and challenges related to the water's tendency for scale formation.

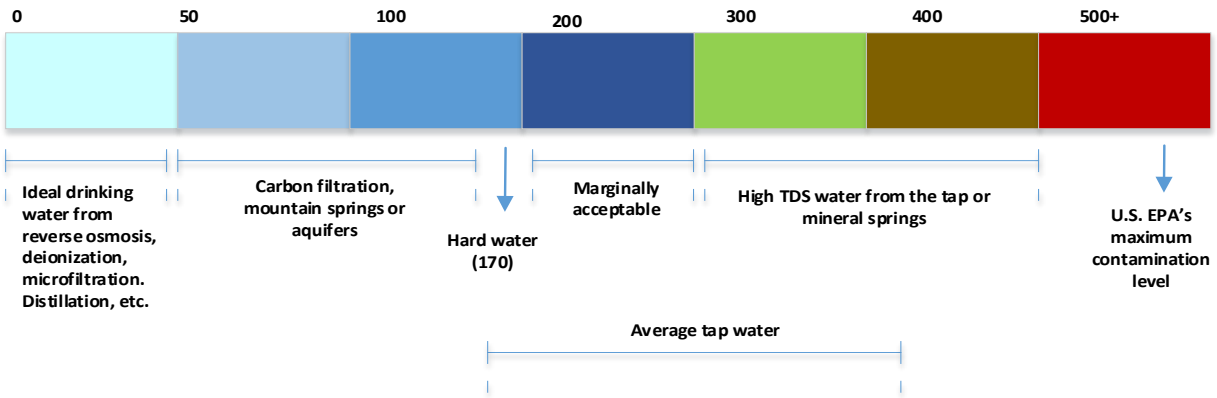


Figure 4. 3 EPA Secondary TDS Regulations for water (adapted from U.S. Environmental Protection Agency, 2009).

Adhering to standards such laid out in The South African Water Quality Guidelines for example, is crucial to ensure that industrial water attains the necessary quality benchmarks, safeguarding its appropriateness for specific industrial purposes.

4.3 Summary

This chapter provides a comprehensive analysis of the characterization of solid and liquid samples used in the study. The solid samples were found to contain significant concentrations of minerals, specifically gypsum and calcite polymorphs. The identification of these polymorphs is important as it provides insights into their unique physical and chemical properties. The analysis of four liquid samples, including scrubber feed, scrubber bleed, dust thickener overflow, and process water, revealed high concentrations of hardness-causing minerals, primarily Ca and Mg. Based on the determined values of non-carbonate hardness, these samples are classified as permanently hard. Furthermore, various physico-chemical parameters of the water samples were calculated, including total dissolved solids (TDS) and electrical conductivity (EC). All water samples exhibited TDS values exceeding 1200 mg/L, indicating high salinity levels and surpassing the maximum contamination level stipulated by the EPA and SANS 214:2015 as well as the The South African Water Quality Guidelines. With an understanding of the mineral content in the solid samples and the importance of maintaining water quality standards, the next chapter focuses on the utilization of conventional and emerging methods for water treatment. The objective is to develop a water treatment process capable of producing water suitable for use within Sibanye's operations, thereby reducing reliance on alternative freshwater purchases and potentially yielding substantial cost savings.

4.4 References

Addy, K., Green, L. and Herron, E., 2004. pH and Alkalinity. University of Rhode Island, Kingston.

Aqion (2022) Water hardness. Aqion. Available at: https://www.aqion.de/site/140 (Accessed: November 5, 2022).

American Public Health Association. 2005. Standard Methods for the Examination of Water and Wastewater, 21 st Edition. Washington, DC, USA

Atekwana, E.A., Atekwana, E.A., Rowe, R.S., Werkema Jr, D.D. and Legall, F.D., 2004. The relationship of total dissolved solids measurements to bulk electrical conductivity in an aquifer contaminated with hydrocarbon. Journal of Applied Geophysics, 56(4), pp.281-294.

Bates, W., 2001. RO Water Chemistry. Hydranautics Membrane Corp.technical paper posted on website http://www. hydranautics. com/docs/papers/04_ro_water_chemistry. pdf.

Buecker, B., 2008. Properly monitor your scrubber chemistry. Power Engineering, 112(7), pp.48-51.

Cappelle, M.A. and Davis, T.A., 2016. Ion Exchange Membranes for Water Softening and High-Recovery Desalination. Emerging Membrane Technology for Sustainable Water Treatment; Elsevier: Amsterdam, The Netherlands, pp.163-179.

Comodi, P., Nazzareni, S., Zanazzi, P.F. and Speziale, S., 2008. High-pressure behaviour of gypsum: A single-crystal X-ray study. American Mineralogist, 93(10), pp.1530-1537.

Department of Water Affairs and Forestry, 1993. South African water quality guidelines: Volume 3-Industrial use. Department of Water Affairs and Forestry.

Dey, D., Herzog, A. and Srinivasan, V., 2007. Chemical precipitation: water softening. Michigan State University, East Lancing.

Entezari, M.H. and Tahmasbi, M., 2009. Water softening by combination of ultrasound and ion exchange. Ultrasonics Sonochemistry, 16(3), pp.356-360.

Guo, M., Xiao, J. and Wang, J., 2019. Impact of the coupled substitution of $CaCO_3$ and $CaSO_4 \cdot 2H_2O$ on chloride binding behaviour in hydrated C3A pastes. Construction and Building Materials, 217, pp.638-650.

Jacques, S.D.M., González-Saborido, A., Leynaud, O., Bensted, J., Tyrer, M., Greaves, R.I.W. and Barnes, P., 2009. Structural evolution during the dehydration of gypsum materials. Mineralogical Magazine, 73(3), pp.421-432.

Jarc, S., Miler, M., Šebela, S. and Zupančič, N., 2017. Sources of sulphate minerals in limestone cave—a possible evidence of anthropogenic activity: a case study in Črna Jama Cave (Slovenia). Environmental Science and Pollution Research, 24(34), pp.26865-26873.

Kemmer, F.N. ed., 1979. The NALCO water handbook. New York: McGraw-Hill.

Koutsoukos, P.G. and Kapetanaki, E., 2016, March. Mixed calcium carbonate and calcium sulphate scale. In CORROSION 2016. OnePetro.

Kumareson, P. and Devanarayanan, S., 1987. Growth of crystals of calcium sulphate in silica gel in presence of additive and their characterisation. Crystal Research and Technology, 22(12), pp.1453-1458.

Lehr, J.H., Gass, T.E. and Pettyjohn, W., 1980. Domestic water treatment. McGraw Hill Book Co. New York, (33093), p.272.

Lisitsin-Shmulevsky, M., Li, X., Hasson, D., Shemer, H. and Semiat, R., 2020. Solubility limits of CaSO4 polymorphs in seawater solutions. Desalination, 475, p.114200.

Minnesota Rural Water Association, 2009. Lime Softening. In: Minnesota Water Works Operations Manual. 4th ed. Minnesota: s.n., p. Chapter 16.

Nazzareni, S., Comodi, P., Bindi, L. and Dubrovinsky, L., 2010. The crystal structure of gypsum-II determined by single-crystal synchrotron X-ray diffraction data. American Mineralogist, 95(4), pp.655-658.

Pedersen, B.F. and Semmingsen, D., 1982. Neutron diffraction refinement of the structure of gypsum, CaSO4. 2H2O. Acta Crystallographica Section B: Structural Crystallography and Crystal Chemistry, 38(4), pp.1074-1077.

Rosenberg, H.S. and Grotta, H.M., 1979. Battelle Development Corp. Scale suppression in lime and limestone scrubbers. U.S. Patent 4,177,245.

United States Geological Survey. Imagens Landsat. 2020, 5.

U.S. Environmental Protection Agency (EPA). 2009. National Primary Drinking Water Regulations. EPA 816-F-09-004. www.epa.gov/safewater/consumer/pdf/
Mcl.pdf.

Van Rosmalen, G.M., Marche, W.G.J. and Bennema, P., 1976. A comparison of gypsum crystals grown in silica gel and agar in the presence of additives. Journal of Crystal Growth, 35(2), pp.169-176.

VinLAB (Pty) Ltd, 2016. DRINKING WATERFOR SANS. [Online] Available at: https://vinlab.com/wp-content/uploads/2016/10/SANS-241-2015.pdf(Accessed:November 26, 2022).

Wang, Y.W., Kim, Y.Y., Christenson, H.K. and Meldrum, F.C., 2012. A new precipitation pathway for calcium sulphate dihydrate (gypsum) via amorphous and hemihydrate intermediates. Chemical Communications, 48(4), pp.504-506.

Wang, Y.W., Christenson, H.K. and Meldrum, F.C., 2013. Confinement leads to control over calcium sulphate polymorph. Advanced Functional Materials, 23(45), pp.5615-5623.

Walton, N.R.G., 1989. Electrical conductivity and total dissolved solids—what is their precise relationship?. Desalination, 72(3), pp.275-292.

Wen, C.Y., Wjm Jr, R.D., Nelsen Jr, J.B., Werkowitz, D.S., Ketteringham, J.M., Davidsson, L.M. and Wiig, K.M., 1975. Scale Control in Limestone Wet Scrubbing Systems. US EPA, EPA-650/2-75-031.

Chapter 5 The effect of lime and soda ash addition on hard water

5.1 Introduction

Chemical precipitation is an established and effective water purification treatment method (Minnesota Rural Water Association, 2009). By introducing lime and soda ash into the water, the pH is elevated, leading to the precipitation and subsequent removal of hardness-causing material. Lime and soda ash effectively reduce water hardness by precipitating calcium and magnesium ions as insoluble compounds, thus preventing scaling in pipes and equipment. This water treatment process also co-removes heavy metals through hydroxide precipitation, making it cost-effective and environmentally friendly. Adjusting pH levels stabilizes water quality and minimizes corrosiveness. Notably, lime and soda ash are economically viable and environmentally benign chemicals, ensuring both efficacy and sustainability in various industrial, municipal, and residential water treatment applications (Fernandez-Prini, 1982; Lime Softening, 2016). Section 4.2.2.4 established that all the water samples collected from Sibanye-Stillwater can be classified as permanently hard due to their substantial non-carbonate hardness. In contrast to temporary hardness (carbonate hardness), which can be reduced by heat treatment alone, the removal of permanent hardness (non-carbonate hardness) necessitates chemical intervention such as lime or soda ash to remove it from water sources effectively (Lime Softening, 2016; Narain et al., 2021; Semesters.in, 2014).

The primary objective of this specific test work was to evaluate the feasibility of lime and soda-ash as softening treatments for the water samples detailed in Section 3.4.2. The softening procedures outlined in Sections 3.4.2.2—3.4.2.5 were followed. Lime and soda ash dosages were computed using the *StaSoft software V5* and the conventional dosage method recommended by the Minnesota Rural Water Association (2009), as summarized in Table 3.2. The subsequent sections will present the results obtained from the water treatments using lime alone and a combination of lime and soda ash.

5.2 Results and Discussion

5.2.1 The effect of varying lime concentration on hardness removal at ambient/room temperatures

Table 5.1 lists the parameters for the varying lime dosage procedure for all four samples (Scrubber bleed (SB), Scrubber feed (SF), Dust-thickener overflow (DTO) and Process water (PW). The final pH and the resulting mass of precipitate are also presented and discussed in the subsequent sections.

Table 5. 1 Varying lime dosage parameters.

20 % STOICHIOMETRIC LIME DOSE						
Sample name	**Initial pH**	**Sample volume (L)**	**Lime dosage (g/L)**	**Temperature (°C)**	**Final pH**	**Mass of precipitate (g)**
SB	3.24	0.25	1.074	25	9.5	1.1
SF	5.18	0.25	0.854	25	9.8	0.91
DTO	6.38	0.25	0.786	25	9.4	0.8
PW	4.81	0.25	0.2	25	8.6	0.22
40 % STOICHIOMETRIC LIME DOSE						
Sample name	**Initial pH**	**Volume of sample (L)**	**Lime dosage (g/L)**	**Temperature (°C)**	**Final pH**	**Mass of precipitate (g)**
SB	3.24	0.25	2.148	25	10	2.2
SF	5.18	0.25	1.708	25	10.2	1.791
DTO	6.38	0.25	1.572	25	10	1.597
PW	4.81	0.25	0.4	25	9.7	0.43
80 % STOICHIOMETRIC LIME DOSE						
Sample name	**Initial pH**	**Volume of sample (L)**	**Lime dosage (g/L)**	**Temperature (°C)**	**Final pH**	**Mass of precipitate (g)**
SB	3.24	0.25	4.296	25	10.4	4.3
SF	5.18	0.25	3.416	25	10.6	3.58
DTO	6.38	0.25	3.144	25	10.3	3.34
PW	4.81	0.25	0.8	25	10	0.947
100 % STOICHIOMETRIC LIME DOSE						
Sample name	**Initial pH**	**Volume of sample (L)**	**Lime dosage (g/L)**	**Temperature (°C)**	**Final pH**	**Mass of precipitate (g)**
SB	3.24	0.25	5.37	25	10.9	5.6
SF	5.18	0.25	4.27	25	11.2	4.56
DTO	6.38	0.25	3.93	25	10.7	4.18
PW	4.81	0.25	1	25	10.5	1.43
120 % STOICHIOMETRIC LIME DOSE						
Sample name	**Initial pH**	**Volume of sample (L)**	**Lime dosage (g/L)**	**Temperature (°C)**	**Final pH**	**Mass of precipitate (g)**
SB	3.24	0.25	6.4	25	11.3	6.7
SF	5.18	0.25	5.12	25	11.5	5.46
DTO	6.38	0.25	4.72	25	11	4.93
PW	4.81	0.25	1.2	25	10.9	1.54
140 % STOICHIOMETRIC LIME DOSE						
Sample name	**Initial pH**	**Volume of sample (L)**	**Lime dosage (g/L)**	**Temperature (°C)**	**Final pH**	**Mass of precipitate (g)**
SB	3.24	0.25	7.518	25	11.8	7.7
SF	5.18	0.25	5.978	25	12.4	6.28
DTO	6.38	0.25	5.502	25	11.6	5.84
PW	4.81	0.25	1.4	25	11.3	1.62
180 % STOICHIOMETRIC LIME DOSE						
Sample name	**Initial pH**	**Volume of sample (L)**	**Lime dosage (g/L)**	**Temperature (°C)**	**Final pH**	**Mass of precipitate (g)**
SB	3.24	0.25	9.666	25	12.1	9.8
SF	5.18	0.25	7.686	25	12.6	7.78
DTO	6.38	0.25	7.074	25	11.9	7.12
PW	4.81	0.25	1.8	25	11.7	1.91

***(Note: mass of precipitate is given for 1 L, although only 250 mL of sample was used)**

5.2.1.1 Lime dosage vs pH, Ca, Mg, total hardness and mass of precipitate

The results observed from the varying lime dosage tests indicate different effects on the following parameters that were monitored and measured. As expected, an increase in lime addition results in an increase in OH^- ions leading to an overall increase in pH. It is also

important to note that the calculated stoichiometric amounts for lime in Table 3.2 proved valid as they produced the required pH > 10.5 for effective chemical precipitation to occur. This pH was observed for all four samples. Figure 5.1 demonstrates the linear relationship between pH and increasing lime addition.

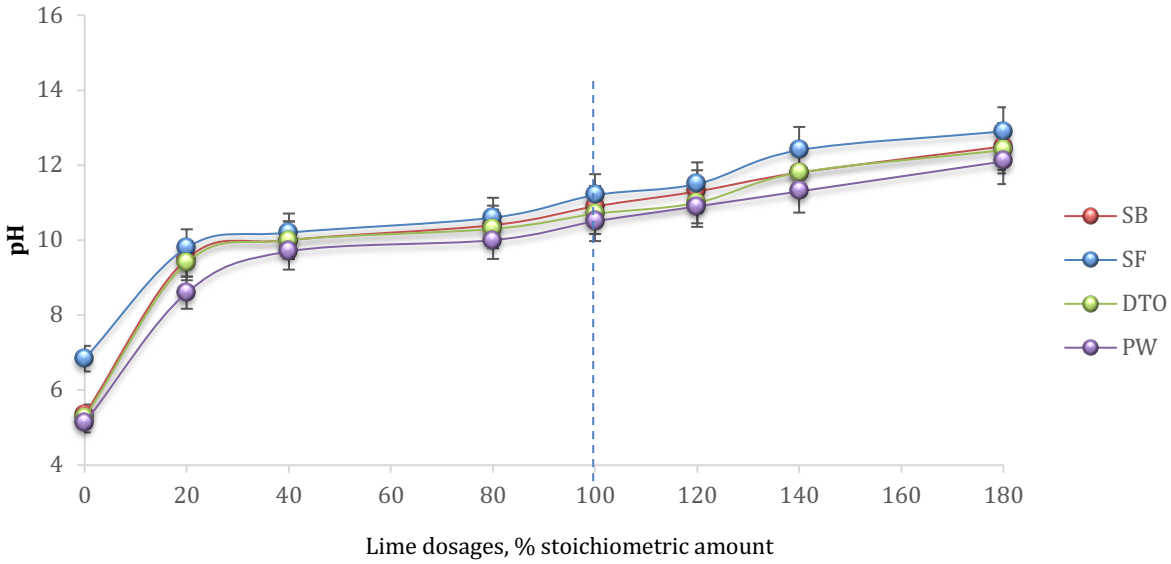


Figure 5. 1 Effect of varying lime dosage on pH

Looking at the Scrubber bleed sample, the Ca concentration (as $CaCO_3$) initially decreased with an increase in lime addition to a minimum (96.75 mg/L), at a lime dosage of 100 % (Figure 5.2) observed at a pH of 10.9. This may be attributed to the precipitation of carbonate hardness as $CaCO_3$. Thereafter, an increase in the concentration was observed as the lime dosage increased. The increase in calcium may be attributed to the addition of excess lime in an essentially "carbonate free" solution (Dey et al., 2007; Smith et al., 2020). Similar observations were made for all the samples.

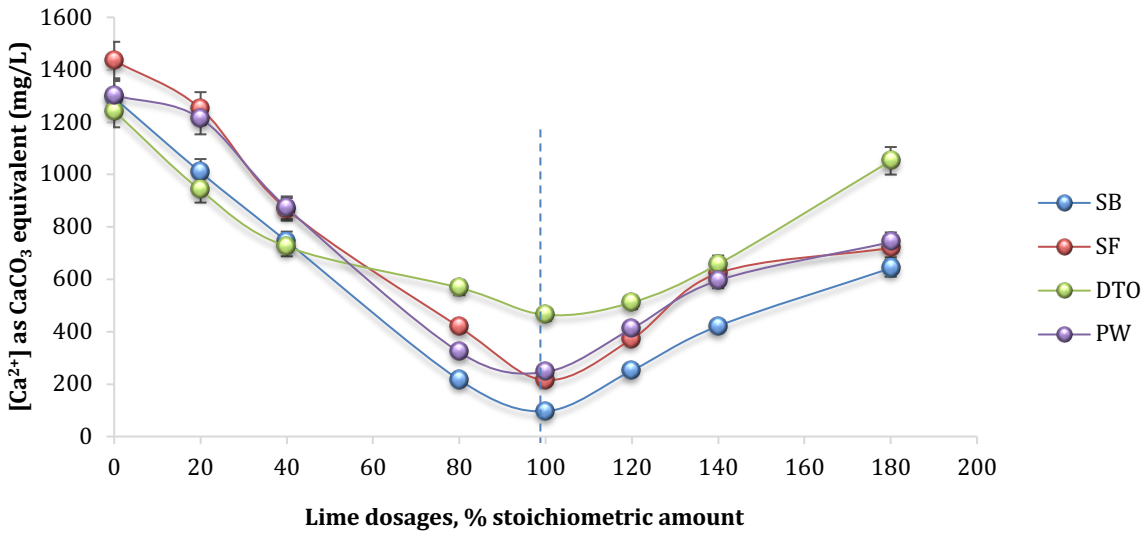


Figure 5. 2 Variation of calcium for varying lime dosages

The concentration of Mg (expressed as $CaCO_3$) exhibited a gradual decline (Figure 5.3) as lime addition increased. This reduction may be attributed to the precipitation of $Mg(OH)_2$ (Equation 3.7). It is well-established that $Mg(OH)_2$ precipitation is highly pH-dependent (Dey et al., 2007; Hamidi et al., 2011; Yang et al., 2014; Veolia Water Technologies & Solutions, 2023), and precipitation typically initiates when the pH exceeds 10.

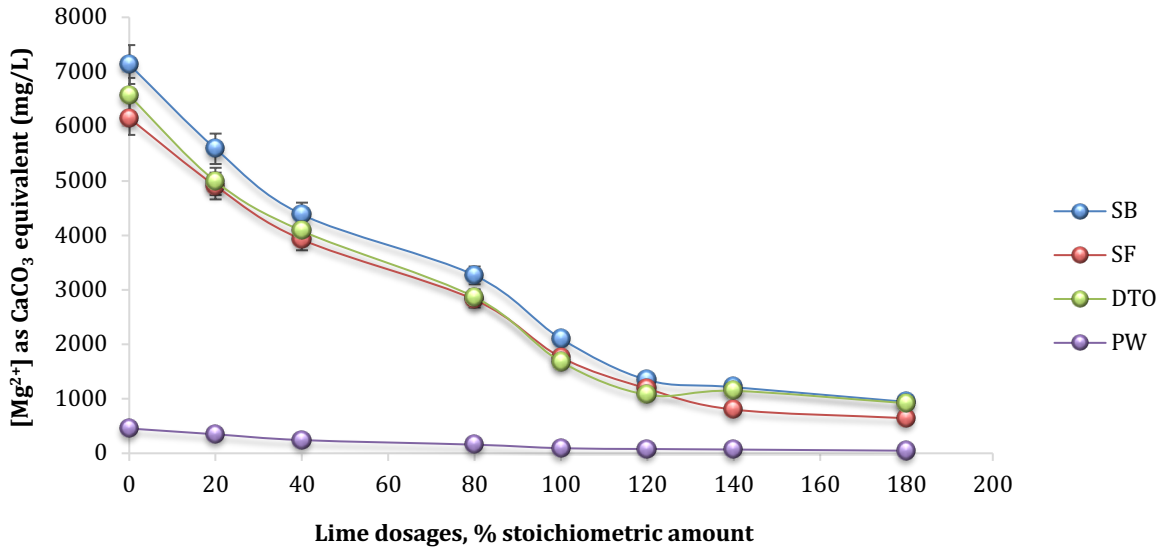


Figure 5. 3 Variation of magnesium for varying lime dosages

In the presence of non-carbonate hardness, treatment with lime alone does not have a significant effect. However, when non-carbonate hardness exceeds 70 ppm in a system with excess hydroxyl alkalinity, the magnesium hardness decreases (Figure 5.3), while calcium hardness increases proportionally (Geldenhuys et al., 2001; Yang et al., 2014; Smith et al., 2020; Veolia Water Technologies & Solutions, 2023). These findings align with observations made by Hamidi et al. (2011) and Geldenhuys et al. (2003), who reported that an increase in pH resulting from lime addition initially led to a decrease in calcium hardness, followed by an increase once a certain pH threshold was reached. On average, the total hardness reached a minimum value at a lime dosage of approximately 100%. However, for stoichiometric dosages exceeding 100%, an overall increase in total hardness was observed (Figure 5.4). This can be attributed to the concurrent increase in calcium concentration as described by Equation 3.1/4.5. In practice, a final total hardness ranging from 75—120 mg/L as $CaCO_3$ is considered acceptable, with observed practical limits for calcium and magnesium concentrations at 30 mg/L and 10 mg/L, respectively. This level of hardness is necessary to prevent corrosion issues associated with overly soft or low-hardness water (Dey et al., 2007; Minnesota Rural Water Association, 2009; Veolia Water Technologies & Solutions, 2023).

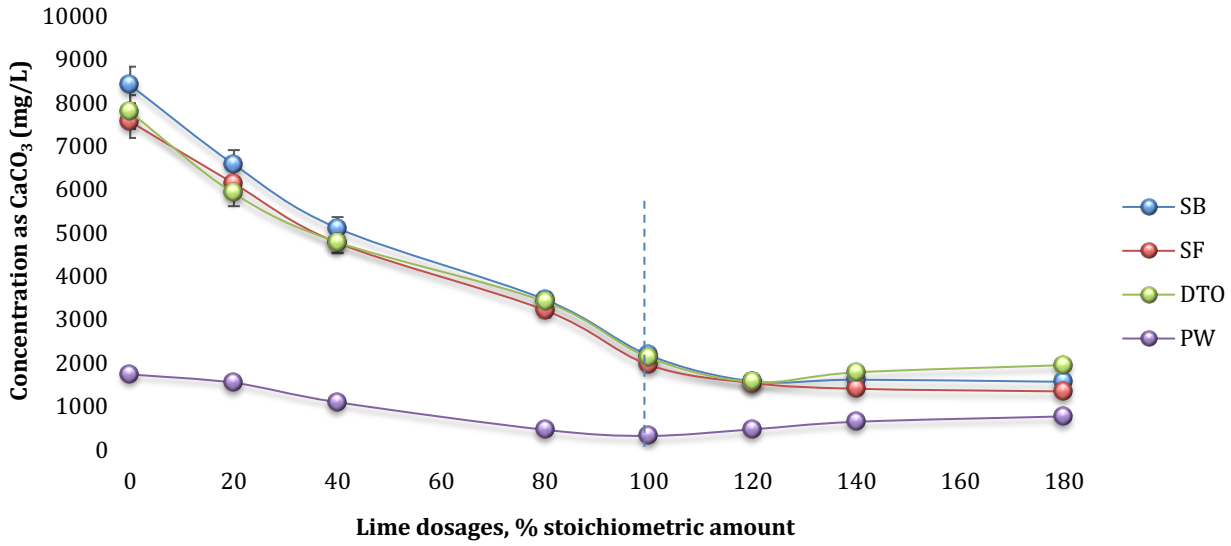


Figure 5. 4 Variation of total hardness for varying lime dosages

From Figure 5.5, it was observed that as the lime dosage was increased, the mass of precipitate formed also increased.

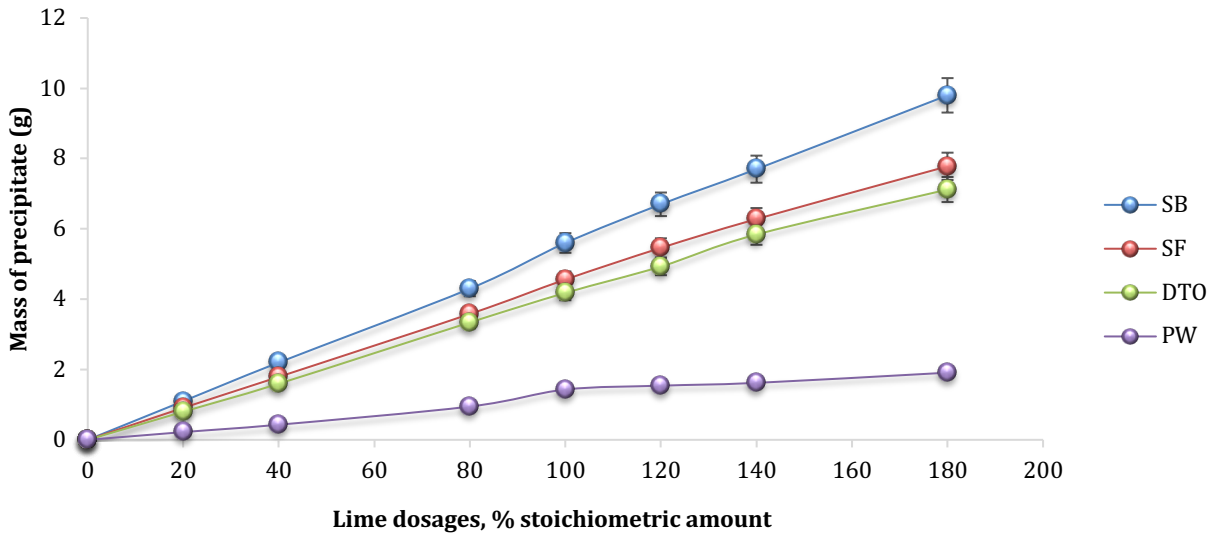


Figure 5. 5 Effect of varying lime dosage on precipitate mass

In summary, when considering both reduced and excess lime conditions, a notable observation emerged: the highest removal of total hardness and Ca was attainable with a 100 % stoichiometric lime dosage. At this dosage, the pH exceeded 10.5, confirming the efficacy of the dosage. While the concentration of Mg continued to decrease and precipitate as $Mg(OH)_2$ with increasing lime dosage, it was observed that the presence of permanent hardness causing minerals persisted in the absence of soda-ash addition. Furthermore, it was noted that complete removal of hardness is not possible due to the slight solubility of certain precipitates that form and subsequently dissolve back into the solution.

Despite the initial total hardness concentrations being significantly above the threshold for "very hard" water (> 8000 mg/L as $CaCO_3$), it is practical to aim for a hardness level of approximately 120 mg/L as $CaCO_3$ (Dey et al., 2007; Seyrig and Shan, 2007). This concentration allows for a balance between hardness removal and the inherent limitations of precipitate solubility.

5.2.1.2 The effect of temperature on the efficiency of lime hardness removal

It has been noted throughout some studies that calcium and magnesium hardness material is reduced by increased temperatures and thus, more effectively removed by warm/hot softening than by cold/ambient softening (Fernandez-Prini, 1982; Minnesota Rural Water Association,

2009; Veolia Water Technologies & Solutions, 2023). The following test work aimed to establish the viability of lime softening, at various temperatures. Only the scrubber bleed and process water samples were tested.

Table 5. 2 Effect of temperature on lime softening parameters for scrubber bleed and process water samples.

Sample name	Initial pH	Volume of sample (L)	Lime dosage (g/L)	Temperature (°C)	Final pH	Mass of precipitate (g)	Mg % reduction	Ca % reduction
SB	3.24	0.25	5.37	25	10.9	5.6	70,5	92,5
	2.9	0.250	0.412	40	10.7	8.21	71,5	96,5
	2.82	0.250	0.685	60	11.2	11.3	72,2	97,5
	2.76	0.250	0.947	80	11.6	15.54	74,5	98,3
	2.42	0.250	1.136	100	11.9	21.6	77,1	98,8
PW	4.81	0.25	1	25	10.5	1.43	79,5	81,1
	4.76	0.250	0.354	40	10.5	1.87	82,3	83,6
	4.39	0.250	0.686	60	10.9	2.9	84,0	86,0
	3.5	0.250	0.739	80	11.3	4.05	85,9	86,7
	2.6	0.250	1.036	100	11.8	5.6	86,8	89,8

***(Note: mass of precipitate is given for 1 L, although only 250 mL of sample was used)**

Table 5.2 shows that due to the inverse relationship between temperature and pH, it is evident that as the temperature of the process water increased, a greater amount of lime was required to achieve the desired pH (> 10.5). An increase in temperature causes the system's equilibrium to shift, absorbing the excess heat and leading to the formation of H^+ ions, which results in a decrease in the solution's pH (Clark, 2020). Figure 5.6 illustrates the relationship between water temperature and the mass of precipitate formed for the lime softening treatment.

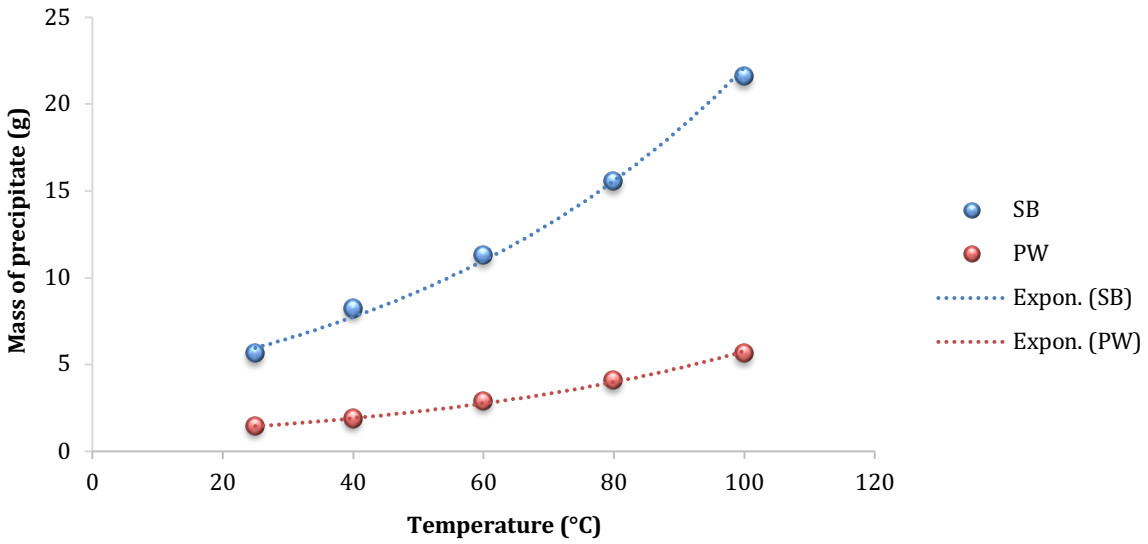


Figure 5. 6 Relationship between temperature and mass of precipitate formed for lime treatment

As discussed in section 2.6.3.1, an increase in temperature promotes the precipitation hardness material by inhibiting dissolution reactions at higher temperature as seen in Figures 5.7 and 5.8 for calcium and magnesium respectively (Fernandez-Prini, 1982; Khan et al., 1995). Consequently, more lime reacted to form more precipitates at higher temperature, resulting in an overall higher lime demand.

The removal efficiency for all metals based on the remaining concentrations of metals in the aqueous solution as shown in Equation 5.1

$$\% \, Removal = (CM_i - CM_f) / CM_i * 100 \qquad [5.1]$$

CM_i denotes the initial concentration of the substance in the solution before any treatment or process occurs. CM_f represents the final concentration of the substance in the solution after the treatment or process has been applied.

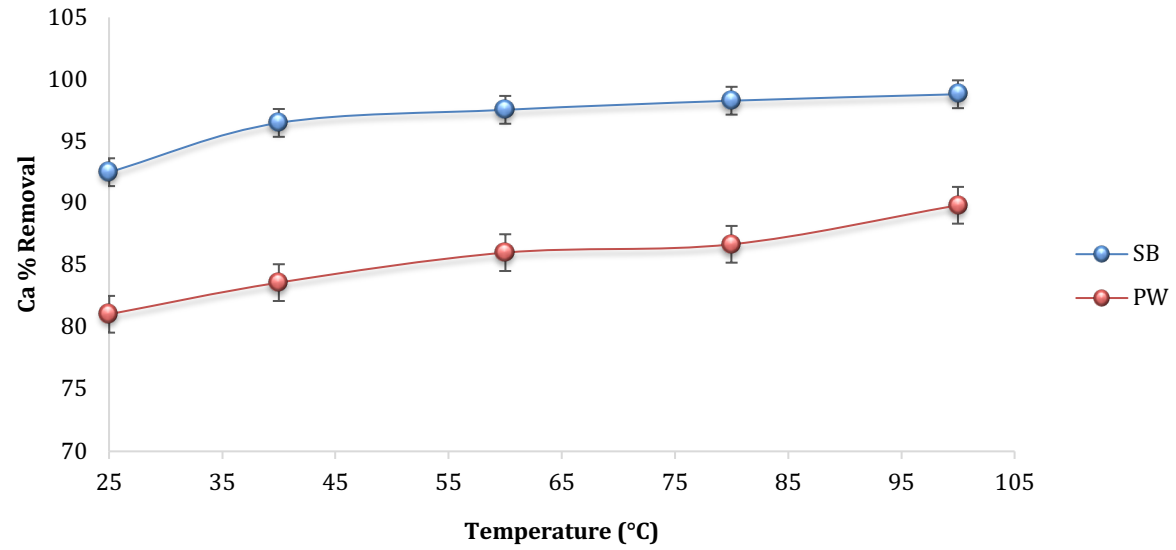


Figure 5. 7 Calcium removal with increasing temperature for lime softening procedure

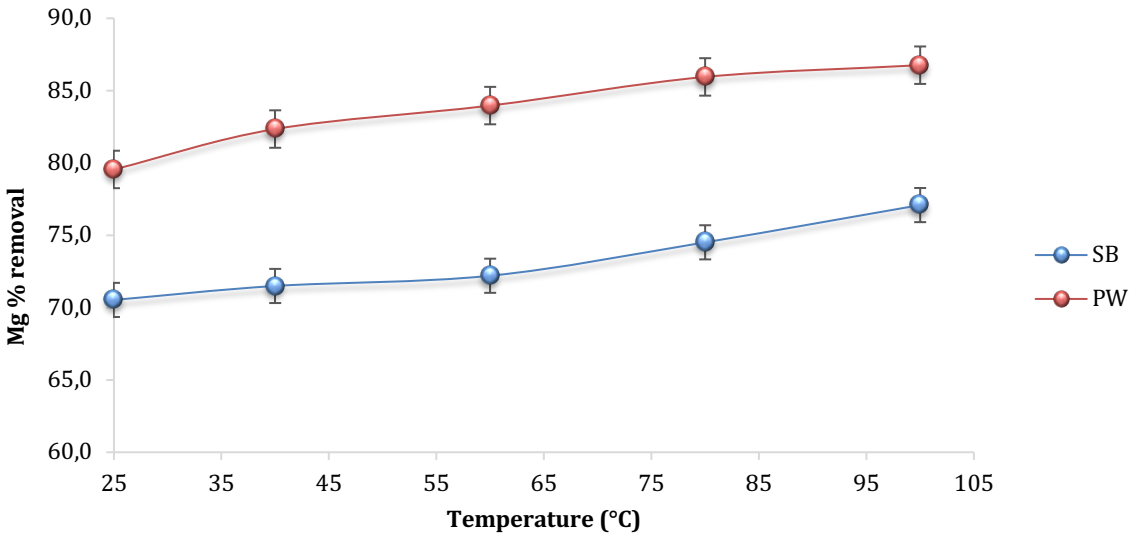


Figure 5. 8 Magnesium removal with increasing temperature for lime softening procedure

5.2.1.3 Traditional excess Lime- Soda ash treatment process at ambient/room temperature (25°C)

The presence of non-carbonate hardness requires the addition of soda ash to the softening treatment for the effective removal of permanent hardness causing minerals (Minnesota rural water association, 2009; Veolia Water Technologies & Solutions, 2023). The lime and soda

ash softening test work parameters at ambient temperatures, final pH and resultant precipitate masses are summarised in Table 5.3.

Table 5. 3 Lime-soda ash-softening parameters.

Sample name	Initial pH	Volume of sample (L)	Lime dosage (g/L)	Soda ash (g/L)	Temperature (°C)	Final pH	*Mass of precipitate (g)
SB	3.24	0.25	5.37	6.85	25	10.9	6.5
SF	5.18	0.25	4.24	6.98	25	11.2	5.2
DTO	6.38	0.25	3.93	6.74	25	10.7	4.31
PW	4.81	0.25	1	1.99	25	10.5	1.5

***(Note: mass of precipitate is given for 1 L, although only 250 mL of sample was used)**

The results from ICP-OES indicate that the lime- soda ash treatment was effective in removing a maximum of 97 % for Ca and over 98 % maximum removal for Mg for the dust thickener overflow and scrubber bleed respectively, at ambient conditions. The final pH of all samples was greater than 10.5, indicating that the calculated stoichiometric dosages in Table 3.1 were valid for effective precipitation. These results are presented and illustrated in Table 5.4 and figure 5.9, respectively

Table 5. 4 Calcium and magnesium concentrations after lime-soda ash treatment at room temperature (25 °C).

25 °C	CALCIUM		MAGNESIUM						
Sample	Final (mg/L)	% Removal	Final (mg/L)	% Removal	Final pH	TH (as mg/L $CaCO_3$)	CH (as mg/L $CaCO_3$)	NCH (as mg/L $CaCO_3$)	Degree of hardness
SB	35	93	55	98	11.4	313	19.5	293.5	Very hard
SF	21	94	153	90	10.6	679.8	94	585.8	Very hard
DTO	15	97	89	94	11.2	402.4	236	166.4	Very hard
PW	26	95	24	78	10.8	384.8	63	321.8	Very hard

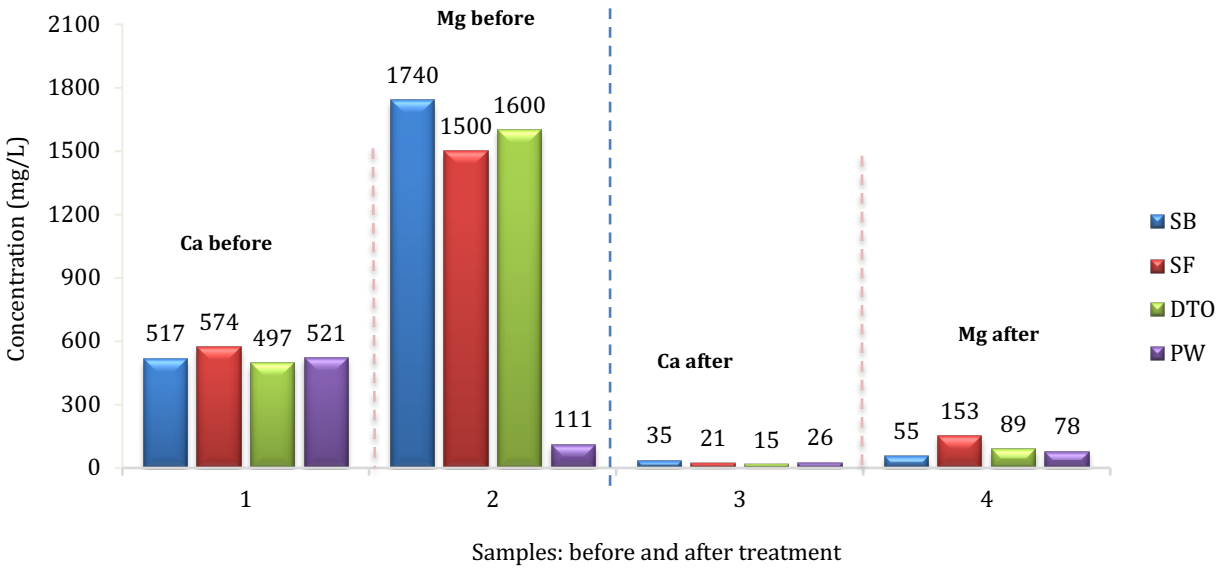


Figure 5. 9 Lime-soda ash treatment for Ca and Mg removal

While the hardness removals were high, Table 5.4 shows that the final concentrations of Ca and Mg after precipitation still rendered the water *very hard* according to Equation 4.4. The water samples were also still regarded as being permanently hard, owing to the high concentration of non-carbonate hardness.

5.2.1.4 The effect of temperature on the efficiency of lime-soda ash treatment

The test work in Section 4.2.2.3 was repeated at higher temperatures of 40 °C, 60 °C, 80 °C, 100 °C. Lime-soda ash treatments ran at elevated temperatures ranges of about 40—60 °C and 80—100 °C are referred to as warm and hot lime softening, respectively (Veolia Water Technologies & Solutions, 2023). This was done to determine whether the non-carbonate hardness and overall residual hardness could be further reduced compared to tests run at ambient temperatures. Only the scrubber bleed and process water samples were tested. Table 5.5 and figures 5.10—5.12 presents the results.

Table 5. 5 Effect of temperature on lime-soda ash softening parameters for scrubber bleed and process water samples.

Sample name	Initial pH	Volume of sample (L)	Lime dosage (g/L)	Soda ash dosage (g/L)	Temperature (°C)	Final pH	Mass of precipitate (g)	Mg % removal	Ca % removal
SB	3.24	0.25	5.37	6.85	25	10.9	6,5	96,8	93,2
	3.1	0.25	6.1	6.85	40	10.7	8,32	97,5	94,0
	2.93	0.25	8.05	6.85	60	11.2	11,05	97,5	94,9
	2.8	0.25	8.19	6.85	80	11.6	14,08	97,6	95,1
	2.46	0.25	8.32	6.85	100	11.9	20,7	97,7	95,3
PW	4.81	0.25	1	1.99	25	10.5	1,5	47,7	95,0
	4.7	0.25	0.354	1.99	40	10.5	2,1	49,9	95,3
	4.28	0.25	1.53	1.99	60	10.9	2,5	52,3	95,4
	3.2	0.25	1.62	1.99	80	11.3	3,98	53,3	95,8
	2.4	0.25	1.67	1.99	100	11.8	5,16	54,3	96,0

***(Note: mass of precipitate is given for 1 L, although only 250 mL of sample was used)**

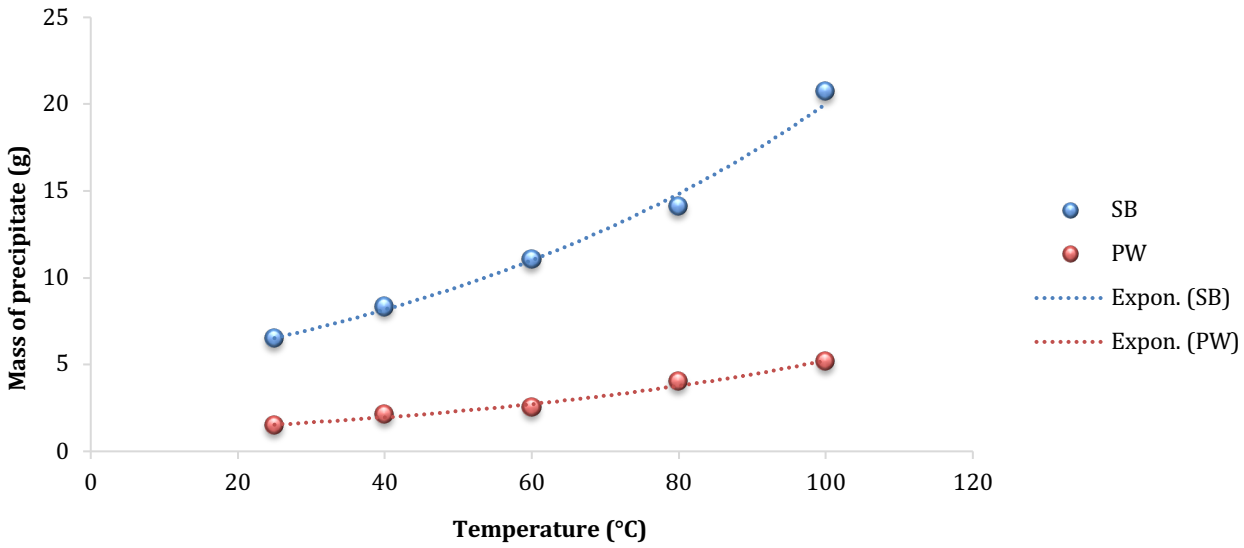


Figure 5. 10 Relationship between temperature and mass of precipitate formed for lime-soda ash treatment

As in the case of lime in Section 3.2.2.3, the inverse relationship between temperature and pH results in a greater amount of lime required to achieve the desired pH of greater than 10.5. Therefore the higher the temperature, the higher the lime demand resulting in more precipitates being formed. Figures 5.11 and 5.12 illustrate the effective removal of Ca and Mg with increasing temperature.

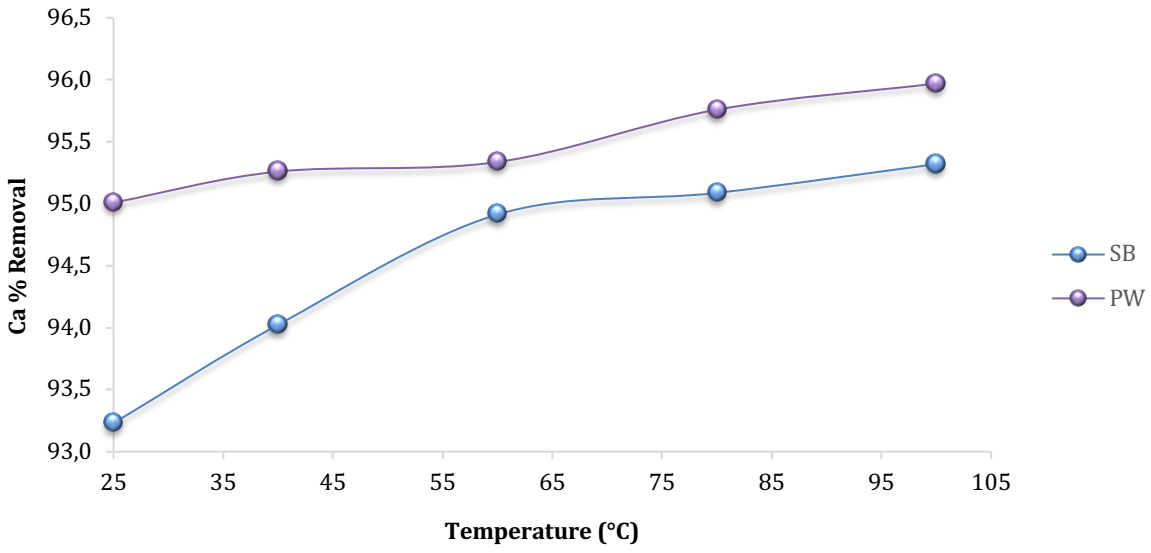


Figure 5. 11 Calcium removal efficiency with increasing temperature for lime-soda softening

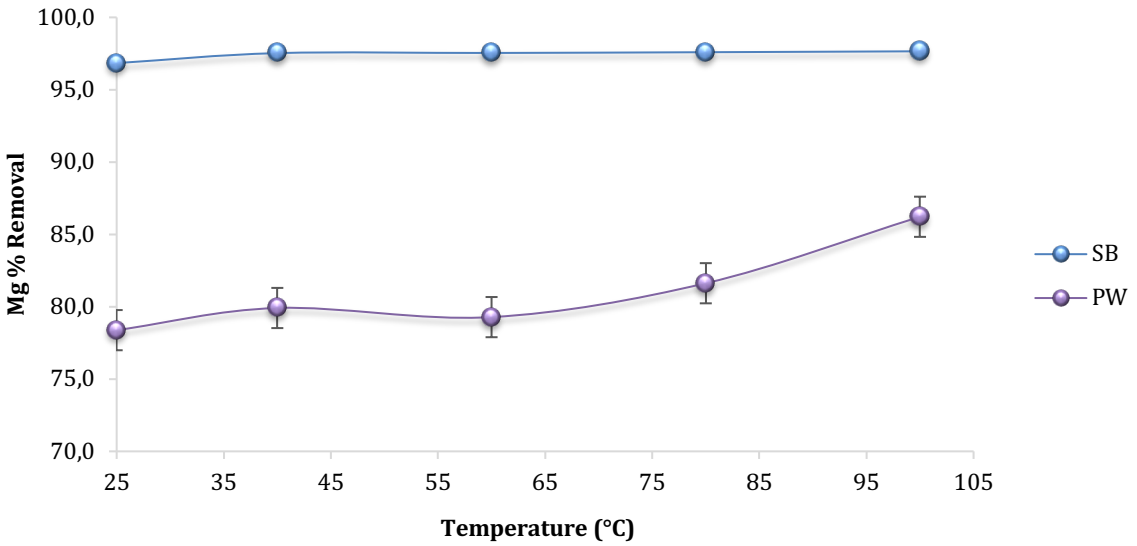


Figure 5. 12 Magnesium removal efficiency with increasing temperature for lime-soda softening

The overall removal efficiency for Mg was higher compared to Ca for the scrubber bleed sample with a maximum removal of 97.7 % at 100 °C. The process water samples removed more Ca than Mg at 96 % also at 100 °C. This role reversal with regards to preferential removal of one ion over the other can be put down to the starting concentrations of both calcium and magnesium in the scrubber bleed and process water samples, respectively. As noted in table 4.9 the scrubber bleed had starting concentrations of calcium and magnesium as 517 and 1740 mg/L, respectively. The process water sample had starting concentrations of calcium and magnesium as 521 and 111 mg/L, respectively. In hard waters with a higher calcium concentration than magnesium, lime-soda softening would primarily remove calcium ions. An increase in temperature would enhance the removal of calcium through more efficient precipitation of calcium carbonate. Magnesium, on the other hand, might not be as effectively removed due to its lower solubility and lesser inclination for precipitation in comparison to calcium unless already available in *much* higher quantities than calcium. These observations align with the solubility products of calcium carbonate ($CaCO_3$; Ksp = 1 .4 × 10^{-8}) and magnesium hydroxide ($Mg(OH)_2$; Ksp = 1.5 x 10^{-11}), reflecting their differing tendencies for dissolution and precipitation under distinct conditions.

5.2.1.5 Co- removal of contaminants for both treatments: ICP-OES results

Metal hydroxide precipitation represents an inexpensive and simple treatment for heavy metal removal from wastewater. The addition of a hydroxide to the water being treated helps to form an insoluble metal hydroxide precipitate. The preferred reagents, from a cost standpoint, are

quick lime, CaO or hydrated lime, $Ca(OH)_2$. Just as in the removal of temporary hardness (Equation 3.7/4.5) the metal ion would react with $Ca(OH)_2$ to form a metal hydroxide precipitate and calcium ions (Equation 5.1) (Kolwalski and Center, 2002; Qasem et al., 2021; Saloua et al., 2020):

$$Metal^{n+} + Ca(OH)_2 \rightarrow Metal(OH)_n + Ca^{2+} \quad [5.2]$$

In addition to the removal of Ca and Mg, the co-removal of contaminants present in the samples was also noted. It is known that pH values of 9—11 improve this process efficiency (Kolwalski and Center, 2002; Qasem et al., 2021; Saloua et al., 2020). Therefore the co-removal of these metals makes sense as both the lime and lime-soda ash treatments were run at pH > 9 with 100 % stoichiometric lime dosages resulting in pH >10.5.

Table 4.6 under section 4.1.2.2.2, presented the ICP-OES analysis of all four samples particularly noting the elements and ions present in the highest concentrations: SO_4^{2-} > S > Na > Mg > Fe > Ca > Si> Mn > K > Ni. During the lime and soda ash softening treatments, changes in the concentration of these elements (in addition to Ca and Mg) were noted. Of the common heavy metals, Ni was present in measurable quantities for both samples (scrubber bleed and process water) analysed. Additionally other contaminants such as Fe, Mn, K, Na and SO_4^{2-} were also present- and is common practice that these ions are also are removed (Kolwalski and Center, 2002; Qasem et al., 2021; Saloua et al., 2020). As mentioned, as of 2017, Sibanye-Stillwater was purchasing its clean water for its processes from Rand water. The co-removal of contaminants might allow Sibanye-Stillwater to treat its scrubber bleed and process waters to concentrations low enough for re-use in their plant water without additional purchase from clean water suppliers. Table 5.6 presents the water quality that Rand Water supplies to the Rustenburg municipality.

Table 5. 6 Rand water elemental quality report (SANS 214:2015).

Sample	Ca [mg/L]	Fe [mg/L]	Mg [mg/L]	Na [mg/L]	SO_4^{2-} [mg/L]	Ni [mg/L]	K [mg/L]	Mn [mg/L]
Rand water	< 0.15	< 0.3	< 0.07	< 0.2	< 0.25	< 0.07	< 0.05	< 0.1

This potential co-removal of contaminants could be an added benefit as their removal from wastewater is important for a clean environment and human health. The tables below (5.7, 5.8 and 5.9) summarise the initial ICP-OES concentrations and the results from the two softening treatments undertaken (lime and soda ash treatment) at various temperatures for the scrubber bleed and process water samples.

Table 5. 7 Initial highest concentrations of elements present in the scrubber bleed and process water samples

Sample	Ca [mg/L]	Fe [mg/L]	Mg [mg/L]	Na [mg/L]	SO_4^{2-} [mg/L]	Ni [mg/L]	K [mg/L]	Mn [mg/L]
SB	517	478	1740	2180	9410	273	71.9	321
PW	521	0.44	111	1530	3340	30.4	20.1	1.07

Table 5. 8 Final concentrations after respective softening treatment (scrubber bleed sample)

Sample	Treatment	Temperature (°C)	% removal	Ca [mg/L]	% removal	Fe [mg/L]	% removal	Mg [mg/L]	% removal	Na [mg/L]
SB				517		478		1740		2180
	Lime	25	92.5	105.99	99.9	0.478	70,5	513.3	-2	2223.6
	Lime-soda	25	93.2	35.16	99.9	0.478	96.8	87	-19.6	2607.3
	Lime	40	96.5	91.5	99.9	0.478	71.5	495.9	-2.4	2232.32
	Lime-soda	40	94	31.02	99.9	0.478	97.5	84.78	-21.7	2653
	Lime	60	97.5	82.7	99.9	0.478	72.2	483.72	-2.8	2241.04
	Lime-soda	60	94.9	26.37	99.9	0.478	97.5	80.04	-29.8	28.29
	Lime	80	98.3	72.9	99.9	0.478	74.5	443.7	-2.8	2241.04
	Lime-soda	80	95.1	30.5	99.9	0.478	95.6	73.08	-32.6	2890.7
	Lime	100	98.8	68.2	99.9	0.478	77.1	398.46	-2.7	2238.9

	Lime-soda	100	95.3	24.3	99.9	0.478	97.8	69.6	-42.8	3113.04
Sample	**Treatment**	**Temperature (°C)**	**% removal**	**SO_4^{2-} [mg/L]**	**% removal**	**Ni [mg/L]**	**% removal**	**K [mg/L]**	**% removal**	**Mn [mg/L]**
SB				9410		273		71.9		321
	Lime	25	16.2	7877.2	88.0	32.76	56.0	31.63	98,0	6.42
	Lime-soda	25	14.8	8008.8	85.0	40.95	50.9	35.27	99,0	3.21
	Lime	40	15.8	7914.8	83.0	46.41	57.1	30.87	99,9	0.32
	Lime-soda	40	15.2	7971.2	82.0	49.14	54.9	32.41	99,9	0.31
	Lime	60	14.1	8074.6	87.0	35.49	56.9	30.96	99,9	0.31
	Lime-soda	60	12.6	8215.6	84.0	43.68	56.1	31.58	99,9	0.32
	Lime	80	16.6	7783.96	89.0	30.03	60.0	28.76	99,9	0.32
	Lime-soda	80	17.7	7736.2	83.7	44.55	58.0	30.19	99,9	0.32
	Lime	100	48.8	4816	92.0	21.84	64.0	25.88	99,9	0.32
	Lime-soda	100	44.6	5214	89.6	28.39	6.4	67.32	99,9	0.32

Table 5. 9 Final concentrations after respective softening treatment (process water sample)

Sample	Treatment	Temperature (°C)	% removal	Ca [mg/L]	% Removal	Fe [mg/L]	% removal	Mg [mg/L]	% removal	Na [mg/L]
PW				521		0.44		111		1530
	Lime	25	81	98.99	99.9	0.044	79.5	31.08	-2.1	1562.13
	Lime-soda	25	95	26	99.9	0.044	78.4	18.87	-20.2	1839.06
	Lime	40	84	83.36	99.9	0.044	82.3	33.3	-2.3	1565.19
	Lime-soda	40	95.3	39.6	99.9	0.044	79.9	6.66	-22	1866.6
	Lime	60	86	72.94	99.9	0.044	84	31.97	-3	1575.9
	Lime-soda	60	95.3	22.92	99.9	0.044	79.3	3.89	-28.3	1962.99
	Lime	80	86.7	79.7	99.9	0.044	85.9	29.3	-2.1	1562.13
	Lime-soda	80	95.8	21.9	99.9	0.044	81.6	6.99	-29.4	1979.82
	Lime	100	89.8	79.19	99.9	0.044	86.8	26.09	-2.4	1566.72
	Lime-soda	100	96.7	17.19	99.9	0.044	86.2	5.77	-43.7	2198.61
Sample	**Treatment**	**Temperature (°C)**	**% removal**	**SO_4^{2-} [mg/L]**	**% removal**	**Ni [mg/L]**	**% removal**	**K [mg/L]**	**% removal**	**Mn [mg/L]**
PW				3340		30.4		20.1		1.07
	Lime	25	16.3	2795.58	85	4.56	54	9.25	98.9	0.012
	Lime-soda	25	13.8	2879.08	83	5.17	49.8	10.09	99,0	0.001

	Lime	40	14.8	2845.68	82.5	5.32	55.6	8.92	99,9	0.001
	Lime-soda	40	14.9	2842.34	81.9	5.5	53.4	9.37	99,9	0.001
	Lime	60	13.9	2875.74	88	3.65	57.2	8.6	99,9	0.001
	Lime-soda	60	11.5	2955.9	83.6	4.99	56.4	8.76	99,9	0.001
	Lime	80	14.3	2862.38	90.4	2.91	58	8.42	99,9	0.001
	Lime-soda	80	16.5	2788.9	82.9	5.2	54	9.24	99,9	0.001
	Lime	100	45.9	1806.94	91	2.74	64.0	7.24	99,9	0.001
	Lime-soda	100	42.3	1927.18	87.1	3.92	64.0	7.24	99,9	0.001

The results from ICP-OES shows that both lime and lime-soda softening treatments were able to co-remove Mn and Fe > 99 % for both water samples. The lime softening treatment alone showed better removal of Ni compared to the lime-soda combination although both treatments showed removal efficiencies > 80 % from both water samples. The increase in sodium concentration, for lime-soda treatment was expected because of the added soda ash reagent and chemical precipitation thus having no effect on sodium reduction. However, there is also a slight increase in sodium for the lime treatment alone that is not expected with lime addition. This may be attributed to some impurities in the reagents and perhaps some experimental error. The lowest co-removals were of potassium and sulphate - although both removals from both samples increased with temperature for both treatments, respectively. The removal of sulphate may be attributed to the precipitation of gypsum (Gaid, 2023). Sulphate had better removals with the lime treatment compared to the lime-soda treatment, although both treatments still had high residual sulphate.

As mentioned in sections 4.2.2.2 and 4.2.2.4, Ca showed better overall removal efficiencies for both samples at all temperatures and for both treatments. The largest reduction in Ca concentration occurred with the lime treatment at 100 °C for the Scrubber water sample, at 99 %. The reduction of Ca from the Scrubber bleed sample with the lime and soda- ash treatment

was efficient up to 95 % at 100 °C. Similar if not better results (97 %), can be achieved through lime treatment at 40 °C. Overall, the energy it would take to heat up the water to elevated temperatures for improved recoveries may not be economically beneficial. It would cost ~ R37 540 886 to heat up 10ML of process water per day (see Appendix 4 for calculations).

For both treatments, it can be concluded that temperature plays an important role in the removal efficiencies of all present metals, with an increase in temperature resulting in an increased removal. With the exception of Fe and Mn as well as Ni, which had reductions of > 99 % and > 80 %, respectively, for both treatments, the lime-soda ash treatment proved the better treatment in the reduction of hardness as well as co-removal of metal contaminants.

5.2.1.6. X-ray diffraction (XRD) analysis of precipitates

The objective of treating both the process water and scrubber bleed samples with lime and a combination of lime-soda ash was initially for the removal of hardness material through precipitation of $CaCO_3$ and $Mg(OH)_2$. This removal of hardness was done by the addition of lime to achieve a pH > 10.5. Additionally observed, was the precipitation and co-removal of contaminant ions also present in the samples. X-Ray Diffraction (XRD) analysis was undertaken on the precipitates formed for each water treatment and the effect of temperature. The XRD scans are presented in Appendix 2.

From the lime treatment, a few compounds had precipitated from both the samples. The precipitates were made up of quartz, magnesium silicate hydrate, calcium silicate anthophyllite, basanite and gypsum. The formation of gypsum ($CaSO_4.2H_2O$) and basanite ($CaSO_4.5H_2O$) would consume sulphates in solution, thus resulting in a reduction of sulphates in both water samples. The precipitates from the lime and soda combination treatment, indicated that lime treatment alone was more efficient. At room temperature, the precipitate was made up of only calcium containing compounds (gypsum and calcite) and quartz. It was expected that with the addition of soda ash, magnesium containing compounds would also be present within the precipitate. However, only at temperatures of 60—100 °C were some magnesium compounds identified, although gypsum made up a majority of the precipitate. This indicated once more, that an increase in temperature led to a more effective removal by chemical precipitation. These observations tie in with those made earlier in sections 4.2.2.2 and 4.2.2.4. While the ICP-OES did indicate reduced levels of other metal contaminants, metal hydroxides particularly those of Ni, Mn and Fe weren't identified in the XRD perhaps due to their lower concentrations in comparison to those of calcium, magnesium and sulphate that were supersaturated.

5.2.1.7 Scaling potential of treated water

To find out how effective the treatments were in the removal of hardness, an added comparison to total hardness calculation would be determining the scaling potential of the treated water. As discussed in section 2.6.1.3, three mathematical models have been developed to predict the tendency of a water sample to form $CaCO_3$ (Abbasnia et al. 2019; Cavano, 2005; Mirzabeygi et al., 2016; Puckorius and Strauss, 1983). These are:

1. The Langelier-Saturation index (LSI)
2. The Ryznar Stability index (RSI)
3. The Puckorious Scaling index (PSI)

For the water samples treated (particularly the scrubber bleed and process water), the LSI > 0, RSI AND PSI > 6 (Shah et al., 2023), respectively. This confirms and validates the results observed under sections 4.2.2.1 and 4.2.2.3 concerning the treated waters still being very hard and having the potential to continue forming scale .

5.3 Summary

Both treatment processes applied for the removal of hardness showed high removal efficiencies for both calcium and magnesium. While the lime and soda ash treatment showed an overall better removal across all temperatures for most metals- lime treatment alone compared fairly well, particularly with the co-removal of contaminants such as Fe and Mn. Depending on the capital available for a water treatment plant, it may be worth opting for a lime only treatment process. This treatment option may require additional cycles to achieve the necessary metal level concentrations the plant may need for the re-use of the water. The use of lime and soda ash at the stoichiometric dosages still rendered the samples very hard and with a high potential to still form scale as indicated by the three scaling indices. It is therefore, necessary to include an additional step to further treat the water to functional concentration and hardness levels. The next section looks into the use of ion exchange as another chemical water softening treatment. The combined use of both ion exchange and lime and soda ash treatment to achieve the desired level of hardness in the water samples is also considered.

5.4 References

Abbasnia, A., Yousefi, N., Mahvi, A.H., Nabizadeh, R., Radfard, M., Yousefi, M. and Alimohammadi, M., 2019. Evaluation of groundwater quality using water quality index and its suitability for assessing water for drinking and irrigation purposes: Case study of Sistan and Baluchistan province (Iran).Human and Ecological Risk Assessment: An International Journal, 25(4), pp.988-1005.

Cavano, R.R., 2005, April. Understanding scaling indices and calculating inhibitor dosages. In CORROSION 2005. OnePetro.

Clark, J., 2020. Polyamides. Chemguide: Helping You to Understand Chemistry.

Damons, R.E., 2001. Development of an Aspen model for the treatment of acid mine drainage.

Dey, D., Herzog, A. and Srinivasan, V., 2007. Chemical precipitation: water softening. Michigan State University, East Lancing.

Drinking Water For Sans. [Online] Available at: https://vinlab.com/wp-content/uploads/2016/10/SANS-241-2015.pdf [Accessed 08 08 2020].

Engineering Congress & Exhibition. Kish, Iran (pp. 21-24).Lime-soda water softening process | limitation of Soda Lime Process (no date). Available at: https://oulms.in/wp-content/uploads/2020/12/BT-101-04Soda-Lime-Process-.pdf (Accessed: November 29, 2022).

Fernandez-Prini, R., 1982. Le Chatelier's principle and the prediction of the effect of temperature on solubilities. Journal of Chemical Education, 59(7), p.550.

Gaid, K., 2023. Drinking Water Treatment, Calco-carbonic Equilibrium and Disinfection (Vol. 5). John Wiley & Sons.

Geldenhuys, AJ, Maree, JP, De Beer, M. & Hlabela, P., 2003. An integrated limestone/lime process for partial sulphate removal. Journal of the Southern African Institute of Mining and Metallurgy, 103(6), pp.345-353.

Greyling, M. and Van Rooy, J.L., 2019. Hydrogeological properties of gypseous soils in South Africa. South African Journal of Geology 2019, 122(3), pp.389-396.

Hamidi, R., Kahforoushan, D., Fatehifar, E., Arehjani, M. and Farmanbordar, S., 2011, November. Simultaneous removal of Ca and Mg Salts using chemical precipitation with lime. In The 7th International Chemical

Kowalski, A. and Center, O.N., 2002, January. Metals removal to low levels using chemical precipitants. In Proceedings of AESF/EPA Conference for Environmental Excellence, Orlando, Florida (pp. 143-150).

Minnesota Rural Water Association, 2009. Lime Softening. In: Minnesota Water Works Operations Manual. 4th ed. Minnesota: s.n., p. Chapter 16.

Mirzabeygi, M., Naji, M., Yousefi, N., Shams, M., Biglari, H. and Mahvi, A.H., 2016. Evaluation of corrosion and scaling tendency indices in water distribution system: a case study of Torbat Heydariye, Iran. Desalination and Water Treatment, 57(54), pp.25918-25926.

Narain, A., Potgieter, J.H., Rencken, G.E. and Smith, J., 2021. Beneficiation of recycled process water at DRDGOLD's ERGO plant, and its effect on gold recovery. Journal of the Southern African Institute of Mining and Metallurgy, 121(7), pp.331-343.

Puckorius, P. and Strauss, S.D., 1983. Get a better reading on scaling tendency of cooling water. Power;(United States), 127(9).

Qasem, N.A., Mohammed, R.H. and Lawal, D.U., 2021. Removal of heavy metal ions from wastewater: A comprehensive and critical review. Npj Clean Water, 4(1), p.36.

Saloua, J., Mohamed, T., Ahmed, M. and Khadija, M., 2020. Industrial rejection: removal of heavy metals based on chemical precipitation and research for recoverable material in byproducts. International Journal of Engineering Technologies and Management Research, 7(2), pp.39-52.

Seyrig, G. and Shan, W., 2007. Chemical precipitation: water softening. ENE, 806.

Shah, M., Shah, V., Dudhat, K. and Patel, D., 2023. Evaluation of geothermal water and assessment of corrosive and scaling potential of water samples in Tulsishyam Geothermal Region, Gujarat, India. Environmental Science and Pollution Research, 30(15), pp.44684-44696.

Sithole, T., Mashifana, T., Mahlangu, D. and Tchadjié, L., 2023. Effect of binary combination of waste gypsum and fly ash to produce building bricks. Sustainable Chemistry and Pharmacy, 31, p.100913.

Smith, T., 2020. Lime Softening—the Forgotten Technology: Optimization Case Studies From South Florida.

Veolia Water Technologies & Solutions, 2023. Handbook of Industrial Water Treatment - Chapter 7 Precipitation Softening. [Online] Available at: https://www.suezwatertechnologies.com/handbook/chapter-07-precipitation-softening [Accessed 01 10 2019].

Yang, X., 2014. Precipitation and removal of ionic compounds from produced water: Observed and modeling results (Doctoral dissertation, Colorado State University).

Chapter 6 The efficiency of ion exchange resins on hard water

6.1 Introduction

Resins are porous, insoluble materials with a high affinity for specific ions in water. They are used for treating hard water by employing ion exchange processes. These resins swap Ca and Mg ions, responsible for water hardness, with Na ions, effectively softening the water and reducing scale build-up in plumbing and appliances. The objective of this test work was to determine the efficiency of two types of resins said to be commonly used in the softening of water due to their ability to attract cations: Weak Acid Cation resin (WAC) and Strong Acid Cation resin (SAC) (Apell et al., 2010; Canepa, et al., 1996; Cappelle, and Davis, 2016; DuPont, Amber series, 2023; Hoffmann and Martinola, 1988). For these resins, water with high TDS and water balances typically tend to be very challenging and difficult to work with (Brown and Sheedy, 2002). Upon inspection of the ICP-OES water analysis, DuPont^{TM} suggested two resins: *Amberlite IRC83H* (WAC; used in the H^+ form) and *Amberlite IRC120Na* (SAC; used in the Na^+ form). The efficiency of these resins in the removal of hardness ions (Ca and Mg) from solution was determined though batch reactions as described in Section 3.2.3.

6.2 Results and discussion

6.2.1 Resin loading/regeneration

Before use, both resins were loaded or regenerated with 1 M HCl for the WAC resin and 1 M NaCl for the SAC resin, respectively. This was done to make sure that both resins' functional groups (H^+ and Na^+, respectively) were fully loaded and available at maximum capacity. The loading for both resins is shown in Figures 6.1 and 6.2. Both resins achieved saturation with H^+ and Na^+ after 45 and 35 minutes, respectively.

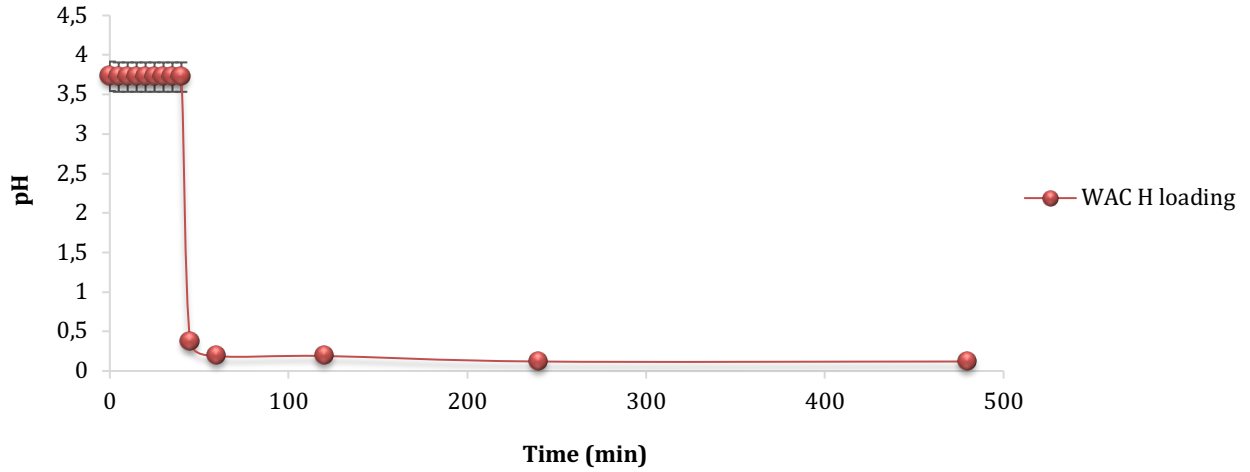


Figure 6. 1 Proton (H^+) loading on WAC resin (*Amberlite IRC83H)*

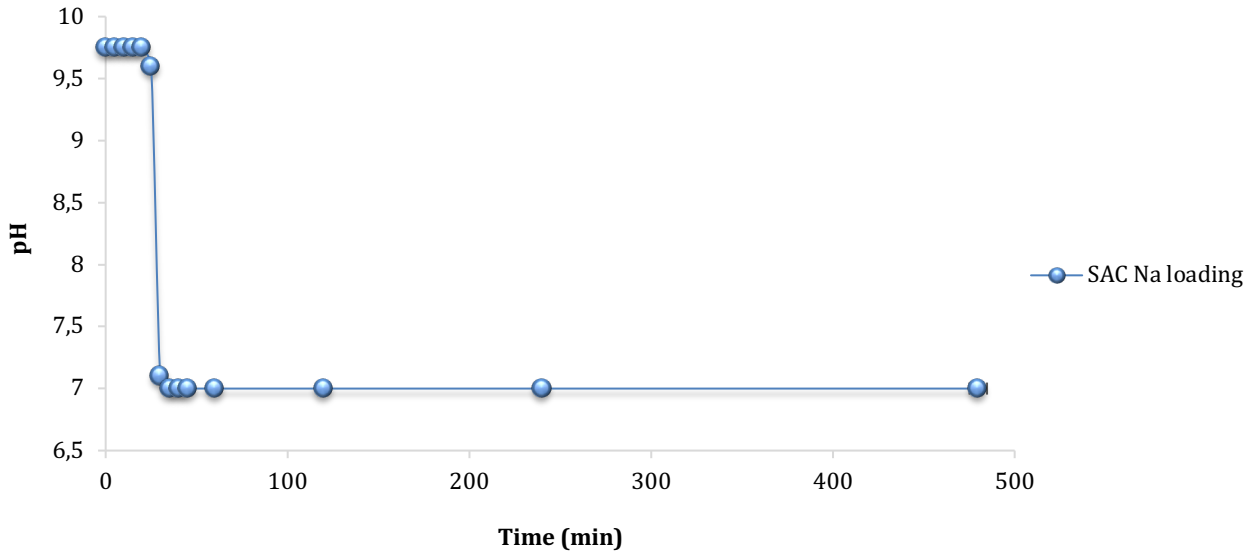


Figure 6. 2 Sodium (Na^+) loading on SAC resin (*Amberlite IRC120Na*)

6.2.2 Determining optimal operating parameters for resin batch reactions

To determine the optimal equilibrium parameters that influence and affect the adsorption of each resin, batch reactions were used. For each resin, the effects of pH, shaker speed, mass of resin and contact time were initially evaluated on the process water sample. The initial pH of

the process water sample was 4.8 with initial [Ca^{2+}] and [Mg^{2+}] as 521 mg/L and 111 mg/L, respectively

6.2.2.1 Effect of pH

6.2.2.1.1 Weak acid cation resin (WAC; Amberlite IRC83H)

Figure 6.3 depicts the results observed for the effect of initial solution pH on the removal efficiency of the WAC resin. Across all initial pHs (1— 2) (as noted in section 3.2.3.2.1), the equilibrium concentrations for both Ca and Mg were reached after 30 minutes.

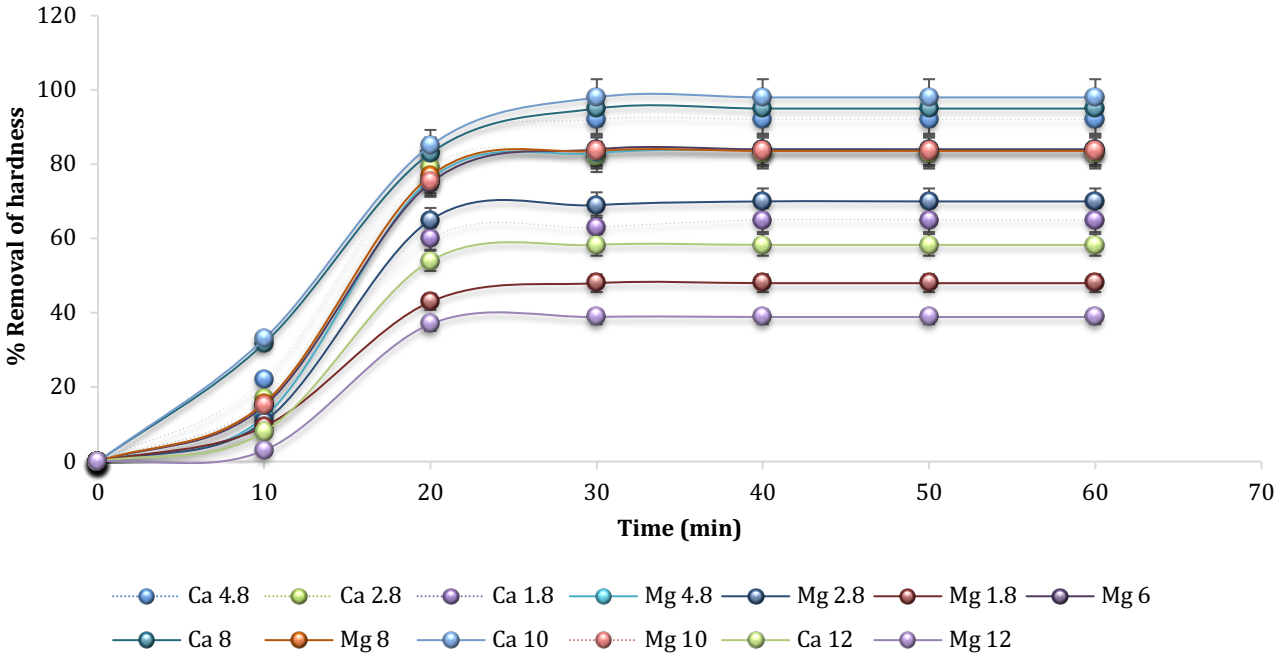


Figure 6. 3 Removal of calcium and magnesium by WAC resin as a function of initial pH of the solution (Initial [Ca^{2+}] = 521 mg/L; initial [Mg^{2+}] = 111 mg/L; stirring speed = 150 rpm, contact time = 60 minutes; Temperature = 25°C)

It can be observed that for pH < 4, the removal efficiencies for both Ca and Mg are the lowest. Weak acid cation resins do not operate particularly well below pH of 4. They have a higher selectivity for H^+ ions than any other ion. Therefore, when they are in the H^+ form and operate in acidic solutions they tend to remain unionized, making them poor ion exchangers. This particular WAC, however, was said to have been specifically designed for water softening and de-alkalization and therefore, the minimum removal efficiency for solutions lower than pH = 4 was found to be ~ 50 % for Mg and 65 % for Ca at pH = 1.8. This resin has a high capacity for hardness removal at neutral to alkaline pHs. For initial solution pHs of 6—10, both Ca and

Mg were efficiently removed by 84 — 98 %. The higher the initial solution pH the better the removal efficiency for the WAC. This trend is true however, for a maximum solution pH of 10. As the pH increases to 12 the removal efficiencies for both Ca and Mg are significantly reduced to ~ 60 % and ~ 40 % respectively. Therefore, pH adjustment (neutral to alkaline) for solutions prior to treatment with the *Amberlite IRC83H* is required for effective removal of hardness ions except at pH ranges where they are no longer stable.

6.2.2.1.2 Strong acid cation resin (SAC; Amberlite IRC120Na)

Similarly, the SAC resin was subjected to initial solution pH ranges from 4 –14 (as noted in section 3.2.3.2.1). As seen in Figure 6.4, the increase in initial solution pH showed no significant effect on the SAC removal efficiency of Ca and Mg between pH 4 —10. This resin is said to be stable across all pH ranges (0—14) as SAC resins with sulphonic functional groups remain ionised at almost the entire pH range (Bandrabur et al., 2012; Dupont, Amber series, 2023).

However, as observed below, at pH >10 the removal efficiency starts to decrease.

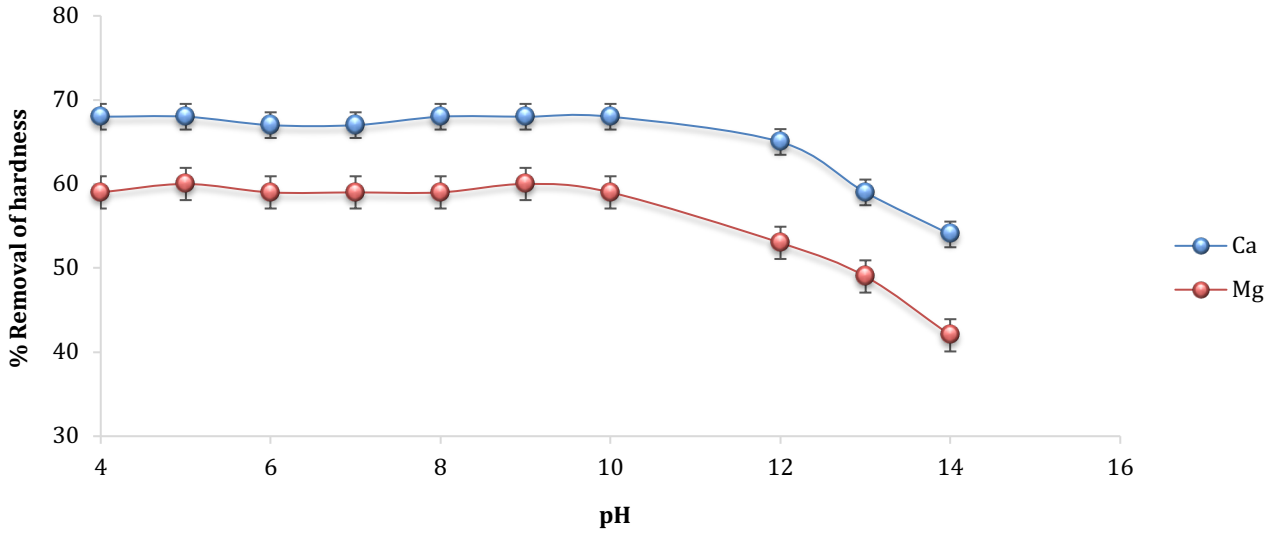
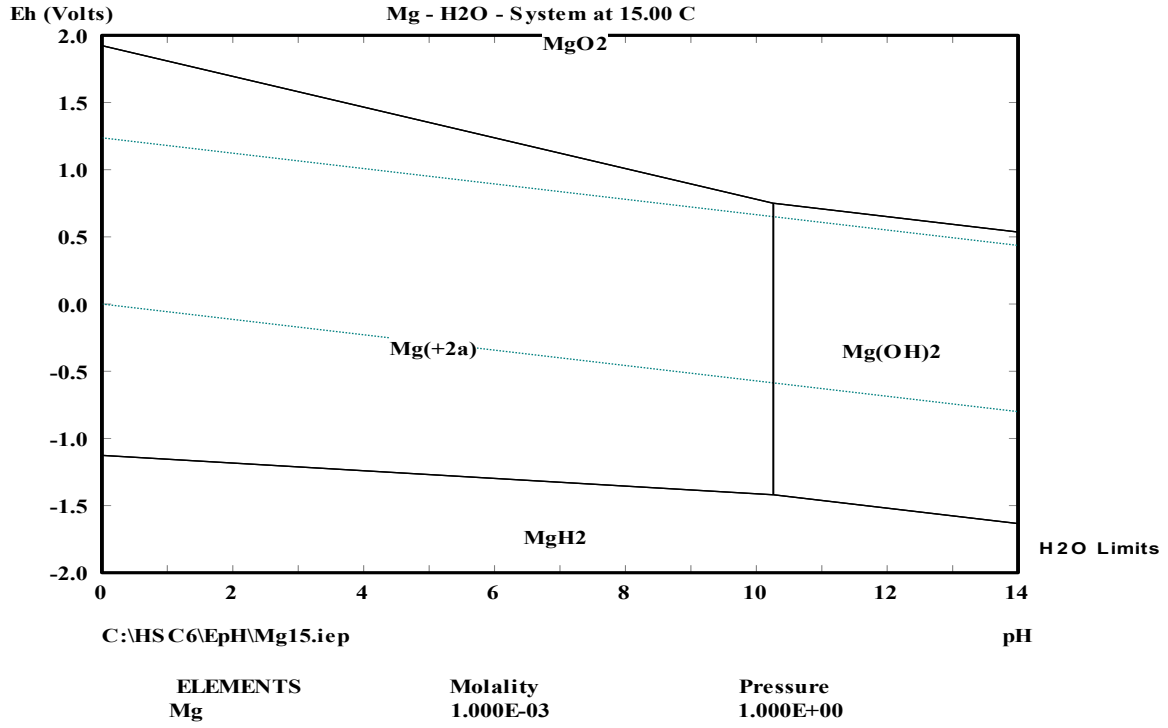


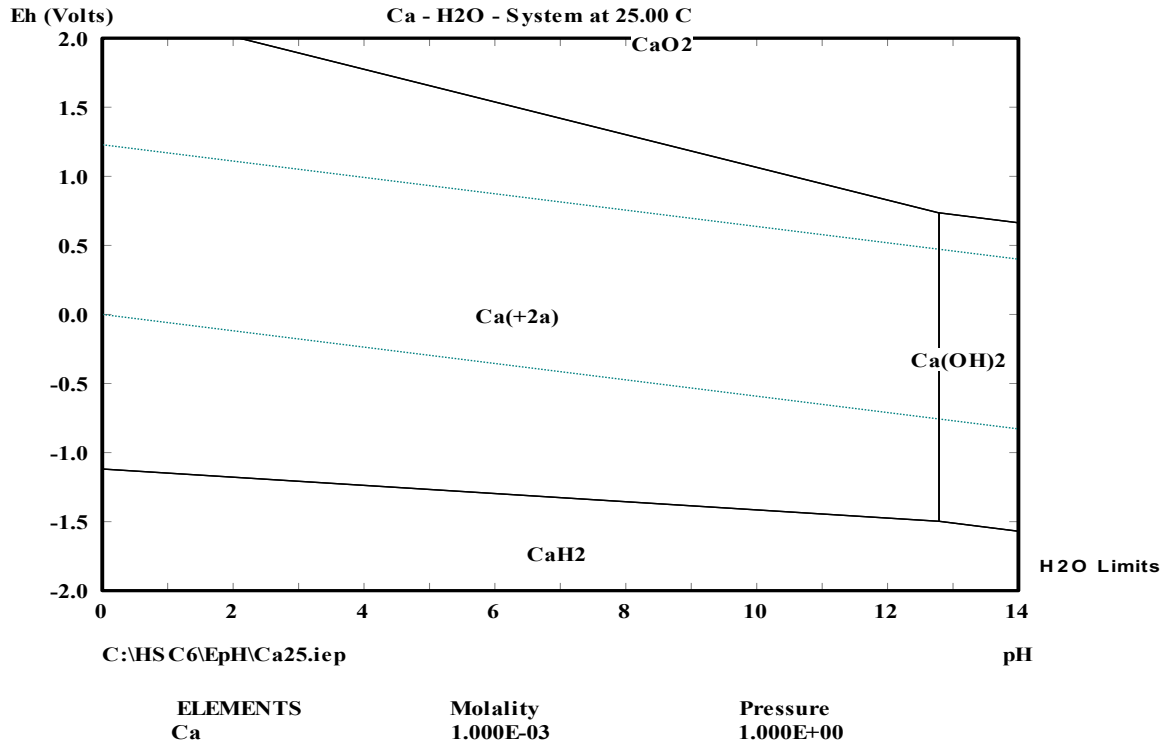
Figure 6. 4 Removal of calcium and magnesium by SAC resin as a function of initial pH of the solution (Initial [Ca^{2+}] = 521 mg/L; initial [Mg^{2+}] = 111 mg/L; stirring speed = 150 rpm, contact time = 60 minutes; Temperature = 25°C)

Considering the pH range where Ca and Mg start to precipitate (pH 10–11), this decrease in removal efficiency may be attributed to the decrease in adsorption capacity of the resin at that

particular pH range. When the pH exceeds 10, the SAC resin's sulphonic acid functional groups become increasingly ionized and less effective at exchanging hydrogen ions for hardness ions. In highly alkaline conditions, the SAC resin clearly isn't as effective at removing hardness ions, and it could even release previously exchanged ions (Harland, 1994). Additionally, according to the speciation diagrams in Figure 6.5 as the pH increases above 10, $Ca(OH)_2$ and $Mg(OH)_2$ become the dominant species.



(a)



(b)

Figure 6. 5 (a) Mg- H_2O and (b) Ca-H_2O Pourbaix diagram (temperature= 25°C; Concentration $1*10^{-3}$)

The precipitation of Ca and Mg species out of solution significantly limits the resin's ability to adsorb Ca and Mg ions. As the pH exceeds 10, the concentration of hydroxide ions substantially rises, leading to the formation of Ca and Mg hydroxides with limited solubility. These hydroxides can precipitate onto the resin beads, creating a layer on the resin surface. Consequently, the contact between the resin and water is hindered, resulting in reduced removal efficiency. This diminishes the resin's effectiveness in removing calcium and magnesium ions, ultimately decreasing hardness removal (Applebaum, 2013; Banerjee et al., 2016), as illustrated in Figure 6.4.

In summary, when the pH exceeds 10, the SAC resin can start to lose its effectiveness for hardness removal. The precipitation of Ca and Mg as hydroxides may additionally hamper the resin's ion exchange process, impeding the removal of hardness ions from water. Therefore, for efficient removal using the SAC resin, it is crucial to consider the solution pH at which Ca and Mg ions remain stable. The SAC resin exhibits a higher affinity for Ca compared to Mg, resulting in maximum removal percentages of 68 % and 60 %, respectively. Both resins demonstrate that operating within moderately acidic to moderately alkaline pH ranges ($4 < pH < 10$) proves most effective for adsorption.

6.2.2.2 Effect of resin mass

In the softening process, accurately determining the mass of resin required for a given volume of sample solution is crucial, especially when considering reagent costs. The results from both resins (Figure 6.6 and 6.7) showed that the removal of both calcium (Ca) and magnesium (Mg) initially increased as the mass of resin increased. This outcome is expected since a higher resin mass provides more ion exchange and adsorption sites, along with a larger surface area, particularly when the initial metal concentration is fixed.

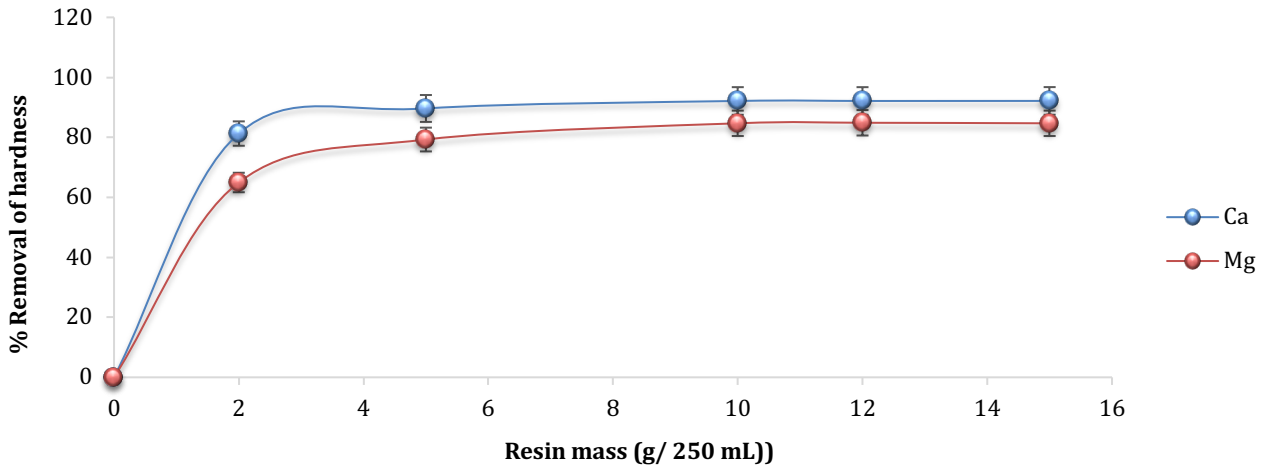


Figure 6. 6 Removal of calcium and magnesium by WAC resin as a function of resin mass. (Initial [Ca^{2+}] = 521 mg/L; initial [Mg^{2+}] = 111 mg/L; stirring speed = 150 rpm, contact time = 60 minutes; Temperature = 25°C; initial natural pH = 4.85).

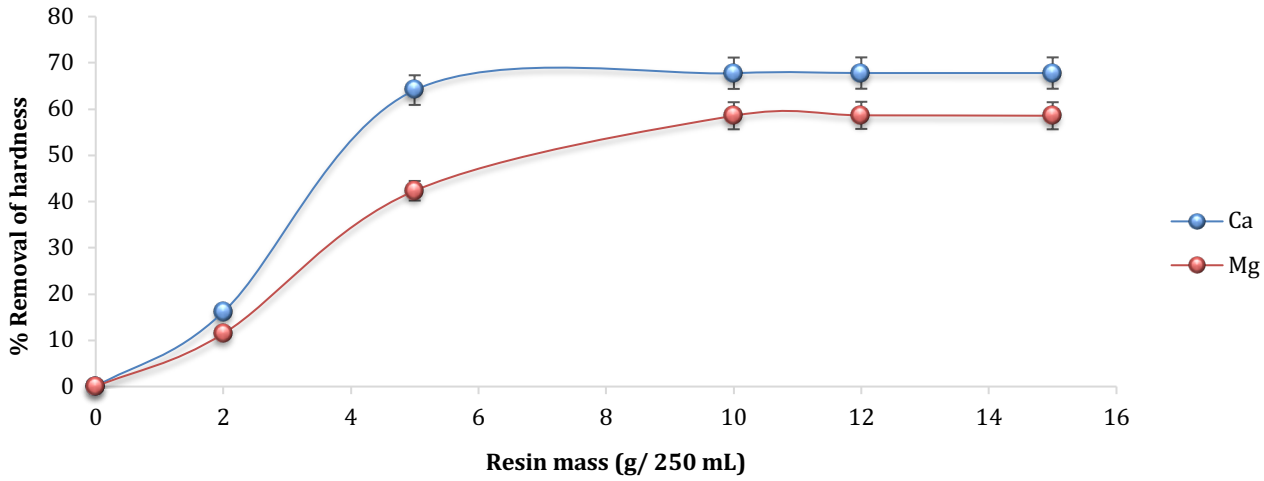


Figure 6. 7 Removal of calcium and magnesium by SAC resin as a function of resin mass. (Initial [Ca^{2+}] = 521 mg/L; initial [Mg^{2+}] = 111 mg/L; stirring speed = 150 rpm, contact time = 60 minutes s; Temperature = 25°C; initial natural pH = 4.85).

The trend of increasing removal efficiency with increasing resin mass becomes less pronounced when the resin mass exceeds 10 g/250 mL. This is may be attributed to a maximum uptake of Ca and Mg. At this point the concentration of Ca and Mg becomes the limiting factor. As a result, the density of the resin decreases during the adsorption process, leaving some parts unsaturated. However, despite this decrease in density, the increase in resin mass leads to a greater availability of ion exchange sites, ultimately improving the overall removal efficiency (Hayani et al., 2016; Tang et al., 2023).

6.2.2.3 Effect of shaking speed

The impact of shaking speed was examined within the range of 50—250 rpm for both resins. The dispersion and distribution of the resin within the solution significantly affect its adsorption capacity. Consequently, the stirring or shaking speed plays a crucial role, especially in mass transfer, as it affects the interaction between the bulk solution and the formation of the external boundary layer near the resin. Therefore, controlling the stirring or shaking speed becomes an important factor to optimize the adsorption process and enhance the overall efficiency of the resin.

6.2.2.3.1 WAC and SAC resin

The effect of the shaking speed on the removal efficiency of the WAC resin is depicted in Figure 6.8. For both Ca and Mg, an increase in shaking speed resulted in an increase in removal efficiency. This trend is observed until 150 rpm after which the removal efficiency remains constant for both ions. The initial increase in removal efficiency can be attributed to the improved mass transfer around the resin (therefore increasing the adsorption capacity) as the shaking speed increases (Albadarin et al., 2012; Yang et al., 2019). At these higher agitation rates, the turbulent flow created by the increased shaking speed promotes better mixing and enhances the transport of ions to the resin surface. This improved mass transfer facilitates a faster exchange of ions between the solution and the resin, potentially reducing the significance of mass transfer limitations. For shaking speeds higher than 150 rpm, however, the constant removal efficiency may be attributed to maximum removal of hard ions, where now mass transfer is no longer limiting but the concentration of hardness ions in solution is (Albadarin et al., 2012; Yang et al., 2019).

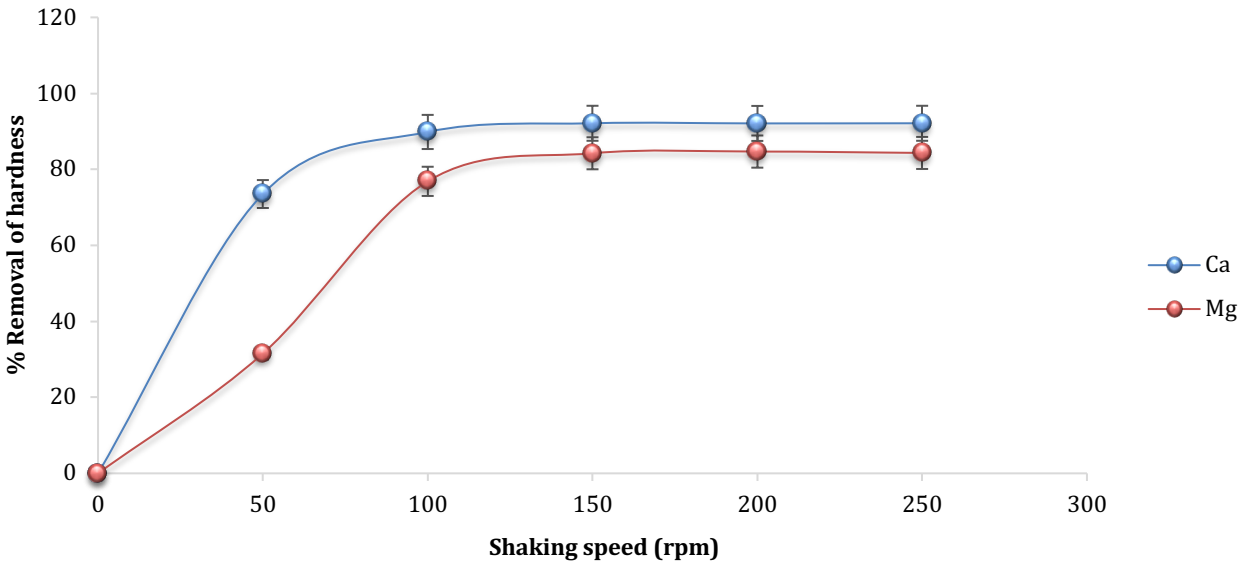


Figure 6. 8 Removal of calcium and magnesium by WAC resin as a function of shaking speed. (Initial [Ca^{2+}] = 521 mg/L; initial [Mg^{2+}] = 111 mg/L; contact time = 24hrs; Temperature = 25°C; initial natural pH = 4.85).

The influence of shaking speed on the removal efficiency of the SAC resin is depicted in Figure 6.9. Initially, there is an increase in removal efficiency as the shaking speed is raised until reaching 150 rpm. However, beyond 150 rpm, the removal efficiency starts to decline. This decrease in efficiency may be attributed to a few reasons:

1. Reduced contact time: While faster agitation may increase the rate of ion exchange initially, if the water passes through the resin bed too quickly, it may not allow sufficient time for the resin to capture and exchange all the hardness ions. Incomplete contact can lead to reduced removal efficiency (Fil et al., 2012; Yang et al., 2019; Yousef et al., 2016).
2. Resin Saturation**:** At very high shaking speeds, the resin may reach its ion exchange capacity more quickly, especially if the hardness level in the influent water is high. Once the resin is saturated, it cannot effectively remove additional hardness ions until it undergoes regeneration (Fil et al., 2012; Yang et al., 2019; Yousef et al., 2016).
3. Ion Back-Exchange/ desorption**:** In some cases, very high shaking speeds may promote the desorption of previously removed hardness ions. This occurs when the resin, due to the rapid agitation, releases ions that it had previously captured, leading to a decrease in removal efficiency. The desorption of Ca and Mg ions from the resin binding sites due to the binding strength of the sulphonic acid functional group on the SAC resin.

As discussed in section 2.6.2 the SAC resin does not have as high an affinity for Ca and Mg as compared to the WAC due to the nature of the functional group (Fil et al., 2012; Yang et al., 2019; Yousef et al., 2016), allowing them to return to the solution. Consequently, at very high shaking speeds the bonding strength between the functional group and the hardness ions may become less pronounced. This reduces the resin's adsorption capacity and leads to a decrease in overall removal efficiency.

4.

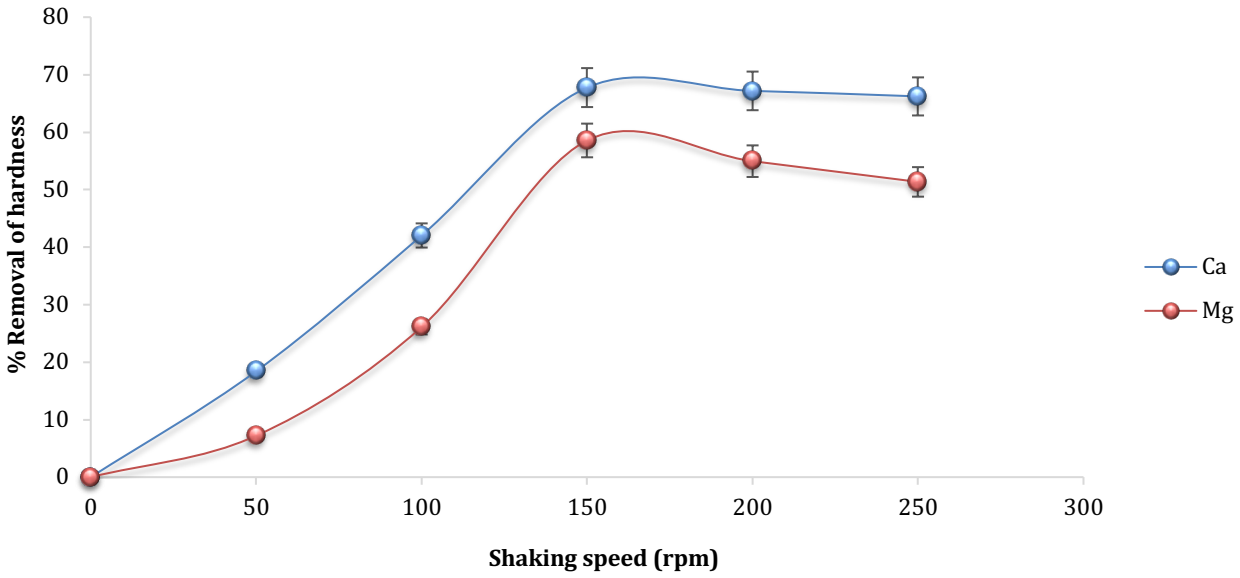


Figure 6. 9 Removal of calcium and magnesium by SAC resin as a function of shaking speed. (Initial [Ca^{2+}] = 521 mg/L; initial [Mg^{2+}] = 111 mg/L; contact time = 24hrs; Temperature = 25°C; initial natural pH = 4.85).

The decrease in removal efficiency observed at shaking speeds beyond 250 rpm for the SAC resin can be further explained by considering the desorption phenomenon. When the shaking speed is increased, the turbulent flow and agitation cause the resin binding sites to be exposed to higher shear forces and increased contact with the solution. As a result, the equilibrium between adsorption and desorption on the resin's binding sites may shift towards desorption. At these higher shaking speeds, the energy imparted to the system can overcome the binding forces between the resin and the adsorbed Ca and Mg ions. This can lead to the desorption of previously adsorbed ions from the resin back into the solution (Cetin, 2014; Fil et al., 2012; Yousef et al., 2016) Consequently, the desorbed ions are no longer effectively retained by the resin, resulting in a reduction in the adsorption capacity and a decrease in the overall removal

efficiency. The desorption process can be influenced by factors such as the strength of the resin-metal ion bond, the concentration of competing ions in the solution, and the solution pH.

The findings observed in this study align with previous research reported in the literature. Studies conducted by Cetin (2014), Fil et al. (2012), and Yousef et al (2016) have also reported similar results regarding the efficiency of cationic exchange resins and the impact of stirring speed on the removal of calcium (Ca) and magnesium (Mg) hardness. Fil et al. (2011) and Yousef et al. (2016) specifically investigated the removal efficiency of nickel (Ni) using the SAC resin and observed a decrease in removal efficiency for stirring speeds exceeding 400 rpm and 250 rpm, respectively. This trend was consistent across different initial Ni concentrations, as noted in Yousef et al.'s (2016) study. These findings highlight the influence of stirring speed on the adsorption capacity and efficiency of ion exchange resins. Additionally, Cetin (2014) conducted research with a sulphonic functional group resin in the H^+ form and achieved maximum removals of Ca and Mg at a stirring speed of 115 rpm. These results demonstrate operational similarities between WAC and SAC resins, further supporting the present findings.

6.2.2.4 Effect of contact time influence on the cationic exchange capacity

The impact of resin contact time on the process water was investigated by maintaining a constant solution pH, shaker speed, and resin mass while allowing the resin to interact with the solution for a duration of 24 hours. The findings obtained for both resins are presented below.

6.2.2.4.1 WAC and SAC resin

The weak acid cation (WAC) resin exhibits an increase in removal efficiency for both metals as the contact time with the resin and solution increases, until the resin reaches saturation (Figure 6.10). During the initial 60 minutes, a rapid uptake of Ca is observed, reaching maximum removal efficiency at 92 %. This equilibrium concentration remains constant throughout the remaining contact time. Similarly, Mg follows a similar trend, with an equilibrium concentration reached after 60 minutes and a maximum removal efficiency of 83 %. This equilibrium concentration also remains unchanged for the duration of the contact time. It is noteworthy that both Ca and Mg reach their equilibrium concentrations within 60 minutes of contact time. Further extending the contact time beyond this period has a negligible effect on the exchange capacity of the resin. This suggests that the resin becomes fully saturated with the target ions, and additional contact time does not significantly enhance the removal efficiency of the WAC resin for Ca and Mg ions.

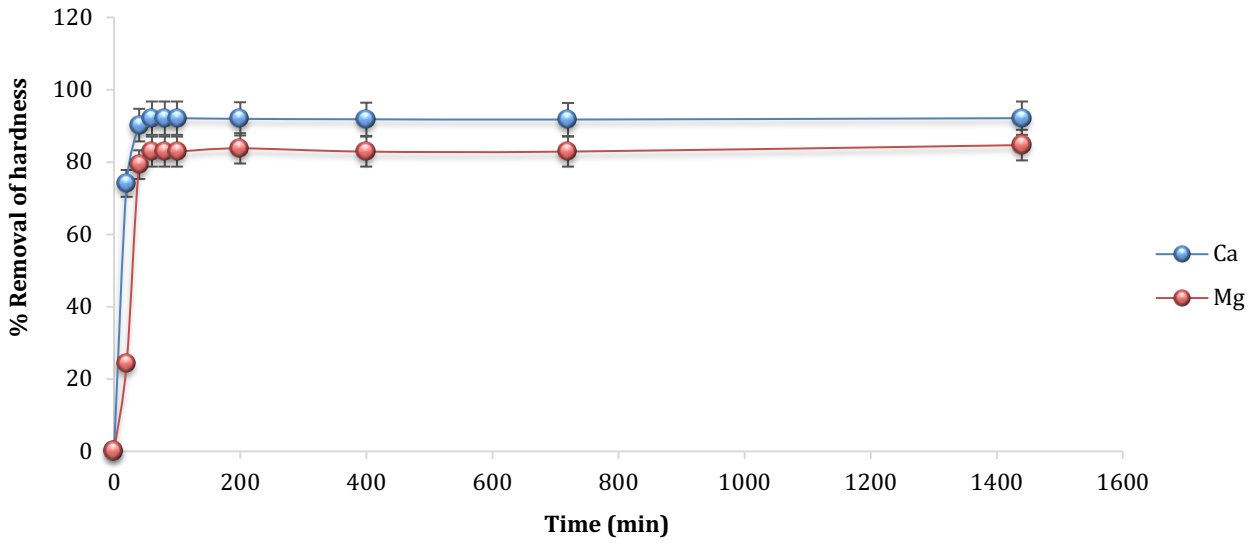


Figure 6. 10 Removal of calcium and magnesium by WAC resin as a function of contact time. (Initial [Ca^{2+}] = 521 mg/L; initial [Mg^{2+}] = 111 mg/L; Contact time = 24hrs; Temperature = 25°C; Initial natural pH = 4.85).

Similar results were observed for the SAC resin in Figure 6.11 with equilibrium concentrations reached after 60 minutes at 67 % and 58 % for Ca and Mg, respectively.

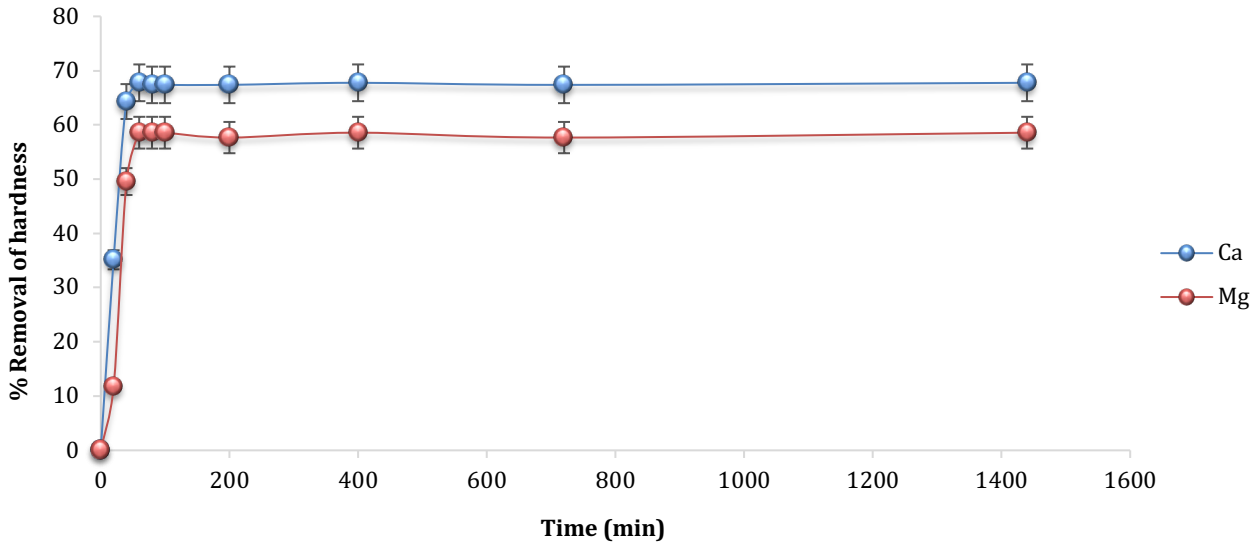


Figure 6. 11 Removal of calcium and magnesium by SAC resin as a function of contact time. (Initial [Ca^{2+}] = 521 mg/L; initial [Mg^{2+}] = 111 mg/L; Contact time = 24hrs; Temperature = 25°C; Initial natural pH = 4.85).

In contrast to this observation, literature has documented the two distinct phases of softening, namely the quick initial phase and the subsequent slower phase, which may sometimes be negligible. The initial rapid phase can be attributed to the abundance of available active sites on the ion exchange resin, enabling efficient adsorption of the target ions. However, as the process continues, the slower phase indicates that the adsorption becomes less effective. The removal efficiency versus time curves exhibit a smooth and continuous convergence towards saturation, suggesting an even coverage of metal ions on the ion exchange resins. This phenomenon indicates that the active sites on the resin are being gradually occupied, leading to a diminishing rate of removal efficiency over time (Yu et al., 2009).

6.2.3 Summary of determined optimal operating parameters for resin batch reactions

The investigation of WAC and SAC resins using batch reactions and varying specific ion exchange parameters has led to the following conclusions:

- Initial Solution pH: The removal efficiency of both resins increased with an increase in pH. However, the WAC resin exhibited lower recoveries at pH values below 4 and above 10. On the other hand, the performance of the SAC resin was not significantly affected by the initial solution pH, except at pH values above 10. It is evident that for efficient and optimal removal of calcium (Ca) and magnesium (Mg), the pH range should be selected where these metals remain stable in their ionized form.
- Shaking Speed: The optimal shaking speed for the batch reactions was found to be 150 rpm. Beyond this speed, poorer removal efficiencies were observed for the SAC resin. This suggests that excessive agitation may hinder the effectiveness of the ion exchange process, possibly due to the lower binding strength of the sulphonic acid functional group at higher speeds as well as reduced contact time between the solution and resin.
- Resin Mass: For a sample solution volume of 250 mL, the optimum resin mass was determined to be 10 g. This resin mass provided the best balance between ion exchange capacity and efficient removal of Ca and Mg from the solution.
- Contact Time: The optimal contact time between the resin and the solution was found to be 60 minutes. At this duration, both resins achieved maximum adsorption of Ca and Mg from the solution. Prolonging the contact time beyond this point did not significantly enhance the removal efficiency of the resins.

- Loading Preference: Interestingly, both resins, despite being specifically designed for softening purposes and having an affinity for Ca and Mg, demonstrated a higher loading preference for Ca compared to Mg in the conducted investigations. This preference was expected for the SAC resin, while the WAC resin was anticipated to exhibit equal loading capacities for both Ca and Mg.

These conclusions highlight the importance of optimizing ion exchange parameters such as solution pH, shaking speed, resin mass, and contact time for effective and efficient removal of Ca and Mg using WAC and SAC resins in batch reactions. The optimal parameters, including the initial solution pH, shaking speed, resin mass, and contact time, identified in the previous investigations were employed in the softening process of all four water samples..

6.2.4 Determining cation resin efficiency in the removal of calcium and magnesium for all samples

The softening process of all four water samples was conducted using both the WAC and SAC resins, and the removal efficiencies of these resins were compared (Figure 6.12 and 6.13) . The optimal parameters determined from previous investigations were applied to ensure effective batch ion exchange reactions. For three of the water samples, which had initial pH values ranging from 4 to 10 according to the ICP-OES analysis in Table 4.7 under section 4.1.2.2.2, the treatment was carried out without adjusting their pH levels. However, the scrubber bleed sample required adjustment, and therefore, it was treated with 1 M NaOH to achieve a target initial pH of 5 (from initial pH ~ 3). In terms of the WAC resin, the removal of calcium (Ca) from all samples demonstrated higher efficiency compared to the removal of magnesium (Mg). The scrubber feed exhibited the highest Ca removal efficiency of 93 %, while the dust thickener and process water samples achieved a maximum removal efficiency of 84 % for Mg. Overall, the WAC resin displayed a minimum removal efficiency of 77 % for both Ca and Mg when considering all samples collectively.

The obtained results allowed for the evaluation of the effectiveness of the WAC and SAC resins in removing hardness from each water sample. By comparing the hardness removal efficiencies across the four water samples, it was possible to determine the variability in the hardness content and assess the suitability of the WAC and SAC resins for different water sources. These

findings would contribute to understanding the efficacy of the selected ion exchange parameters in achieving the desired level of hardness removal for various water samples.

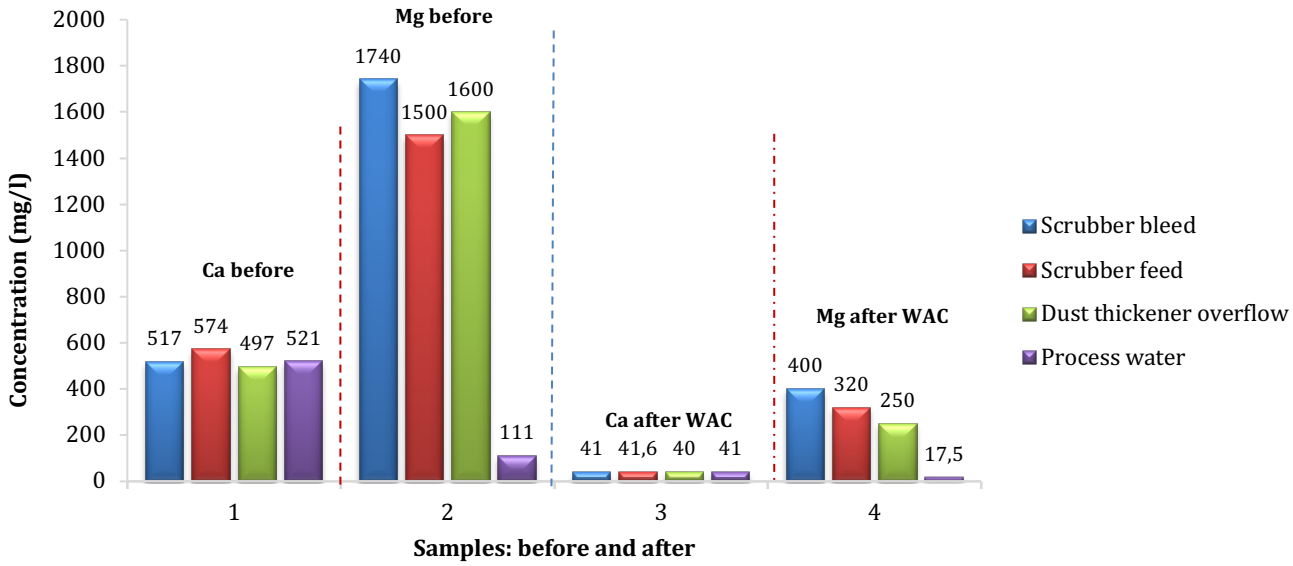


Figure 6. 12 Removal of calcium and magnesium by WAC resin. (Contact time = 60 minutes; Temperature = 25°C; Shaking speed 150 rpm; Resin mass = 10 g; Solution pH 4 –10).

Figure 6.13 depicts the removal efficiency of the SAC resin for Ca and Mg. Calcium was the most adsorbed compared to Mg with a maximum removal efficiency of 68 % for all samples and 59 % maximum Mg removal for the process water sample.

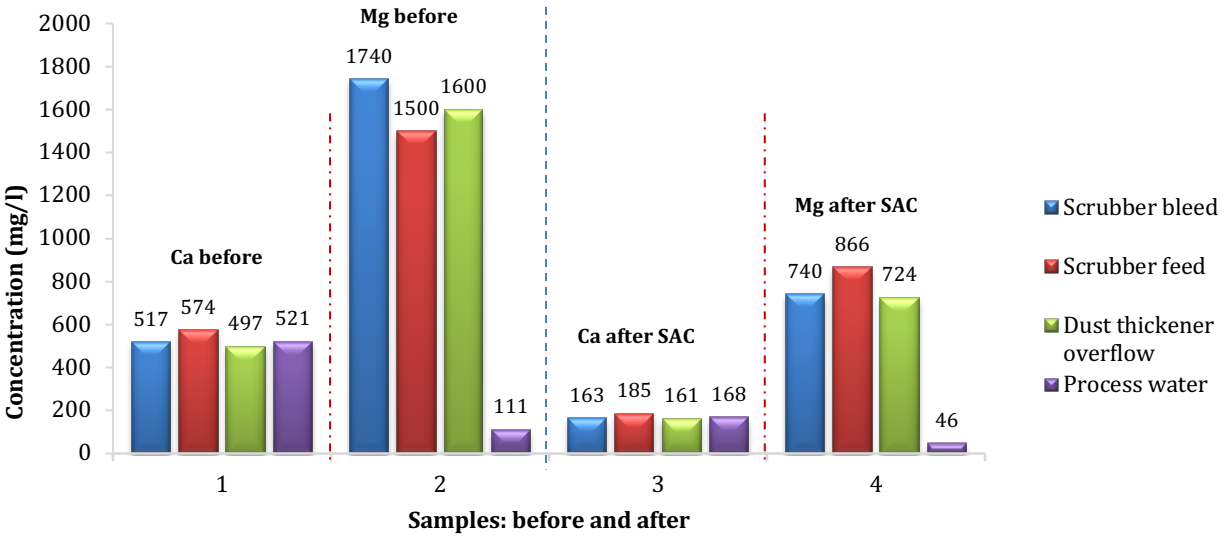


Figure 6. 13 Removal of calcium and magnesium by SAC resin. (Contact time = 60 minutes; Temperature = 25°C; Shaking speed 150 rpm; Resin mass = 10 g; Solution pH 4 –10).

While the removal efficiencies of both the WAC and SAC resin were relatively satisfactory, the final concentrations of Ca and Mg in the solutes still rendered the samples as being *very hard.*

The WAC resin outperformed the SAC resin in terms of removal efficiency. This superiority can be attributed to the specific design of the WAC resin, which not only possesses a high affinity for Ca and Mg hardness ions but is also tailored to effectively remove hardness ions from solutions with high TDS content (Brown and Sheedy, 2002). However, it is important to note that additional treatment steps were required to further reduce the hardness levels in these water samples to achieve a soft or moderately hard water classification. To accomplish this, a combination of chemical precipitation using lime and soda ash, as well as ion exchange, was employed in the subsequent sections of the study. The integration of these treatment methods allows for comprehensive and efficient softening of the water samples, ensuring that their hardness levels fall within the desired range of 0—60 mg/L or 61—120 mg/L as $CaCO_3$. This multi-step approach ensures the production of water that meets the required standards for various applications.

6.2.5 Determining resin efficiency with lime-soda ash pre-treatment of hard water (combined softening treatment)

Due to the persistently high hardness levels observed in the samples treated with lime-soda ash and ion exchange individually, a decision was made to combine both treatments in order to achieve an overall softening process. The feed samples used for this combined treatment were the ones previously treated with lime and soda ash, as indicated in Section 5.2.1.4, Table 5.5. Following the lime and soda ash treatment, these samples exhibited solution pH values above 10.5, requiring further adjustment to achieve the desired initial pH range described in Section 4.3.1.1.1 ($5 < pH > 10$). To accomplish this, the samples were treated with 1M HCl. Utilizing the optimal parameters determined in Section 4.3.1.2, the feed samples underwent subsequent treatment using both the WAC and SAC resins. The final concentrations of Ca and Mg after the dual treatment with lime-soda ash and ion exchange are presented in Table A3.1 in Appendix 3. This table provides a comprehensive overview of the effectiveness of the combined treatment approach in achieving the desired softening outcome for the samples.

After the application of lime and soda ash treatment, the WAC resin further improved the removal of Ca and Mg from the scrubber bleed, scrubber feed, dust thickener overflow, and process water samples. The Ca removal percentages increased by 54 %, 38 %, 41 %, and 40 %, respectively, while the Mg removal percentages were enhanced by 65 %, 90 %, 87 %, and 27 %, respectively. Similarly, the SAC resin demonstrated improved Ca removal percentages of 49 %, 19 %, 28 %, and 37 % for the respective samples. For magnesium, the SAC resin achieved reductions of 64 %, 88 %, 71 %, and 17 % in the same order, respectively. The overall effectiveness of the combined softening processes involving lime-soda ash and ion exchange is illustrated in Figures 6.14 to 6.17. Notably, Figure 6.14 demonstrates that the scrubber bleed sample achieved an impressive overall Ca removal of 97 % when subjected to both lime-soda ash treatment and the use of the WAC resin. Similarly, a remarkable 98 % removal of Ca was achieved for the scrubber feed and dust thickener overflow samples, as well as a 97 % removal for the process water sample. Regarding magnesium in Figure 6.15, the combined softening treatments resulted in excellent removal rates of over 99 % for the scrubber bleed, scrubber feed, and dust thickener overflow samples, while the process water sample achieved an 84 % removal. These findings highlight the highly effective nature of the combined softening processes in achieving substantial reductions in both Ca and Mg concentrations, leading to significant overall hardness removal.

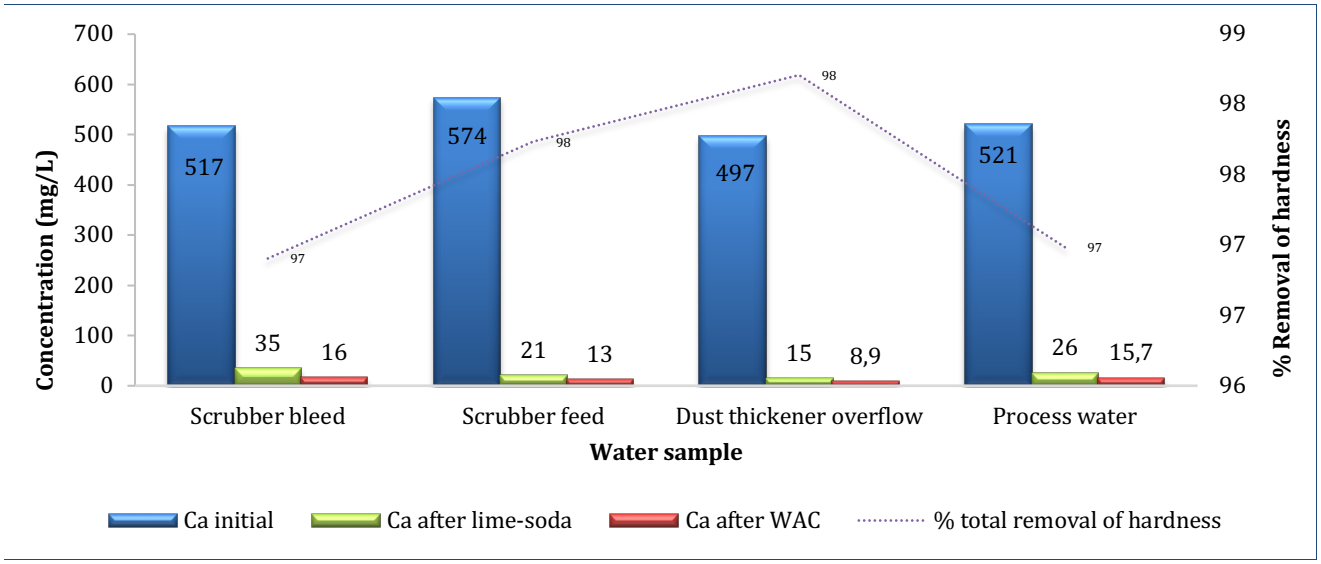


Figure 6. 14 Final Ca concentration after dual softening of water samples with lime-soda ash and WAC resin

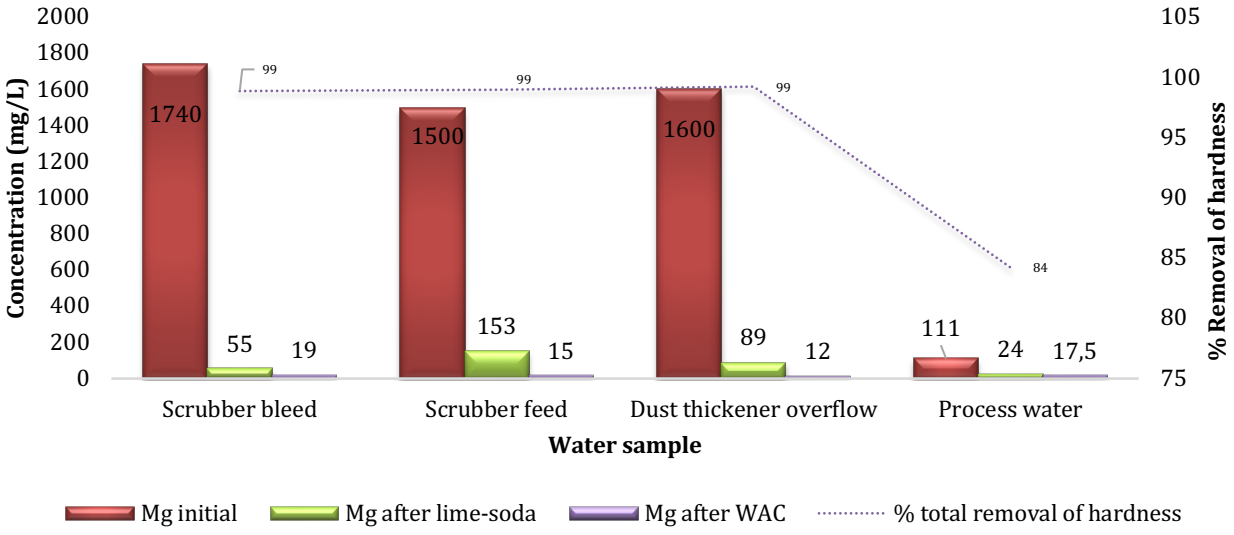


Figure 6. 15 Final Mg concentration after dual softening of water samples with lime-soda ash and WAC resin

The utilization of SAC resin after the lime-soda ash treatment yielded noteworthy results, as depicted in Figures 6.16. These results demonstrate that an overall removal of 97 % of Ca was attained from the scrubber bleed, scrubber feed, and process water sample. Additionally, a 98% removal rate was observed for the dust thickener overflow sample.

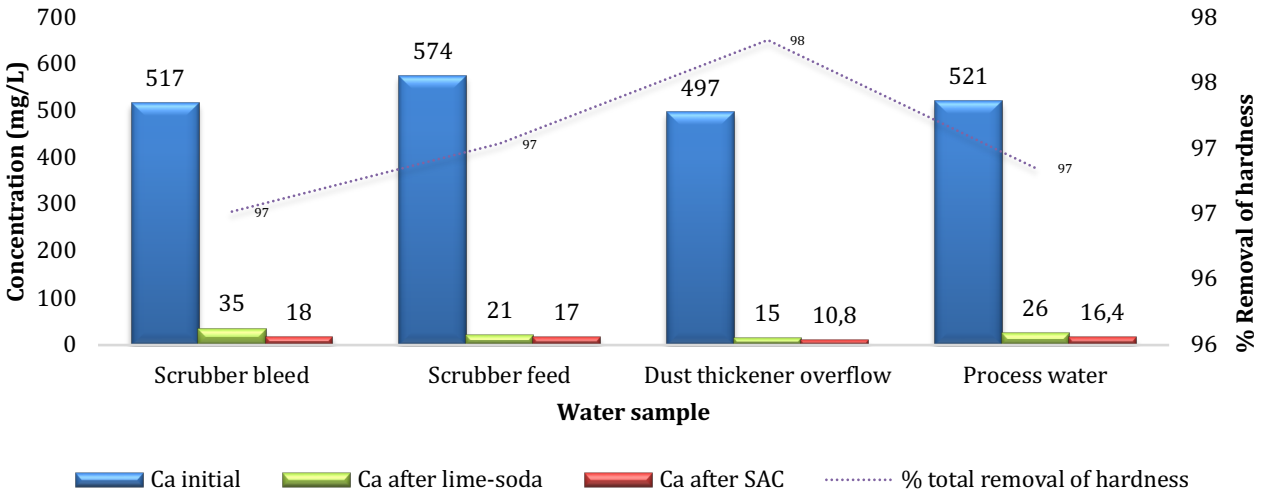


Figure 6. 16 Final Ca concentration after dual softening of water samples with lime-soda ash and SAC resin

Magnesium exhibited remarkable removal efficiencies in the scrubber bleed and scrubber feed samples, achieving a remarkable 99 % reduction in Figure 6.17. Additionally, the dust thickener overflow and process water samples showed considerable removal efficiencies of 98 % and 82 %, respectively. These findings highlight the exceptional effectiveness of the combined softening processes in significantly reducing magnesium concentrations in the treated samples.

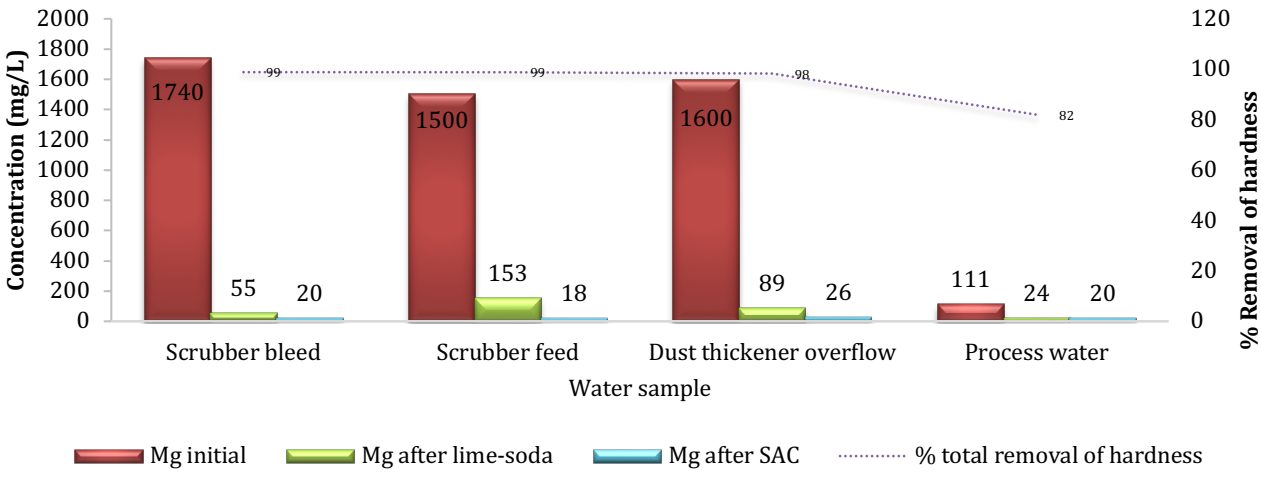


Figure 6. 17 Final Mg concentration after dual softening of water samples with lime-soda ash and SAC resin

Table 6.1 displays the concentrations of Ca and Mg in the treated water samples after the combined softening process involving lime soda-ash treatment and ion exchange. These concentrations are crucial for determining the hardness level of the treated water, as outlined in Equation 4.4.

Table 6. 1 Total hardness after lime -soda ash and ion-exchange combined softening treatment.

	WAC		SAC		Total hardness (TH) mg/L as $CaCO_3$			
Sample	Ca (mg/L)	Mg (mg/L)	Ca l (mg/L)	Mg (mg/L)	WAC	Degree of hardness	SAC	Degree of hardness
SB	16	19	18	20	117,9	Moderately hard	127	hard
SF	13	15	17	18	94	Moderately hard	116,3	Moderately hard
DTO	8,9	12	10,8	16	71,45	Moderately hard	133,6	hard
PW	15,7	17,5	16,4	19	111	Moderately hard	123	hard

The combined treatment of lime-soda ash and WAC resin proved to be more effective compared to the combined treatment with the SAC resin. Once again, the WAC resin demonstrated superior performance, resulting in moderately hard solutions with hardness levels ranging from 60—120 mg/L as $CaCO_3$. However, except for the scrubber feed sample, the SAC resin yielded hard water (120—180 mg/L as $CaCO_3$) even after the combined treatment with lime-soda ash. It is worth noting that practical limits of approximately 30 mg/L for Ca and 10 mg/L for Mg are considered acceptable to prevent excessively corrosive water due to low or no hardness (Dey et al., 2007; Minnesota Rural Water Association, 2009; Veolia Water Technologies & Solutions, 2023). Consequently, a total residual hardness of approximately 75-120 mg/L as $CaCO_3$ was achieved through the combined softening process of lime-soda ash and the WAC resin. An example of a lime and soda ash treatment plant in South Africa is the Rand Water Zuikerbosch Water Treatment Plant, located near Johannesburg. With a processing capacity of approximately 640 ML per day, it is one of the largest water treatment plants in the country, serving the Gauteng province, including Johannesburg and Pretoria. The Rand Water Zuikerbosch Water Treatment Plant utilizes hydrated lime to soften the water and remove minerals such as Ca and Mg, which contribute to water hardness. The plant is designed to

produce water with a final hardness level of approximately 120—80 mg/L as $CaCO_3$, aligning with the South African National Standards for Drinking Water (SANS-241-2015). The water samples analysed in this study exhibited very high hardness and TDS values. After undergoing the combined softening treatment, the TDS values are provided in Table 6.2.

Table 6. 2 TDS values after combined softening treatment.

Sample	TDS (mg/L)	
	WAC	SAC
SB	1100	1238
SF	867	1195
DTO	685	1296
PW	1056	1243

The final TDS values resulting from the combined softening treatment using lime-soda ash and the WAC resin are all below the drinking quality requirement limit of 1200 mg/L specified in SANS 214:2015. This outcome confirms the effectiveness of the proposed treatment plan. Meeting these TDS limits aligns with the objectives of reducing water hardness and producing water suitable for use and reuse within the plant. As a result, the need for freshwater purchases from Rand Water is significantly mitigated.

6.3 Summary of cationic resin efficiency of WAC (Amberlite IRC 83H) and SAC (Amberlite IRC 120Na)

The objective of this section was to assess the efficiency of cationic resins in removing hardness ions, specifically Ca and Mg. Although both resins are designed for softening and de-alkalization purposes, the WAC resin exhibited superior adsorption and softening capabilities. Considering the initial extremely high levels of hardness observed in all the samples (as indicated in section 4.2.2.4, Table 4.8), particularly the significant concentration of non-carbonate or permanent hardness, the achieved final hardness levels are commendable as they align with those in achieved in practice. Furthermore, these hardness levels attained through the combined softening treatment of lime-soda ash and the WAC resin are recommended in practical applications to mitigate corrosion concerns.

6.4 References

Albadarin, A.B., Mangwandi, C., Ala'a, H., Walker, G.M., Allen, S.J. and Ahmad, M.N., 2012. Kinetic and thermodynamics of chromium ions adsorption onto low-cost dolomite adsorbent. Chemical engineering journal, 179, pp.193-202.

Applebaum, S.B., 2013. Demineralization by ion exchange: in water treatment and chemical processing of other liquids. Elsevier.

Amber series (2022). Home. Available at: https://wwww.dupont.com/brands/amber-series.html/(accessed: January 19, 2022).

Apell, J.N. and Boyer, T.H., 2010. Combined ion exchange treatment for removal of dissolved organic matter and hardness. Water Research, 44(8), pp.2419-2430.

Bandrabur, B., Tataru-Farmus, R.E., Lazar, L., Bulgariu, L. and Gutt, G., 2012. Use of Strong Acid Resin Purolite C100E for Removing Permanent Hardness of Water-Factors Affecting Cationic Exchange Capacity. Scientific Study & Research. Chemistry & Chemical Engineering, Biotechnology, Food Industry, 13(3), p.295.

Banerjee, D., Kim, D., Schweiger, M.J., Kruger, A.A. and Thallapally, P.K., 2016. Removal of TcO 4− ions from solution: materials and future outlook. Chemical Society Reviews, 45(10), pp.2724-2739.

Bezuidenhout, G.A., Davis, J., Van Beek, B. and Eksteen, J.J., 2012. Operation of a concentrated mode dual-alkali scrubber plant at the Lonmin smelter. Journal of the Southern African Institute of Mining and Metallurgy, 112(7), pp.657-665.

Brown, C. and Sheedy, M., 2002, November. A new ion exchange process for softening high TDS produced water. In SPE International Thermal Operations and Heavy Oil Symposium and International Horizontal Well Technology Conference. OnePetro

Canepa, P., Garombo, C., Szpyrkowicz, L. and Zilio-Grandi, F., 1996. Comparison between ion exchange and nanofiltration for softening of industrial water. Filtration & separation, 33(2), pp.131-135.

Cappelle, M.A. and Davis, T.A., 2016. Ion Exchange Membranes for Water Softening and High-Recovery Desalination. Emerging Membrane Technology for Sustainable Water Treatment; Elsevier: Amsterdam, The Netherlands, pp.163-179.

Cetin, G., 2014. Removal of hardness of earth alkaline metals from aqueous solutions by ion exchange method. International Scholarly Research Notices, 2014.

Dey, D., Herzog, A. and Srinivasan, V., 2007. Chemical precipitation: water softening. Michigan State University, East Lancing.

Drinking Water For Sans. [Online] Available at: https://vinlab.com/wp-content/uploads/2016/10/SANS-241-2015.pdf [Accessed 08 08 2020].

Fil, B.A., Boncukcuoğlu, R., Yilmaz, A.E. and Bayar, S., 2012. Adsorption of Ni (II) on ion exchange resin: Kinetics, equilibrium and thermodynamic studies. Korean Journal of chemical engineering, 29, pp.1232-1238.

Harland, C.E., 1994. Ion exchange: theory and practice (No. 29). Royal society of Chemistry.

Hayani, A., Mountadar, S., Tahiri, S. and Mountadar, M., 2016. Softening of hard water by ion-exchange with strongly acidic cationic resin. Application to the brackish groundwater of the coastal area of El Jadida province (Morocco). Journal of Materials and Environmental Science, 7, pp.3875-3884.

Hoffmann, H. and Martinola, F., 1988. Selective resins and special processes for softening water and solutions; A review. Reactive Polymers, Ion Exchangers, Sorbents, 7(2-3), pp.263-272.

Minnesota Rural Water Association, 2009. Lime Softening. In: Minnesota Water Works Operations Manual. 4th ed. Minnesota: s.n., p. Chapter 16.

Tang, Q., Wu, H., Zhou, M. and Yang, D., 2023. Preparation of a new gel-type lignin-based cationic adsorption resin for efficient removal of Ca2+ from aqueous solutions. International Journal of Biological Macromolecules, 241, p.124505.

Veolia Water Technologies & Solutions, 2023. Handbook of Industrial Water Treatment - Chapter 7 Precipitation Softening. [Online] Available at: https://www.suezwatertechnologies.com/handbook/chapter-07-precipitation-softening [Accessed 01 10 2019].

Yang, J., Yu, S., Chen, W. and Chen, Y., 2019. Rhodamine B removal from aqueous solution by CT269DR resin: static and dynamic study. Adsorption Science & Technology, 37(9-10), pp.709-728.

Yousef, N.S., Farouq, R. and Hazzaa, R., 2016. Adsorption kinetics and isotherms for the removal of nickel ions from aqueous solutions by an ion exchange resin: application of two and three parameter isotherm models. Desalination and Water Treatment, 57(46), pp.21925-21938.

Yu, Z., Qi, T., Qu, J., Wang, L. and Chu, J., 2009. Removal of Ca (II) and Mg (II) from potassium chromate solution on Amberlite IRC 748 synthetic resin by ion exchange. Journal of hazardous materials, 167(1-3), pp.406-412.

Chapter 7 The effect of magnetic water treatment on hard water

7.1 Introduction

The previously evaluated methods for water softening, which involve traditional chemical approaches, have proven to be effective in preventing scale formation. However, concerns regarding operating costs and the significant alteration of water chemistry have raised environmental and economic considerations. These factors drive the exploration of alternative physical methods that can offer similar benefits without the use of chemicals. As discussed in Chapter 2, MWT has emerged as a potential solution in line with the global shift towards sustainability and environmental responsibility. However, the treatment mechanisms of MWT have been subject to debate, with conflicting theories and claims of varying efficiency. Therefore, the objective of this test work is to investigate and potentially confirm the impact of MWT on scaling in hard water.

Gabrielli et al. (2001) emphasized the importance of investigating the effectiveness of magnetic treatment on scaling waters through two key aspects. Firstly, they suggested monitoring the variation in ionic calcium concentration at the outlet of the magnetic device to assess the impact of magnetic treatment. Secondly, they recommended evaluating the scaling potential of the treated water to determine the extent to which scale formation is mitigated. In addition to the above statement, the efficiency of the magnetic treatment on the solution must also be evaluated in terms of observing changes in significant water parameters such as pH, dissolved oxygen (DO), electrical conductivity (EC) and oxidation-reduction potential (E_h) of the solution.

7.2 Results and discussion

7.2.1 Preliminary MWT time exposure effects on solution pH and dissolved oxygen (DO)

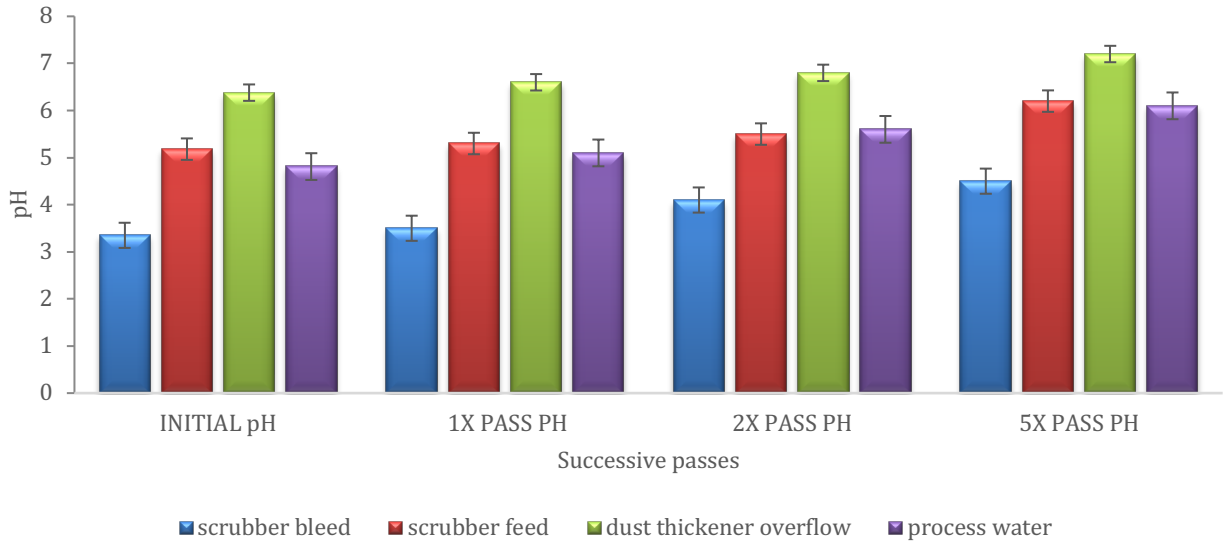


Figure 7. 1 MWT effect on solution pH

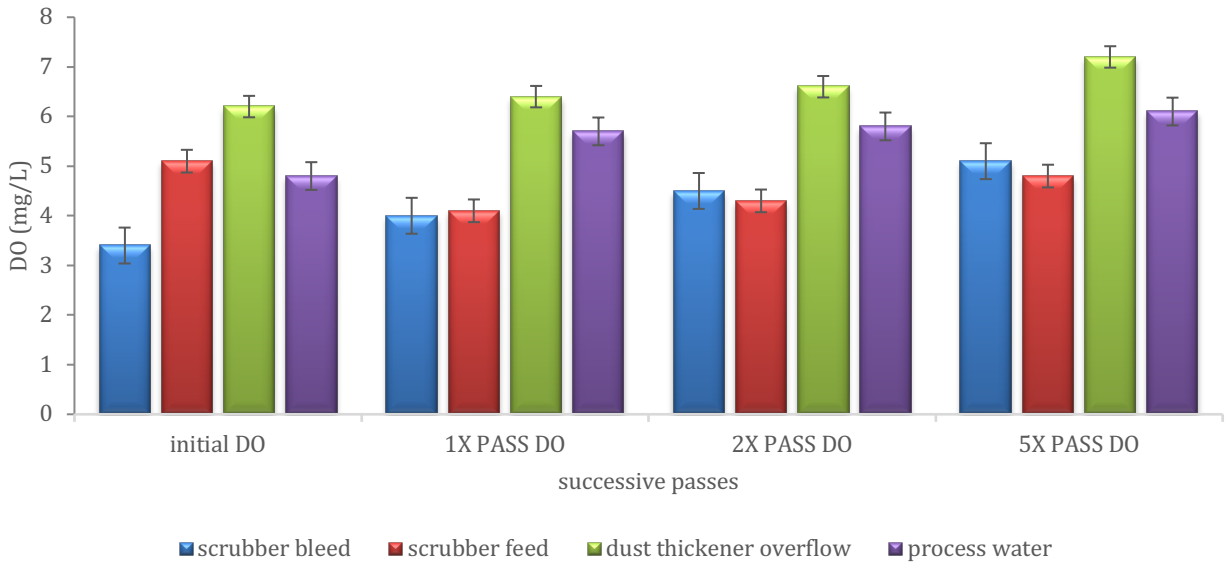


Figure 7. 2 MWT effect on solution DO

The initial setup of the simple MTD, as depicted in Figure 3.6, aimed to determine if any measurable influence on DO and pH could be observed. The preliminary tests conducted using the MWT device indicated an increase in pH and DO with successive passes through the

treatment device, as shown in Figures 7.1 and 7.2. However, it is important to note that while it can be assumed that the increase in DO is due to the MTD, it could also be attributed to the stirring effect when the sample exits the device. Therefore, based on these tests and the setup used, it was challenging to draw definitive conclusions about the effectiveness of the MTD in altering the DO of water samples. Subsequently, further tests were conducted using an adjusted MTD configuration, as shown in Figure 3.8. While magnetic treatment devices (MTDs) are available in different configurations (Baker & Judd, 1995), the subsequent test work was performed using an adjusted MTD setup as described in section 3.2.4.2, that exhibited some efficiency. This adjusted setup was based on similar setups described in the literature, such as those by Gabrielli et al. (2001), McMahon (2009), and Yap et al. (2021).

7.2.2 Effect of adjusted MTD exposure on electrical conductivity, calcium concentration, dissolved oxygen and DO and oxidation-reduction potential

The impact of the MTD on [Ca^{2+}], EC, DO, and E_h was assessed. The solutions were subjected to the magnetic effect for a duration of 60 minutes, and the following figures illustrate the observed results. Control experiments were also conducted in the absence of the magnetic effect, and the corresponding results are presented below.

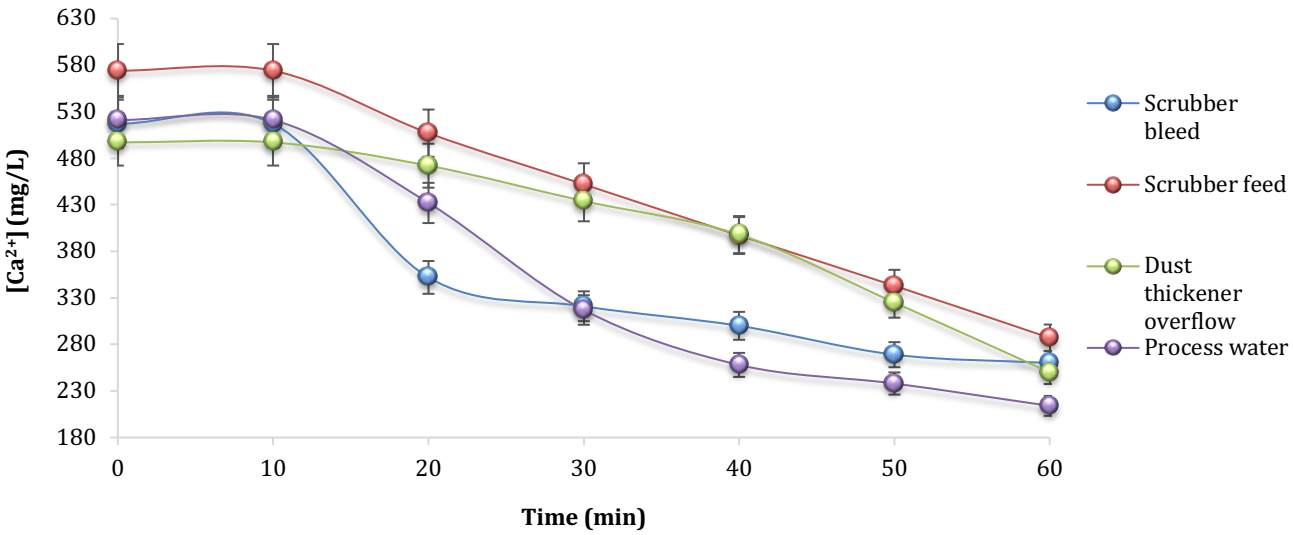


Figure 7. 3 Effect of MTD on [Ca^{2+}] for all four water samples

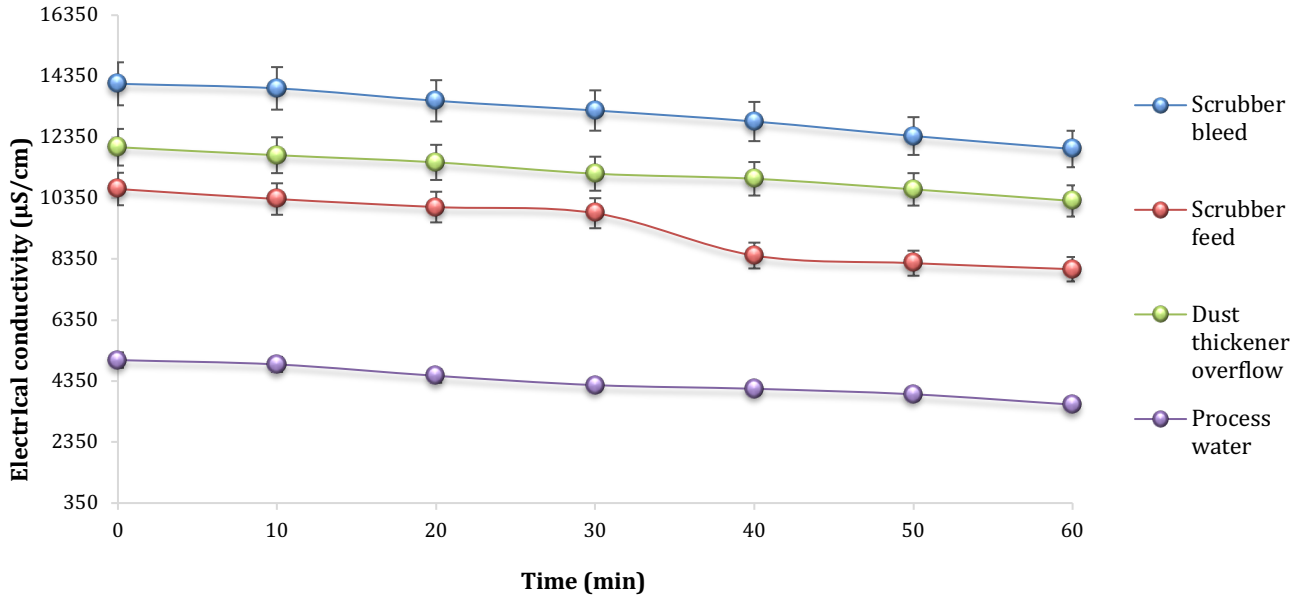


Figure 7. 4 Effect of MTD on EC for all four water samples

The electrical conductivity (EC) showed a decreasing trend over the 60-minute period. This decrease corresponded to lower estimated TDS values based on Equation 4.7 from Chapter 4. In this study, the relationship between TDS and EC followed a linear pattern with a high coefficient of determination (R^2) close to 1, as shown in Figure 7.5. These findings align with the observations of Taylor et al. (2018), who also reported a linear relationship for EC values below 75,000 µS/cm. They further demonstrated that TDS values could be estimated with minimal error using Equation 7.1:

$$TDS\ (mg/L) = k_e * EC\ (\mu S/cm) \quad [7.1]$$

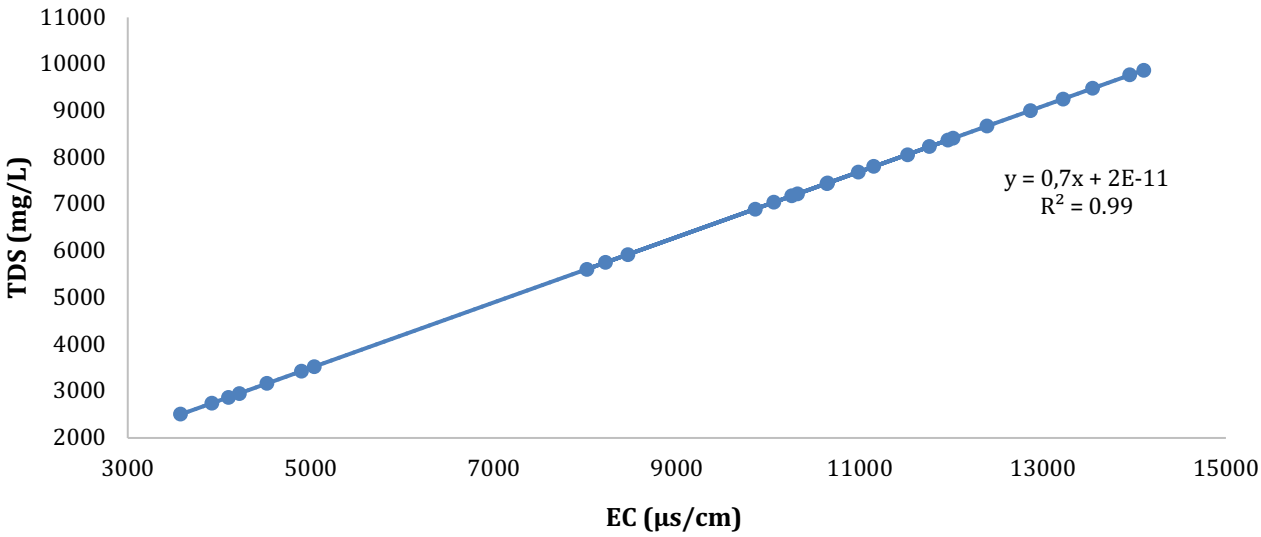


Figure 7. 5 Relationship between TDS and EC for all water samples.

Measuring the TDS value is crucial as it provides insights into the ionic composition of the solution. The observed decrease in both EC and TDS indicates that ions are undergoing precipitation, resulting in a reduction of ion concentration in the solution, as reflected by the changes in EC. This finding is further supported by Figure 7.3, which shows a decrease in the concentration of Ca in the solution over time under the magnetic effect. The impact of the magnetic effect on pH, DO, and E_h is presented in Figures 7.6—7.8. Exposure to the magnetic effect over time leads to an increase in pH and DO levels. This initial observation was also evident in the preliminary tests shown in Figures 7.1 and 7.2, conducted with the setup depicted in Figure 3.6. The increasing pH of the system is associated with the formation of stable hydroxides in the neutral to alkaline pH range, as illustrated in Figure 6.5 in Chapter 6.

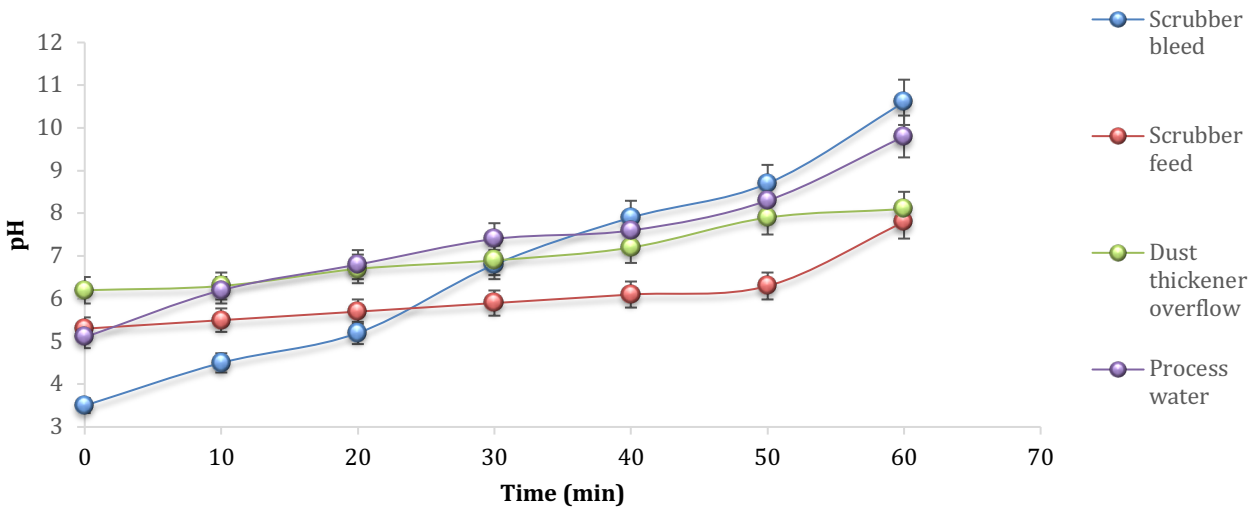


Figure 7. 6 Effect of MTD on pH for all four water samples

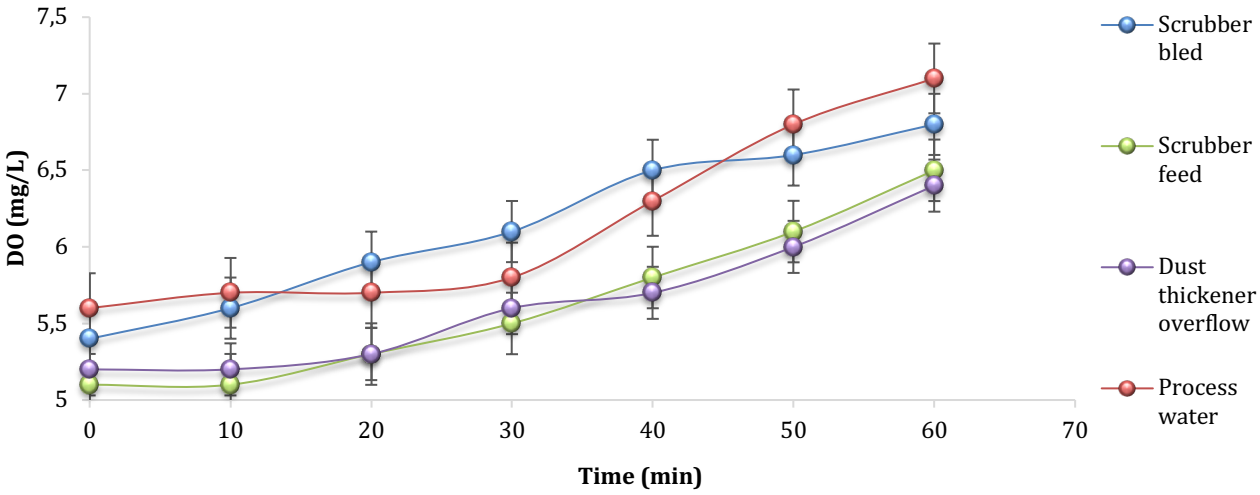


Figure 7. 7 Effect of MTD on DO for all four water samples

Previous research has established that the presence of a magnetic field can cause changes in the pH of a solution, which is closely linked to the concentration of protons (Lin et al., 2020; Mghaiouini et al., 2020). It is hypothesized that these modifications occur due to alterations in the bonding between water molecules and between water and hydronium molecules. The proposed hypothesis suggests that the magnetic field induces an increase in the formation of

hydrogen bonds between water and hydronium molecules, which helps counteract the external energy imparted by the magnetic field (Lin et al., 2020; Mghaiouini et al., 2020). Electromagnetic fields have also been found to influence the pH of tap water. This phenomenon can be explained by the absorption of energy by the dipolar moment when exposed to an electromagnetic field. This energy leads to the dissociation of water molecules, resulting in the release of more OH^- ions and the absorption of H^+ ions. Consequently, both the pH and DO of the water increase (Lin et al., 2020; Mghaiouini et al., 2020).

Additionally, in the current study, the oxidation-reduction potential (E_h) decreased over time during exposure to the magnetic field.

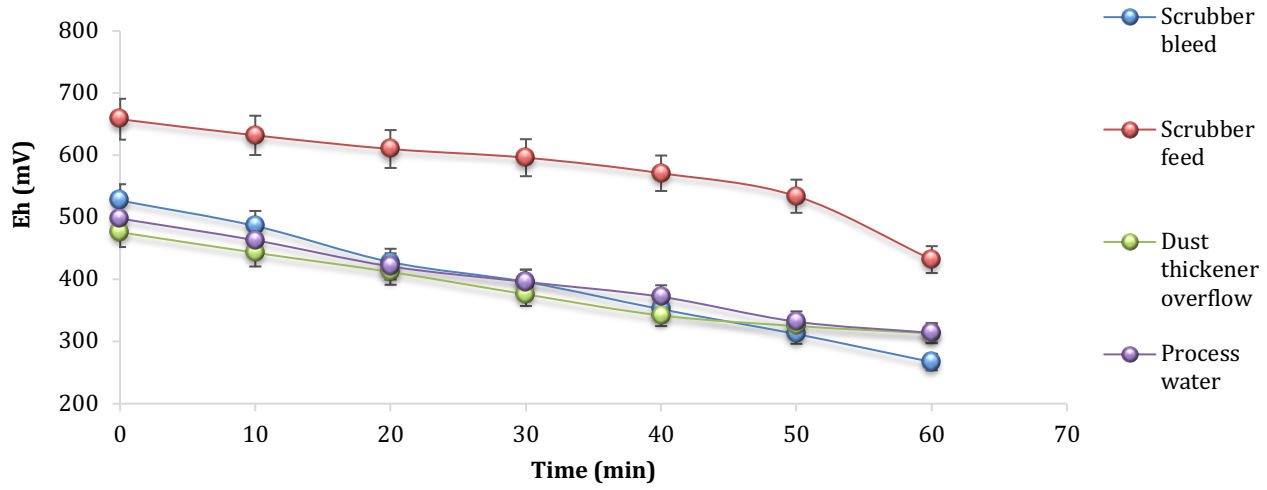


Figure 7. 8 Effect of MTD on E_h for all four water samples

The observations made in this study align with findings from the literature, where a perpendicular flow of water through a magnetic device resulted in an increase in pH and DO, while E_h decreased (McMahon, 2009; Yap et al., 2021). This concept is primarily derived from the theory of an electric motor, which explains that when a current passes through a wire coil in a magnetic field, it generates torque, leading to the movement of the coil. This movement, in turn, generates electricity through the flow of electrons. The reverse electric motor principle describes the opposite process, where electricity is utilized to generate torque (Kramer, 2012). When applied to water magnetization, the parameters described in Equations 7.2 and 7.3 exhibit the following characteristics:

$$H_2O \rightarrow H^+ + OH^- \quad [7.2]$$

$$4\ OH^- \rightarrow 2\ H_2O + O_2 + 4e^- \quad [7.3]$$

According to Equation 7.2 (Dasmeh, 2009; Le Chatelier, 1884; Perlt et al., 2017), under equilibrium, water molecules can ionize, forming H^+ and OH^- ions.

The process can be summarized as follows:

1. When water flows perpendicular to a magnetic field, it mechanically disturbs the field, resulting in the creation of a current.
2. The induced current facilitates the flow of electrons.
3. The electrons combine with H^+ ions, leading to the formation of ionized water molecules with metastable bonds.
4. The chemical balance is disrupted when there is an excess of OH^- ions, causing the pH to rise. To restore equilibrium, Le Chatelier's principle suggests that the excess OH^- ions undergo oxidation, resulting in the formation of O_2, H_2O, and an electron (Equation 7.3).
5. The presence of electrons in water can be measured through the Eh (redox potential) measurement. A decrease in Eh indicates an increase in electron density in the water.

This understanding of the magnetic effect on water and its chemical equilibrium is supported by findings from Dasmeh (2009) and Perlt et al (2017). Both studies provided substantial evidence that magnetic fields can significantly influence the properties of water and its chemical equilibrium. Dasmeh's research (2009) emphasized the structural and ionic behaviour changes in water due to magnetic fields, while Perlt et al (2017) expanded on these findings using molecular dynamics simulations to show how magnetic fields can alter thermodynamic properties and reaction kinetics. These studies collectively suggest that magnetic fields have the potential to be used in various practical applications to enhance chemical processes and water treatment methods.

Figure 7.9 illustrates the percent change in $[Ca^{2+}]$, DO, pH, E_h, and EC for the scrubber bleed sample with and without the MTD. The graph clearly demonstrates that the MTD has an impact on these water parameters, whereas the absence of the MTD shows minimal changes. It is worth noting that the only parameter that exhibited a slight variation in the absence of the MTD was

DO. This slight increase in DO can be attributed to the turbulence in the water flow, which enhances the oxygen transfer rate and consequently elevates the oxygen levels.

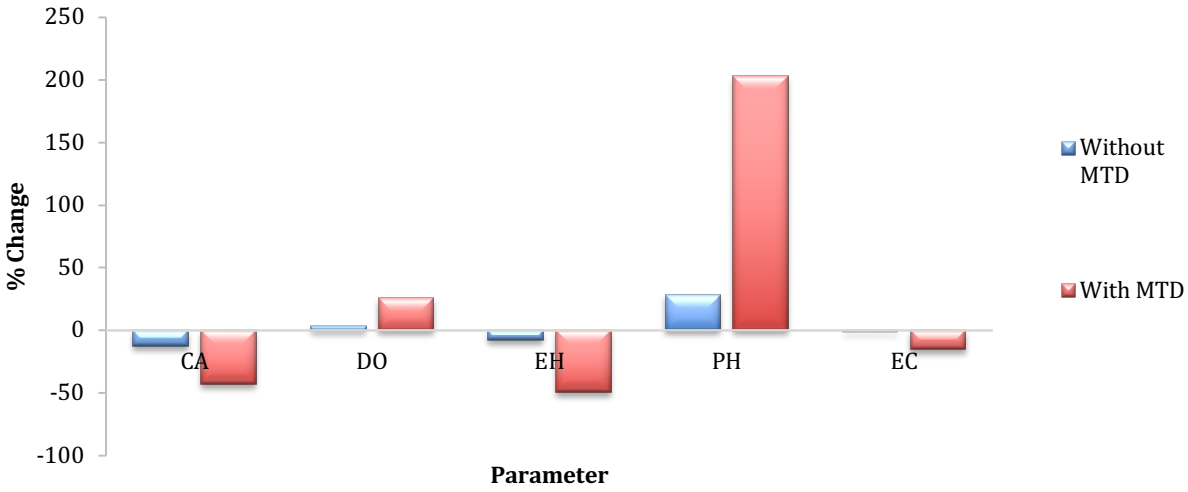


Figure 7. 9 Percent change of [Ca^{2+}], DO, E_h pH and EC without and with an MTD

7.2.3 Influence of the magnetic strength variation on hard water

7.2.3.1 Effect of number of magnets/ length of MTD on calcium concentration

By altering the number of permanent magnets, the effective magnetic field strength was modified from 1.3 T (with 10 magnets) to 0.4 T (with 2 magnets). As anticipated, this adjustment had an impact on [Ca^{2+}], as a consistent decrease in ionic concentration was observed with an increasing number of magnets for both water samples. As discussed in section 2.8.3, the change in the [Ca^{2+}] with varying numbers of magnets and magnetic field strength can be attributed to the phenomenon of magnetic field-induced precipitation or aggregation. When the magnetic field is stronger, it can influence the behaviour of charged particles like calcium ions in the water (Alimi et al., 2015; Coey and Cass, 2000; Mosin and Ignatov, 2015a; 2015b). The increased magnetic field strength might facilitate the formation of clusters or aggregates of calcium ions, leading to their reduced concentration in the solution. This phenomenon could be due to the magnetic forces affecting the interactions between ions, causing them to come together and form solid particles more quickly. As a result, the presence of more magnets and a stronger magnetic field might accelerate the removal of Ca ions from

the solution through precipitation or aggregation, leading to the observed decrease in [Ca^{2+}] (Alimi et al., 2015; Coey and Cass, 2000; Mosin and Ignatov, 2015a; 2015b).

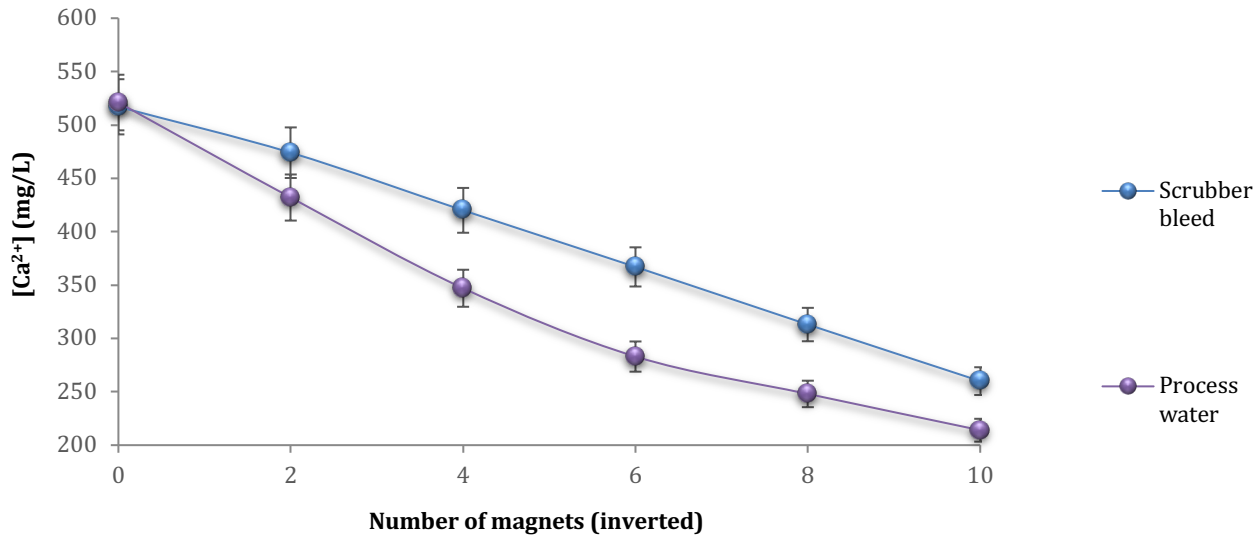


Figure 7. 10 Relationship between number of magnets/ effective magnetic strength and [Ca^{2+}]

7.2.3.2 Effect of magnetic pole orientation on calcium concentration (inverted vs, non-inverted arrangement)

These tests were conducted to examine and compare the influence of magnetic field strength when the magnetic poles were inverted. The following graphs illustrate the impact of magnetic field strength on the scrubber bleed and process water samples, considering both inverted and non-inverted poles.

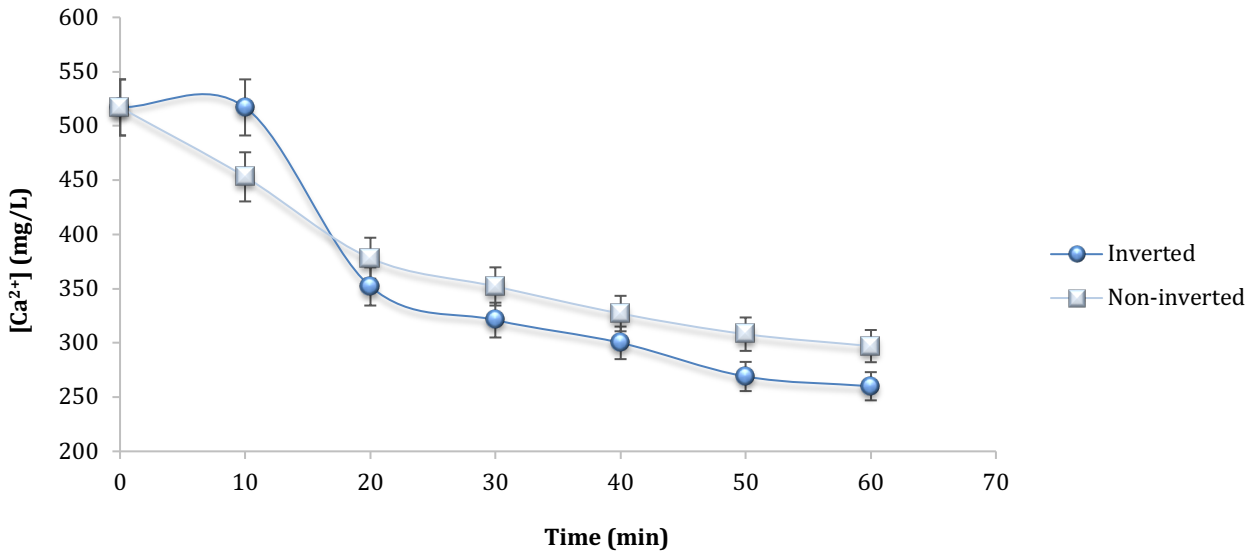


Figure 7. 11 Inverted vs non-inverted magnetic poles and the effect on [Ca^{2+}] of the scrubber bleed sample

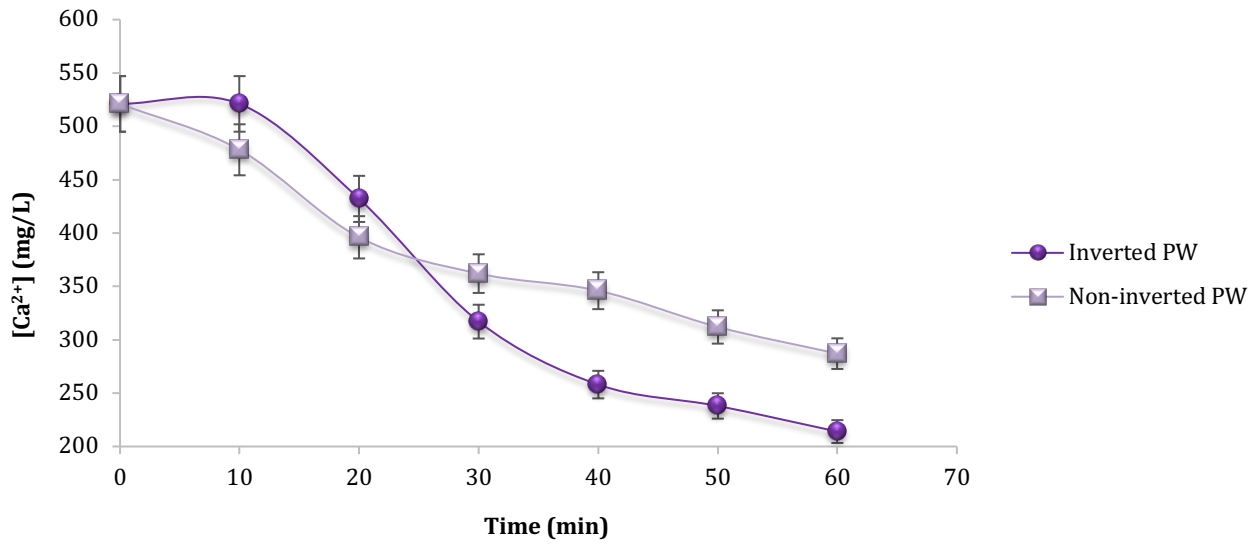


Figure 7. 12 Inverted vs non-inverted magnetic poles and the effect on [Ca^{2+}] of the process water sample

Moreover, it should be noted that magnets with inverted and non-inverted configurations exhibit distinct magnetic field waveforms. Figure 7.13 demonstrates that the non-inverted configuration produces a more homogeneous waveform compared to the inverted configuration.

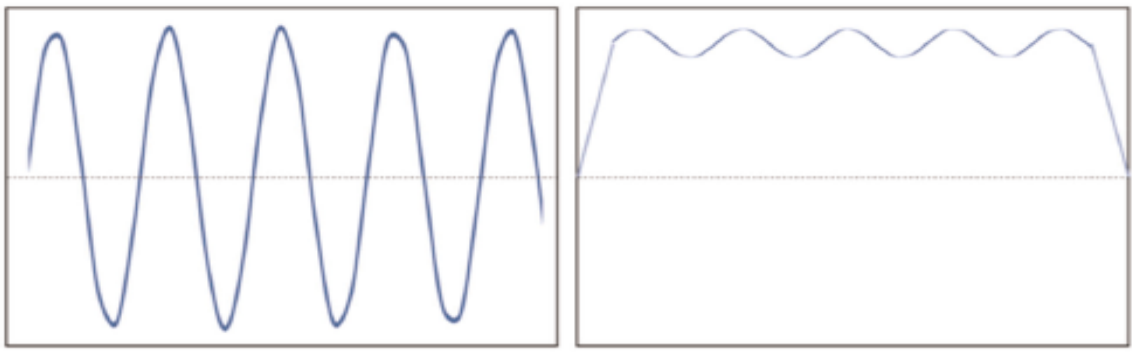


Figure 7. 13 Schematic representation of waveforms for inverted (left) and non-inverted (right) magnetic pole orientation for MTD (Redrawn from Gabrielli et al (2001))

The inverted configuration exhibited a greater reduction in Ca compared to the non-inverted configuration. This observation can be attributed to the constant variation in magnetic field strength (flux) associated with the inverted configuration, whereas the non-inverted configuration maintained a uniform and steady magnetic field. In the inverted configuration, the magnetic field strength, often referred to as magnetic flux, experiences continuous fluctuations due to the inherent geometry and arrangement of the setup. This fluctuating magnetic field has the potential to induce dynamic changes in the movement and behaviour of charged particles, including ions like Ca, within the solution being treated. These dynamic changes can lead to enhanced interactions between the magnetic field and the ions, resulting in a more efficient removal of calcium (Gabrielli et al., 2001; Mazaheri-Tehrani and Faiz, 2022; Sohaili et al., 2016). On the other hand, the non-inverted configuration maintains a uniform and steady magnetic field throughout the treatment process. This consistent field strength creates a relatively stable environment, which can affect how ions respond to the magnetic field. While the non-inverted configuration still induces interactions between the magnetic field and ions, these interactions might be less intense and variable compared to the inverted configuration (Gabrielli et al., 2001; Mazaheri-Tehrani and Faiz, 2022; Sohaili et al., 2016). As a result, the reduction in calcium might be less pronounced in the non-inverted setup.

7.2.3.3. The combined effect of magnetic pole orientation and number of magnets on calcium concentration (inverted vs. non-inverted arrangement)

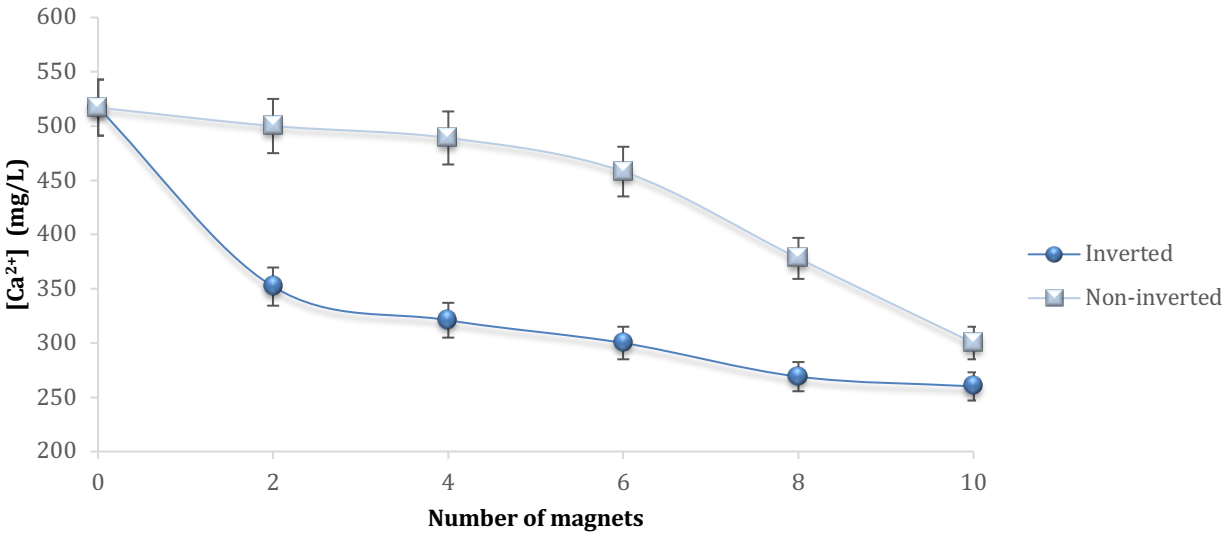


Figure 7. 14 Variation of $[Ca^{2+}]$ against the number of magnets and orientation of magnetic poles for the scrubber bleed sample

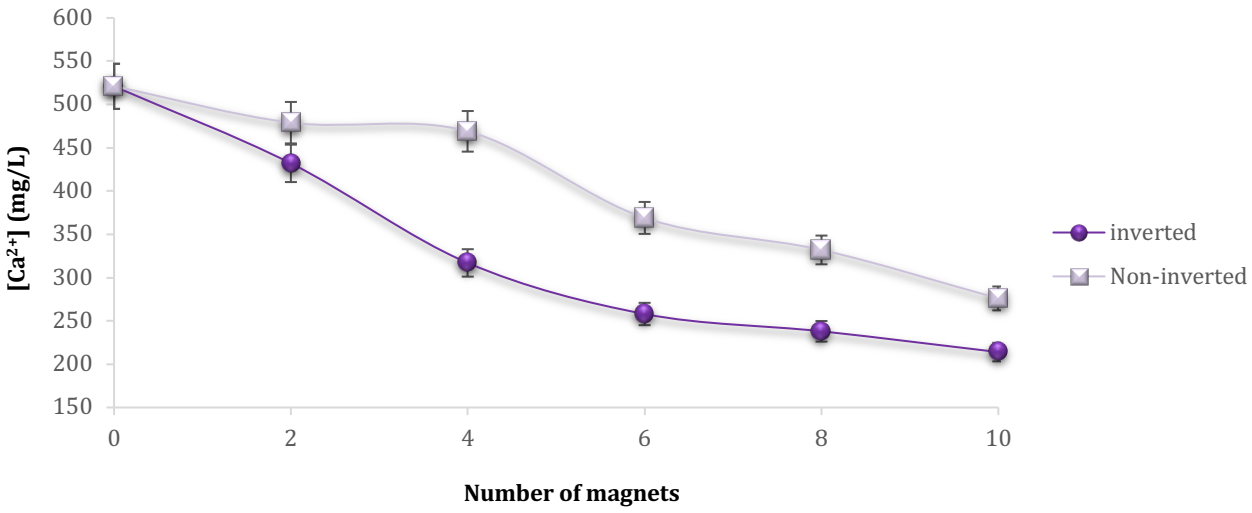


Figure 7. 15 Variation of $[Ca^{2+}]$ against the number of magnets and orientation of magnetic poles for the process water sample

The combined effect of the number of magnets and their orientation validated the findings and conclusions of the previous individual tests in Sections 7.3.2.1 and 7.3.2.2, respectively In both

samples, a higher number of magnets in the inverted orientation resulted in the highest efficiency in terms of Ca removal. These results differed from the findings of Alabi et al. (2015), who suggested that an effective MTD requires a uniform magnetic field (non-inverted). However, they aligned with the findings of Gabrielli et al (2001), Figure 7.16, who observed that the curve representing Ca removal with inversion was shifted by the same amount compared to the curve without inversion. When the orientation of 10 pairs of magnets was flipped, the efficiency dropped from 50 % to 35 %.

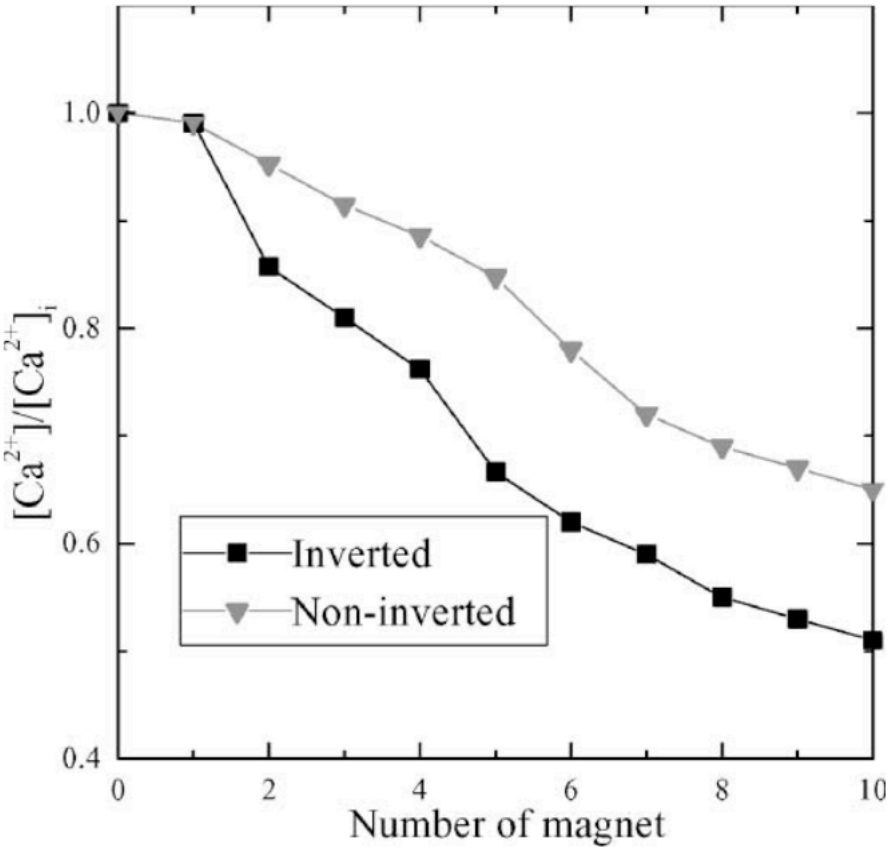


Figure 7. 16 Variation of the concentration of the ionic calcium against the length of the magnetic device obtained by varying the number of inverted or non-inverted pairs of permanent magnets (Gabrielli et al., 2001).

By utilizing 10 pairs of magnets, the MTD efficiency decreased from 50 % with inverted pairs to 42 % without inversion in this present study.

7.2.4 The influence of flow rate on calcium concentration in MTD.

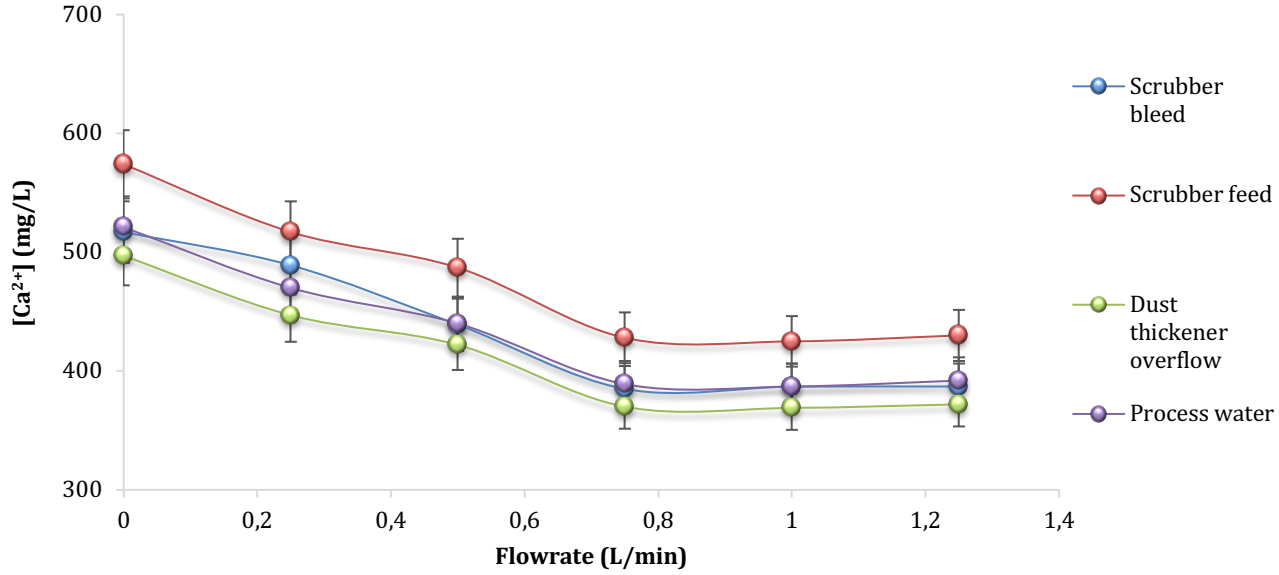


Figure 7. 17 Effect of flowrate on the MTD removal efficiency

By increasing the initial flowrate from 0.25 L/min to 0.5, 0.75, and 1 L/min, the removal of Ca from the solution also increased as seen in Figure 7.17. The highest removal was observed at a flowrate of 0.75 L/min, after which the Ca concentration started to gradually increase. These findings suggest that the magnetization effect is more pronounced at mid flow rates for this MTD. At this flow rate, the MTD may be more effective as a balance between retention time, magnetic field strength, and water turbulence is struck, allowing for optimal interaction between the magnetic field and calcium ions. Thus, these results indicate that optimum flow rates for a specific MTD must be established to enhance the exposure time of water to the magnetic effect, leading to an overall improvement in the efficiency of Ca removal (Othman et al., 2019, Sohaili, 2016).

7.2.5 The influence of pipe material of a MTD on calcium concentration

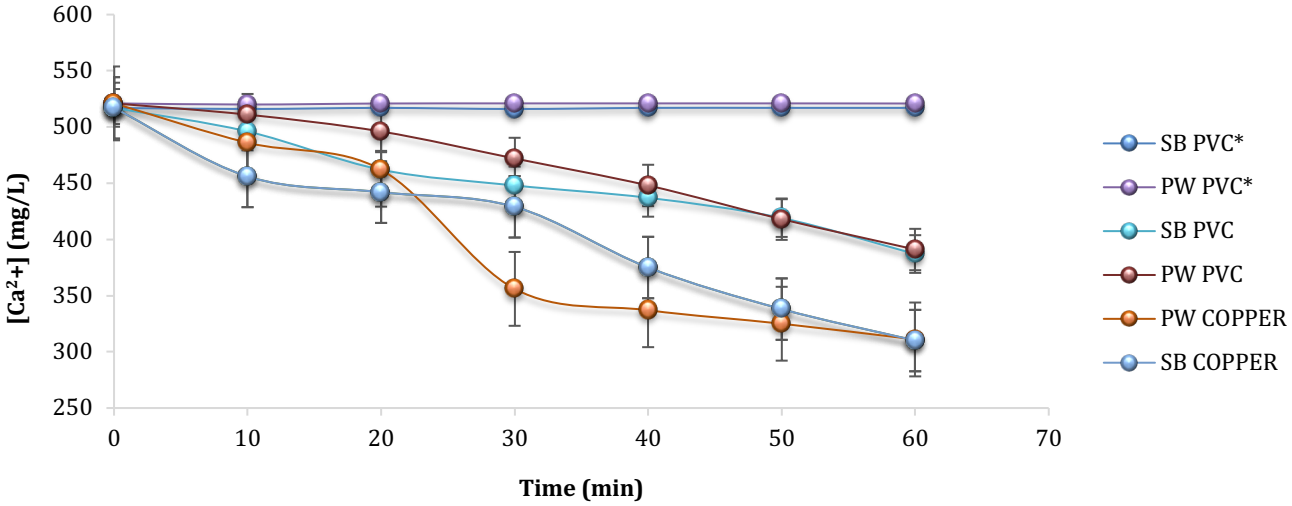


Figure 7. 18 Variation of [Ca^{2+}] against the pipe material of the MTD

To assess the impact of different pipe materials on the efficiency of the MTD, an investigation was conducted using various insulating and conducting materials. The objective was to understand how the choice of pipe material affects the magnetic field and subsequently the performance of the MTD. The materials tested included two types of polyvinyl chloride (PVC): a rigid white form (referred to as PVC*) and a flexible clear tubing (PVC), as well as copper. These materials were selected to represent different electrical conductivity properties. The results, as shown in Figure 7.18, revealed distinct variations in the MTD efficiency depending on the pipe material used. Copper exhibited the highest efficiency, followed by the clear PVC. This can be attributed to the high electrical conductivity of copper, allowing for better transmission of the magnetic field throughout the pipe as also observed in the work of Gabrielli et al (2001). As a result, the magnetic effect on the water passing through the copper pipe was maximized, leading to significant removal of calcium ions. On the other hand, the white rigid PVC* demonstrated no noticeable change in the concentration of Ca. This lack of effect can be attributed to the insulating properties of PVC*, which hindered the passage of the magnetic field. Consequently, the magnetic treatment was unable to induce significant changes in the water composition. Furthermore, the galvanized steel pipe exhibited the highest efficiency among the tested materials, as observed in previous findings (Figure 7.3). The galvanized steel

pipe allowed for better magnetic field transmission compared to PVC*, resulting in effective removal of Ca ions from the water.

These observations indicate that the effectiveness of the MTD is strongly influenced by the electrical conductivity properties of the pipe material. Conducting materials such as copper and galvanized steel enable better propagation of the magnetic field, facilitating enhanced interactions with water molecules and resulting in improved removal of Ca ions. In contrast, insulating materials like PVC* limit the transmission of the magnetic field, hindering its impact on the water composition. These findings emphasize the importance of selecting appropriate pipe materials to optimize the performance of the MTD. Conducting materials with higher electrical conductivity can facilitate a stronger magnetic effect, leading to more efficient removal of undesirable ions from the water.

7.2.6 The effect of MTD on the scale produced

The MTD experiments yielded consistent results with the previous test work in Sections 7.2.2 to 7.2.5, as evidenced by the parameters observed and depicted in Figures 7.19 to 7.21. The X-ray diffraction (XRD) analysis was performed to determine the relative abundance of precipitates formed during the experiments, and the results are presented in Tables 7.1 and 7.2.

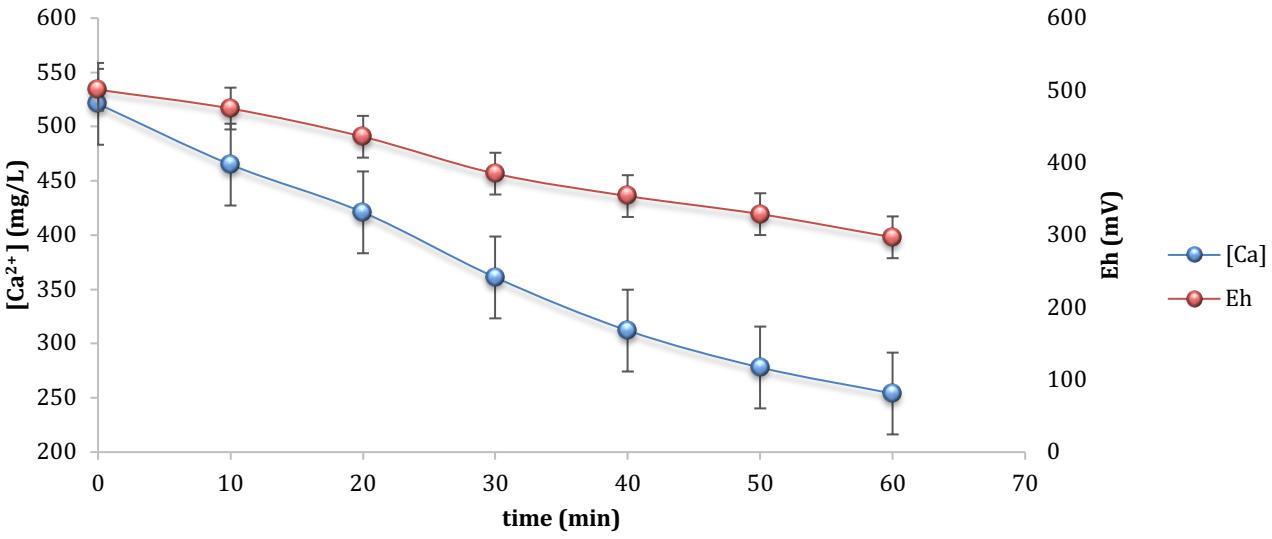


Figure 7. 19 [Ca^{2+}] and E_h as a function of time

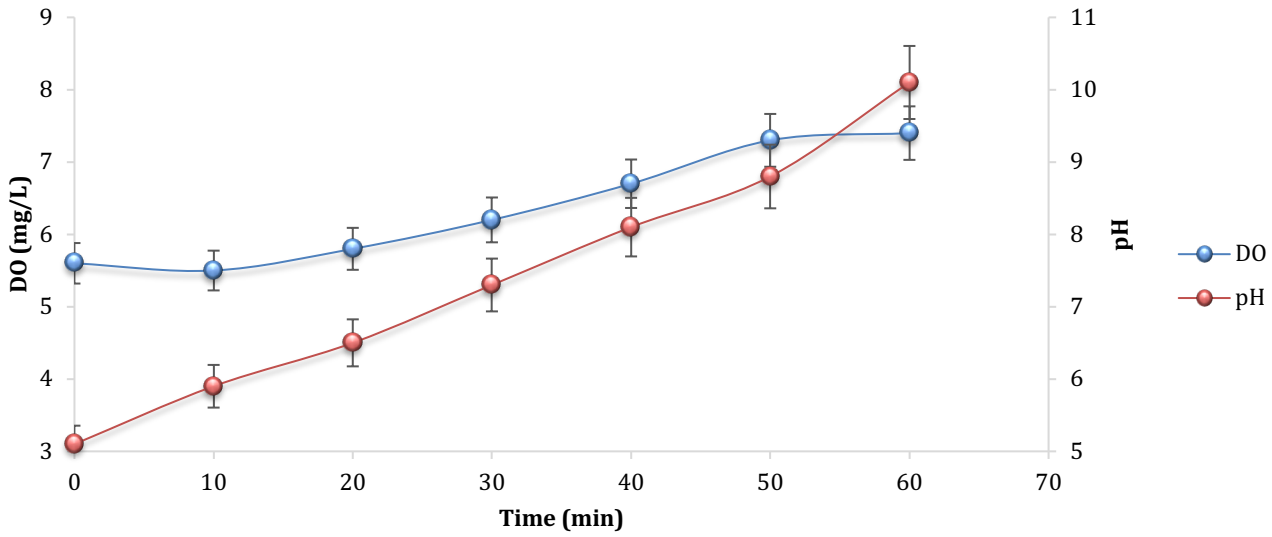


Figure 7. 20 DO and pH as a function of time

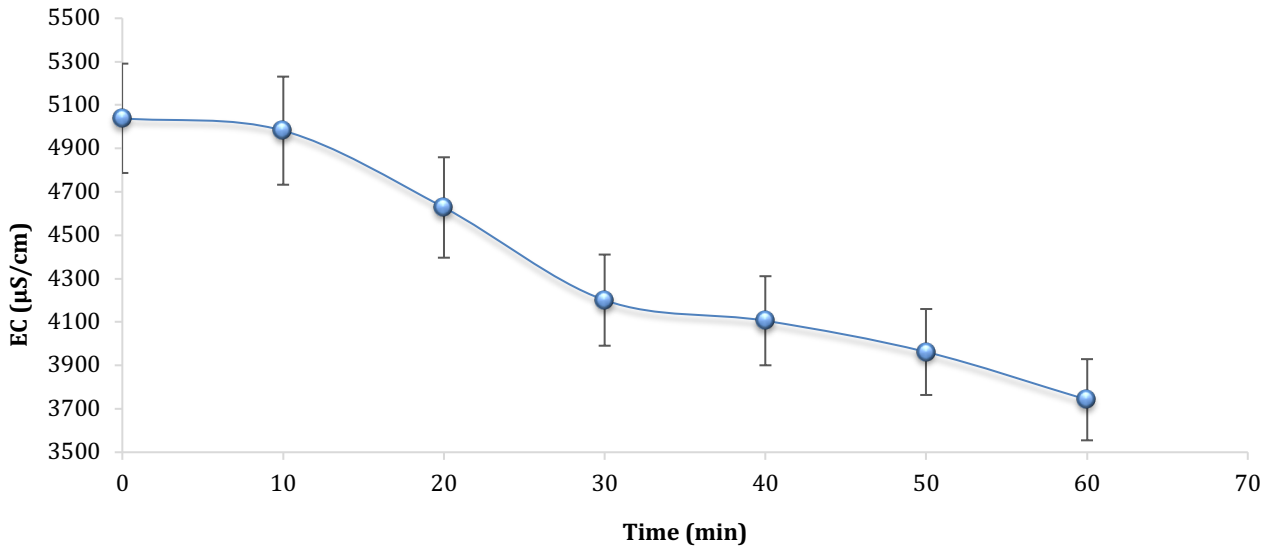


Figure 7. 21 EC as a function of time

Table 7. 1 X-ray diffraction average results (Relative Abundance) after 60 minutes exposure to the MTD.

Compound name	Formula	Relative abundance
Gypsum	$CaSO_4$	Predominant (> 80% mass)
Calcite	$CaCO_3$	Major (> 15 % mass)
Aragonite	$CaCO_3$	Minor (> 5% mass)

The original scale samples that were analysed using XRD in Chapter 4 only indicated the presence of calcite as the only polymorph present in the sample (i.e. that resulted from untreated hard water). After exposure to the MTD the presence of another polymorph, aragonite, was identified. Although in small quantities (5 %), this presence indicates that the crystal structure of $CaCO_3$ (20 % of the total precipitate) had been changed to some degree- even though the sample was exposed to the MTD for only 60 minutes as noted in Figure 7.22. while there are some studies who claim changes to the morphology of gypsum (Mwaba, 2007), there were no noticeable changes to gypsum in this study except for a slight decrease its intensity.

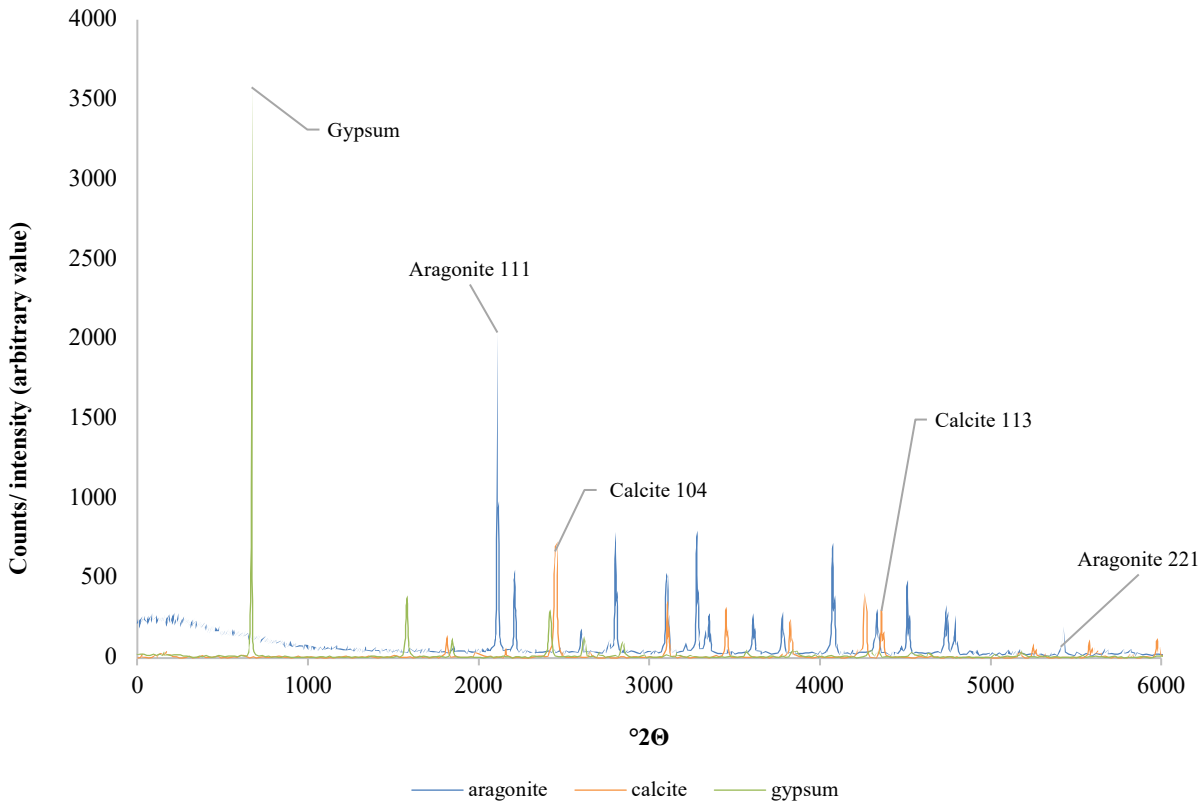


Figure 7. 22 XRD analysis for crystals formed after 60 minutes exposure to MTD

Similar observations were made by Chang and Tai (2010) as well as Sronsri et al., 2020 where it was observed that aragonite seed crystals did not exhibit growth in the absence of magnetization at room temperature. However, these seed crystals demonstrated growth in the presence of a magnetic field. Notably, a magnetic field of greater intensity exhibited its effects within a shorter time frame. The sample was again exposed to the MTD for 3 hours to determine if time was a determining factor in the mass of Aragonite formed. Table 7.2 presents the XRD average results and the relative abundance of the mineral phases that formed.

Table 7. 2 X-ray diffraction average results (Relative Abundance) after a 3-hour exposure to the MTD.

Compound name	Formula	Relative abundance
Gypsum	$CaSO_4$	Predominant (> 80% mass)
Calcite	$CaCO_3$	Minor (> 5 % mass)
Aragonite	$CaCO_3$	Major (> 15% mass)

After subjecting the system to a magnetic field for 3 hours, the crystal exhibited a composition of 5 % calcite and 15 % aragonite (Figure 7.23), indicating a shift towards increased aragonite formation compared to the initial treatment duration of 60 minutes.

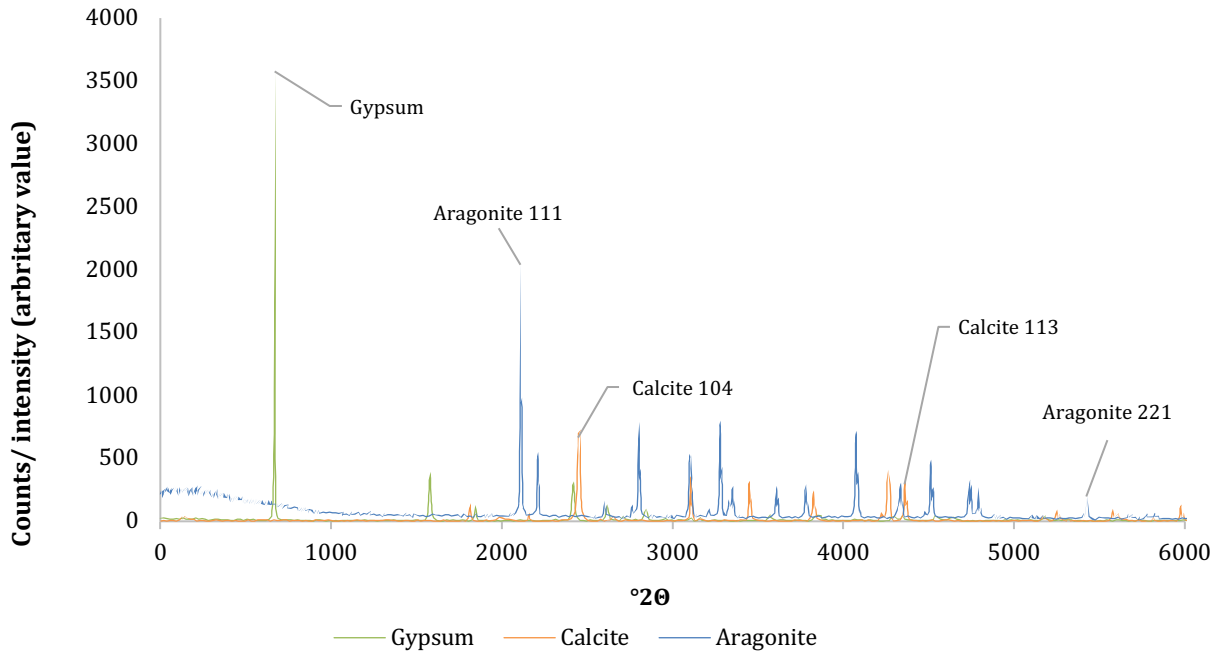


Figure 7. 23 XRD analysis for crystals formed after 3 hours exposure to MTD

It was also noted that no scale was found to have adhered to the insides of the pipe when the solution was removed for analysis.

This result provides evidence that the presence of a magnetic field effectively decreased the formation of calcite within the system. The higher concentration of aragonite in the precipitate may be attributed to the acceleration of the precipitation process induced by the magnetic field as discussed in Chapter 2, Section 2.8.3. The higher aragonite concentration within the precipitate may also be attributed to the catalysing effect of the applied magnetic field, which accelerates the kinetics of the precipitation process. The magnetic field's influence on molecular alignment and intermolecular forces fosters more rapid nucleation and growth of aragonite crystals, leading to its heightened presence in the final precipitate. It is noteworthy that under normal conditions, the formation of scale typically takes several months. However, in this system, the magnetic field facilitated the precipitation of aragonite in less than an hour. This accelerated process favoured the formation of aragonite over time, as aragonite exhibits a faster precipitation rate compared to calcite. The significant reduction in the amount of calcite observed in the precipitate highlights the substantial impact of the magnetic field in suppressing calcite formation. It is important to recognize that calcite is the primary constituent of scale, which is responsible for adhesion to heating and piping surfaces. On the other hand, aragonite, being a softer crystal, remains suspended in the solution and does not adhere to surfaces until

it settles in areas of reduced flow rate. Hence, the decrease in the amount of calcite in the precipitate directly correlates to a reduction in scale formation. This discovery highlights that magnetic fields could be used to prevent the build-up of scale. They can affect how the particles form, making it more likely for a specific type of particle (aragonite) to form instead of another type (calcite)

7.2.7 Proposed Mechanism of MWT

In Chapter 2, sections 2.8.2 and 2.8.3, this study delved into the potential mechanisms underlying the successful application of MWT. Specifically, regarding the formation of $CaCO_3$, the dissolved calcium and carbonate ions in water attract dipolar water molecules, resulting in the formation of a Stem Layer around the ions. This Stem Layer keeps the ions apart, preventing their combination and the subsequent formation of solid calcium carbonate. However, when water molecules flow, their dipolar nature gives rise to an electric current. As this flowing water passes through a magnetic field, the Lorentz effect alters the random orientation of dipolar water molecules, causing them to align in a more ordered manner. This alteration of the Stem Layer structure brings the calcium and carbonate ions closer together, facilitating the formation of nucleation sites for precipitation. Importantly, this precipitation occurs uniformly throughout the bulk of the solution rather than on metal surfaces, favouring the formation of aragonite over calcite. This study concludes that magnetization enhances the rate of precipitation, leading to the preferential formation of aragonite over calcite. This shift in crystal formation is attributed to the increased efficiency of nucleation and the altered conditions brought about by the magnetic field. The magnetic field's influence on the motion and behaviour of water molecules can enhance mass transfer and reaction kinetics. This can accelerate the precipitation process and lead to the preferential formation of aragonite over calcite, which has a faster precipitation rate and less likely to adhere to surfaces. One possible interpretation might be that the observed alteration in crystal morphology, as noted in this study, results in the development of fragile crystals that are prone to breakage and can be easily carried away by fluid flow forces. As noted and detailed by Prywer, (2004), another explanation could involve the surface area on the face of crystals originating from magnetically treated solutions, potentially fostering looser agglomeration tendencies. As a consequence, this could prompt the formation of larger crystals within the bulk solution. These larger crystals may then establish themselves as more favourable or competitive sites for crystal growth compared to the pipe surfaces. Therefore, this phenomenon could potentially lead to a decrease in crystal or

scale formation on heat transfer surfaces. Overall, these insights shed light on the underlying mechanisms through which MWT affects the precipitation of calcium carbonate, highlighting the acceleration of precipitation and the subsequent formation of aragonite as key outcomes of magnetic treatment.

7.3 Summary

Through the MWT test work conducted, several important findings have emerged: Firstly, MWT has demonstrated a notable impact on the physico-chemical properties of hard water, specifically affecting parameters such as pH, DO, EC, ion concentration, and E_h. Furthermore, the study identified specific factors that influence the MWT process, such as the number of magnets employed, magnetic orientation, flow rate, and the material of the pipe in the MTD setup. These parameters were found to be crucial in determining the effectiveness of MWT for different water types. The review of existing literature on magnetic force treatment of water and aqueous solutions, particularly in the context of hard scale prevention, reveals an ongoing lack of a consistent theory regarding the mechanism of action. However, recent publications within the past decade have advanced our understanding of the field's influence on water structure, primarily through changes in hydrogen bonding induced by the Lorentz force. One notable result from the study is the rapid formation of aragonite, a less common form of calcium carbonate, under conditions that would typically favour the formation of calcite. This unexpected outcome highlights the role of MWT in altering the precipitation process and influencing the crystal polymorph formed. The formation of aragonite, a softer crystal that does not readily adhere to surfaces, can contribute to the inhibition of scale formation. The reduced presence of calcite in the precipitate suggests a lower propensity for scale adhesion on heating and piping surfaces. It is worth noting, based on previous literature, that aragonite may eventually convert to calcite over time, as calcite is the more stable polymorph. Therefore, further investigation is necessary to determine the timescale required for this conversion to occur. Additionally, understanding the "memory effect" of magnetic treatment is crucial, as it pertains to the long-term effectiveness of magnetically treated water in preventing scale build-up even after the magnetic field has been switched off. This can provide insights into the lasting impact of MWT and its potential as a sustainable solution.

In summary, there is no denying the effectiveness of MWT. However, to gain wider acceptance and utilization of MWT, it is essential to deepen the understanding of the underlying mechanisms at play. The tests conducted on MWT in this study have offered insights into how

magnetic treatment impacts water properties, particularly by promoting the formation of aragonite over calcite and the need for further investigation into conversion rates and the possible persistence of MWT's preventive effects.

7.4 References

Alabi, A., Chiesa, M., Garlisi, C. and Palmisano, G., 2015. Advances in antiscale magnetic water treatment. Environmental Science: Water Research & Technology, 1(4), pp.408-425.

Chang, M.C. and Tai, C.Y., 2010. Effect of the magnetic field on the growth rate of aragonite and the precipitation of $CaCO_3$. Chemical Engineering Journal, 164(1), pp.1-9.

Dasmeh P, Searles DJ, Ajloo D, Evans DJ, Williams SR., 2009. On violations of Le Chatelier's principle for a temperature change in small systems observed for short times. J Chem Phys.; 131:214503.

Gabrielli C, Jaouhari R, Maurin G, Keddam M., 2001. Magnetic water treatment for scale prevention. Water Res.; 35:3249–59.

Klempner G, Kerszenbaum I., 2008. Handbook of large turbo-generator operation and maintenance. Hoboken: Wiley.

Kramer M., 2012. The DC motor. http://large.stanford.edu/courses/2012/ph24 0/kramer2/. Accessed 24 Oct 2022.

Le Chatelier H.L, 1884. On a general statement of the laws of chemical equilibrium. C R Acad Sci Paris.; 99:786–9 [in French].

Lin, L., Jiang, W., Xu, X. and Xu, P., 2020. A critical review of the application of electromagnetic fields for scaling control in water systems: mechanisms, characterization, and operation. NPJ Clean Water, 3(1), p.25.

Mazaheri-Tehrani, E. and Faiz, J., 2022. Airgap and stray magnetic flux monitoring techniques for fault diagnosis of electrical machines: An overview. IET Electric Power Applications, 16(3), pp.277-299.

McMahon, C.A., 2009. Investigation of the quality of water treated by magnetic fields.

Mghaiouini, R., Elmlouky, A., Salah, M., Al-Antary, T.M., Monkade, M., El Bouari, A. and Ghidan, A.Y., 2020. Effect of electromagnetic fields on the ph of water under kinetic conditions. Fresenius Environmental Bulletin, 29, pp.7922-7933.

Mwaba, M.G., Gu, J. and Golriz, M.R., 2007. Effect of magnetic field on calcium sulphate crystal morphology. Journal of crystal growth, 303(2), pp.381-386.

Othman, A., Sohaili, J. and Supian, N.S., 2019. A Review: Methodologies Review of Magnetic Water Treatment As Green Approach of Water Pipeline System. Pertanika Journal of Science & Technology, 27(1).

Perlt E, von Domaros M, Kirchner B, Ludwig R, Weinhold F., 2017. Predicting the ionic product of water. Sci Rep-UK.; 7:10244.

Prywer, J., 2004. Explanation of some peculiarities of crystal morphology deduced from the BFDH law. Journal of crystal growth, 270(3-4), pp.699-710.

Sohaili, J., Shi, H.S., Zardari, N.H., Ahmad, N. and Muniyandi, S.K., 2016. Removal of scale deposition on pipe walls by using magnetic field treatment and the effects of magnetic strength. Journal of Cleaner Production, 139, pp.1393-1399.

Sronsri, C., Kongpop, U. and Sittipol, W., 2020. Quantitative analysis of calcium carbonate formation in magnetized water. Materials Chemistry and Physics, 245, p.122735.

Taylor, M., Elliott, H.A. and Navitsky, L.O., 2018. Relationship between total dissolved solids and electrical conductivity in Marcellus hydraulic fracturing fluids. Water Science and Technology, 77(8), pp.1998-2004.

Chapter 8 The proposed conceptual water treatment process and the techno-economic evaluation

8.1 Proposed conceptual water treatment process

From the results obtained in Chapter 6, the combined use of lime-soda ash and ion exchange proved beneficial in the removal of hardness. In this regard, the potential full-scale installation of a lime-soda and ion-exchange treatment process was investigated. For the initial levels of hardness present in the samples presented in this study, this proposed water treatment process including an alternative gypsum crystallization stream (part of SAVMIN process (van Niekerk, 2002)) is presented in Figure 8.1

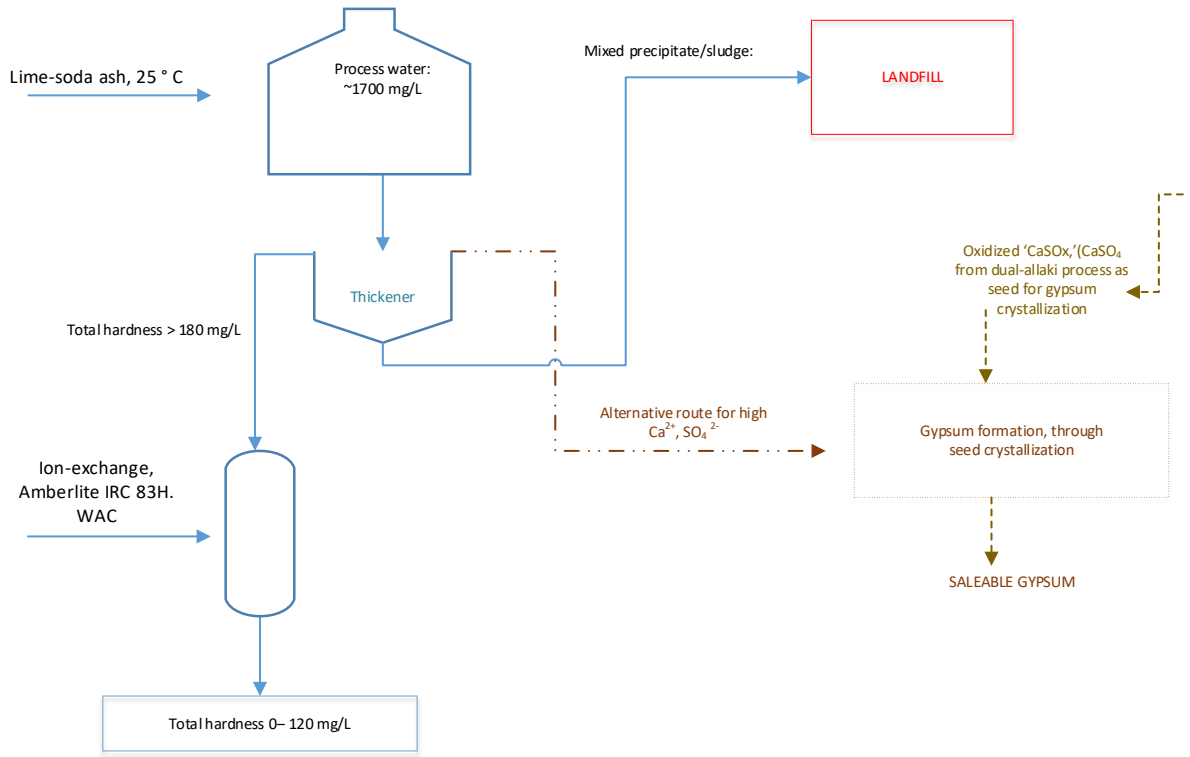


Figure 8. 1 Proposed flowsheet for the water softening process

8.1.1 General process description

- Phase 1 will include the addition of lime and soda ash to the sample in the neutralization reactor, allowing enough time for precipitation of hardness material to occur (according to equations 3.6—3.8). The mixed precipitate that forms, while mostly made up of calcium compounds (as noted in the XRD analyses), may also include some heavy

metals such as Fe, Ni and Mn (depending on the initial concentration). The precipitate is removed through a thickener/settler and sent to a landfill. The resulting effluent/overflow should have a residual total hardness of 120—180 mg/L. This effluent is still high in sulphate concentration, which was marginally reduced through precipitation of sulphate compounds including gypsum.

- Phase 2 involves the application of a weak acid cation resin to the water sample (effluent) pre-treated with lime and soda ash. By ensuring that optimal operating parameters are applied for the correct scale (as determined in Chapter 6), hardness removals of more than 80 % can be achieved resulting in a residual total hardness of 0-120 mg/L.
- Phase 2*: Alternative stream:* The work of van Niekerk (2002) on the SAVMIN process confirmed that neutralisation and heavy metal removal of acid mine water was achieved by high lime treatment. The initial addition of lime may causes the solution phase to become supersaturated with gypsum, due to the high concentration of sulphates that may be already present in the feed water, as this study. The solution is contacted with gypsum crystals in order to provide active surfaces of gypsum, which acts as a catalyst for the precipitation of the 'supersaturated' gypsum (Damons, 2001). The formation of gypsum is described by the following stoichiometric reaction:

  $$Ca^{2+} + SO_4^{2-} \rightarrow CaSO_4.2H_2O \qquad [8.1]$$

  While not part of the scope of the present study, this alternative route may prove beneficial in terms of value recovery through the formation of a saleable product. There is a market for high quality gypsum in the cement industry in South Africa (Greyling and Rooy, 2019; Sithole et al., 2023) where it is indispensably used as a retarding agent. This is one alternative that Sibanye-Stillwater is looking into (Bezuidenhout et al., 2012) especially with mounting pressure under the current regulations on Waste Classification and Management (Act 59 of 2008; amended in 2014, act 26). This regulation “Minimum Requirements for Waste Disposal by Landfill” (Second edition, 1998) deals with the standards and assessment of waste for landfill disposal.
- In addition, Sibanye-Stillwater currently has no available option for disposing of the waste from the dual-alkali plant other than to dump it in a hazardous landfill site. The waste produced is a combination of $CaSO_3$ and $CaSO_4$ called ‘CaSOx’. If dewatered sufficiently and $CaSO_3$ is oxidised fully to $CaSO_4$ (Bezuidenhout et al., 2012), this ‘waste’ may curb some costs in the partial SAVMIN process if it is used as the seed

material required for alternative gypsum crystallization section.

8.2 The techno-economic evaluation of the proposed water treatment process

A techno-economic evaluation of an existing or proposed treatment process at Sibanye-Stillwater can provide significant value by assessing both its technical and economic viability. This analysis helps in identifying cost-saving opportunities, optimizing resource allocation, improving efficiency, and supporting strategic decision-making to enhance profitability and sustainability. In this investigation, the feasibility of implementing a treatment method using lime and soda ash followed by ion exchange was assessed, based on the results obtained from Chapter 6. Additionally, an alternative treatment process involving gypsum crystallization for the high calcium and sulphate solution resulting from the lime and soda ash treatment was explored. The SAVMIN process, which incorporates lime treatment and gypsum crystallization, had been comprehensively evaluated by Van Niekerk in 2002 for treating 5 ML per day of acid mine drainage. The economic evaluation in the present study closely followed Van Niekerk's methodology by estimating costs based on his work. For this study, an estimated 10 ML of process water per day was evaluated to determine the feasibility and cost-effectiveness of the proposed treatment methods.

8.2.1 Lime- soda softening evaluation

8.2.1.1 Lime and soda ash make–up and dosing

Hydrated lime and soda ash are readily available at Sibanye-Stillwater. The lime is received as a fine powder in road tankers and transferred to a storage silo. The lime is currently directly added to the first-stage reactor of the dual-alkali system using a screw feeder. Similarly, for the proposed water treatment plant, a screw feeder will control the lime addition into neutralisation reactor for metal precipitation and the addition can be controlled by a pH meter situated in the reactor. Soda ash is also received in fine powder form by road tankers and transferred to a storage silo. It is currently used for the sodium requirements in the dual-alkali as an absorber for SO_2. Soda ash addition can be made to the reactor based on the stoichiometric dosages required for the Process water to be treated.

According to the required lime and soda ash dosage calculation procedure outlined by Minnesota Rural Water Association (2009) (Chapter 3), as well as the lime-soda ash softening test work outlined in section 4.2, the average lime consumption to raise the pH to above pH 11.0 was 1000 mg/l. The required hydrated lime and soda ash dosage is:

- $Ca(OH)_2$ = 1000 mg/l

  = 1.0 kg/m^3 of process water
- Na_2CO_3 = 1990 mg/L ~ 2000 mg/L

  = 2 kg/m^3 of process water

8.2.1.2 Process Design Criteria

8.2.1.2.1 Neutralisation Reactor and Thickener/Settler

The process design criteria for the installation of a Neutralisation Reactor and Settler of a lime-soda treatment process (followed by an alternative gypsum crystallization process) is presented in Table 8.1 based on Van Niekerk's (2002) estimation. The design calculations for the reactor and settler are presented in Appendix 4.

The neutralisation reactor was designed for the following duties (Van Niekerk, 2002):

- Retention time = 30 minutes
- Mixing intensity = 70 watts per cubic meter (W/m^3)

The neutralisation settler was designed for the following hydraulic and solids loading:

- Upflow rate = 0.7 m/hr
- Solids loading rate = 80 kg suspended solids per square meter per hour (SS/m^2/hr)

Table 8. 1 Process design criteria for the Neutralisation Reactor and Thickener/Settler.

Neutralisation Reactor		
Number of reactors		*2*
Average working days per month	Days	30
Total volume of process water for treatment	ML/day	10
	m^3/s	0.12
Retention time	minutes	30
Volume of each reactor	m^3	90
Mixing intensity	W/m^3	0.70
Lime dosing rate	Kg/m^3 process water	1
	Kg/s	0.12
	ton/month	300
Soda ash dosing rate	Kg/m^3 process water	2
	Kg/s	0.12
	ton/month	600
Operating temperature	°C	25
Thickener/Settler		
Number of thickeners		1
volumetric flowrate	m^3/s	0.12
Upflow rate	m/hr	0.7
Solids loading rate	Kg/m^3hr	80
Retention time	minutes	30
Volume of settler	m^3	180
Thickener underflow density	SG	1.45

8.2.1.3 Capital expenditure (CAPEX) estimate

The economic evaluation undertaken by van Niekerk (2002) estimated the CAPEX of a 20 ML/day lime and gypsum treatment facility focusing on the following disciplines:

- Mechanical Equipment
- Civil Engineering
- Structural Steel
- Piping & Valves
- Electrical & Instrumentation
- Installation
- Transport
- Commissioning

The summary of the CAPEX estimation study is provided in Table 8.2 for a plant that is anticipated to operate for 10 years. The evaluation carried out by van Niekerk in 2002 was adjusted for inflation of approximately 6 % per year, based on data from Sinnot (2005) and the South African Reserve Bank's Monetary Policy (2020), to calculate the current study's capital and operational expenses for a throughput of 10 ML/day.

Table 8. 2 The Capital expenditure for a lime-soda ash treatment and alternative gypsum crystallization stream.

Lime soda ash treatment and alternative gypsum crystallisation: 10 Ml/day						
Description	**Mechanical**	**Civil**	**Electrical**	**Instruments**	**Other**	**Total**
Lime storage	R6 109 214	R3 052 246				
Neutralisation reactor and thickener	R869 591	R5 864 943				
Interconnecting pipework		R46 8822				
Electrical equipment			R4 557 093			
Instrumentation and controls				R307 516		
Transportation costs					R195 6947	
Commissioning					R947 344	
TOTAL ZAR	**R6 978 805**	**R8 917 189**	**R4 557 093**	**R307 516**	**R2 904 291**	**R23 664 894**
TOTAL USD						**$15 776 326**

8.2.1.4 Monthly operating costs (OPEX)

The monthly operating expenditure (OPEX) estimation followed the evaluation done in reference to the lime treatment pilot plant by van Niekerk (2002). An inflation of ~ 6% per annum (Sinnot, 2005; South African Reserve Bank, Monetary Policy 2020) was applied to the evaluation done by van Niekerk (2002) to estimate the current study's operating costs. Chemical usage, electrical power consumption, the necessary operating personnel and labour as well as an average of 30 operational days per month were all taken into account when calculating the operating costs. The unit costs for chemicals and electricity were based on pricing indices as of February 2023, as reported by Alibaba.com (2023) and GlobalPetrolPrices.com (2023) and an average 15 ZAR/USD based on the operational cost for the treatment of 10 ML/day was approximated. Based on Van Niekerk's estimations (2002) the amount of necessary machinery and equipment were also scaled up from 5 ML/day to 10 ML/day for the current study's potential operating costs.

Table 8. 3 Monthly reagent costs.

Reagent	Dosage (kg/m^3 process water)	Unit Cost (USD/kg)	Quantity (kg)	Total (USD)	Total ZAR
Hydrated lime	1	0.122	300 000	36 800	552 000
Soda ash	2	0.42	600 000	504 000	7 560 000
Total Monthly Reagent Costs				**$540 800**	**R8 112 000**

Table 8. 4 Electrical costs.

Equipment Item	Number installed	Unit Cost (USD/kWh)	Monthly Unit Power Requirement (kWh)	Total (USD)	Total (ZAR
Process Water Feed Pumps	3	0.074	12240	2717.28	40 759.2
Neutralisation Reactor Mixers	2	0.074	7920	1,172.16	17582.40
Neutralisation Settler Bridge	1	0.074	720	53.28	799.20
Hydroxide/Gypsum Recycle Pumps	2	0.074	12240	1811.52	24 172.80
Lime Screw Feeder	1	0.074	1440	106.56	1598.40
Lime Slacker Tank Mixer	1	0.074	720	53.28	799.20
Lime Settler Bridge	1	0.074	720	53.28	799.20
Lime Recycle Pumps	1	0.074	2664	197.14	2957.1
Milk of Lime Dosing Pumps	1	0.074	10080	745.92	11 188.8
Total Monthly Power Costs				**$6710.41**	**R100 656.10**

Table 8. 5 Labour costs

Personnel	Number Required	Unit Cost (R//hr)	Monthly Working Hours	Total
Engineer	1	253	160	40 480
Assistants	1	124	240	29 760
Operator	2	62	240	14 880
Labourer	5	62	240	14 880
Total Monthly Labour Costs				**R100 000**
				$6 666.67
Total OPEX Costs ZAR				**R8 312 000**
Total OPEX Costs USD				**$554 0133**

The total monthly operating costs for the lime soda- ash and alternative stream for gypsum crystallization are R8 312 000 and the capital expenditure amounts to R23 664 894.

Considering Sibanye-Stillwater had purchased ~20 ML fresh water for its operations for R200 000 000 in 2017 (~R 300 726 051 in 2023) (Water conservation and water demand management, 2017; Team, 2021), this lime-soda ash cost to soften its current Process Waters is within the assumed budget. The added benefit is that 300 ML can be processed for under R9 000 000 every month.

8.2.2 Ion- exchange softening evaluation using the Amberlite IRC83H (WAC)

The ion exchange operating costs were calculated with the use of *WAVE SOFTWARE* from DuPont™. Typical ion exchange feed will be 100 m^3/h of the pre-treated water from lime-soda ash softening (Chapter 5, Table 5.4). WAC runs effectively around 20 bv/h and will require 5m^3 of resin for 1 column (work on 2 columns; total resin of 10m^3).

- Regeneration takes about 3.5 hours using HCl.
- Each regeneration cycle will use 1500 L of 33 % HCl.
- Estimate regeneration every 20 hours.
- Total chemical requirements is on average 1800 L (33 % HCl) per day.
- Cost of HCl is USD 6/L of 33 % HCl purity
- Cost of resin is USD11/L and 10,000 L need to be replaced every 3 years.
- Cost of electricity is currently USD 0.075/kWh.
- Product will have total hardness between 0—120 mg/L as $CaCO_3$

To calculate the cost of softening water through WAC and the energy costs, we need to consider the resin replacement cost, the operating cost of the resin system, and the energy cost of operating the system.

8.2.2.1 Resin Replacement Cost:

The total cost of resin replacement every 3 years would be:

10 m^3 x USD 11/L = **USD 110,000**

8.2.2.1.1 Operating Cost:

The annual operating cost of the resin system can be calculated as follows:

Resin Usage:

The volume of resin used per year can be calculated as follows:

20 bv/h x 24 hours/day x 365 days/year = **175,200 bed volumes/year**

Chemical Usage:

The total chemical requirements for regeneration per day would be:

1800 L/day x USD 6/L = **USD 10,800/day**

Total Operating Cost:

Therefore, the total annual operating cost of the resin system would be:

(175,200 bed volumes/year x USD1/bed volume) + (USD10,800/day x 365 days/year) = USD 175,200 + USD 3,942,000 = **USD 4,117,200/year**

Energy Cost:

To calculate the energy cost, we need to know the power consumption of the system and the cost of electricity.

Assuming that the WAC system requires 1 kW of power per m^3/h of flow rate, the total power consumption would be:

100 m^3/h x 2 columns x 1 $kW/m^3/h$ = 200 kW

Assuming an energy cost of USD 0.075/kWh, the energy cost per day would be:

200 kW x 24 hours/day x USD 0.075/kWh = **USD 360/day**

Therefore, the total energy cost per year would be:

USD 360/day x 365 days/year = **USD 131,400/year**

Total Cost:

The total cost of softening water through WAC over a three-year period would be:

- Resin Replacement Cost + Operating Cost x 3 years + Energy Cost x 3 years

= USD 110,000 + USD 4,117,200/year x 3 years + USD 131,400/year x 3 years

= **USD 13 729 200**

- This would amount to ~ **R68 464 000/ year**.

8.3 Summary

The evaluation of the water softening process using Weak Acid Cation (WAC) resin reveals significant operational costs. The resin replacement every three years amounts to USD 110,000. The annual operating cost of the resin system, including chemical usage for regeneration, stands at USD 4,117,200. Additionally, the energy cost, based on a power consumption of 200 kW, amounts to USD 131,400 per year. Over a three-year period, the total cost of the process sums up to USD 13,729,200. These expenses highlight the substantial financial implications associated with maintaining efficient water softening operations, amounting to approximately R68,464,000 annually. This operating cost also falls within the assumed budget for Sibanye-Stillwater. For both treatment options, the operating costs would at best amount to ~ R176 464 000 per year. At this cost including the Capex for the lime-soda ash treatment plant, the full cost to install and operate would be just over R200 000 000. Depending on what the capital expenditure for an ion exchange plant is, this full treatment process may not be economically feasible. Hence, it is worthwhile to investigate, for future reference, the potential revenue and returns that could be generated through the treatment of process water, including the exploration of possible saleable by-products, such as for example, gypsum.

8.4 References

Damons, R. E., 2001. Development of an Aspen Model for the Treatment of Acid Mine Drainage, M.Tech, Cape Town: The Cape Technikon.

GlobalPetrolPrices.com. (n.d.). South Africa Electricity Prices. Retrieved February 14 2023, from https://www.globalpetrolprices.com/South-Africa/electricity_prices/

Greyling, M. and Van Rooy, J.L., 2019. Hydrogeological properties of gypseous soils in South Africa. South African Journal of Geology 2019, 122(3), pp.389-396.

Monetary Policy (2020) Monetary policy. South African Reserve Bank. Available at: https://www.resbank.co.za/en/home/what-we-do/monetary-policy (Accessed: February 1, 2023).

Sinnot, R. K., 2005. Coulson and Richardson's Chemical Engineering Design. 4th ed. Oxford: Elsevier Butterworth-Heinemann.

Sithole, T., Mashifana, T., Mahlangu, D. and Tchadjié, L., 2023. Effect of binary combination of waste gypsum and fly ash to produce building bricks. Sustainable Chemistry and Pharmacy, 31, p.100913.

van Niekerk, A., 2002. Evaluation of the Savmin Sulphate Removal Process. Johannesburg: The Coalteh Research Association

Chapter 9 Conclusions and recommendations

The water samples analysed in this study exhibited extremely high levels of hardness, exceeding 3000 mg/L as $CaCO_3$. Additionally, the samples had elevated concentrations of total dissolved solids and sulphates, which posed challenges in identifying effective treatment methods. The main findings from the treatment methods conducted are as follows:

1. Lime and soda ash water softening: The combined use of lime and soda ash is commonly recommended for treating hard water with permanent hardness. However, it was observed that lime treatment alone also effectively reduced hardness. While lime and soda ash treatment exhibited the best overall hardness removal, especially at higher temperatures, both treatments demonstrated the additional advantage of removing heavy metals such as Fe, Ni, and Mn by over 80 %. It is important to note that the heating requirement for a daily consumption of 10 ML/day would not be economically viable. Therefore, considering the available capital, lime-only treatment with multiple cycles may be considered and recommended to minimize reagent costs associated with soda ash.
2. Ion exchange: Despite the application of weak acid cation (WAC) and strong acid cation (SAC) resins for hardness removal, the water hardness remained high. Calcium was more effectively adsorbed compared to Mg with a maximum removal efficiency of 68 % for all samples, while the maximum magnesium removal efficiency reached 59 % for the process water sample. Overall, the WAC resin exhibited higher efficiency compared to the SAC resin. This can be attributed to its high affinity for Ca and Mg hardness ions and its specific design for removing hardness ions from solutions with high total dissolved solids.
3. Combined use of lime-soda ash and ion exchange: The combination of lime-soda ash treatment and WAC resin in the softening process demonstrated superior performance compared to the combination with SAC resin. Once again, the WAC resin yielded moderately hard solutions with $CaCO_3$ concentrations ranging from 60—120 mg/L.
4. In contrast, the SAC resin, even when used in combination with lime-soda ash treatment, resulted in hard water with calcium carbonate levels ranging from 120—180 mg/L, except for the scrubber feed sample. Nevertheless, these hardness levels are

considered satisfactory within the water industry, as it is common practice to maintain a hardness residue within the range of 120—180 mg/L of $CaCO_3$.

5. Overall, the combined treatment approach involving lime-soda ash and the WAC resin proved to be the more effective option, ensuring desirable hardness levels in the treated water samples, while the SAC resin exhibited slightly higher hardness residues in most cases.
6. Magnetic water treatment: The magnetic treatment device (MTD) showed efficiency, particularly in reducing calcite formation. The magnetic influence altered water properties such as pH, DO, EC, and [Ca^{2+}], indicating the involvement of specific mechanism(s). The rapid formation of $CaCO_3$ and the preferential formation of aragonite over calcite were attributed to the Lorentz force. The solutions tested in this study primarily precipitated $CaSO_4$ due to the initial high concentrations of Ca^{2+} and SO_4^{2-}. It is recommended to conduct additional studies to determine the effect of magnetic treatments on mixed salt solutions with comparable quantities and assess if other minerals with polymorphs behave similarly to $CaCO_3$.
7. A conceptual water treatment process was proposed, combining lime-soda ash treatment with ion exchange using a WAC resin. An alternative stream based on the SAVMIN process for gypsum precipitation after lime and soda ash treatment was also suggested. However, before considering this route, it is crucial to conduct laboratory and pilot tests to assess the efficiency of removing excess Ca^{2+} and SO_4^{2-} through gypsum precipitation for hardness levels similar to those addressed in this study.
8. The proposed 10 ML treatment plant is estimated to cost over R200,000,000. It is worth noting that this treatment process offers the potential advantage of generating a saleable product, gypsum. This is significant in meeting strict legislative targets and aligning with the broader goal of maintaining a circular economy. By utilizing the treatment process outlined, the plant not only addresses water hardness issues but also has the potential for economic benefits through the commercialization of gypsum, contributing to the sustainable utilization of resources and promoting environmental responsibility.

Appendices:

Appendix 1

3.1 Ion exchange resin properties

Physical and chemical properties of WAC resin (Amberlite IRC 83 H) (DuPont, Amber series, 2023)

Matrix	Polyacrylic, macroporous
Type	Weak acid cation
Functional group	Carboxylic acid
Physical form	Amber, opaque, spherical beads
Ionic form as shipped	H^+ Form
Total exchange capacity	≥ 4.50 eq/L
Water retention capacity	40 – 50 %
Particle size	
Particle diameter	500 – 750 µm
Uniformity coefficient	≤ 1.70
>300 µm	≤ 2.0 %
Whole Uncracked Beads	≥ 95 %
Swelling	$H^+ \rightarrow Na^+$: ≤ 60 %
Bulk Density, as Shipped	700 g/L

Operating conditions of WAC resin (Amberlite IRC 83 H) (DuPont, Amber series, 2023)

Maximum Operating Temperature	100°C (212°F)		
Bed Depth, min.	700 mm (2.3 ft)		
Flowrates			
Service	5 – 50 bv*/h		
Regeneration			
HCl	2 – 4 bv/h		
H_2SO_4	2 – 4 bv/h		
NaOH	2 – 4 bv/h		
Displacement Rinse	2 bv at 2 – 4 BV/h		
Fast Rinse	2 – 4 bv at service flow rate		
Regenerant (100% basis)	**HCl**	**H_2SO_4**	**NaOH**
Concentration	2 – 5%	0.5 – 0.7%	2 – 4%
De-alkalization(%Operating Capacity	105 – 110%	105 – 110%	105 – 110%
Softening (% Total Capacity)	110 – 160%	110 – 160%	110 – 160%

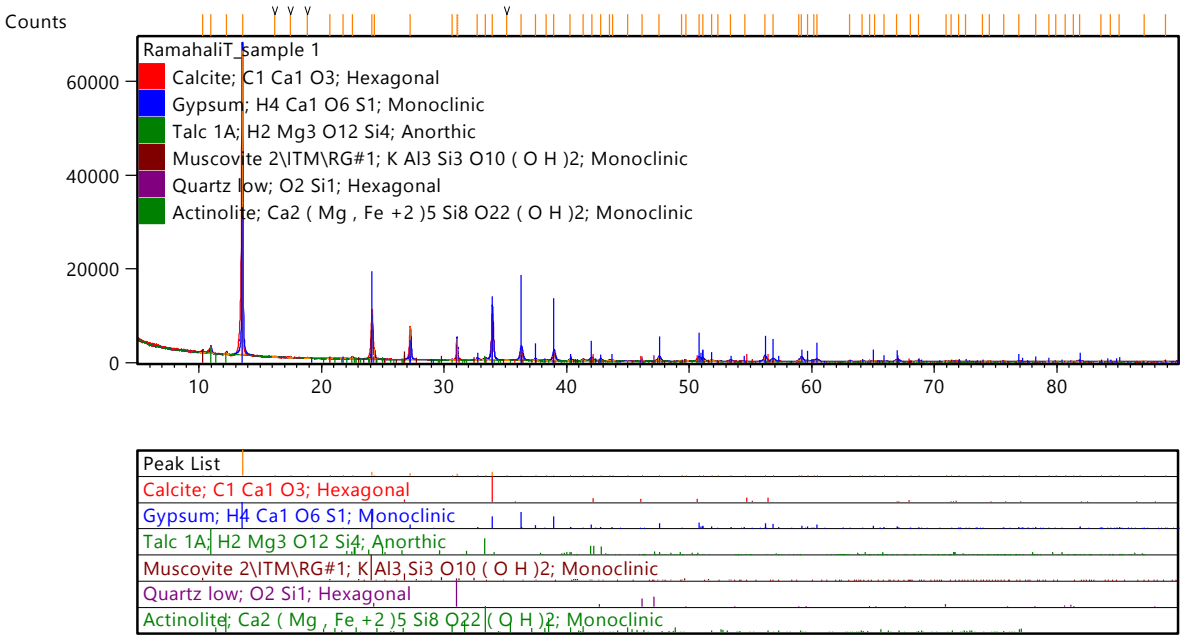
Physical and chemical properties of SAC resin (Amberlite IRC 120Na) (DuPont, Amber series, 2023)

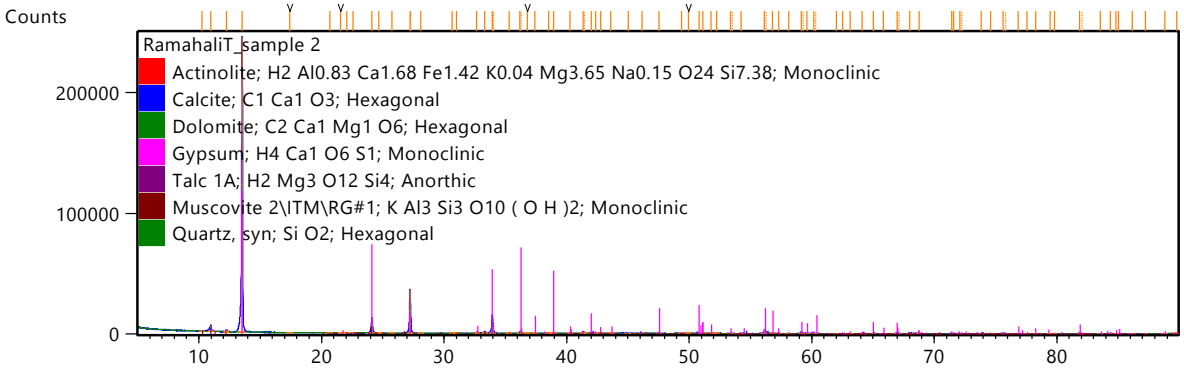
Physical form	Amber spherical beads
Matrix	Styrene-divinylbenzene copolymer
Functional group	Sulfonate
Ionic form as shipped	Na^+
Total exchange capacity	> 2.00 eq/L (Na^+ form)
Moisture holding capacity	45 to 50 % (Na^+ form)
Shipping weight	840 g/L
Uniformity coefficient	<1.9
Harmonic mean size	0.600 to 0.800mm
<0.300mm	2 % max
Maximum reversible swelling	$Na^+ \rightarrow H^+$ < 11 %

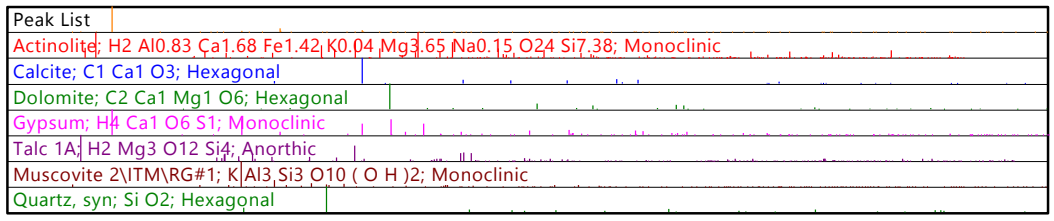
Operating conditions of WAC resin (Amberlite IRC 83 H) (DuPont, Amber series, 2023)

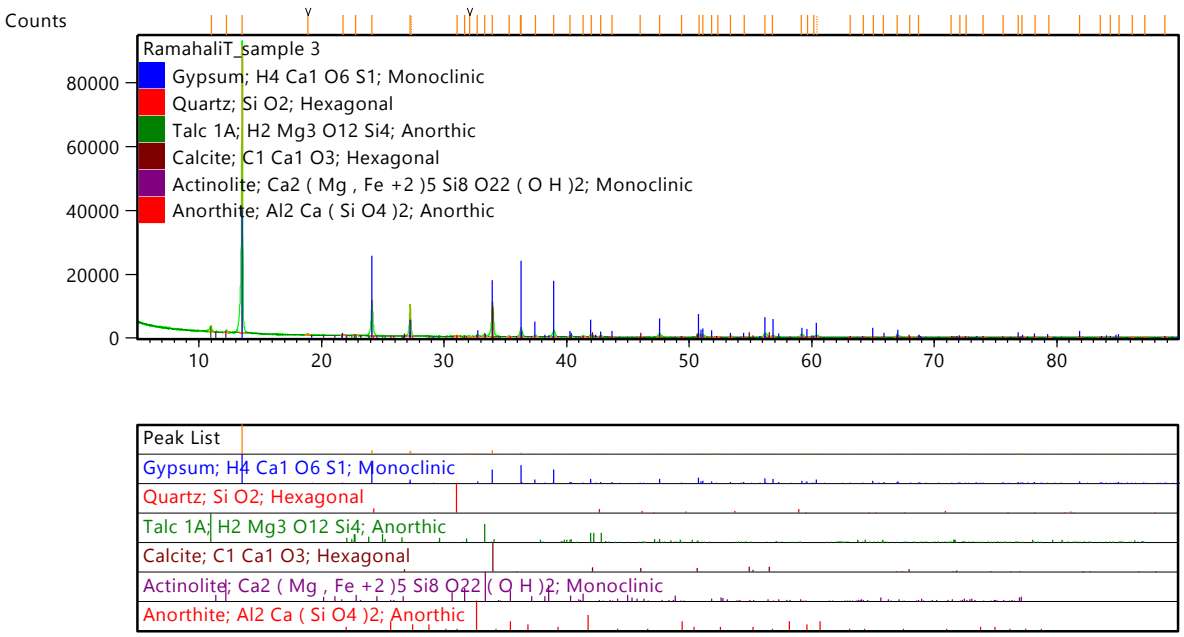
Maximum operating temperature	135°C		
Minimum bed depth	700mm		
Service flow rate	5 to 40 bv/h		
Regenerant	HCI	H_2SO_4	NaCI
Level (g/L)	50 to 150	60 to 240	80 to 250
Concentration (%)	5 to 8	0.7 to 6	10
Minimum contact time	30 minutes		
Slow rinse	2 bv at regeneration flow rate		
Fast rinse	2 to 4 bv at service flow rate		

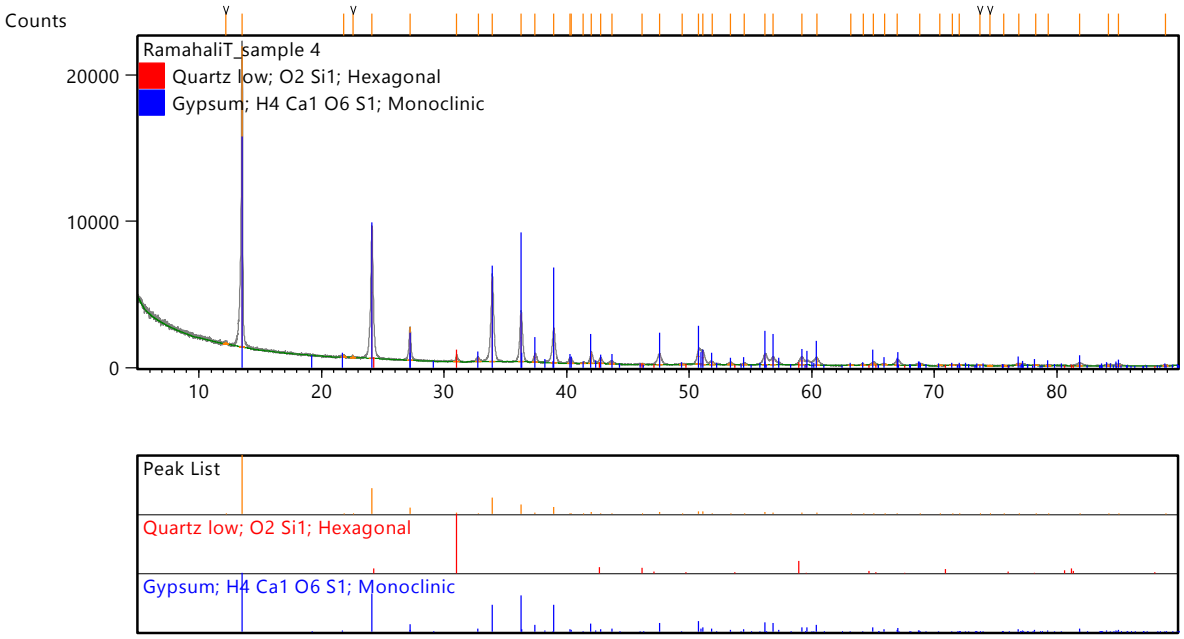
1.2 XRD results for scale samples

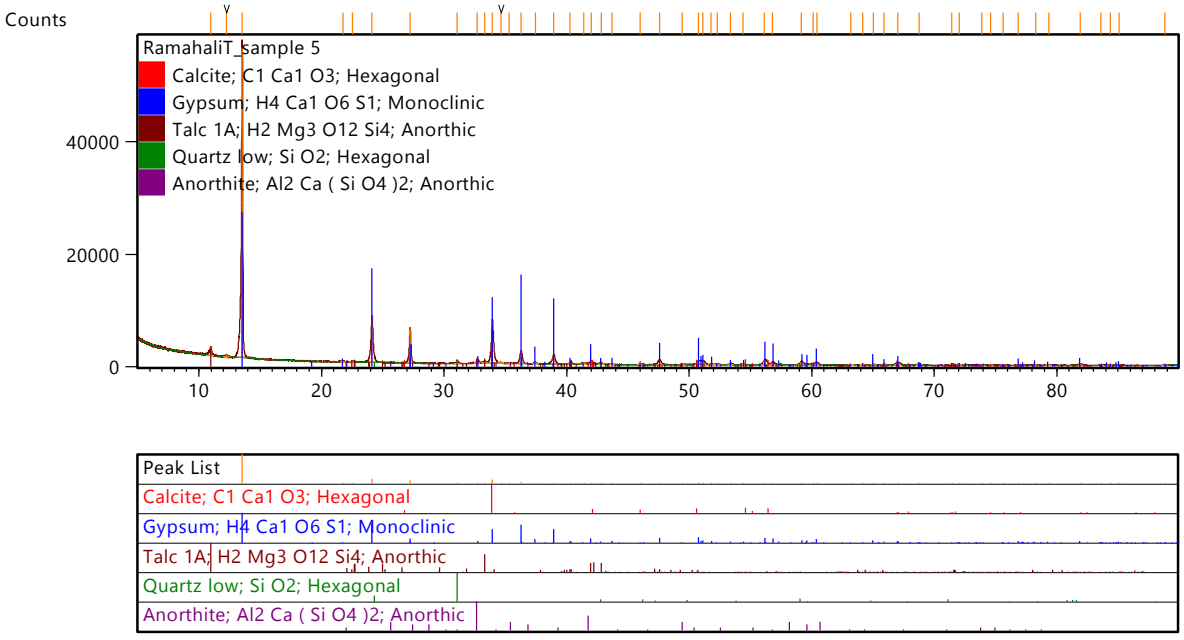


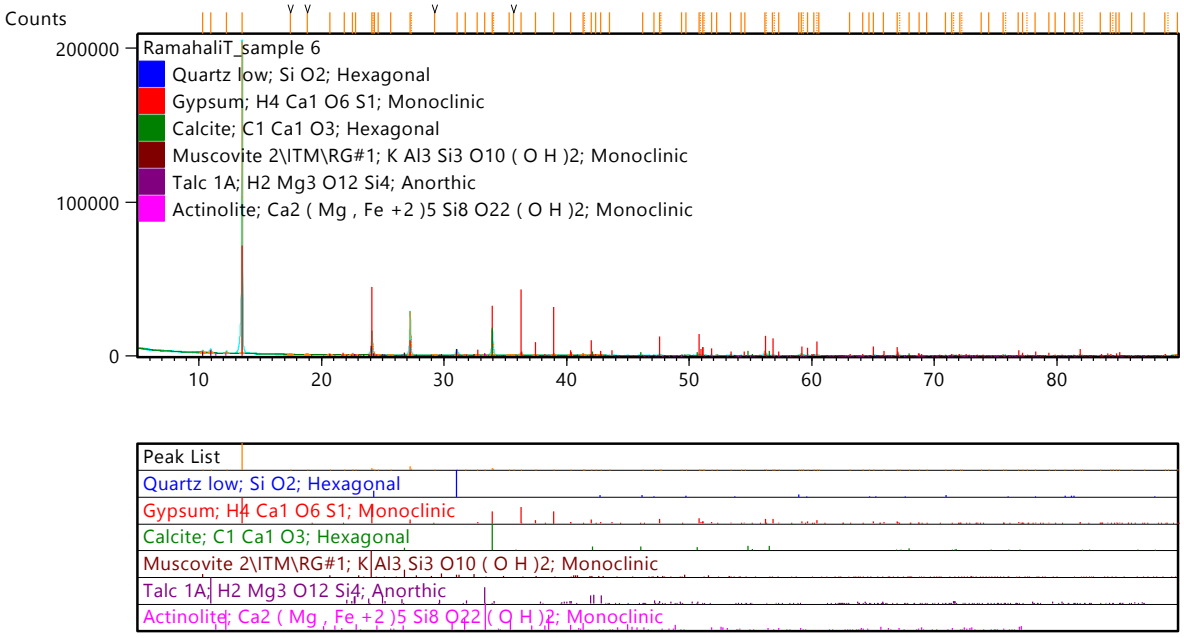


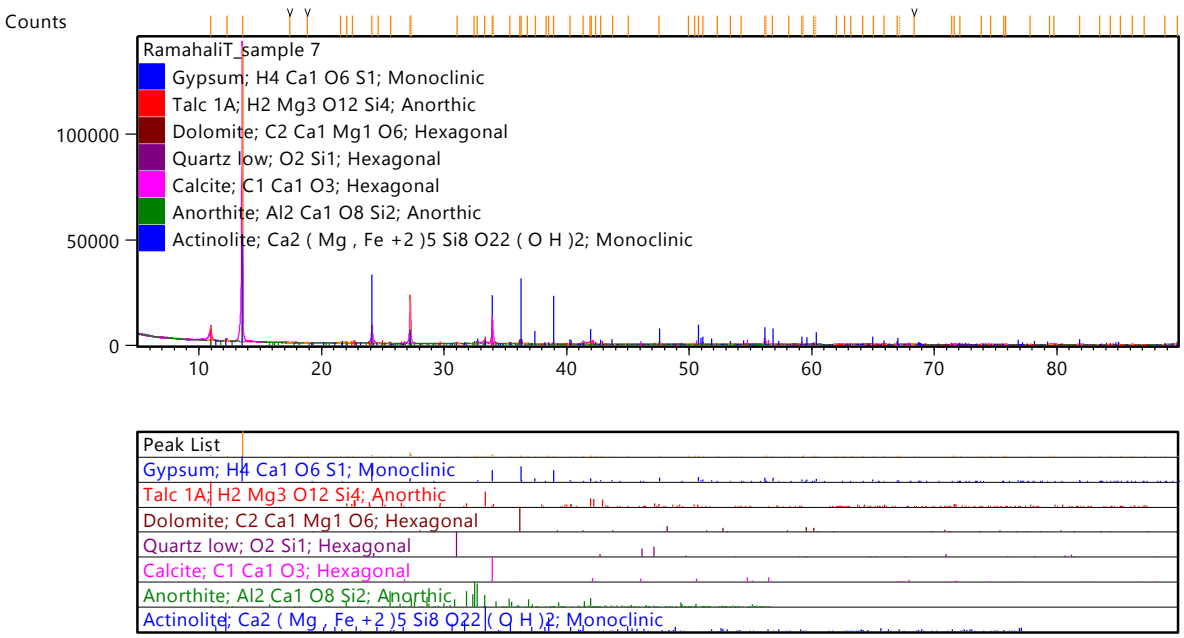



Counts
RamahaliT_sample 3
Gypsum; H4 Ca1 O6 S1; Monoclinic
Quartz; Si O2; Hexagonal
Talc 1A; H2 Mg3 O12 Si4; Anorthic
Calcite; C1 Ca1 O3; Hexagonal
Actinolite; Ca2 (Mg , Fe +2)5 Si8 O22 (O H)2; Monoclinic
Anorthite; Al2 Ca (Si O4)2; Anorthic
80000
60000
40000
20000
0
10
20
30
40
50
60
70
80
Peak List
Gypsum; H4 Ca1 O6 S1; Monoclinic
Quartz; Si O2; Hexagonal
Talc 1A; H2 Mg3 O12 Si4; Anorthic
Calcite; C1 Ca1 O3; Hexagonal
Actinolite; Ca2 (Mg , Fe +2)5 Si8 O22 (O H)2; Monoclinic
Anorthite; Al2 Ca (Si O4)2; Anorthic


Counts
RamahaliT_sample 4
Quartz low; O2 Si1; Hexagonal
Gypsum; H4 Ca1 O6 S1; Monoclinic
20000
10000
0
10
20
30
40
50
60
70
80
Peak List
Quartz low; O2 Si1; Hexagonal
Gypsum; H4 Ca1 O6 S1; Monoclinic

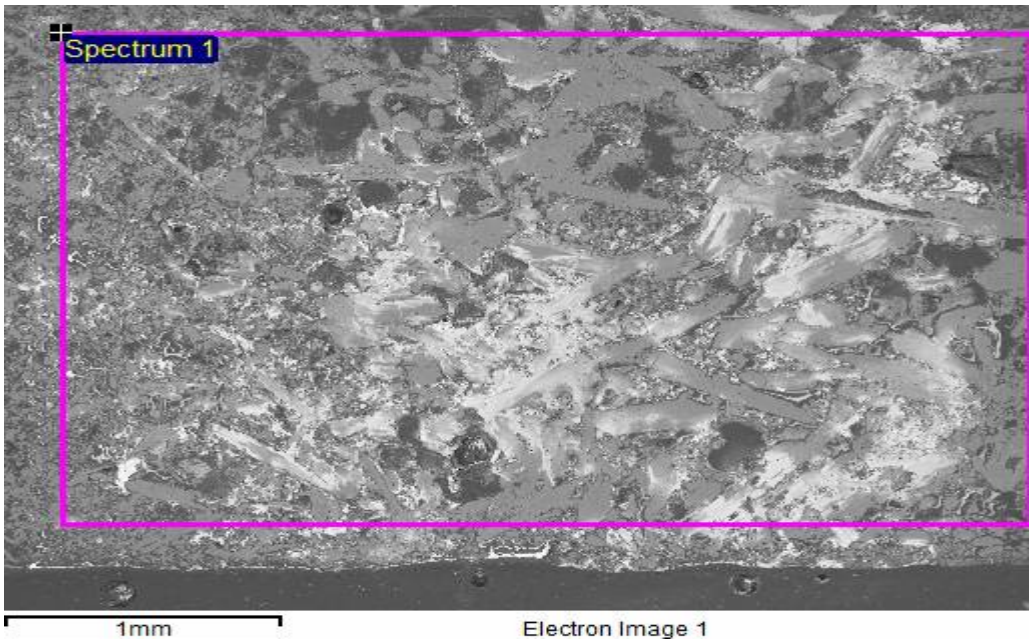

Counts
RamahaliT_sample 5
Calcite; C1 Ca1 O3; Hexagonal
Gypsum; H4 Ca1 O6 S1; Monoclinic
Talc 1A; H2 Mg3 O12 Si4; Anorthic
Quartz low; Si O2; Hexagonal
Anorthite; Al2 Ca (Si O4)2; Anorthic
40000
20000
0
10
20
30
40
50
60
70
80
Peak List
Calcite; C1 Ca1 O3; Hexagonal
Gypsum; H4 Ca1 O6 S1; Monoclinic
Talc 1A; H2 Mg3 O12 Si4; Anorthic
Quartz low; Si O2; Hexagonal
Anorthite; Al2 Ca (Si O4)2; Anorthic


Counts
RamahaliT_sample 6
Quartz low; Si O2; Hexagonal
Gypsum; H4 Ca1 O6 S1; Monoclinic
Calcite; C1 Ca1 O3; Hexagonal
Muscovite 2\ITM\RG#1; K Al3 Si3 O10 (O H)2; Monoclinic
Talc 1A; H2 Mg3 O12 Si4; Anorthic
Actinolite; Ca2 (Mg , Fe +2)5 Si8 O22 (O H)2; Monoclinic
200000
100000
0
10
20
30
40
50
60
70
80
Peak List
Quartz low; Si O2; Hexagonal
Gypsum; H4 Ca1 O6 S1; Monoclinic
Calcite; C1 Ca1 O3; Hexagonal
Muscovite 2\ITM\RG#1; K Al3 Si3 O10 (O H)2; Monoclinic
Talc 1A; H2 Mg3 O12 Si4; Anorthic
Actinolite; Ca2 (Mg , Fe +2)5 Si8 O22 (O H)2; Monoclinic

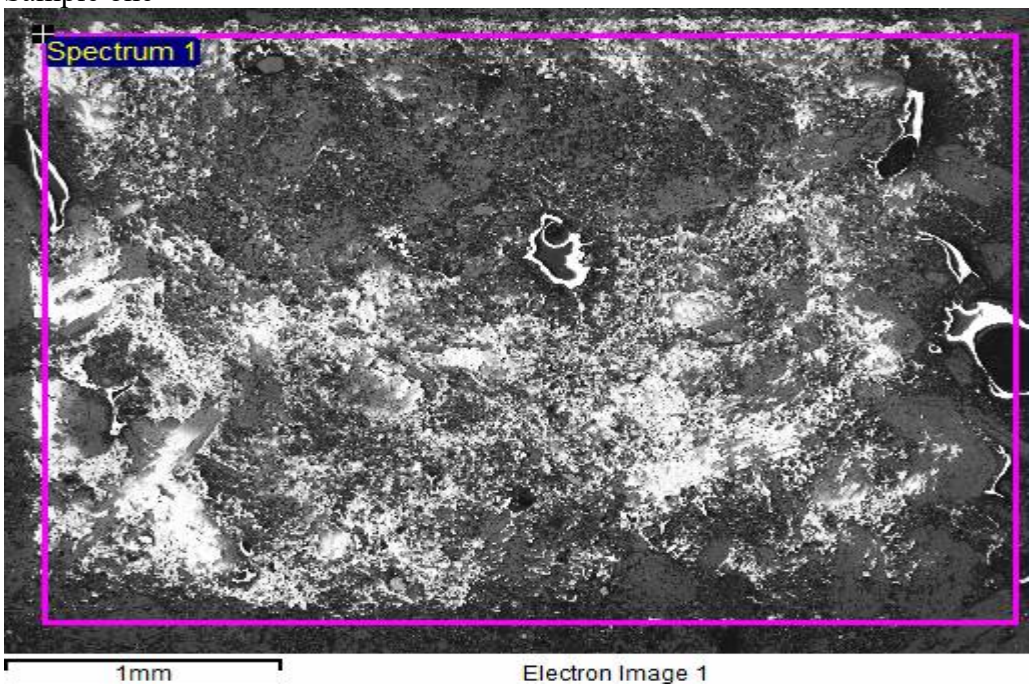

Counts
RamahaliT_sample 7
Gypsum; H4 Ca1 O6 S1; Monoclinic
Talc 1A; H2 Mg3 O12 Si4; Anorthic
Dolomite; C2 Ca1 Mg1 O6; Hexagonal
Quartz low; O2 Si1; Hexagonal
Calcite; C1 Ca1 O3; Hexagonal
Anorthite; Al2 Ca1 O8 Si2; Anorthic
Actinolite; Ca2 (Mg , Fe +2)5 Si8 O22 (O H)2; Monoclinic
100000
50000
0
10
20
30
40
50
60
70
80

Peak List
Gypsum; H4 Ca1 O6 S1; Monoclinic
Talc 1A; H2 Mg3 O12 Si4; Anorthic
Dolomite; C2 Ca1 Mg1 O6; Hexagonal
Quartz low; O2 Si1; Hexagonal
Calcite; C1 Ca1 O3; Hexagonal
Anorthite; Al2 Ca1 O8 Si2; Anorthic
Actinolite; Ca2 (Mg , Fe +2)5 Si8 O22 (O H)2; Monoclinic

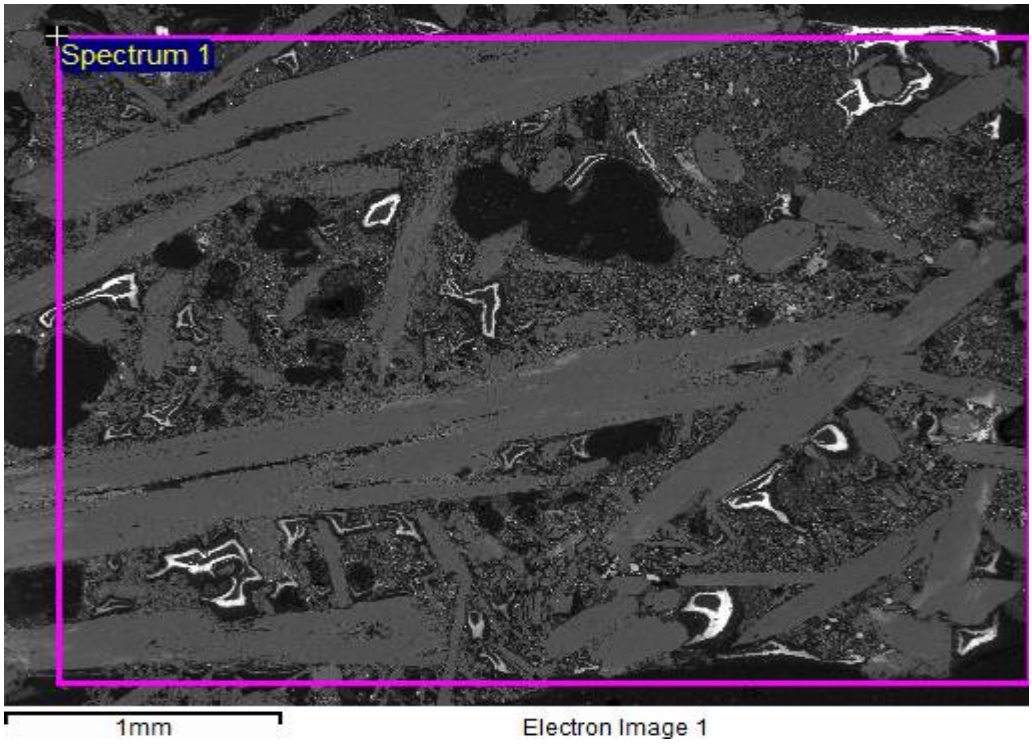
1.3 SEM photomicrographs of all solid samples



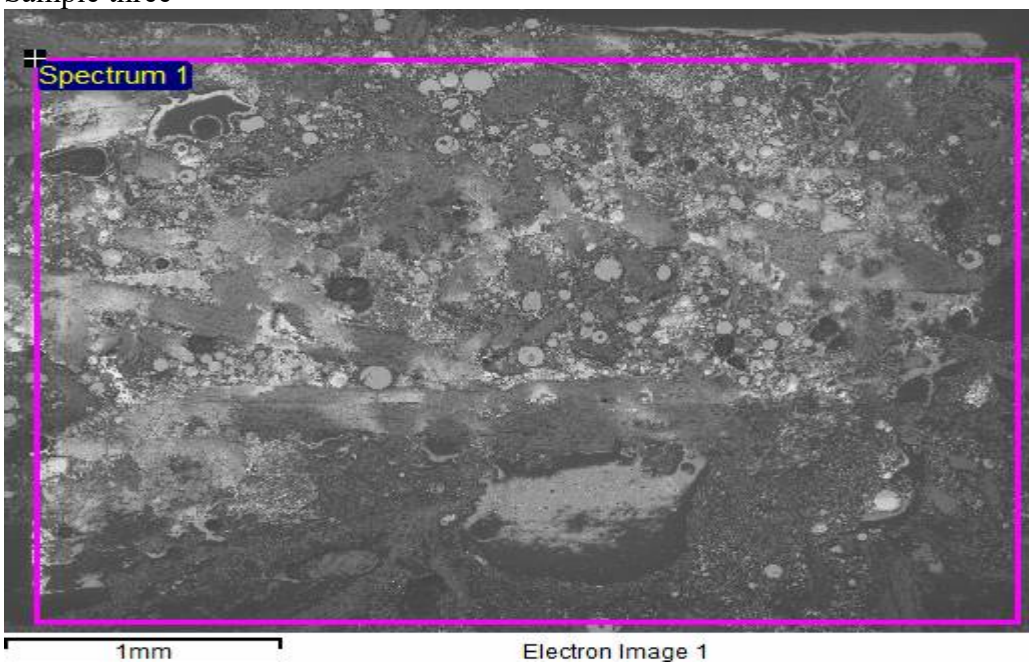
Sample one



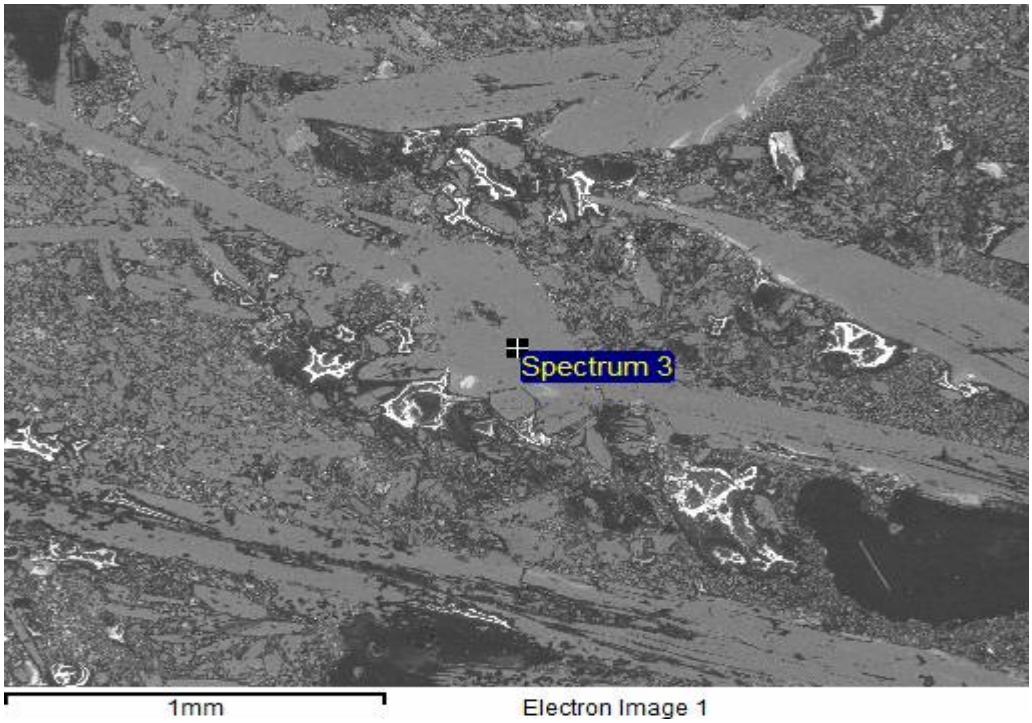
Sample two



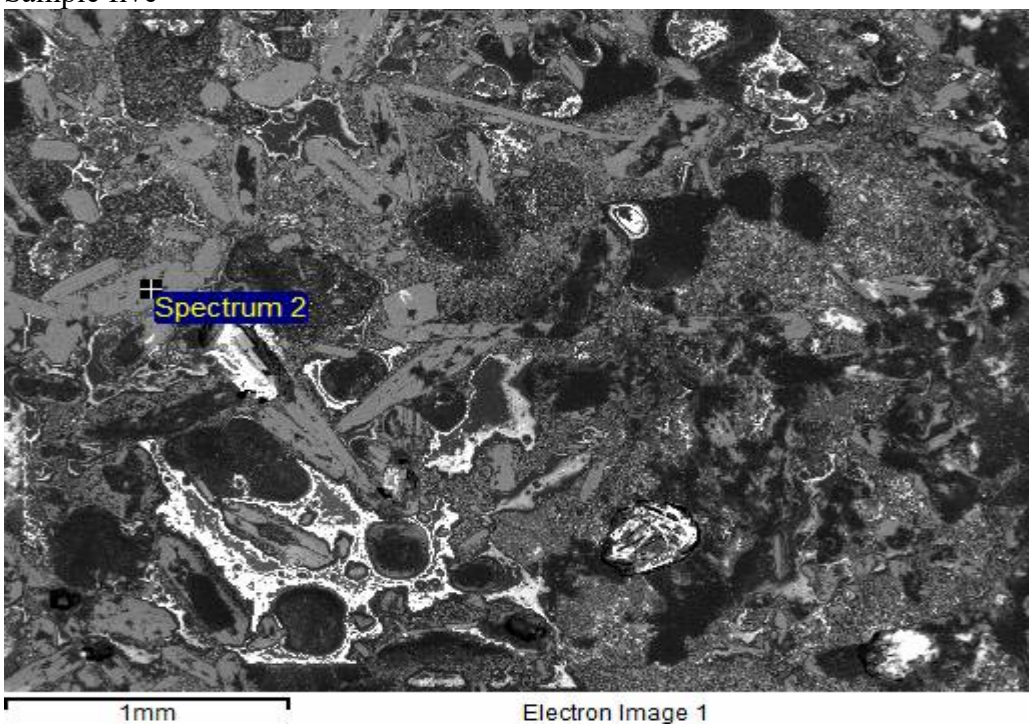
Sample three



Sample four



Sample five



Sample six

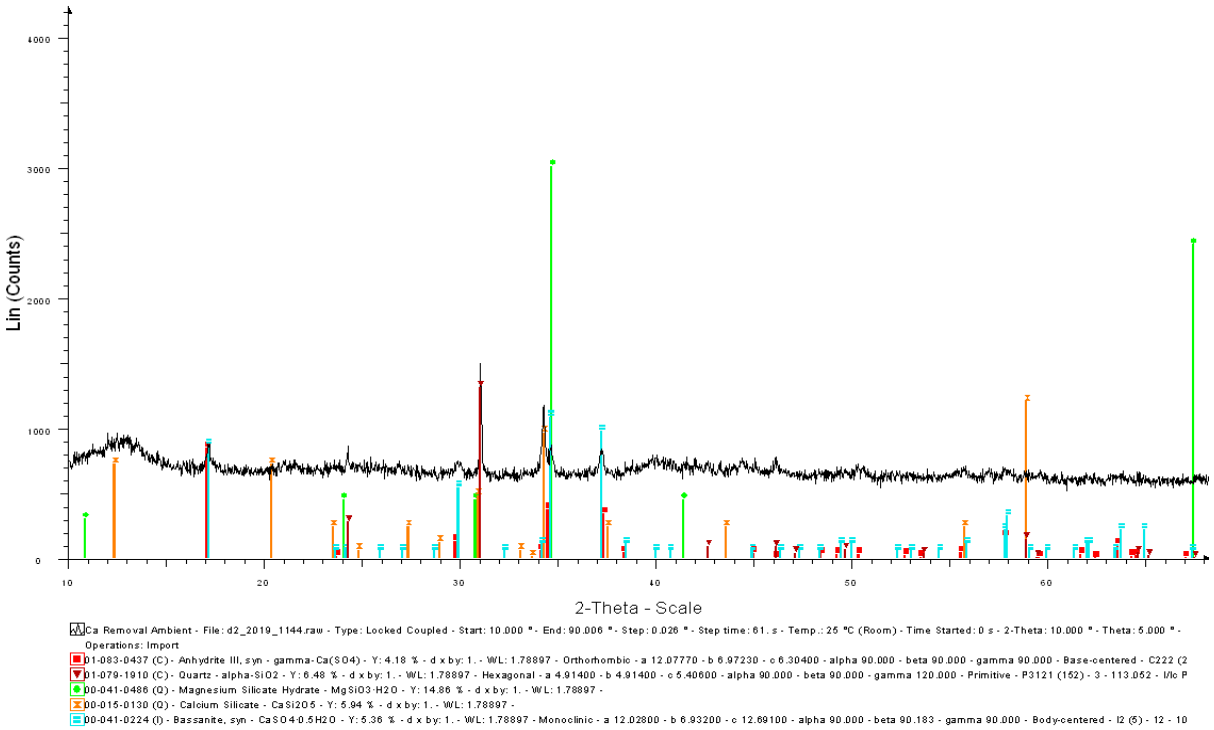


Sample seven

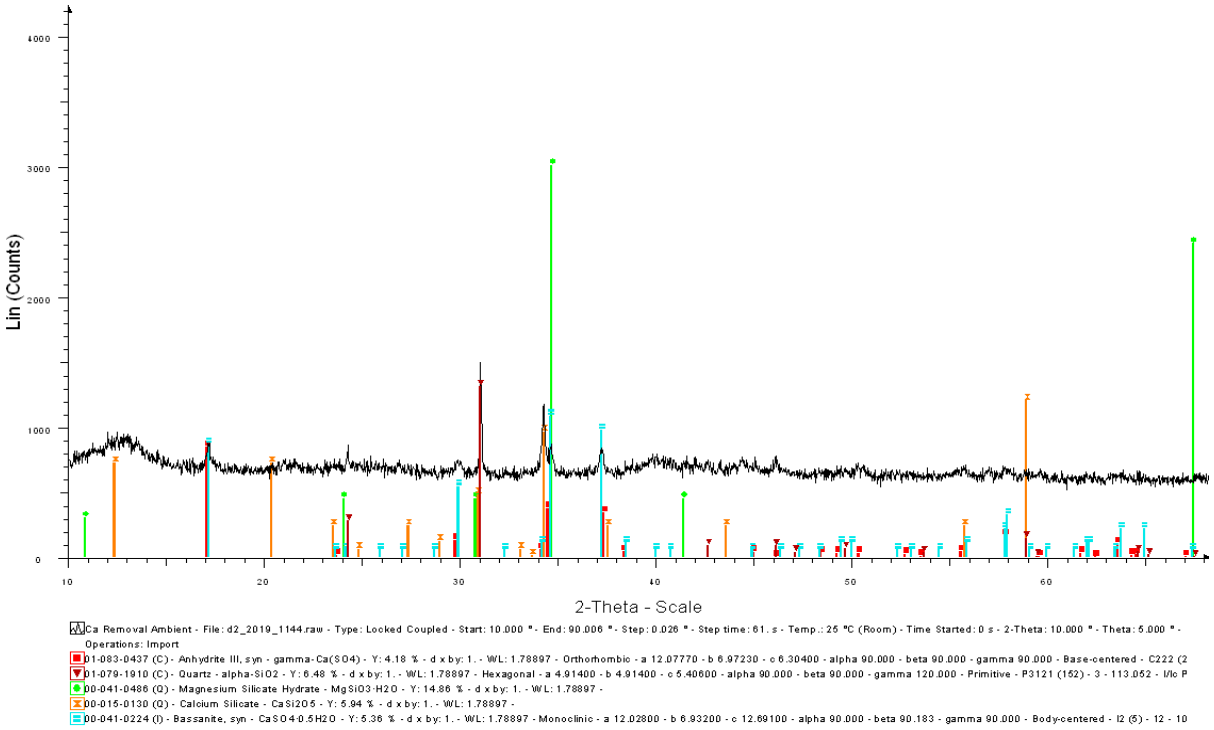
Appendix 2:

2.1 XRD analysis for lime and lime-soda treatments

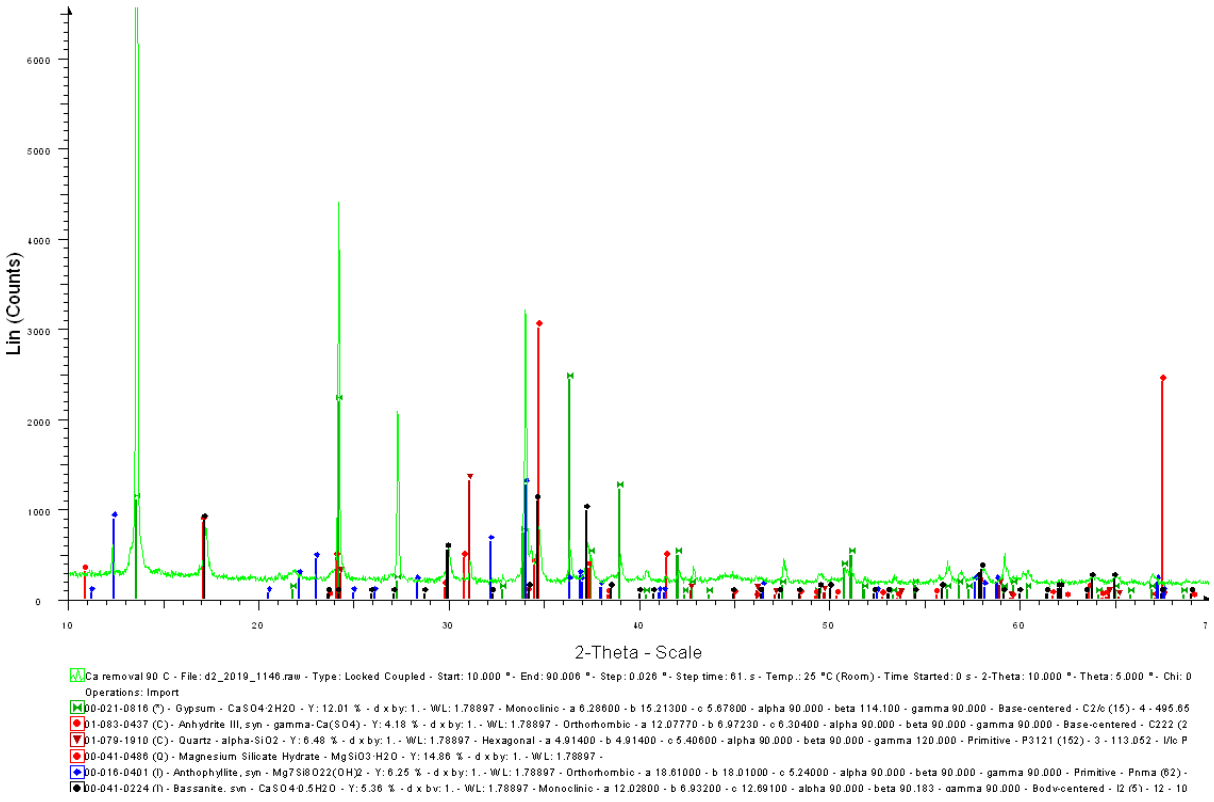
Lime softening at 20 °C



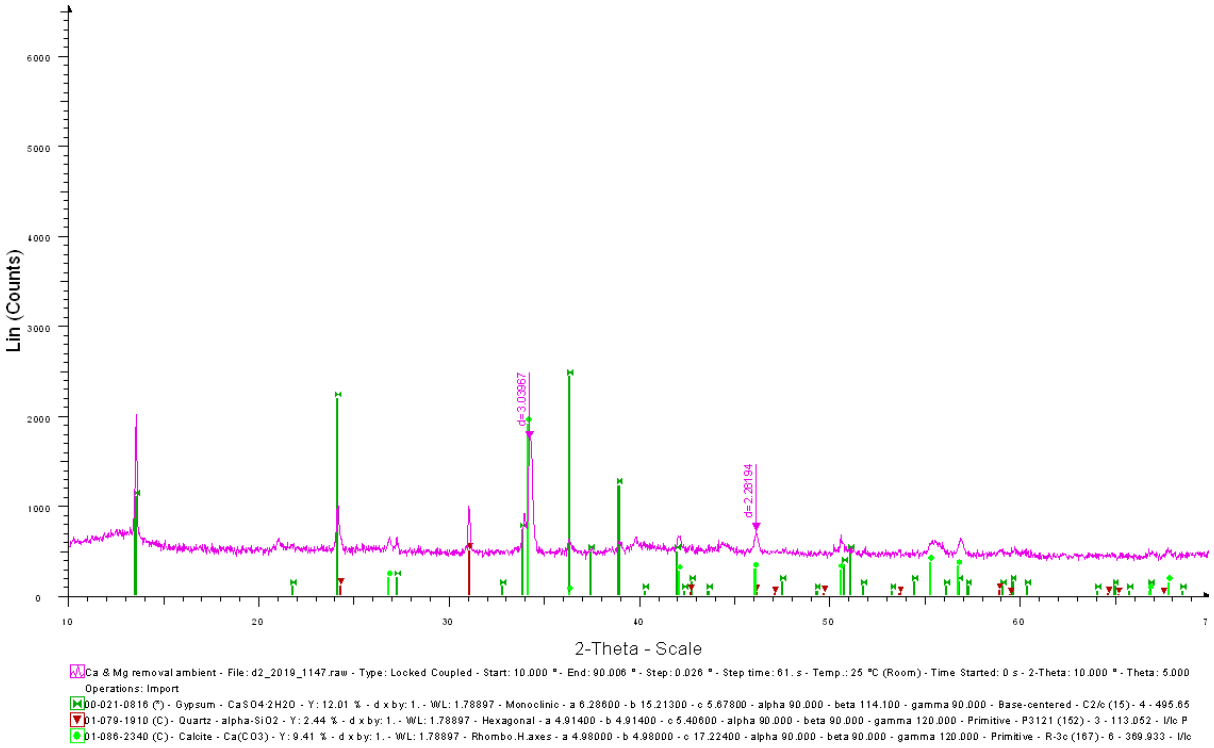
Lime softening at 60 °C



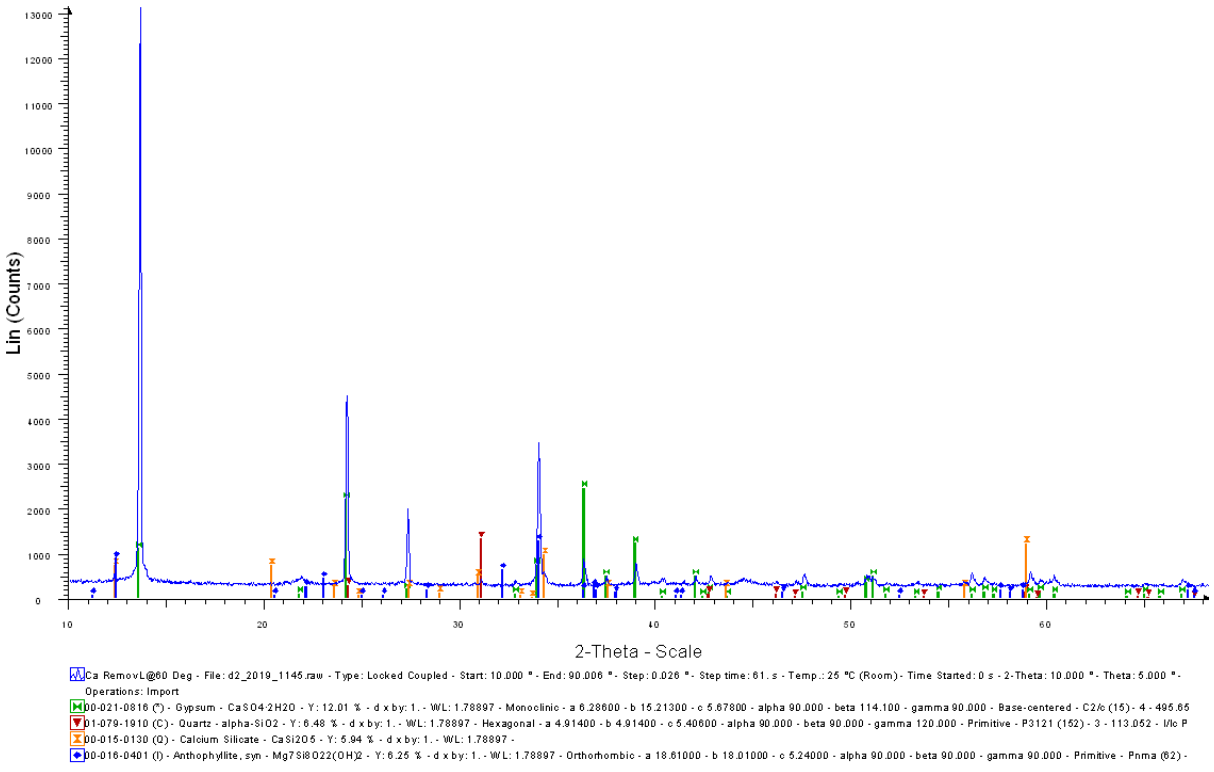
Lime softening at 100 °C



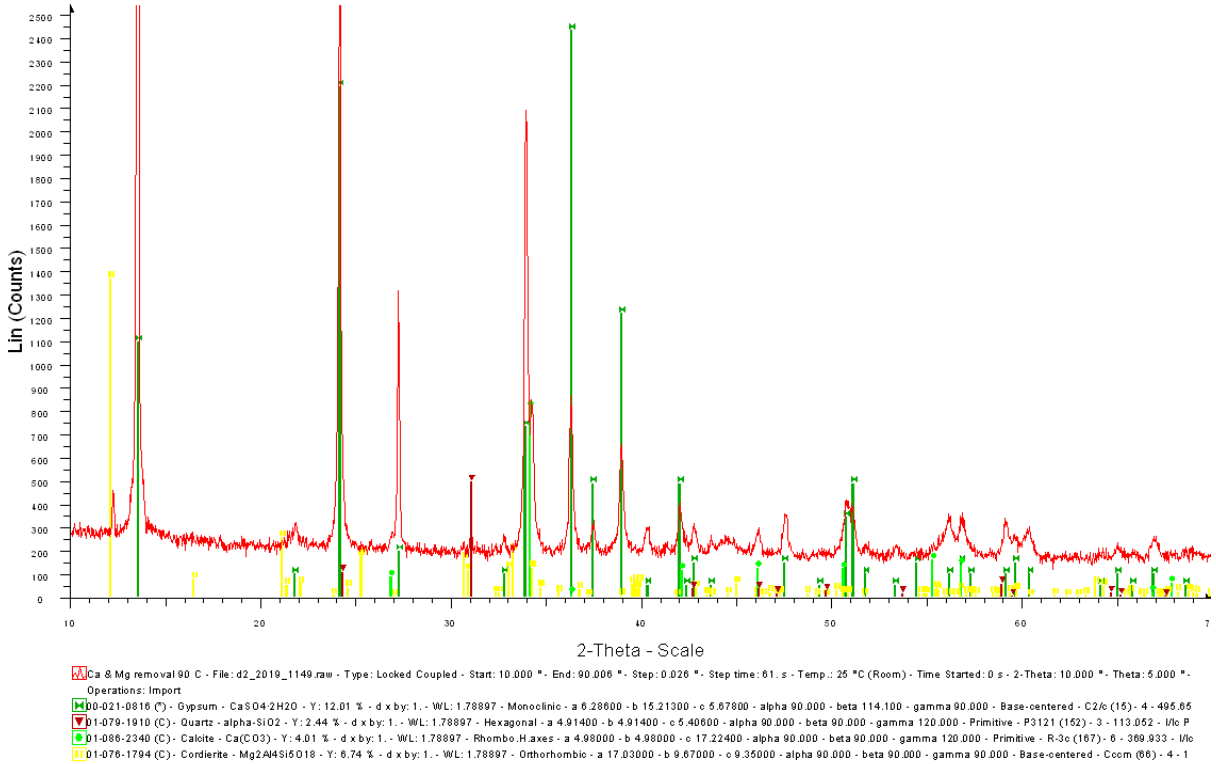
Lime soda softening at 20 °C



Lime soda softening at 60 °C



Lime soda softening at 100 °C



Appendix 3:

3.1 Combined softening results from lime-soda ash and ion-exchange.

	AFTER LIME AND SODA		WAC TREATMENT				SAC TREATMENT			
SAMPLE	**Ca [mg/l]**	**Mg [mg/L]**	**Ca [mg/L]**	% removal	**Mg [mg/L]**	% removal	**Ca [mg/L]**	% removal	**Mg [mg/L]**	**% removal**
SB	35	42	16	**54**	19	**65**	18	**49**	20	**64**
SF	21	153	13	**38**	15	**90**	17	**19**	18	**88**
DTO	15	89	8,9	**41**	12	**87**	10,8	**28**	26	**71**
PW	26	24	15,7	**40**	17,5	**27**	16,4	**37**	20	**17**

Appendix 4:

4.1 Energy balance

In section 4.2, the results showed that lime-soda softening was more efficient as temperature increased with Ca and Mg most efficiently removed at 100 °C. Significant operating costs would be associated with the heating requirement for 10 ML/day.

*Heat/Energy requirement to raise temperature (KJ) = m. C_p. ΔT

Where:

m = mass of eluant

Cp = heat capacity of the eluant

ΔT = change in eluant temperature

* 3600 KJ is equivalent to 1 kWh

A summary of the energy balance calculation for heating process water from ambient conditions to 100 °C is summarized in the table below:

Heating requirements per day			
Initial temperature		20	°C
Required heating temperature		100	°C
C_p (heat capacity)		4.18	J/g.°C
Volume		10 000	m^3/day
Energy/Heating requirement		3 344 000	MJ
Conversion: MJ→ kWh		MJ/3600	
Energy/ heating requirement	**daily**	928	MWh
	monthly	27 867	MWh

The monthly estimated unit cost per kilowatt is presented below. The determined cost indicate heating of the process water would not be economically viable.

Monthly heating/electricity cost				
Water heating requirement	**Unt cost (USD/kWh)**	**Quantity (kWh)**	**Total (USD)**	**Total (ZAR)**
	0.074	27 867 000	2 062 158	37 540 886

4.2 Neutralisation Reactor Design Calculations

By following the design outline by van Niekerk (2002), a total of two neutralisation reactors were chosen, each with a retention time of 30 minutes. The volume of each reactor was calculated as follows:

Total volumetric flowrate =

$$= 10 \frac{\text{ML}}{\text{day}} \times \frac{1000}{24 \times 60 \times 60}$$

$$= 0.12 \text{ m}^3/s$$

Volume of neutralisation reactor =

$$\frac{Retention\ time \times volumetric\ flowrate}{number\ of\ reactors}$$

$$= \frac{30\ minutes \times 0.12 \times 60}{2}$$

$$= 90 \text{ m}^3$$

Neutralisation Settler/Thickener Design Calculations

By following the design outline by Van Niekerk (2002), a total of two neutralisation reactors were chosen, each with a retention time of 30 minutes and upflow velocity of 0.7 m/hr. The volume of each reactor was calculated as follows:

Total volumetric flowrate =

$$= 10 \ \frac{\text{ML}}{\text{day}} \times \frac{1000}{24 \times 60 \times 60}$$

$$= 0.12 \ \text{m}^3/s$$

Volume of settler/ thickener=

$$\frac{Retention\ time \times volumetric\ flowrate}{number\ of\ reactors}$$

$$= \frac{30\ minutes \times 0.12 \times 60}{1}$$

$$= 180 \ \text{m}^3$$

4.3 Lime and Soda ash Design Dosage and Consumption

From section 5.1.1.2, the required lime and soda ash dosage was determined as 1.0 kg/m^3 and 2 kg/m^3 of process water. The monthly reagent consumption is therefore calculated as follows:

Lime consumption=

Lime dosage × volumetric flowrate

$$= 1 \frac{\text{kg}}{\text{m3}} \times 10 \frac{\text{ML}}{\text{day}} \times \frac{1000\text{x}30}{1000}$$

=300 ton/month

Soda ash consumption=

Soda ash dosage× volumetric flowrate

$$= 2 \frac{\text{kg}}{\text{m3}} \times 10 \frac{\text{ML}}{\text{day}} \times \frac{1000\text{x}30}{1000}$$

= 600 ton/month